# AN ENERGY CONVERSION SCHEME USING A PERMANENT MAGNET GENERATOR AND A PWM, GTO CONVERTER

By

FADHIL ABBAS MEHDI AL-QRIMLI

Thesis submitted in accordance with the requirements of
the University of Liverpool for the degree of
Doctor in Philosophy

The University of Liverpool
Department of Electrical Engineering And Electronics

January 1991

To my beloved ( kids ):

Haidar

Ali .....

My Wife Atared

## *ABSTRACT*

*The work presented in this thesis has concentrated on the development and design of a system that can be used in conjunction with an alternative source of energy to produce an energy conversion scheme. A permanent magnet synchronous generator is used for this project together with a three-phase fully controlled converter. High field permanent magnet generators are also tested and can be used in future work. The converter power devices used are the Gate Turn Off thyristors, which are controlled by a pulse width modulation technique. The work divides into three parts. In the first part, the permanent magnet generator parameters are determined together with its performance characteristics and Optimal output power from the generator is discussed.*

*The second part of this work concerns the design and construction of the three-phase GTO converter, using a new method of pulse width modulation to improve performance characteristics. Two bridges are discussed; one of them has three-power devices as switches with twelve-diodes. This bridge works as a full wave rectifier with delay angle limitation of* $\pm 30°$*. The other bridge has 6-power devices as switches. This bridge works in full two quadrant operation (*$\pm 180°$ *delay angle). The permanent magnet generator and the PWM, GTO converter are tested together to form a variable source of energy. This is discussed in chapters Three and Four.*

*The third part of this work concentrates on the use of this system for alternative sources of energy. One of these sources used, for example, is a wind energy system. Tidal power systems are also considered. A programmable digital controller for the output power of the system is designed and*

*implemented to form a complete system of power conversion. This is discussed in chapters Five and Six. Some suggestions for future work are discussed in chapter Seven.*

## ACKNOWLEDGEMENT

I would like to express my sincere gratitude and appreciation to Professor K.J. Binns for his enthusiastic encouragement, help and his moral support during the preparation of this thesis.

I greatly acknowledge Dr. P.H. Mellor for his guidance, help and useful discussion and advice during the course of my research.

I am also very grateful to the Ministry of Higher Education and Scientific Research of Iraq for their sponsorship and financial support for this work.

Thanks to all my colleagues and friends for their help during the research, and all the staff of the Department of Electrical Engineering and electronics for their encouragement. My thanks extended to Mr. K. Mealor for his help in preparing the equipment needed for this research.

Special love and loyalty to my wife Atared, and my children Haidar and Ali for their patience, when I spent so much time away from them during this research.

Finally, but not last, I am indebted to my parents, sisters, brothers, and my uncle Shihab Al-Qrimli, for their generosity, patience, encouragement and for always being there with their support.

# *TABLE OF CONTENTS*

# *LIST OF SYMBOLS*

| | |
|---|---|
| $C_p$ | turbine efficiency. |
| $C_T$ | torque coefficient. |
| $emf$, $E_o$ | electromotive force per phase. |
| $f_g$ | oscillator frequency. |
| $f_m$ | machine frequency. |
| $i_{a1}$ , $i_a$ | stator current. |
| $i_{a2}$ | converter a.c. current. |
| $i_c$ | capacitor filter current. |
| $I_{d1}$ | d.c. current of first converter. |
| $I_{d2}$ | d.c. current of second converter. |
| $n$ | shaft speed. |
| $P_m$ | mechanical power on the shaft. |
| $P_{wd}$ | wind power. |
| $R$, $Y$, $B$ | machine and converter phases. |
| $R_a$ | armature resistance per phase. |
| $T_s$ | torque developed on the shaft. |
| $V_{tl}$ | line voltage. |
| $v$ | wind speed. |
| $V_{d1}$ | d.c. voltage of first converter. |
| $V_{d2}$ | d.c. voltage of second converter. |
| $V_{tp}$ , $V_{Rp}$ | phase voltage. |
| $V_{tcl}$ | converter line voltage. |
| $V_{tcp}$ | converter phase voltage. |
| $X_d$ | direct axis synchronous reactance. |
| $X_l$ | leakage reactance. |
| $X_q$ | quadrature axis synchronous reactance. |
| $X_s$ | synchronous reactance. |

GREEK LETTERS:

| | |
|---|---|
| $\beta$ | commutation angle. |
| $\phi$ | power-factor angle. |
| $\phi_{opt}$ | Optimal power-factor angle. |
| $\eta_c$ % | converter efficiency. |
| $\eta_s$ % | combined system efficiency. |
| $\alpha_1$ | delay angle of the first converter. |
| $\alpha_2$ | delay angle of the second converter. |
| $\Omega$ | Ohm. |
| $\omega$ | angular speed of rotation. |
| $\rho$ | air density. |
| $\lambda$ | blade tip to wind speed ratio. |

ABBREVIATIONS:

| | |
|---|---|
| A/D | analogue to digital converter. |
| CLK | clock. |
| EPROM | erasable programmable read only memory. |
| GTO | gate turn off thyristor. |
| IGBTs | insulated gate bipolar transistors |
| PLL | phase locked loop. |
| PM | permanent magnet. |
| PWM | pulse width modulation. |
| rpm | revolution per minute. |
| WECS | wind energy conversion systems. |

# *LIST OF FIGURES*

*CHAPTER ONE*

# INTRODUCTION

The hazards of Nuclear power generation and the increasing costs of fossil fuels has caused interest to be focused on the search for, and efficient utilisation of, alternative sources of energy for conversion into electric power. The renewable energy from the wind and tide provide feasible alternatives. Wind or tidal turbines are coupled to electrical machines for power generation and transmission. However the energy from these sources is variable with regard to both speed and power and consequently the energy generated by the electrical machine can be variable in terms of frequency and voltage. In order to match these sources to the transmission network, the voltage and frequency must be synchronised by methods such as the following:

1- Direct connection by,

a- Mechanical methods such as, gear box control, and pitch control of the wind turbine blades.

b- Electrical methods such as, implementing magnetic pole changes in the electric generator connected to the turbine.

2- Indirect connection, using power converters in different schemes such as, a D.C. generator and inverter, or an A.C. generator and A.C./D.C./A.C. converter system.

Stand alone wind energy conversion systems (WECS) have many applications in which a variable output frequency is acceptable, since they are not connected directly to the a.c. network. These systems usually consist of small wind turbines which are normally used for battery charging in isolated areas not connected to the grid of the a.c. utility network, and include such applications as remote communications, lighting, commercial

green house heating, and in the leisure markets (to provide energy for navigational instruments on yachts, or for caravan batteries). In practice even a very small wind generator can serve a useful purpose by ensuring that batteries have longer lifetimes due to regular charging, and do not have to be carried away for charging. Some manufacturers have aimed their wind turbine design at mass production using low cost, high volume techniques [24]. Moreover, small wind turbines can be connected indirectly to the a.c. network in conjunction with some kind of short-term energy storage such as:-

1-Mechanical short-term energy storage systems [9], using flywheels.

2-Electrical short-term energy storage systems [24], using batteries.

The typical characteristics of the prime movers which provide the source of renewable wind energy are discussed in Chapter 5. Here, the presently available types of electric generators and power conditioning systems are considered. There are many kinds of a.c. generators used in wind energy conversion systems (WECS), including synchronous [1, 8], slip ring induction [2-7, 33], squirrel cage induction [35], or d.c. generators [24, 31, 34]. Of synchronous generators, one particular type is a permanent magnet (PM) synchronous generator [13-17, 22].

A number of schemes have already been proposed for converting wind energy into a form suitable to feed into an existing a.c. utility network [3-21, 27-29], or as a stand alone system for use in remote areas [24, 30-35]. The proposals for the systems that are connected to the a.c. network broadly fall into two categories:

1- Constant speed, constant frequency systems, including systems which are connected directly to the a.c. network and are synchronised by mechanical or electrical methods.

2- Variable speed, constant frequency systems, including systems which are indirectly connected to the a.c. network, for example through the use of power electronic converters.

Wind energy conversion systems can be connected to the utility network in synchronous [4, 6], or in asynchronous connection [5, 7-12]. Each system has its own advantages and disadvantages which have been discussed extensively in the literature [23-26]. If the generator is connected directly to the utility network then some form of synchronisation is needed. A mechanical gear box is required with the wind-turbine to adjust the rotor speed to maintain the generator speed constant with changing wind-velocities. This mechanical control is relatively expensive compared with the alternative of a variable speed generator connected through power electronic devices to the utility network. However the integration of power electronics within a wind energy conversion system does have its disadvantages. Amongst these are greater complexity of control and control circuitry, and more importantly the difficulty in obtaining highly rated power devices with sufficient switching capability. The demand of both constant voltage and frequency in a power source is crucial in matching it to the utility network, since the latter has itself these constraints. The energy extracted from a variable-speed power generator with the use of solid-state devices, is generated with very much higher efficiency than that from constant speed power generators. Several different techniques have been proposed to obtain steady 50 Hz power from

a.c. generators driven by a variable-speed wind or tidal turbine [4-12, 18], and they are discussed later.

The use of an induction generator with a variable speed turbine is useful to some extent for low power applications, because of the cheapness of the system as whole, and the cessation of generation if the utility fails, thus making line repair elsewhere on the grid safe [24]. In general, induction generators suffer from a poor power-factor and low efficiency, typically in the order of 80% [37]. In wind-energy applications, the induction generator acts as a motor if the wind speed drops below a certain prescribed limit, which is clearly a disadvantage of this machine. Furthermore it can cause disturbances to the power-factor angle within the line. For example a self-excited induction generator has been used by Arrillaga and Watson [5], but it has poor characteristics for high power demands due to the need of a large capacitor bank at the output of the generator to produce the excitation. The rectifier used in this scheme was a 3-phase line commutated 6-pulse controlled rectifier, and required high power semiconductors to carry the large currents generated by the capacitors used for excitation. In an alternative scheme Sato and Umida [8] used a squirrel-cage induction generator with a 6-pulse forced commutated a.c./d.c. converter (normal thyristors with commutation circuits), connected to a PWM d.c. chopper circuit and a line-commutated inverter. This system has good characteristics compared with the previous system [5], but has the disadvantage of low efficiency as a whole, (since an induction machine was used with maximum efficiency stated as 75 %), and a high harmonic content in the line current. Furthermore the inverter connected to the utility network was conventional in that it would draw a lagging power-factor. Another disadvantage of this

converter system, is that the d.c. inductor and the chopper components must be very large to handle the high powers.

Induction generators are used also in static Kramer system [32], where the speed of the induction generator is controlled through slip energy recovery. The recovered slip power is fed back to the stator of the generator through a rectifier and a line commutated inverter. An alternative system called the Scherbius system, uses a silicon controlled rectifier instead of the diode rectifier in the static Kramer system. Both systems have the disadvantage of discontinuous operation at synchronous speed because of low slip voltage at this speed. The other disadvantage is the need for a high power rating of the semiconductor devices, which need to deal with high rotor voltages at high speeds and high currents at low speeds. A more complex system proposed by Holmes and Elsonbaty [33] used a Cycloconverter with doubly fed induction generator overcome some of these difficulties. However like before, this system has the disadvantage that it could not operate at synchronous speed and had low efficiency at high negative slip.

The alternative to induction generation schemes is to use synchronous generators. Synchronous generators have a higher efficiency of about 95% than their induction counterparts, and are normally used for power generation from constant speed turbines such as in hydrostations. Synchronous generators have the ability to control the reactive power supplied to their loads simply by means of adjustment of their field current. The induction generator does not have this capability and also needs additional power-factor improvement [7, 10, 11]. The major disadvantage of synchronous generators is that they run in synchronism with the prime mover

on their shaft. A wind turbine, for example attached to a synchronous generator would cause large variations in load angle and current if directly connected. There is thus a need for some external control in order to maintain a stable load voltage and current. Modern power electronic devices and recent advances in digital control electronics make these schemes more realisable. These advances have led to more compact less complex power electronic circuits and a higher efficiency at reduced cost. The efficiency, power handling capability, and lower speed operation with increased number of poles makes synchronous machines very attractive.

Interest in permanent magnet machines for drive systems was almost non-existent twenty years ago [14]. Recently much work has been carried out by scientists to develop new permanent magnet materials, and researchers in the field of machine design have similarly developed new permanent magnet machines [13-17]. The PM-synchronous generator has a constant field excitation fixed by the power of the permanent magnet in the rotor. High power, efficient generators can be realised with well designed rotors which make full use of the magnet stored energy. Many types of permanent magnets are used in the design of PM-synchronous machines such as $SmCo_5$, NdFeB and (Ceramic-8) Ferrite [13-16]. A PM-synchronous generator of a particular a.c. power can be smaller than a wound rotor synchronous generator of the same power and can have a very high power to volume ratio. The excitation field windings are replaced by permanent magnets and consequently, there is no need for slip rings, brushes, or rotor windings. As a result there is minimal rotor loss and its cooling is unnecessary. A machine with this specification is a largely maintenance free machine. In general permanent-magnet synchronous generators are more

reliable, robust and efficient compared with wound rotor synchronous generators. The increased number of poles of the generator is useful in wind-power systems since the generator can be directly coupled to the turbine rotor without a gear box. Turbines with low cut-in speeds can be used. Therefore, more useful energy is produced in the vast majority of applications than one matched to high wind speeds. This is especially important at low wind speeds in the summer.

The disadvantage of PM-synchronous generators is the constant field excitation which lead to inherent voltage regulation, which cannot be corrected easily like the wound rotor synchronous generators. The output voltage can only be controlled by an external power conditioner, which effectively acts as a variable power factor load to supply VAR power to adjust the armature reaction flux. This can be achieved by connecting the output of the PM-synchronous generator to an a.c./d.c. forced commutated converter working at leading power-factor, as is proposed in this research. The work in this thesis is based upon an 8-pole multistacked permanent-magnet synchronous generator which has been previously used in windmill power systems [13]. The type of magnet in the rotor is a Ceramic-8 Ferrite. This machine is also used in the present work using a PWM, GTO converter as a power conditioner.

A number of topologies of power electronic converters have been used in alternative energy conversion schemes. Conventional thyristor phase controlled rectifiers are extensively used in a.c. to d.c. rectification and inversion because they require no special means for commutation and are easily controlled. These converters have an inherent short coming in that the

power factor decreases as the phase control angle increases, and that lower frequency harmonics of the current drawn from a.c. line are relatively large. However with most classes of 3-phase fully-controlled static power converter, small improvements of power factor and a reduction in line current harmonics can be achieved [43-66]. For example, the performance of the power converter can be improved by adding two auxiliary thyristors to the conventional six-pulse bridge as proposed by Stefanovic [44]. These thyristors are connected between the d.c. rails supply and have the function of reducing the conduction period of each phase by returning current through the neutral wire. However, although this method results in some improvement in the power-factor, and reduced harmonics on the d.c. side, it has the disadvantage of increasing the harmonic content on the a.c. side, in addition to complex firing control and the expense of the auxiliary thyristors. In an alternative scheme modified gate signals were used by Dewan and Dunford [45] with a conventional converter. The system employs a flywheeling action through the power bridge; though it has limited operation as regards the delay angle $\alpha$ in that it operates like a conventional six-pulse converter for $\alpha$ between 0° and 60°, flywheeling operation being between 60° and 90°. Further more the gating signals are more complex in the inversion mode.

In the majority of the converter topologies [43-66] the energy transfer is controlled by varying the phase angle. The use of switch mode techniques and step-up choppers, in the d.c. link can result in improvements in the energy transmission from a system of both variable voltage and frequency to a system of both constant voltage and frequency (i.e.a utility a.c. network) [67-70]. Koczara and Michalski [70] used a step-up chopper in the d.c. link between a rectifier and a six-pulse power converter. In this case the proposed

system consisted of a synchronous generator connected to a 3-phase full-wave bridge rectifier and fed through a step-up chopper circuit to a converter (working with a.c. line commutation), which is operated at a constant phase angle. The step-up chopper used in the d.c. link between the rectifier and the converter decreases the converter reactive power (or in other words improves the power factor) on the a.c. side. However, the converter line current of the a.c. side connected to a utility network still has the same rectangular shape as the conventional six-pulse bridge converter (i.e.with a large line current harmonic content), and consequently requires the additional expense of smoothing reactors and capacitors in addition to the chopper. These type of converters however are becoming relatively less efficient, and require more space for the large, expensive capacitors and reactors, when compared with those using PWM techniques although this should be considered against the cost effectiveness of the line commutated thyristor circuits compared with the force commutated devices required in a PWM scheme.

With the introduction of fast-switching power devices such as IGBTs and GTOs, a pulse width modulation (PWM) control technique can be used for static fully-controlled 3-phase converters [71-87]. Some of the PWM techniques already use normal thyristors with auxiliary commutation circuits [71-74], while others use power transistors. However because of the limited current capability of high voltage IGBTs, and the additional base drive required of bipolar transistors, GTOs are in general preferred for medium to high power applications.

Many PWM control techniques [75-87] have been used in a fully-controlled 3-phase bridge converters and have resulted in an improved

power factor with the capability of a variable d.c. voltage with constant delay angle. The use of PWM control can also reduce the line current harmonics, and hence less filtering is necessary on both a.c. and d.c. sides of the converter. Different pulse-width modulation strategies are possible with such converters [80-87]. No single modulation strategy can, however provide optimum performance for the source and the output. In the presented work, the input and output performance of a 3-phase a.c./d.c. fully controlled converter is improved by using a sinusoidal pulse-width modulation (SPWM) technique. Variable input power-factor with full regulation of the output d.c. voltage is achieved. The converter is a current source type, providing a flywheeling action through the main bridge, and maintains a constant d.c. current and a sinusoidal input current. Consequently the line current harmonics are reduced, resulting in a substantial reduction of the reactive power compensation and filter requirements on the a.c. and d.c. sides. An optimised modulation strategy is used to reduce the harmonic content to a very low value. The PWM, GTO converter is designed to work at leading and lagging power-factor, which makes it suitable for use with a PM-synchronous generator.

The GTO converter with the 8-pole permanent magnet generator forms an energy conversion scheme suitable for wind energy conversion. The output from the PM-synchronous generator is converted to d.c. power which can be used for charging a battery or for heating applications, if the system is of the stand alone type. If the system needs to be connected to the a.c. network, a second converter can be used, working in the inversion mode. Such a conversion scheme can have the ability to convert the power in both directions, as would be required by tidal power generation schemes. The

benefits of using the proposed PWM, GTO converter with the PM-synchronous generator are a reduction in the harmonic losses in the generator and the ability to run the generator at any power factor. Optimum characteristics of high power and high efficiency can be achieved from the system by running the generator at leading power-factor. Thus the disadvantage of inherent voltage regulation in the PM-synchronous generator is overcome.

Since the output power from a wind-turbine is strongly affected by wind speed, the controller of the GTO converter is designed to match a high range of shaft speeds from 250 rpm up to 1000 rpm. This wide range of speed is controlled by using a phase locked loop (PLL) circuit. The controller is also programmed to control the output power of the permanent magnet generator, so that, the generator can deliver maximum power per $I^2R$ loss at all speeds and at any load current. Thus, at any speed the PM-generator delivers power at its maximum efficiency. Therefore, the generator will follow all wind speed changes converting all the available mechanical power to electrical power. In this mode of operation a system efficiency over 88% is achieved.

*CHAPTER TWO*

# THE PERMANENT-MAGNET SYNCHRONOUS GENERATOR, MODEL AND PERFORMANCE CHARACTERISTICS

## 2.1 INTRODUCTION

The permanent magnet (PM) synchronous machine used in this project has an 8-pole multistacked imbricated rotor of the type described in references [15, 17] and is shown in fig.(2-1a). In this particular machine Ferrite Ceramic-8 magnets are used. The stator of this machine is that of a conventional induction motor as shown in fig.(2-1b), and has a 3-phase, double layer distributed winding. The machine dimensions are presented in Table (2-1).

The rotor has five axially magnetised discs which are arranged together with steel discs along the rotor axis with like poles facing one another. The steel discs are placed between the permanent magnet discs to separate them and to form an iron path, which guides the flux radially to pole shoes as shown in fig.(2-2) [22]. Fig.(2-2a) shows the three components of the rotor separately for clarity. They are assembled to the permanent magnet discs in such a way to provide a field of alternate north and south poles around the periphery as shown in fig.(2-2b). The unusual design of the rotor is such that the flux density on the pole face is higher than that on the magnet surface. Thus, the axial magnet configuration is designed such that the ratio of total surface area of the magnet to the total rotor surface area exceeds unity. This ratio is higher than other traditional designs of permanent magnet machine, and produces a machine with a higher power density. This rotor design has been optimised through the use of a 3-dimensional finite-element analysis [TOSCA] described by Low [22].

The rotor shown in fig.(2-2b) may be expected to have some saliency due to its geometry. The permanent magnet machine can be assumed to

behave like a conventional salient pole machine as shown in the phasor diagram of fig.(2-3b), but with fixed field current. Therefore the synchronous reactance is divided into two components, direct and quadrature-axis reactances, $X_d$ and $X_q$, and similarly the armature current $I_a$ has been resolved into its direct and quadrature components, $I_d$ and $I_q$ respectively. The synchronous reactances of the present PM-generator, $X_d$ and $X_q$ have been determined experimentally, as shown later in fig.(2-7), and were found to be nearly equal. This agrees with previous work completed on this generator by Low [17]. Hence, the PM-generator is assumed for simplicity to have a cylindrical rotor rather than a salient pole. The equivalent theoretical model presented for the generator similarly assumes a cylindrical rotor, an assumption which is confirmed experimentally by the generator performance. The other parameters of the generator equivalent circuit have been determined experimentally using the methods described below and are as shown in table(2-2).

## 2.2 DETERMINATION OF THE EQUIVALENT CIRCUIT PARAMETERS:

The permanent magnet generator parameters were measured initially for a salient pole rotor. In the tests current and voltage harmonics are assumed to be negligible. The generator is further assumed to supply a balanced three-phase load. Fig.(2-3) represents the equivalent circuit per-phase of the PM-generator, which is derived from the standard model of the synchronous machine. This model combines both the rotor and stator parameters. The rotor parameters are modelled by the induced emf $E_o$ caused by permanent magnet field, and a synchronous reactance $X_s$. The synchronous reactance value includes the leakage reactance $X_l$, which models

the stator leakage flux. The stator winding resistance is represented by $R_a$. The core loss has been neglected at the moment, and but reconsidered later when analysing the maximum power transfer of the generator and the optimal power-factor angle at which this occurs.

### 2.2.1 Measurement of the induced emf:

The PM-synchronous generator is driven by a d.c. motor at different speeds, from a very low speed 50 rpm up to a suitable maximum value 1500 rpm. The general experimental circuit diagram including this test is shown in fig.(2-4). This generator has an 8-pole rotor, thus its synchronous speed is 750 rpm. The permanent magnet excitation is found from the open circuit induced voltage which varies linearly with the generator frequency. The set of readings of the open circuit terminal line voltage $V_{ll}$ are given as a function of speed in fig.(2-5). A linear relationship can be seen from the graph showing no pronounced drop in voltage at higher speeds due to iron loss effects. The induced emf $E_o$ per phase is represented by the line shown in fig.(2-5), which is equal to the line terminal voltage $V_{ll}$ divided by $\sqrt{3}$.

The emf voltage $E_o$ is used in the calculation of the parameters of the PM-generator and its characteristics. A constant value is assumed for $E_o$ at any specified speed of the PM-synchronous generator, under all load conditions.

### 2.2.2 Measurement of the direct and quadrature axis synchronous reactances:

The PM-synchronous generator is different from conventional synchronous generators, since it has a special condition of constant field excitation caused by the permanent magnet in the rotor. The experimental tests used to measure $X_d$ and $X_q$ therefore need to be modified from the conventional synchronous generator methods.

#### 2.2.2a Measurement of direct-axis synchronous reactance:

A zero power-factor test is employed to test the generator at two conditions, zero power-factor leading and zero power-factor lagging. In this type of measurement the direct axis value of synchronous reactance $X_d$ is calculated [36-42], whether the generator is a cylindrical rotor or a salient-pole machine.

In this test, the zero power factor currents give rise to armature reaction which acts in the direct polar axis in space, and causes either magnetisation (at zero power-factor leading) or demagnetisation (at zero power-factor lagging) as shown in fig.(2-6). The equivalent circuit of one phase of the PM-synchronous generator for leading power-factor operation is shown in fig.(2-6a). Similarly fig.(2-6b) shows the phasor diagram representing zero power-factor lagging. The quadrature component of the armature current is negligible, therefore the effect of $X_q I_q$ will be considered equal to zero. The voltage equation of the PM-synchronous generator represented by the circuit model shown in fig.(2-6a) is given in vector form as:

$$\vec{E_o} - \vec{V_{tp}} = \vec{I_a}(R_a + jX_d) \qquad (2.1)$$

Since an inductive load is connected to the generator, the stator current $I_a$ will lag the terminal voltage $V_{tp}$ by approximately 90°. Referring to fig.(2-6b), it can be seen that the $I_aR_a$ drop is small and in phase quadrature with $V_{tp}$, and therefore the voltage drop across the direct axis-synchronous reactance $X_d$ is in phase with the induced voltage $E_o$. It follows then, that the synchronous reactance at zero power-factor lagging can be found from the line values, $E_{ol}$, $V_{tl}$, and $I_a$ by:

$$X_d = \frac{E_{ol} - V_{tl}}{\sqrt{3}\, I_a} \tag{2.2}$$

At zero power-factor leading, shown in fig.(2-6c), a similar effect appears, but the voltage equation, after neglecting the resistance effect is

$$E_{tp} - V_o = X_d I_a \tag{2.3}$$

and therefore,

$$X_d = \frac{V_{tl} - E_{ol}}{\sqrt{3}\, I_a} \tag{2.4}$$

To determine the synchronous reactance $X_d$ experimentally it is a matter of running the PM-machine as a generator, and connecting a variable three-phase balanced, purely inductive load (zero power-factor lagging) to its terminals. The load inductance is varied for different values of current keeping the generator speed constant. Then, the load is replaced by a variable three-phase balanced, purely capacitive load (zero power-factor leading), and a second set of readings are recorded, again keeping the generator speed constant. This test was repeated for different speeds, and

an example of the results are plotted in fig.(2-7). From this figure it can be determined that, the direct-axis synchronous reactance $X_d$ may be assumed to be constant at a given speed. As expected the value was found to vary linearly with frequency, and varies little over a wide range of stator current.

**2.2.2b Measurement of quadrature-axis synchronous reactance:**

The PM-synchronous generator delivers maximum power for a given current and speed at a leading power-factor. The phasor diagram which represents this condition is shown in fig.(2-8). Where it can be seen that the maximum power delivered from the generator to the load occurs when $I_a$ is in phase with ( $E_o$ ), i.e. $I_a$ lies in the quadrature axis and the direct component of the armature current is zero. Therefore at this condition the synchronous reactance is equal to the quadrature-axis synchronous component $X_q$. If the power factor angle $\phi_{opt}$ at which the output power is maximum can be determined, then from the phasor diagram,

$$V_{tp} \sin(\phi_{opt}) = I_a X_q \tag{2.5}$$

Rearranging equation (2.5) and substituting line values results in:

$$X_q = \frac{V_{tl} \sin(\phi_{opt})}{\sqrt{3}\, I_a} \tag{2.6}$$

The experimental values obtained using this method are also plotted in fig.(2-7). From this figure it is obvious that $X_q$ and $X_d$ are approximately equal over a wide range of load current, indicating that this machine behaves in its operation much like a cylindrical rotor generator. While, the synchronous reactances $X_q$ and $X_d$ have been calculated using these methods,

there are alternate methods available [17, 42], using d.c. inductance bridge techniques or finite element methods [103] which are beyond the scope of the present discussion.

### 2.2.3 RESISTANCE MEASUREMENT OF THE STATOR WINDING :

Copper loss in electrical machines is caused by the ohmic resistance of the stator windings. The resistance of the stator winding of the 8-pole permanent magnet synchronous generator was measured by applying a d.c. voltage across two phases of the stator winding leaving the third phase open circuited as shown in fig.(2-9). Then, the resistance per phase $R_a$ is equal to the reading of voltmeter divided by ( $2I_a$ ). This resistance was found to be equal to 1.26Ω per phase. This value is increased by 20% to account for skin effect, and the temperature increase, giving $R_a = 1.52\Omega$.

### 2.2.4 LEAKAGE REACTANCE MEASUREMENT:

The leakage reactance ( $X_l$ ) is an important factor in the design and construction of the machine. It is defined as the leakage flux due to the slots, the end of the winding, and the harmonic leakage [104]. The analysis of the leakage reactance is beyond the scope of this work, but a value of $X_l$ has been determined to give a complete model of the generator. The phasor diagram representing the PM-synchronous generator at leading power-factor is redrawn in fig.(2-10). Hence the air gap voltage per phase $V_{gp}$ is derived from this figure as,

$$V_{gp} = \sqrt{(V_{tp} \sin \phi - X_l I_a)^2 + (V_{tp} \cos \phi - R_a I_a)^2} \qquad (2.7)$$

The measured values of $V_{tp}$, $\phi$, $R_a$ , and $I_a$ have been substituted into this equation and a graph is plotted for $V_{gp}$ versus $V_{tp}$ as shown in fig.(2-11). This graph is plotted for constant value of stator current (6.15 Amp), constant frequency, but variable power-factor. A computer program was written based on equation (2.7) to find the best value of ( $X_l$ ), which would give a linear relationship between air gap voltage and the terminal phase voltage. A linear relationship is obtained when $X_l$ is approximately equal to (0.5 Ω) as shown in fig.(2-11). These conditions have been realised experimentally. Thus, if $X_l$ is reduced to zero the line will lose its linearity and bend downward as shown in fig.(2-11). Similarly, the line will bend upward when $X_l$ is increased to more than (0.5 Ω) as shown in the same figure. A similar value of $X_l$ (0.5 Ω) was calculated previously from the measurement of the machine dimensions by Low[17].

## 2.3 ANALYSIS OF THE EQUIVALENT CIRCUIT OF THE 8-POLE PM-SYNCHRONOUS GENERATOR:

As mentioned previously it is sufficient to model the permanent magnet generator using a cylindrical rotor equivalent circuit. The average of the measured values of $X_d$ and $X_q$ found from above where used for the single value of synchronous reactance ( $X_s$ ). Any variation in $X_s$ due to changing saturation conditions in the machine is negligible. It will be seen later that the theoretical model based upon these assumptions is supported by experimental results. At this stage the effect of core loss is neglected and the leakage reactance is included in the synchronous reactance value.

The equivalent phasor diagrams of the machine at leading and lagging power-factors are shown in figs.(2-12a and 2-12b) respectively. From the phasor diagram at leading power-factor, the induced emf voltage $E_o$ is given by,

$$E_o^{\,2} = (V_{tp}\cos\phi + I_a R_a)^2 + (V_{tp}\sin\phi - I_a X_s)^2 \qquad (2.8)$$

Rearranging this equation results in

$$V_{tp}^{\,2} + 2V_{tp}I_a(R_a\cos\phi - X_s\sin\phi) + I_a^{\,2}(R_a^{\,2} + X_s^{\,2}) - E_o^{\,2} = 0 \qquad (2.9)$$

The second order equation (2.9) is solved and the output voltage $V_{tp}$ is found to be,

$$V_{tp} = I_a\left[\sqrt{\left(\frac{E_o}{I_a}\right)^2 - (R_a\sin\phi + X_s\cos\phi)^2} - R_a\cos\phi - X_s\sin\phi\right] \qquad (2.10)$$

The corresponding line voltage $V_{tl}$ is then,

$$V_{tl} = \sqrt{3}\,I_a\left[\sqrt{\left(\frac{E_o}{I_a}\right)^2 - (R_a\sin\phi + X_s\cos\phi)^2} - R_a\cos\phi - X_s\sin\phi\right] \qquad (2.11)$$

The total output power $P_o$ of the generator is given by,

$$P_o = 3V_{tp}I_a\cos\phi \qquad (2.12)$$

Using equation (2.11) the output power of the generator can be written as a function of stator current and power-factor angle as:

$$P_o = 3I_a^{\,2}\left[\sqrt{\left(\frac{E_o}{I_a}\right)^2 - (R_a\sin\phi + X_s\cos\phi)^2} - R_a\cos\phi - X_s\sin\phi\right]\cos\phi$$

(2.13)

At a given rotor speed the induced emf voltage $E_o$ of the generator is assumed to be constant, and $R_a$ and $X_s$ are also constant. The only variables in equations (2.11) and (2.13) are the stator current $I_a$ and power-factor angle $\phi$ . The voltage and power characteristics given by equations (2.11) and (2.13) respectively are discussed in section (2.5) where they are compared against load tests on the machine.

## 2.4 CORE LOSS REPRESENTATION:

The core loss is defined as the sum of the hysteresis losses, and the eddy current losses in the magnetic material. This power loss is dependent on the frequency of the machine, the voltage induced in the armature, and other factors related to the properties of the magnetic material. The core loss ($P_{closs}$) of the synchronous generator is assumed to be also proportional to the square of the air gap flux [37], and thus

$$P_{closs} \propto (V_{gp})^2 \tag{2.14}$$

Where $V_{gp}$ is the voltage caused by the resultant air gap flux. This voltage can be found from equation (2.7) given in section (2.2.4), given a knowledge of the leakage reactance.

The core loss $P_{closs}$ of the 8-pole PM-synchronous generator is determined experimentally by subtracting all the output power, the friction and windage loss and the copper loss from the measured input shaft power, and is illustrated by the following formula,

$$P_{closs} = P_{in} - P_{ot} - P_{wf} - 3I_a{}^2 R_a \tag{2.15}$$

Where,

$P_{in}$ is the input power of the prime mover on the shaft to the generator including friction and windage loss.

$P_{ot}$ is the total output power of the generator measured by the two wattmeter method.

$P_{wf}$ is the windage and friction loss of the PM-synchronous generator alone.

Experimentally the core loss, and the windage and friction loss of the generator are normally measured together. Therefore equation (2.15) becomes:

$$(P_{closs} + P_{wf}) = P_{in} - P_{ot} - 3I_a^2 R_a \qquad (2.16)$$

A series of load tests were performed on the machine. In each the stator current and speed kept constant, and the load is changed to give the power-factor angles from -90° lagging to 90° leading. The test was repeated for five different values of stator current and the results are plotted in fig.(2-13). In this figure, the core loss is plotted as a function of the square of the normalised air gap voltage, which is obtained by the division of the air gap voltage found from equation (2.7) by the induced emf $E_o$. A straight line is obtained which confirms that the core loss is proportional to the square of induced voltage in the air gap. The friction and windage losses $P_{wf}$ can be separated from the core loss by the intersection of the line graph with the y-axis, where the voltage and therefore the core loss is zero. The friction and windage loss was found to be equal to 30 watt at a speed of 750 rpm.

The core loss is represented theoretically by a shunt resistor $R_c$ in the equivalent circuit as shown in fig.(2-20). This resistance is found experimentally from the slope (m) of the core loss graph given in fig.(2-13), where,

$$m = \tan \Psi = \frac{P_{closs}}{(\frac{V_{gp}}{E_o})^2} \tag{2.17}$$

Rearranging this equation results in

$$\frac{(E_o)^2}{m} = \frac{(V_{gp})^2}{P_{closs}} \tag{2.18}$$

Since the core loss $P_{closs}$ is equal to $(\frac{(V_{gp})^2}{R_c})$ , then from eqn.(2.18)

$$R_c = \frac{(V_{gp})^2}{P_{closs}} = \frac{(E_o)^2}{m} \tag{2.19}$$

The parameters of the experimental line shown in fig.(2-13), obtained at a speed of 750 rpm (50 Hz) are

$$P_{closs} = 31.645(\frac{V_{gp}}{E_o})^2 + 30 \qquad (Watts) \tag{2.20}$$

The constant 30 watts represents the windage and friction loss $P_{wf}$ of the PM-synchronous machine at (750 rpm). At 50 Hz the induced emf $E_o$ is equal to $(\frac{176}{\sqrt{3}})$, then referring to eqns.(2.19 and 2.20), the core loss resistance is determined as

$$R_c = \frac{(\frac{176}{\sqrt{3}})^2}{31.645} = 326 \qquad Ohm$$

This result is used to determine the generator performance at maximum power transfer.

## 2.5 OUTPUT VOLTAGE AND POWER CHARACTERISTICS:

The measured line voltage and output power characteristics of the generator are shown in figures (2-14) and (2-15) respectively. The results are presented at a rotor speed of 750 rpm, which gives a stator frequency of 50 Hz, and at various constant armature currents. The corresponding characteristics obtained from the equivalent circuit analysis of section (2.3) are also plotted in the figures.

The variation of the voltage $V_{tl}$ with respect to power-factor angle $\phi$ is given in fig.(2-14). The rise of the terminal voltage with increasing leading power-factor angle is due to the effect of the armature reaction which tends to aid the rotor flux in the air gap at leading power-factor angle $\phi$, and opposes the rotor flux at lagging power-factor. The measured values of $V_{tl}$ are in the main coincident with the predicted values, calculated by eqn.(2.11). However the measured values of the voltage curve when the stator current is 6.15 Amp, are shifted slightly from the predicted values. This is because in the experimental test it was difficult to keep the stator current constant (6.15 Amp) at the maximum value and a small variation occurred in the test currents.

Figure (2-15) plots the output power $P_o$ of the PM-synchronous generator at constant stator current and variable power-factor angle $\phi$ from -90° lagging to 90° leading. Here the predicted values were obtained using equation (2-13). The output power $(P_o)_{max}$ delivered from the generator is a maximum at a leading power-factor. The maximum output power point $(P_o)_{max}$ moves to the right from unity power-factor towards leading power-factor as the stator current increases.

The PM-synchronous generator was also tested at different frequencies to ensure the accuracy of the mathematical model presented. Results for the generator running at 30 Hz are plotted in fig.(2-16) to show the voltage curves versus power-factor angle. Similarly fig.(2-17) shows the relationship of the output power to the power-factor angle at this frequency. Again as would be expected the maximum power points occur at leading power-factor. A good comparison was obtained between the measured and predicted results.

Furthermore the generator was tested at constant speed, measuring its output power as a function of the stator current, for different constant values of power-factor. These results are shown in fig.(2-18).

The induced stator voltage was observed not to be a pure sinusoidal waveform because of the effect of the tooth ripple. Tooth ripple is caused by the slots between the stator teeth which encompass the stator coils. These slots causes variations in field path reluctance and so induce ripples on the machine emf waveforms. There are methods of reducing these ripples, such as skewing the stator slots or the rotor magnets, increasing the air gap length

and using narrow slots. The experimental waveforms of both stator voltage and current at different power-factor angles are shown in fig.(2-19). It is clear that the voltage at leading power-factor is more sinusoidal than the others in the figure because of the filtering action of the load capacitor.

## 2.6 THEVENIN'S EQUIVALENT CIRCUIT OF PM-GENERATOR WHICH INCLUDES CORE LOSS:

Core loss is normally represented by a shunt resistor $R_c$ connected across the induced voltage in the air gap as shown in the equivalent circuit diagram in fig.(2-20). To ease the analysis the equivalent circuit can be reduced to the simpler Thevenin circuit shown in fig.(2-20b). This Thevenin equivalent circuit has been considered mainly to obtain an accurate model of the output power characteristics of the 8-pole machine, in particular to obtain the optimal power-factor angle $\phi_{opt}$ at which the output power is maximum. The Thevenin equivalent voltage source (TVS) shown in fig.(2-20b) is given by:

$$E'_o = \frac{R_c E_o}{R_c + jX_a} = \left| \frac{R_c E_o}{\sqrt{R_c^2 + X_a^2}} \right| \quad \angle \{ -\tan^{-1}(\frac{X_a}{R_c}) \} \tag{2.21}$$

where

$$X_a = X_s - X_l \tag{2.22}$$

The Thevenin impedance $Z'$ is then:

$$Z' = (R_a + jX_l) + \frac{R_c(jX_a)}{(R_c + jX_a)} \tag{2.23}$$

## 2.7 OPTIMAL POWER-FACTOR AND MAXIMUM POWER OF THE GENERATOR:

The PM-synchronous generator supply maximum power $(P_o)_{max}$ to the load certain factors when the angle $\phi$ between the terminal phase voltage $V_{tp}$ and the stator line current $I_a$ is at an optimal leading value. From the Thevenin equivalent circuit of the PM-synchronous generator shown in fig.(2-20b), and phasor diagram shown in fig.(2-21), it can be seen that the maximum power transfer occurs when the stator current $I_a$ is in phase with the Thevenin voltage source $E'_o$, (i.e. the power-factor angle between $E'_o$ and $I_a$ should be equal to zero deg.). Therefore at this condition the power-factor angle ($\phi$) is,

$$\phi_{opt} - \tan^{-1}\left(\frac{I_a X'}{E'_o - I_a R'}\right) \tag{2.24}$$

To find the optimal power-factor angle ($\phi_{opt}$) in terms of the original equivalent circuit parameters, $R_a, R_c, X_a$ , and $X_l$ , first the Thevenin impedance $Z'$ is expressed as:

$$Z' = R_a + jX_l + \frac{R_c jX_a(R_c - jX_a)}{R_c^{\,2} + X_a^{\,2}} \tag{2.25}$$

resolving into real and imaginary parts

$$Z' = \left(R_a + \frac{R_c X_a^{\,2}}{(R_c^{\,2} + X_a^{\,2})}\right) + j\left(X_l + \frac{R_c^{\,2} X_a}{(R_c^{\,2} + X_a^{\,2})}\right) \tag{2.26}$$

Equating the real part of eqn.(2.25) to R′, and the imaginary part to X′ results in,

$$R' = (R_a + \frac{R_c X_a^{\,2}}{(R_c^{\,2} + X_a^{\,2})}) \tag{2.27}$$

and

$$X' = (X_l + \frac{R_c^{\,2} X_a}{(R_c^{\,2} + X_a^{\,2})}) \tag{2.28}$$

Substituting the magnitude of the Thevenin voltage source ( TVS ) represented by eqn.(2.21), R′ and X′ into eqn.(2.24), results in

$$\phi_{opt} = \tan^{-1}\left[\frac{I_a\{X_l X_a^{\,2} + R_c^{\,2}(X_l + X_a)\}}{E_o\sqrt{(R_c^{\,4} + R_c^{\,2} X_a^{\,2})} - I_a\{R_a R_c^{\,2} + X_a^{\,2}(R_a + R_c)\}}\right] \tag{2.29}$$

Or alternatively the optimal power-factor angle ($\phi_{opt}$) can be written in terms of $\omega$ as

$$\phi_{opt} = \tan^{-1}\left[\frac{\omega I_a\{L_l(L_a\omega)^2 + R_c^{\,2}(L_l + L_a)\}}{E_o\sqrt{R_c^{\,4} + (R_c L_a\omega)^2} - I_a\{R_a R_c^{\,2} + (L_a\omega)^2(R_a + R_c)\}}\right] \tag{2.30}$$

The parameters in the above equation are the experimental values found previously and are listed in table(2-2).

The optimal power-factor angle is essentially independent of frequency as shown in fig.(2-22). It also has an approximately linear relationship with the stator current $I_a$. Equation (2.29) is supported experimentally as shown by the results plotted in fig.(2-23), where $\phi_{opt}$ is plotted against stator current. The solid line represents the theoretical optimal power-factor angle ($\phi_{opt}$), and the other points represent the experimental values obtained with a passive load connected to the generator.

Fig.(2.24) shows the maximum power $(P_{ot})_{max}$ transfer as function of stator current ( $I_a$ ) for 50 Hz at the optimal power-factor angle. $(P_{ot})_{max}$ can be seen to be directly proportional to ( $I_a$ ). Similar results were obtained at 30 Hz and 40 Hz.

The optimal angle $\phi_{opt}$ is almost constant for a wide speed range of 250-900 rpm of the PM-synchronous generator as shown in fig.(2-22). This represents good performance by the machine, since by keeping constant stator current $I_a$ and constant power-factor angle $\phi$ , maximum power $(P_{out})_{max}$ is achieved over this wide range of speed 250-900 rpm. This control will be carried out automatically by the power-factor controller of the proposed PWM, GTO converter and is discussed in chapter six.

## 2.8 GENERATOR EFFICIENCY:

Efficiency is a very important factor when assessing the cost and practical use of generators. The 8-pole PM-synchronous generator discussed here exhibits very high efficiency even though a low cost Ceramic-8 Ferrite permanent magnet material is used in the rotor. The generator is at its most efficient when operating at leading power-factors and high load currents.
The basic definition of generator efficiency is defined as the ratio of output power $P_{ot}$ to input power $P_{in}$ , i.e.:

$$\eta\% = \frac{P_{ot}}{P_{in}} \; x \; 100\% = \frac{P_{ot}}{P_{ot} + losses} \; x \; 100\% \qquad (2.31)$$

The output power can be measured by application of the well known two-wattmeter method between the machine phases. Input power measurement is simply a matter of calculating the torque speed product on the prime mover or generator shaft. Some of the mechanical power delivered to the shaft is lost to friction and windage ($P_{wf}$).

The machine electrical losses may be classified into two main types, stator winding loss which is load current dependent and magnetic core loss ( $P_{closs}$ ), which is mainly independent of load current. Stator winding loss is simply the ohmic loss due to the resistance of the stator windings ( $I_a^2 R_a$ ). The core loss is calculated from equation (2.20). The windage and friction loss at 50 Hz is included in this equation. The efficiency at 50 Hz can now be defined in a more precise manner as:

$$\eta\% = \frac{P_{ot}}{P_{ot} + 31.645\left(\frac{V_{gp}}{E_o}\right)^2 + 30 + 3I_a^2 R_a} \; x \; 100\% \qquad (2.32)$$

Hence we can compute the theoretical efficiency of the generator from equation (2.32) after calculating the air gap voltage from equation (2-7)in the previous sections. Fig.(2-25) shows the generator efficiency at 50 Hz for different values of stator current, and indicates the generator efficiency from zero power-factor lagging to zero power-factor leading. The deviation between the predicted and measured efficiency at high currents reaffirms the explanation given in section (2.5) on the clarification of the output characteristics. The PM-synchronous generator has similarly high efficiency at low frequencies. For example the experimental efficiency curves at 30 Hz are plotted as shown in fig.(2-26).

| Parameter | Value | Unit |
|---|---|---|
| Rotor diameter | 151 | mm |
| Rotor length excluding end plates | 151.5 | mm |
| Rotor length including end plates | 159.94 | mm |
| Number of stacked magnets in the rotor | 5 | discs |
| Rotor magnetic material Ferrite Ceramic-8 | | |
| Stator internal diameter | 152.7 | mm |
| Stator external diameter | 240.5 | mm |
| Stator length | 151.7 | mm |

**Table(2-1) Dimensions of the 8-pole PM machine.**

| Parameter | Value | Unit |
|---|---|---|
| Number of phases | 3 | phase |
| Number of poles | 8 | pole |
| Number of stator slots | 36 | slots |
| Stator/phase voltage | 101.6 | Volt |
| Stator/phase current | 4 | Amp |
| Stator/phase resistance $R_a$ | 1.5 | Ohm |
| Core loss resistance $R_c$ | 326 | Ohm |
| Synchronous reactance $X_s$ | 15 | Ohm |
| Leakage inductance $L_l$ | 1.6 | mH |
| Armature reaction inductance $L_a$ | 46 | mH |
| Synchronous inductance $L_s$ | 48 | mH |
| Synchronous speed $n$ | 750 | rpm |

**Table(2-2) PM machine parameters at 50 Hz.**

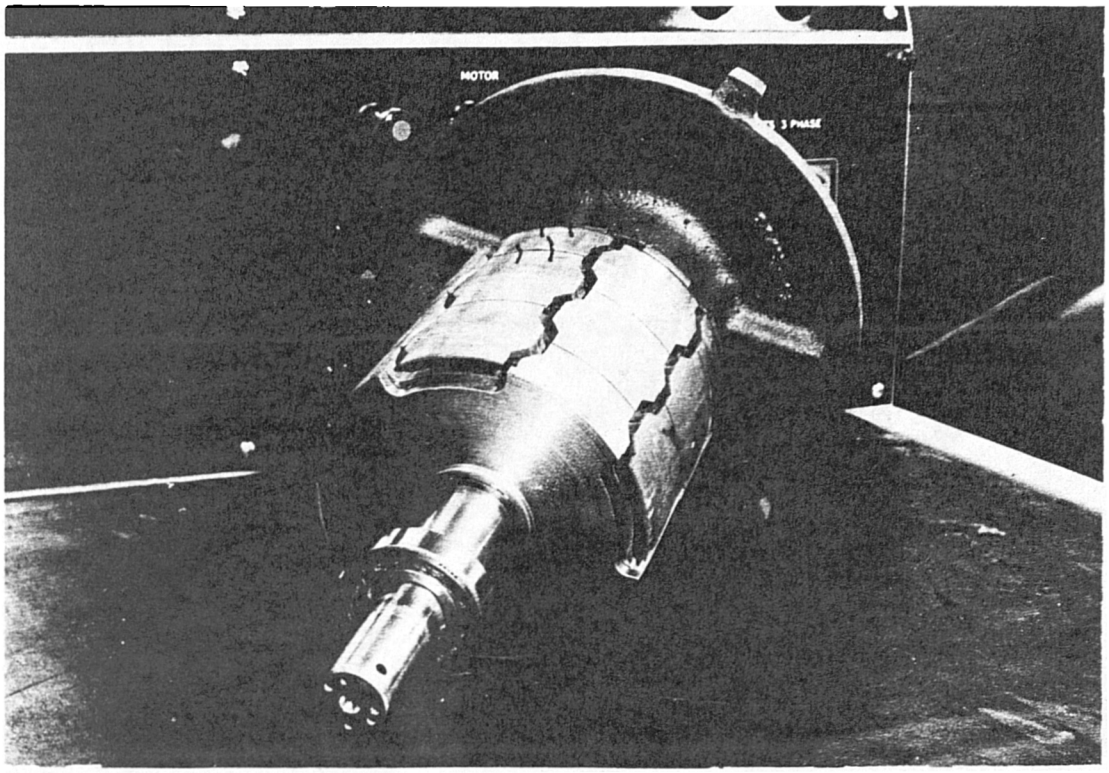


a- PM-Rotor.

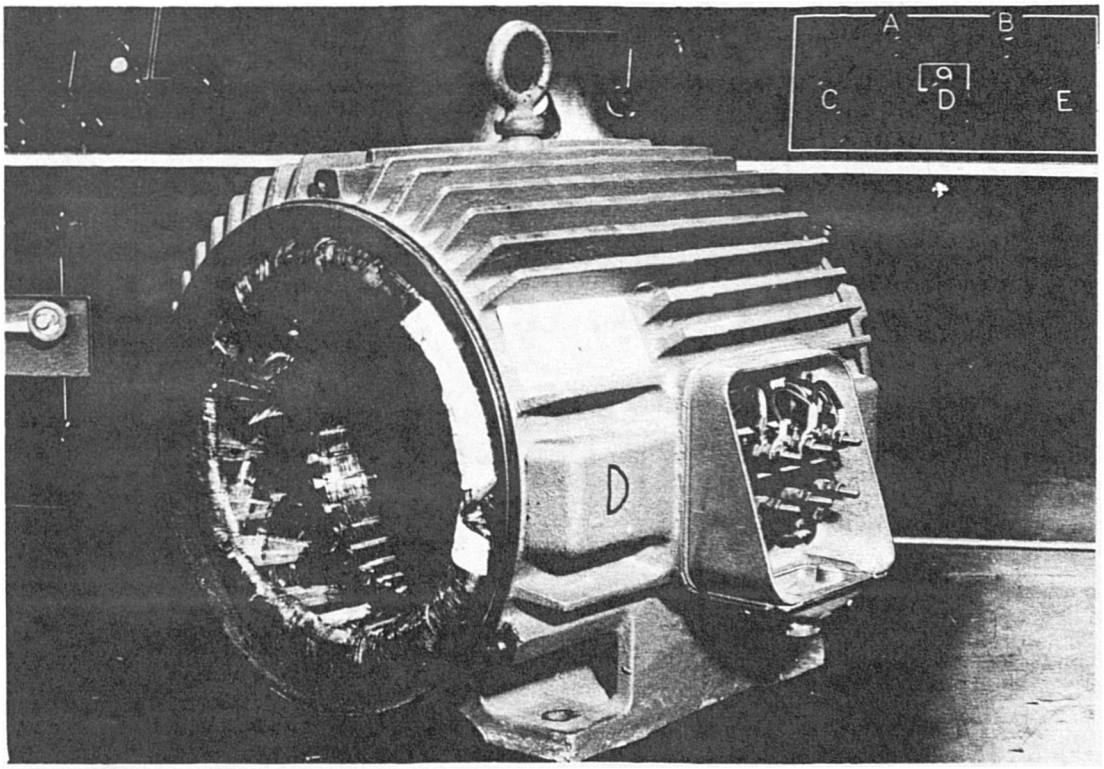


b- Conventional Stator.

Fig.(2-1) 8-Pole multistacked imbricated rotor PM-synchronous generator.

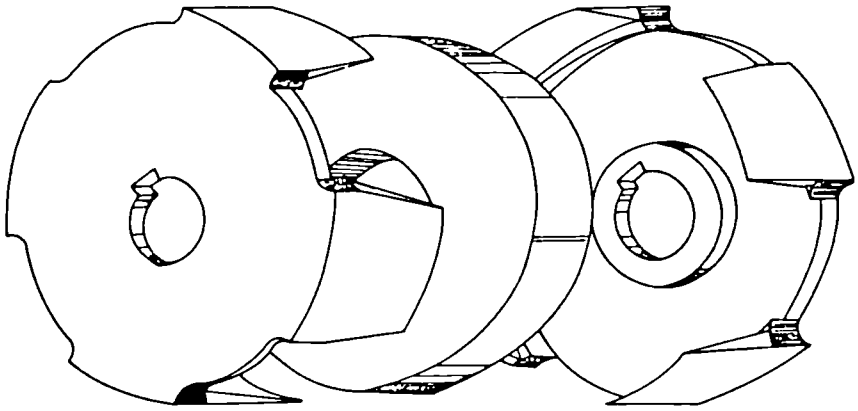

a- A rotor unit.

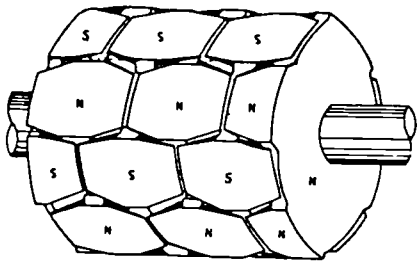


b- An assembled rotor.

Fig.(2-2) Permanent Magnet Rotor.

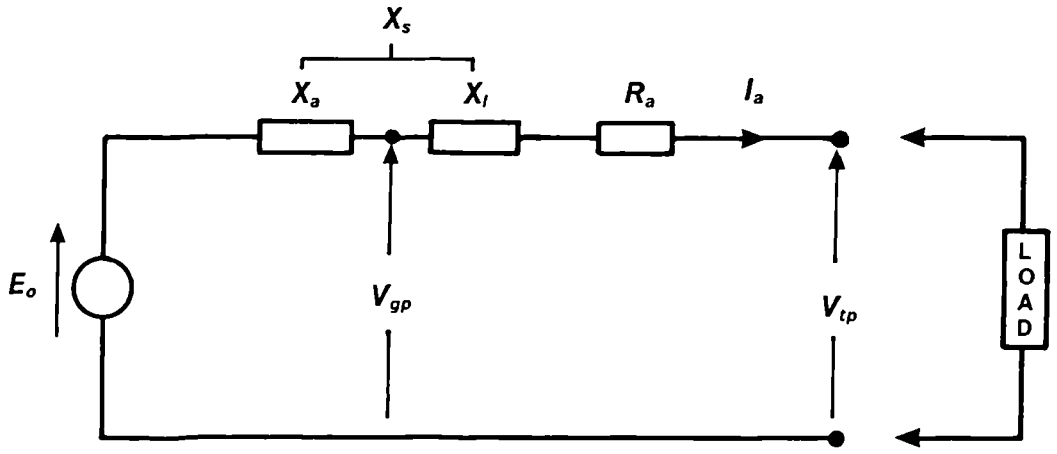


a- Equivalent circuit.

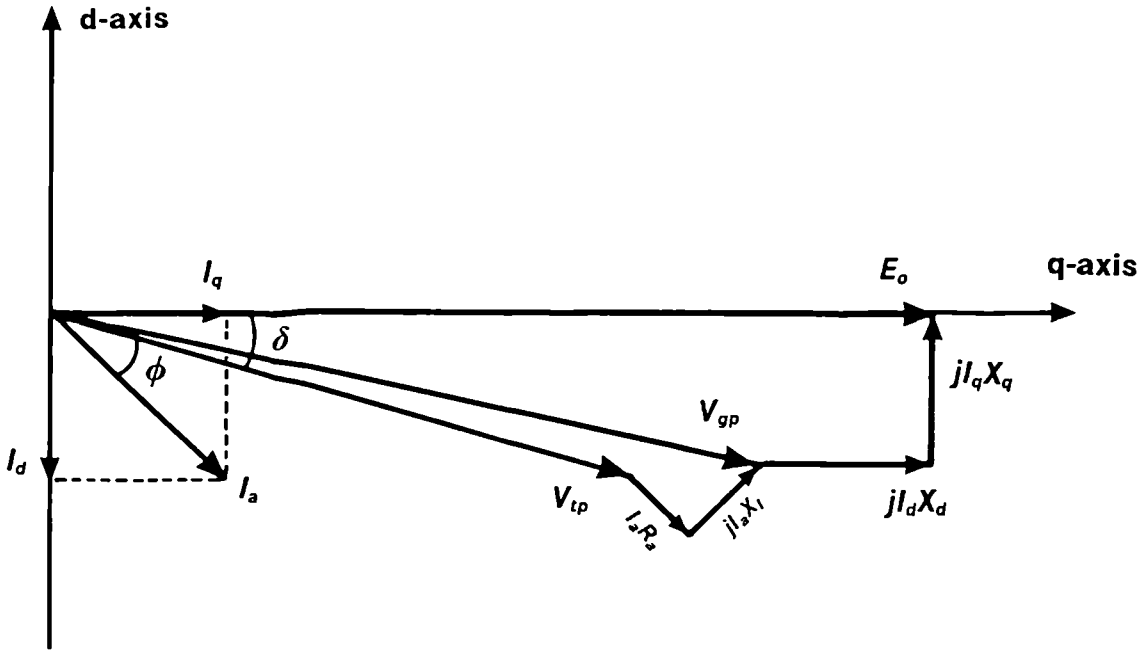


b- Phasor diagram for a salient pole machine.

Fig.(2-3) PM-generator equivalent circuit and phasor diagram.

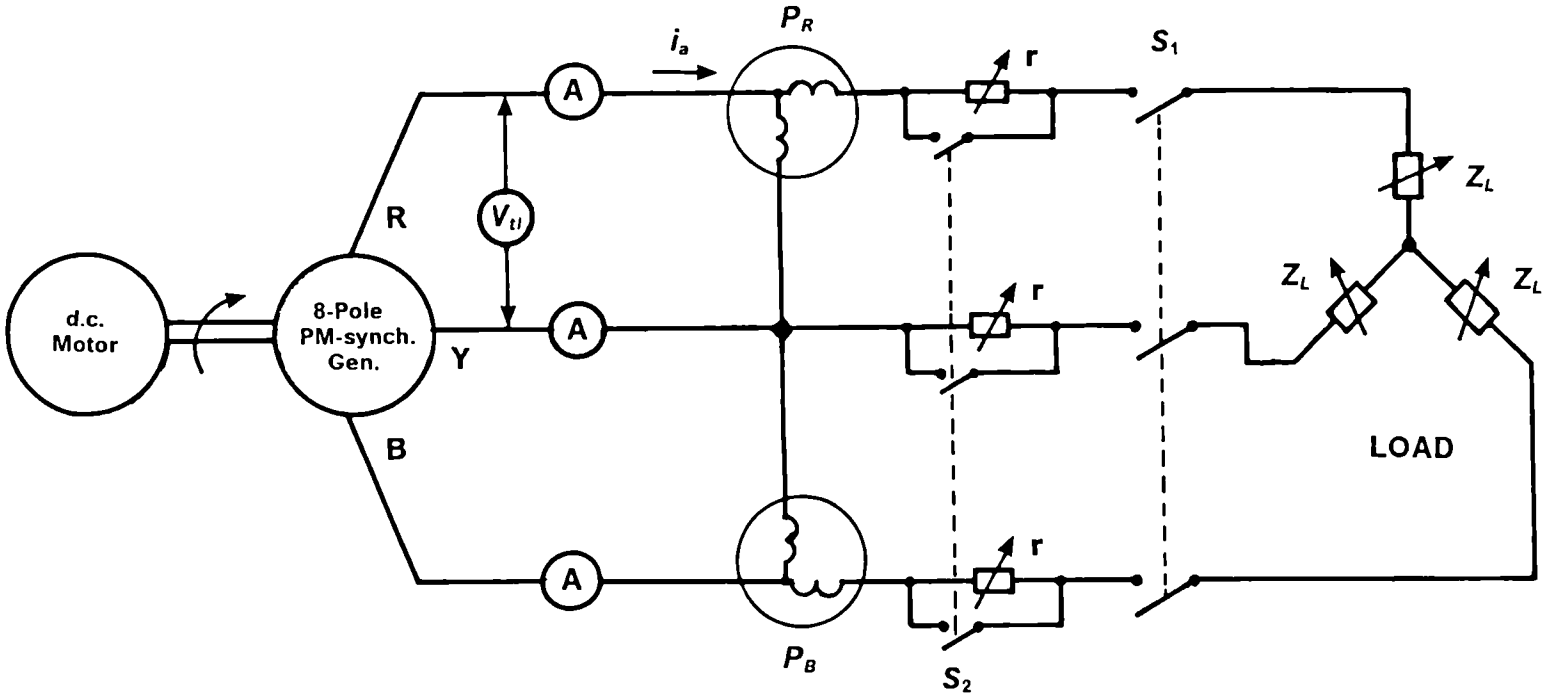


**Fig.(2-4) General circuit diagram of the experimental work for testing the PM Generator.**

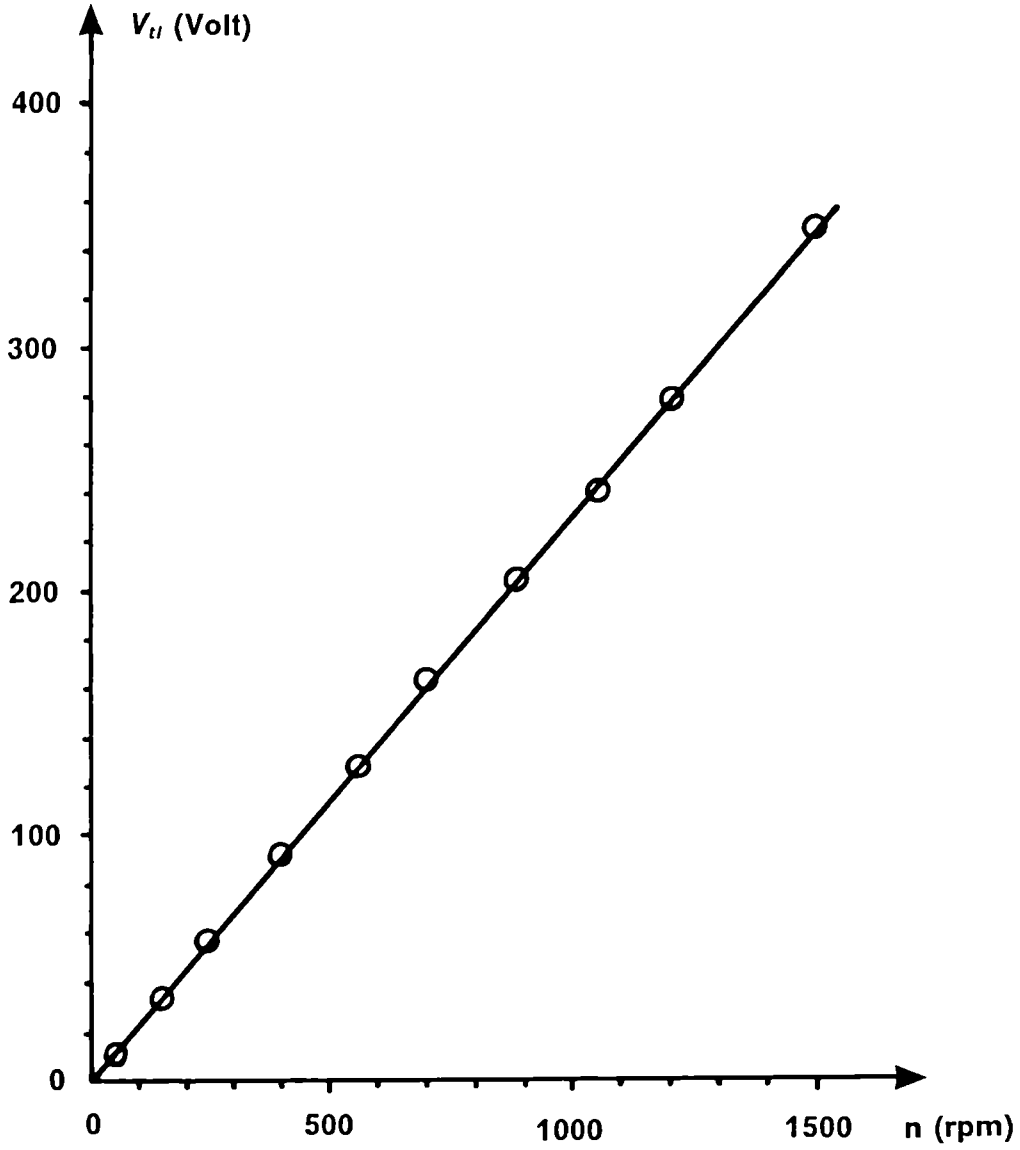


Fig.(2-5) Determination of induced emf of the PM-generator.

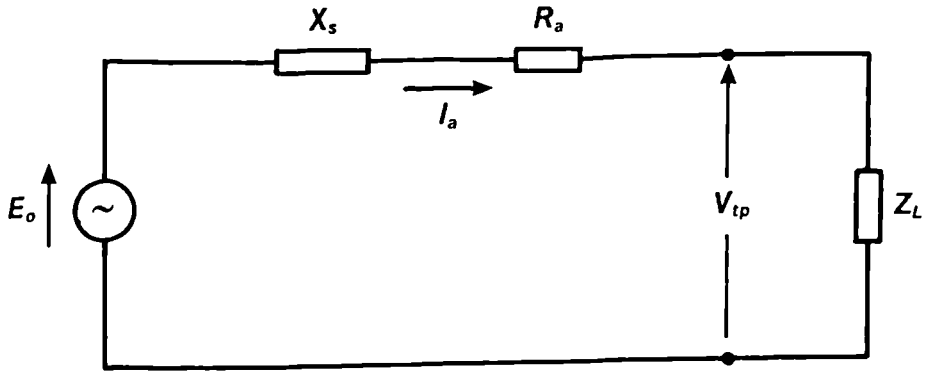


(a-) Purely Capacitive or Inductive load, connected to the generator.

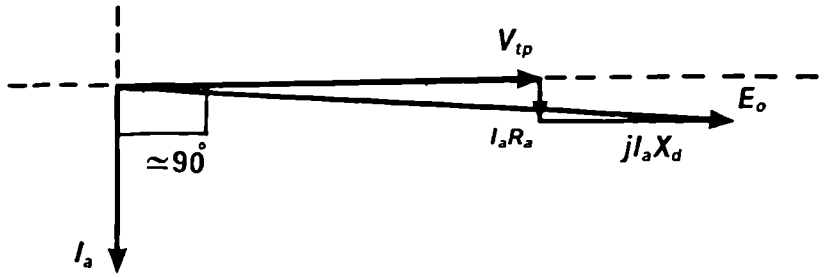


(b-) Phasor diagram of Zero power-factor lagging.

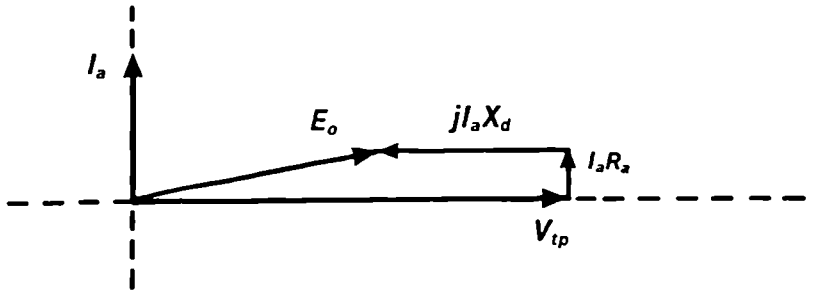


(c-) Phasor diagram of Zero power-factor leading.

Fig.(2-6) The equivalent circuit of the PM-Synchronous generator used for zero power-factor test.

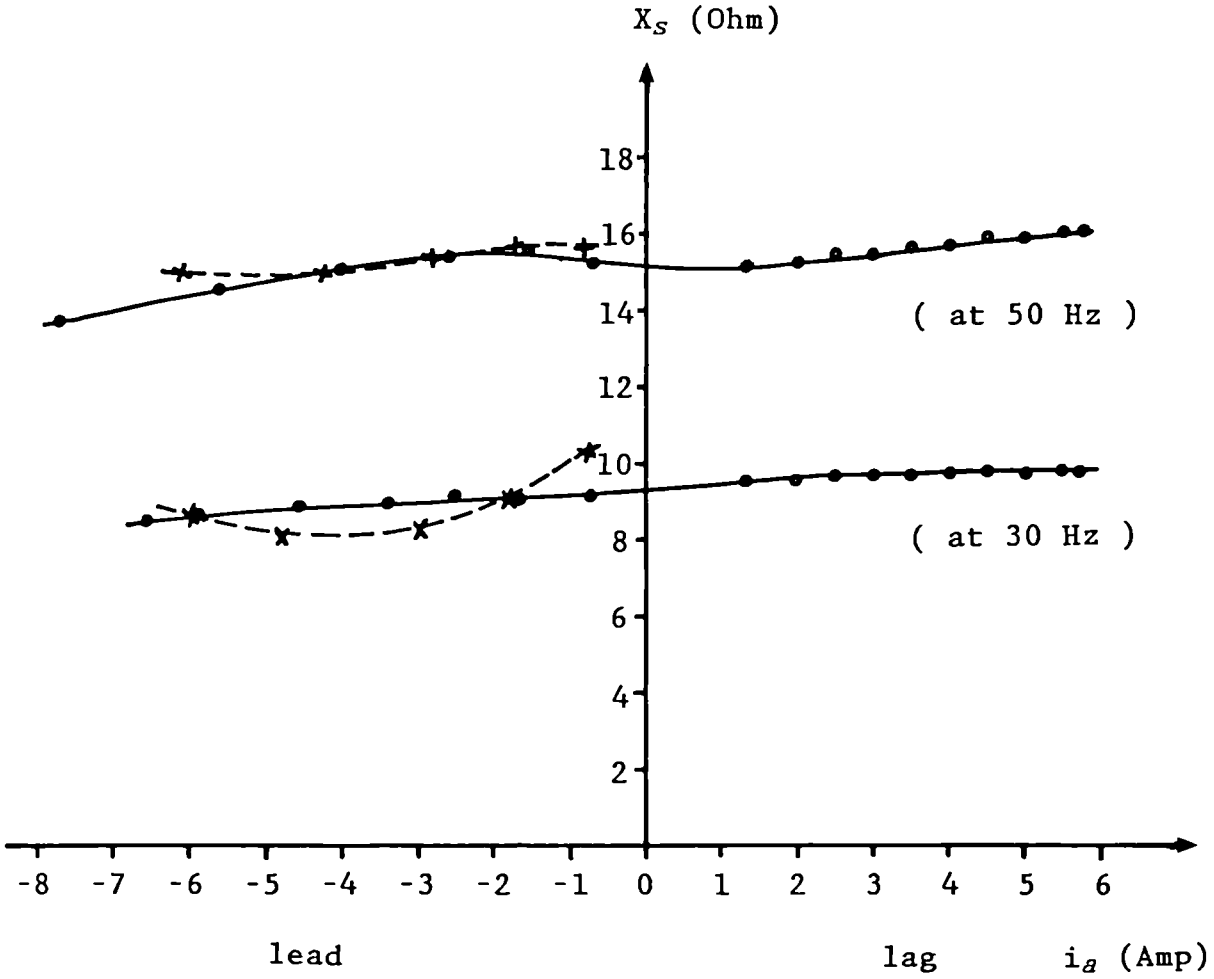


o .... $X_d$

x .... $X_q$

**Fig.(2-7) Direct and quadrature axis synchronous reactance variations with armature current at zero power-factor.**

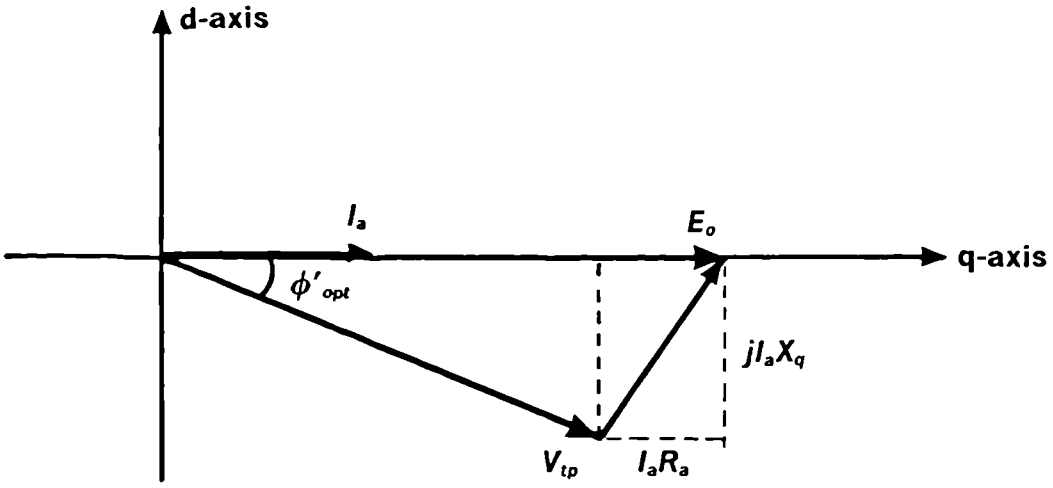


Fig.(2-8) Phasor diagram for the PM-generator at condition of maximum power.

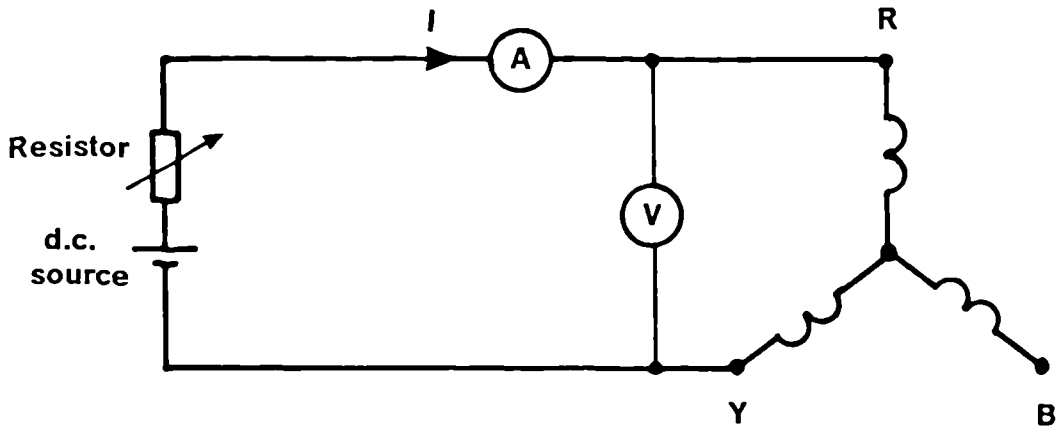


Fig.(2-9)Stator winding resistance measurement.

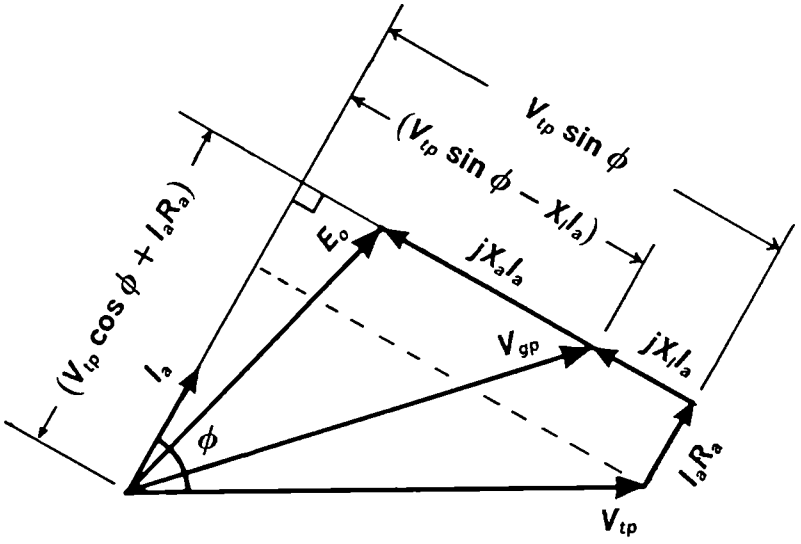


**Fig.(2-10) Phasor diagram of the 8-Pole PM Synchronous generator at leading power-factor**

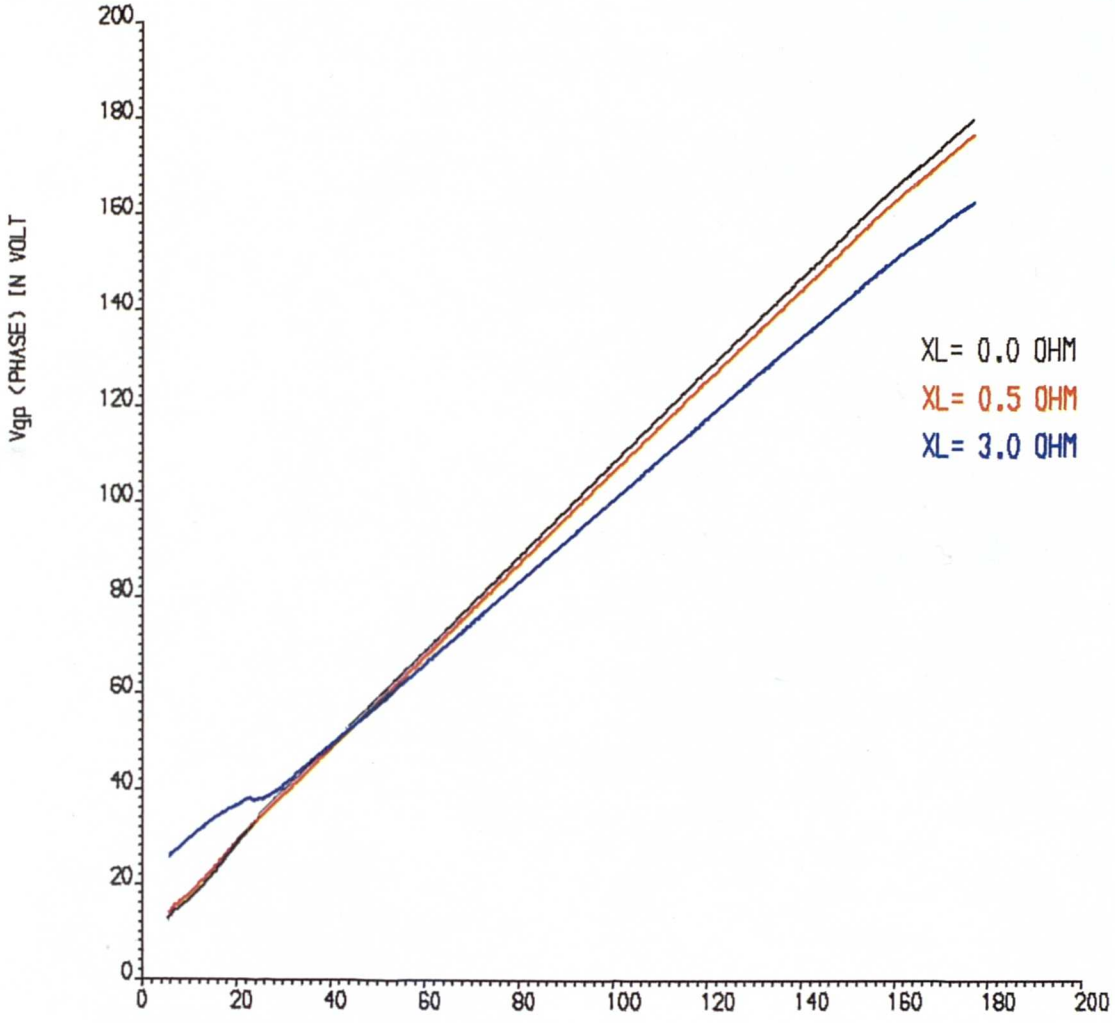


FIG.( 2-11 ) AIR GAP PHASE VOLTAGE VERSUS TERMINAL PHASE VOLTAGE AT 50 HZ, AND IA = 6.15 AMP

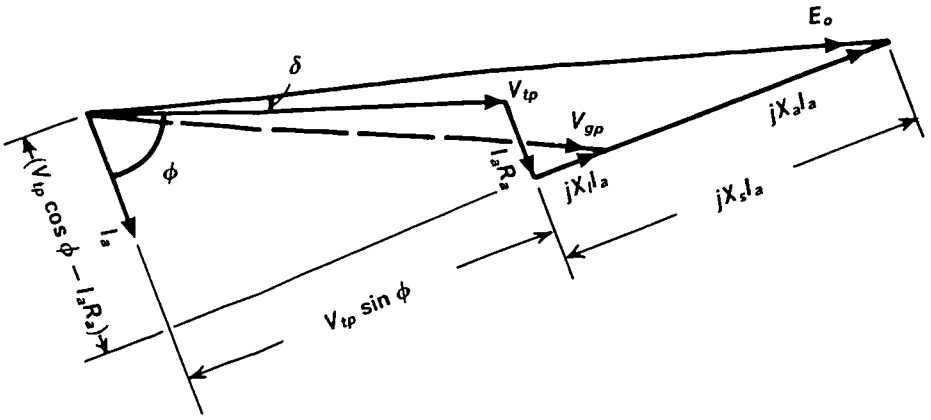


a- At lagging power-factor.

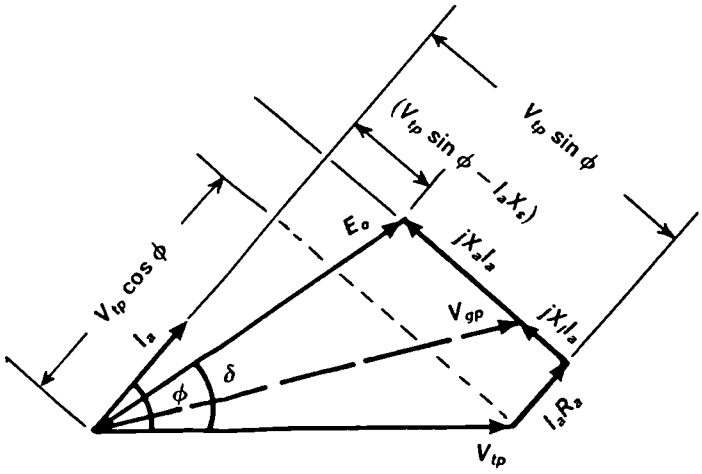


b- At leading power-factor.

Fig.(2-12) Phasor diagram of a cylindrical rotor PM-generator.

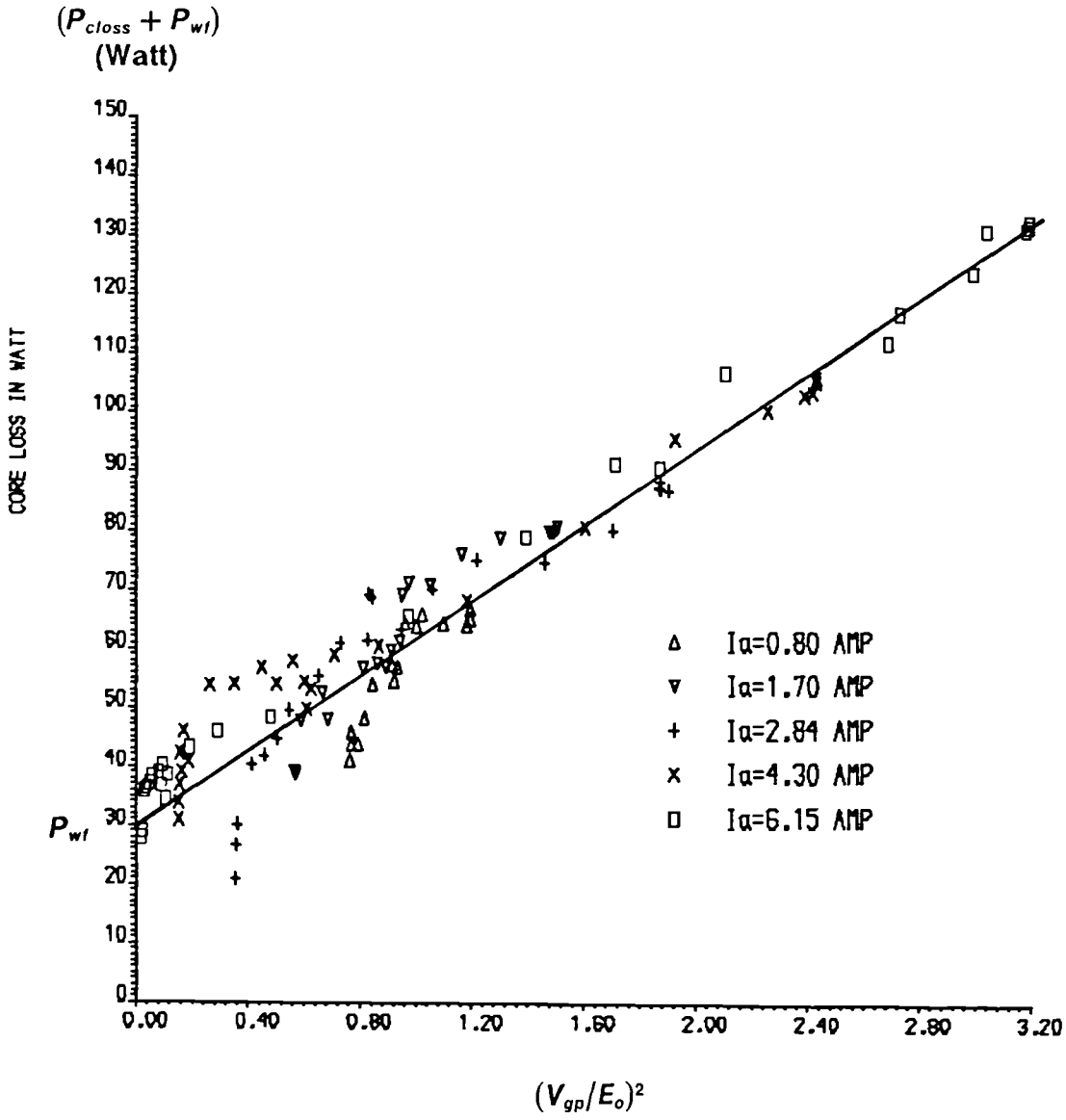


**Fig.(2-13) Generator core loss for different stator current at 50 Hz.**

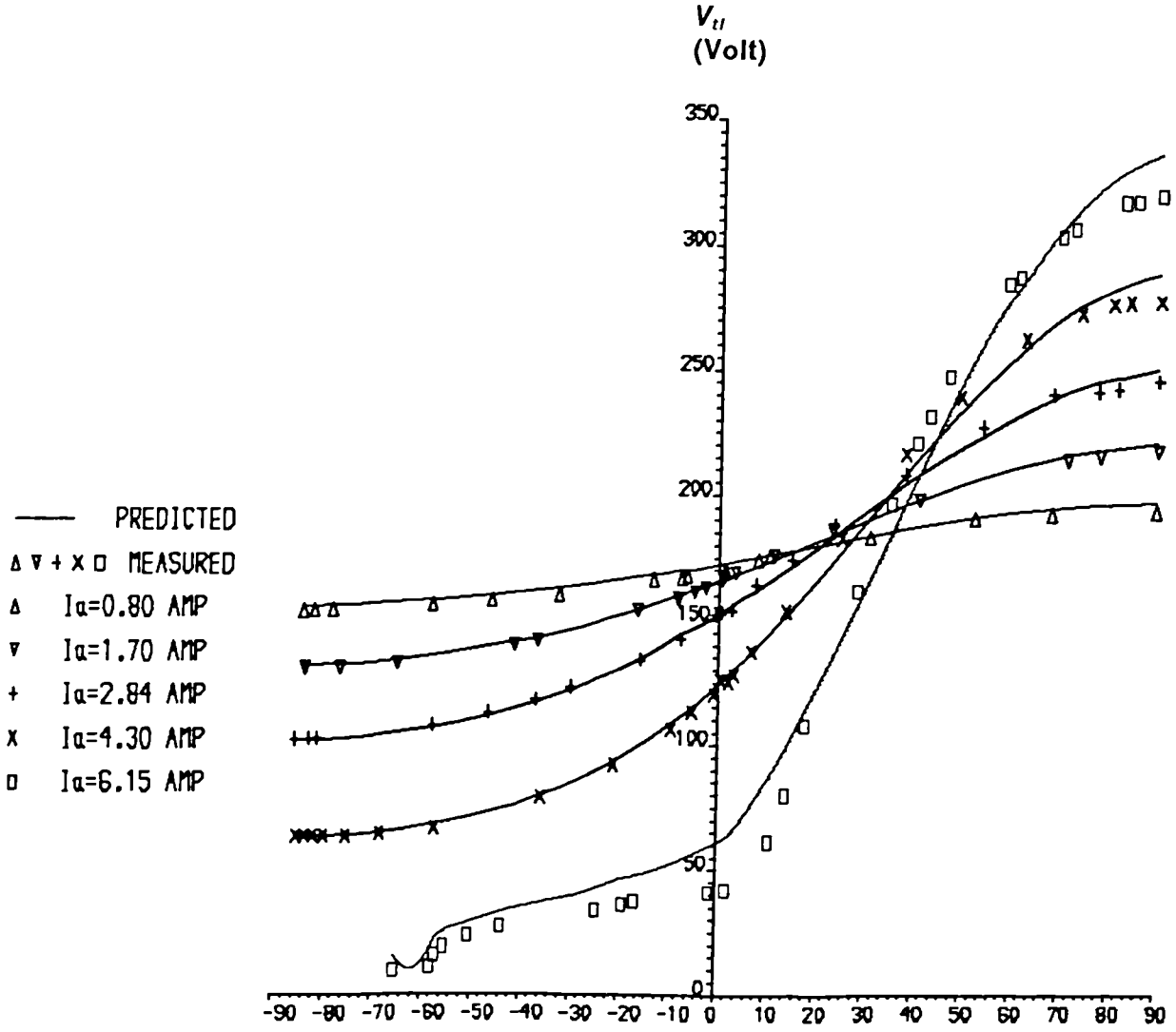


Fig.(2-14) Terminal line voltage $V_{tl}$ at 50 Hz.

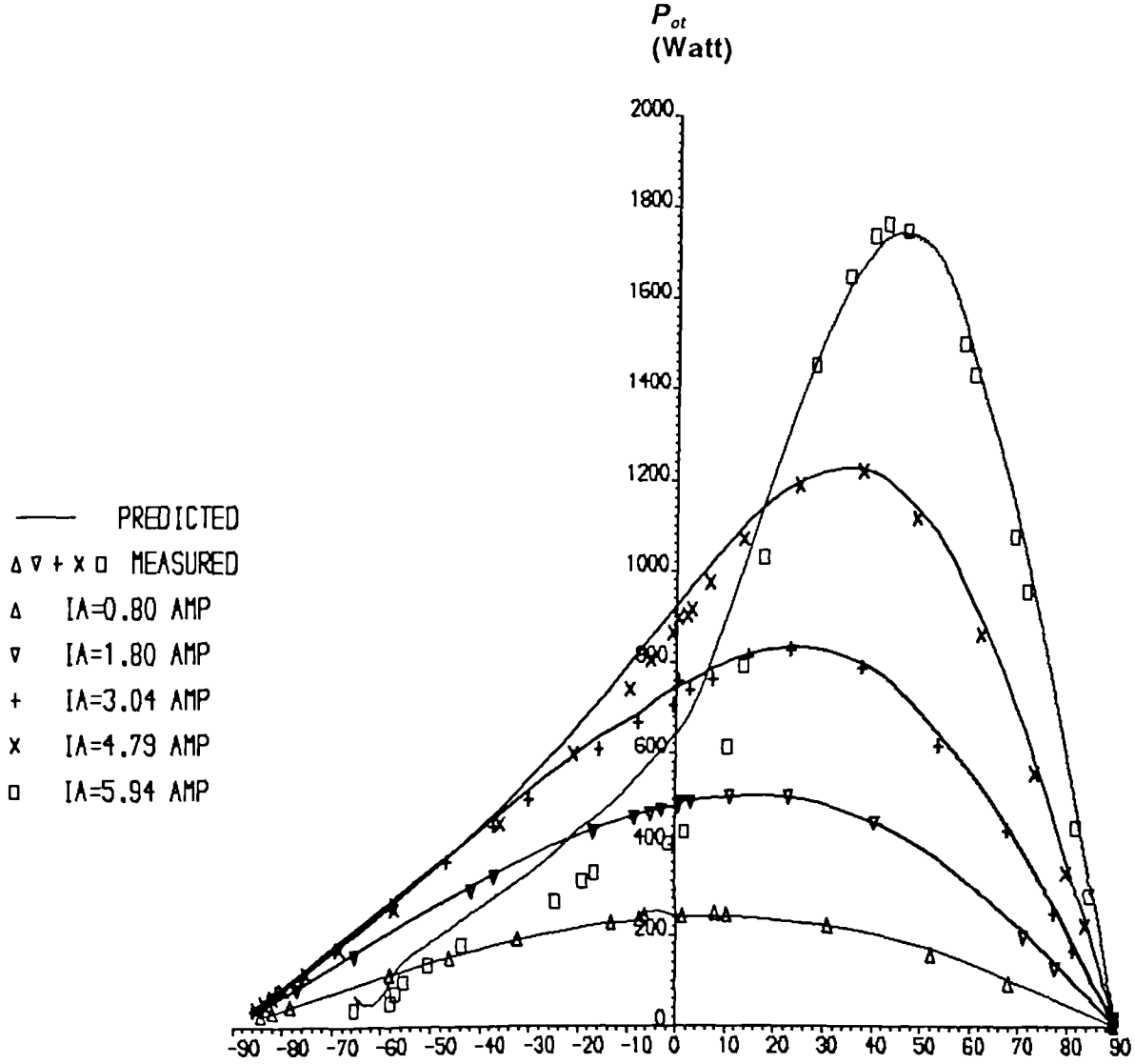


**Fig.(2-15) Generator output power $P_{ot}$ at 50 Hz.**

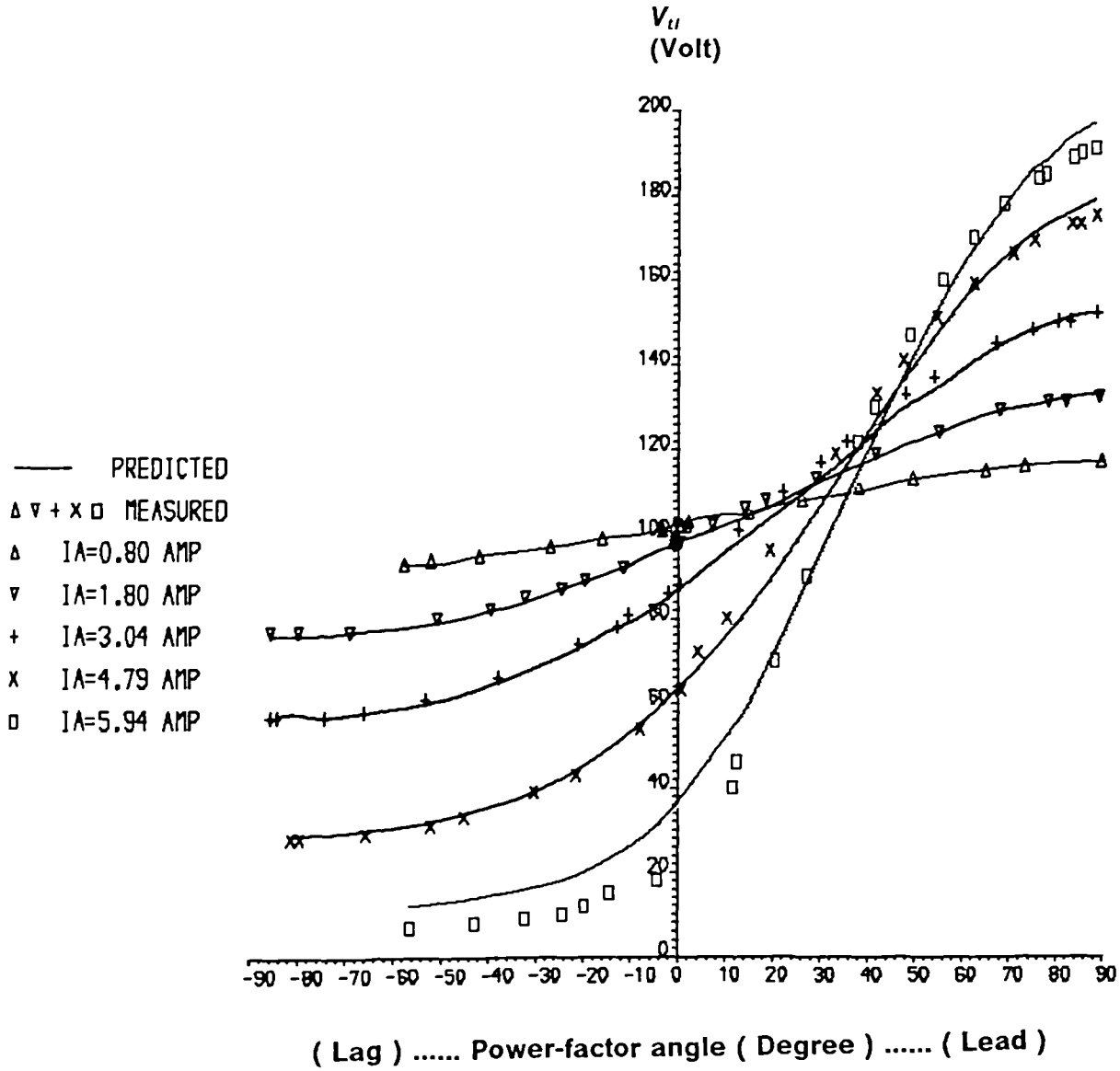


**Fig.(2-16) Terminal line voltage $V_{tl}$ at 30 Hz.**

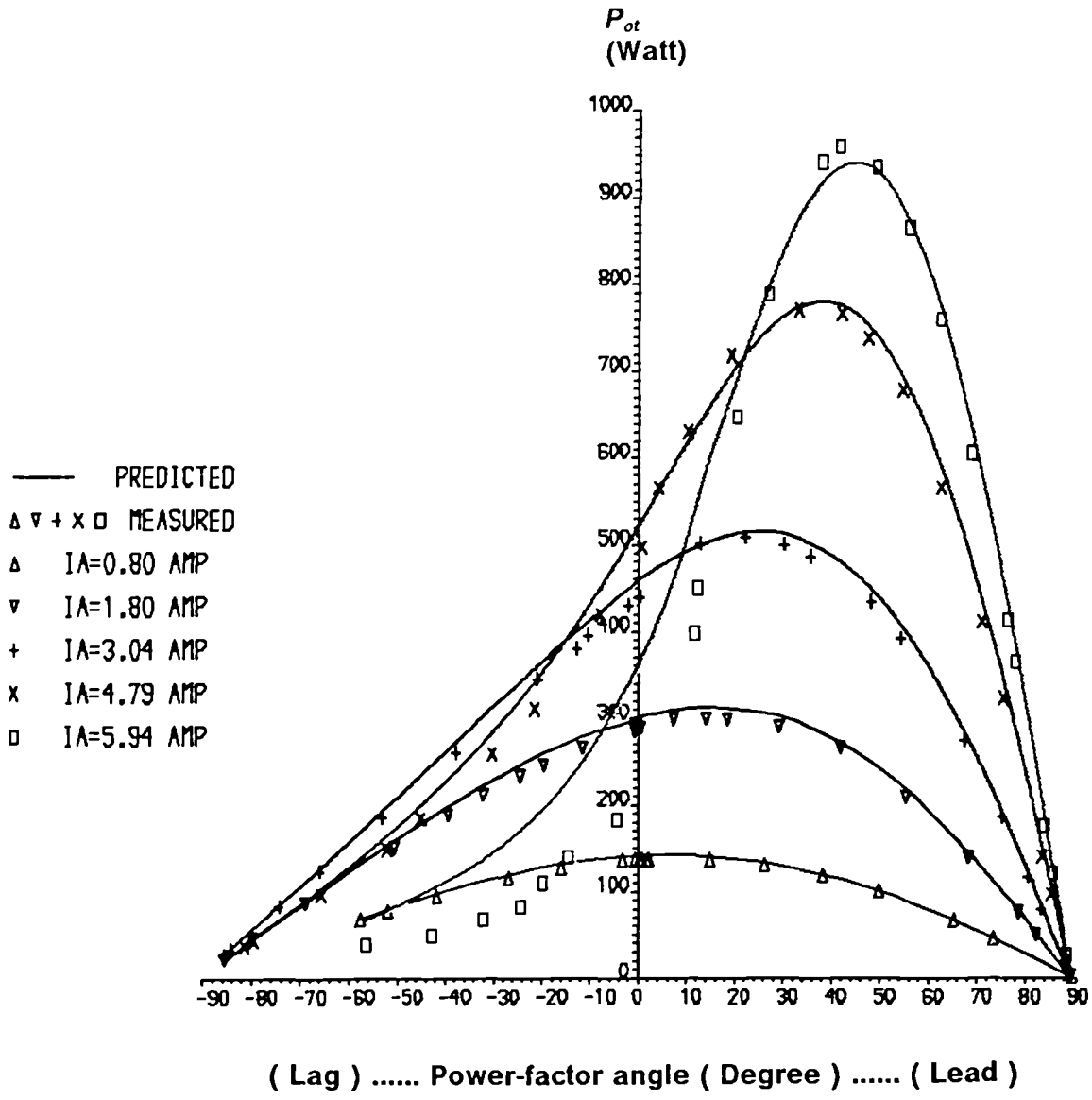


**Fig.(2-17) Generator output power $P_{ot}$ at 30 Hz.**

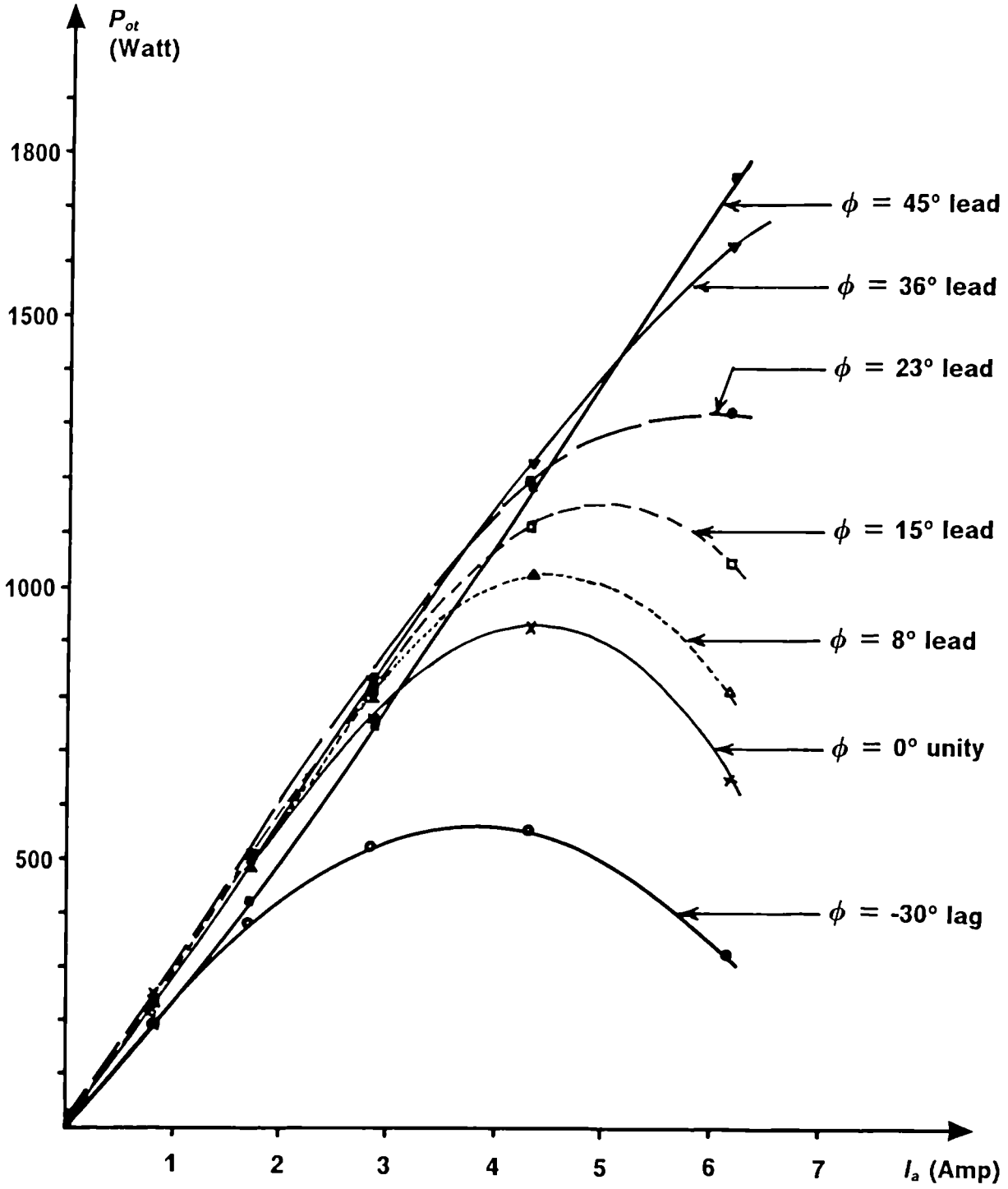


**Fig.(2-18) Output power at constant power-factor angle versus stator current at 50 Hz.**

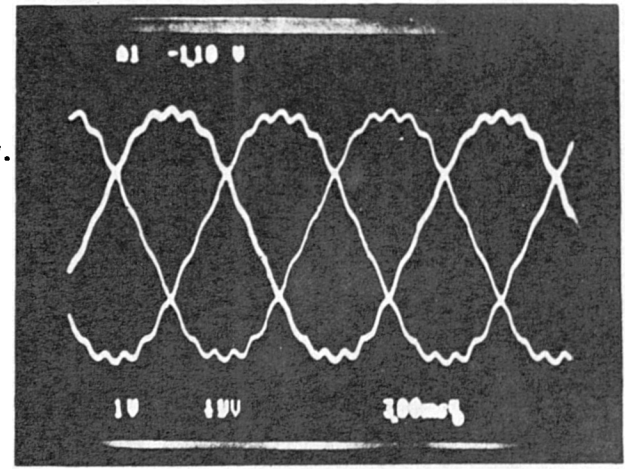

100 V/div.

$V_{ll}$

a- No load 3-phase line voltage.

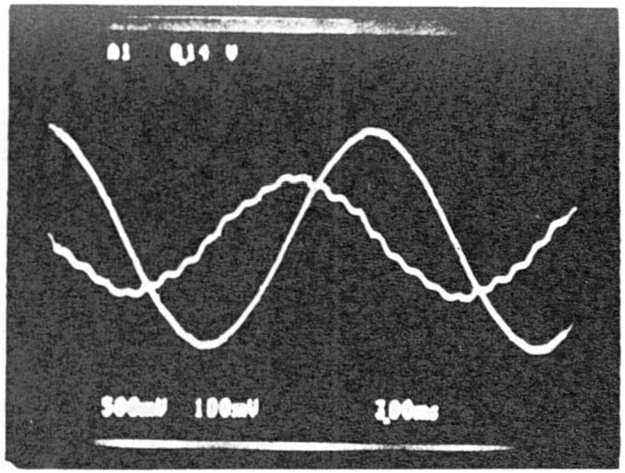

2.5 A/div.

50 V/div.

$i_a$

$V_{ln}$

b- At inductive load.

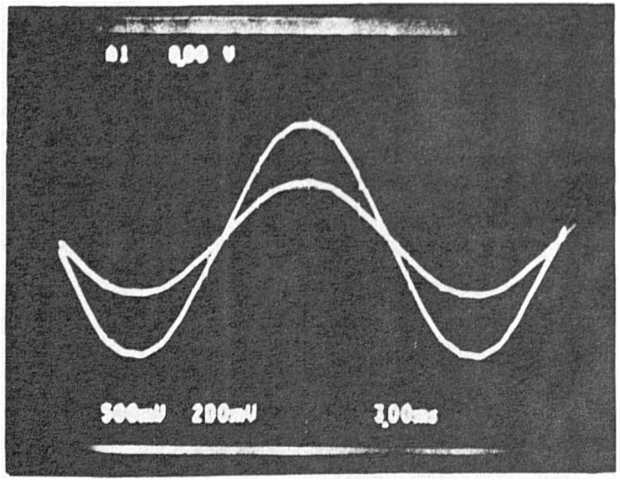

50 V/div.

5 A/div.

$V_{ln}$

$i_a$

c- At resistive load.

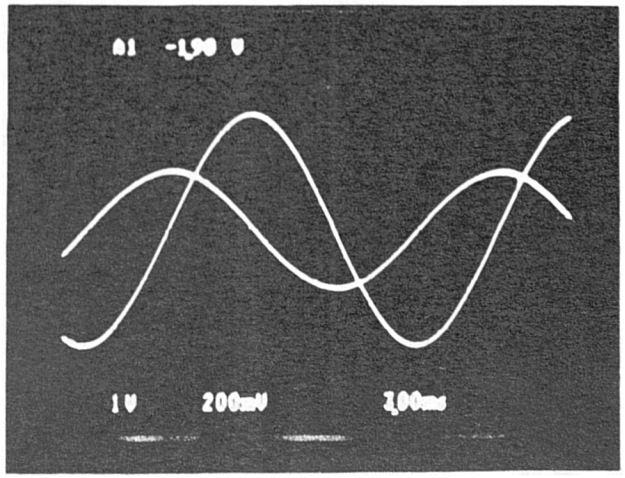

100 V/div.

5 A/div

$V_{ln}$

$i_a$

d- At capacitive load.

**Fig.(2-19) Stator terminal voltage and current of the PM-synchronous generator.[ $i_a = 4\ Amp$, $T/div. = 3\ ms/div.$ ]**

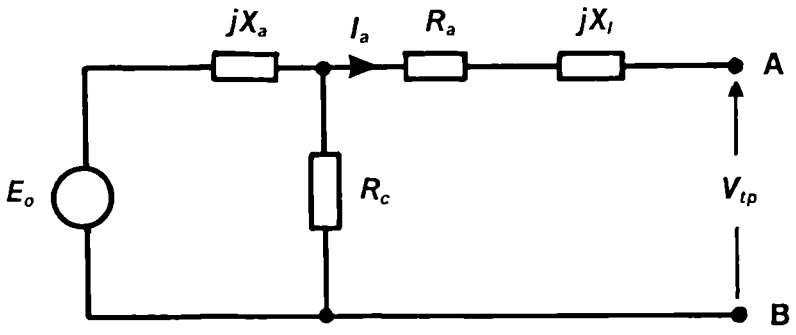


a- Machine equivalent circuit.

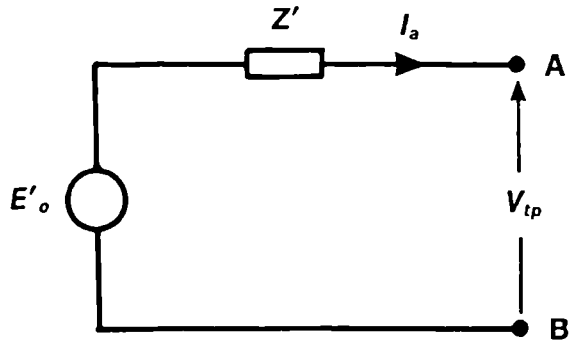


b- Thevenin's equivalent circuit.

Fig.(2-20) Equivalent circuit of the PM-synchronous generator and its Thevenin's equivalent circuit including core loss.

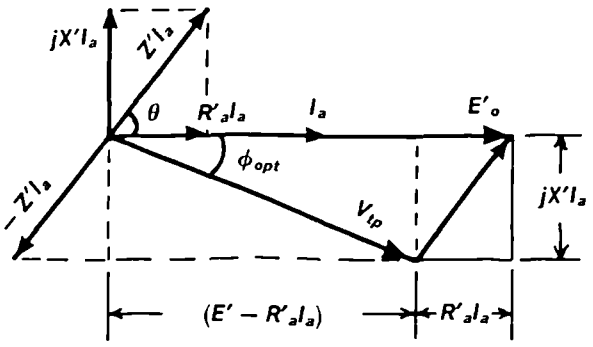


Fig.(2-21) Phasor diagram for optimal power-factor angle.

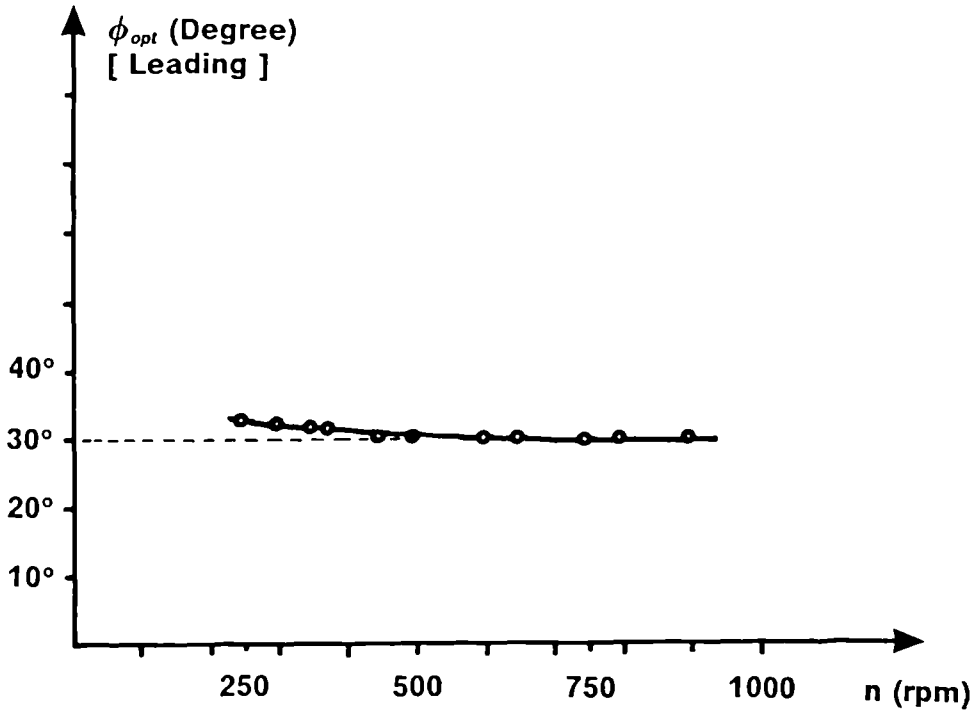


Fig.(2-22) Optimal power-factor angle versus speed at $I_{a1} = 3.5$ Amp.

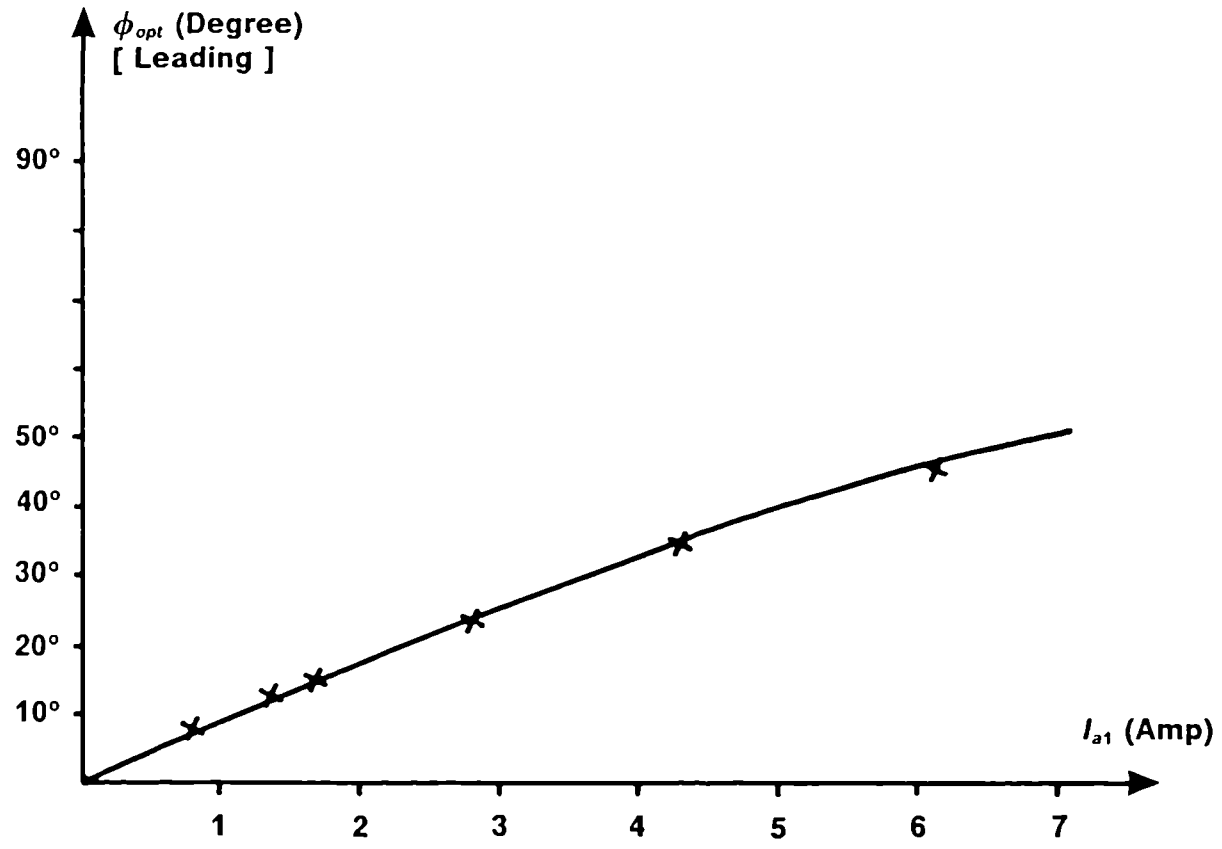


Fig.(2-23) Optimal power-factor angle versus stator current at maximum power transfer.

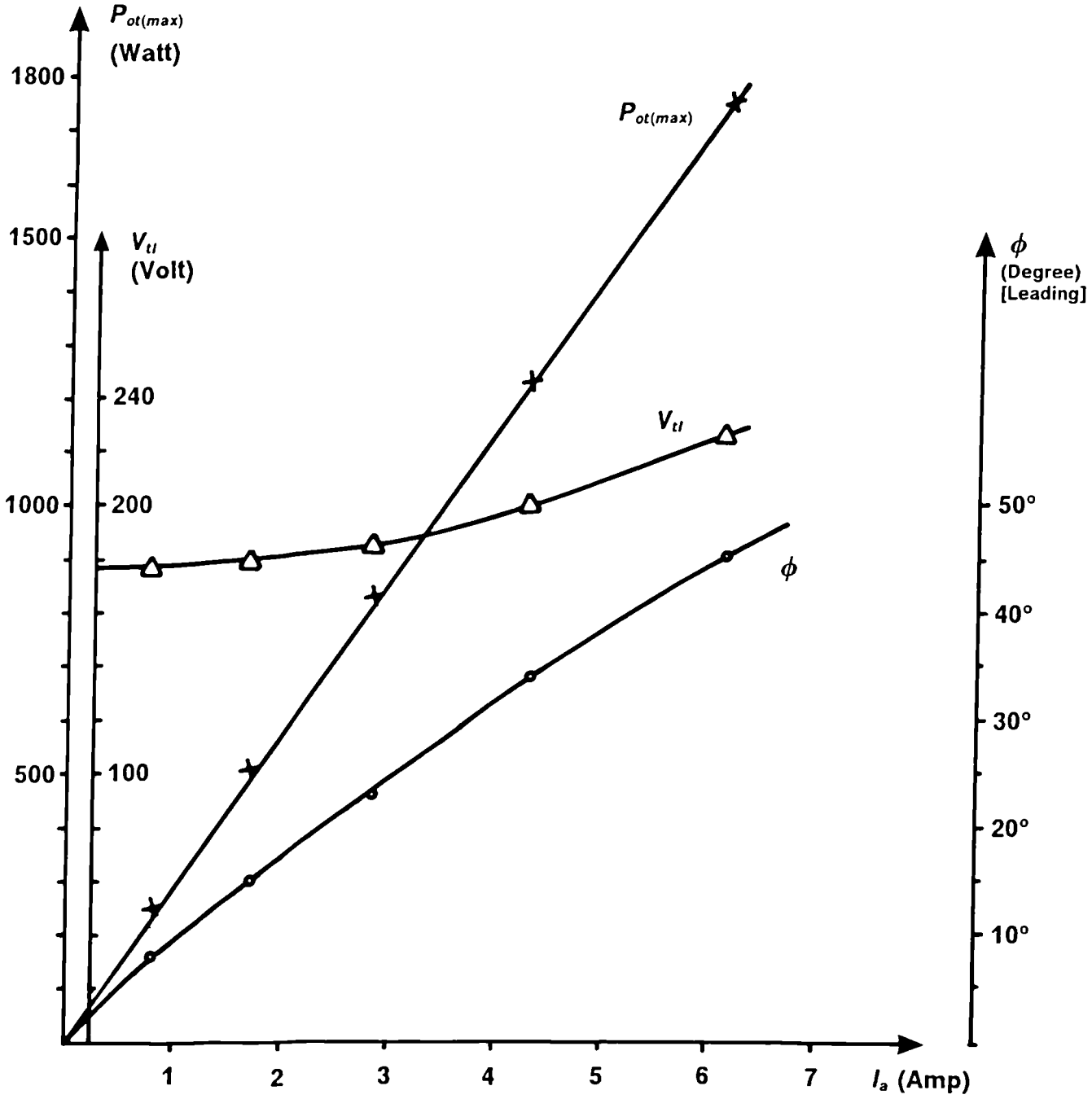


Fig.(2-24) Maximum power, line voltage (at max. power), and power-factor angle versus stator current at 50 Hz.

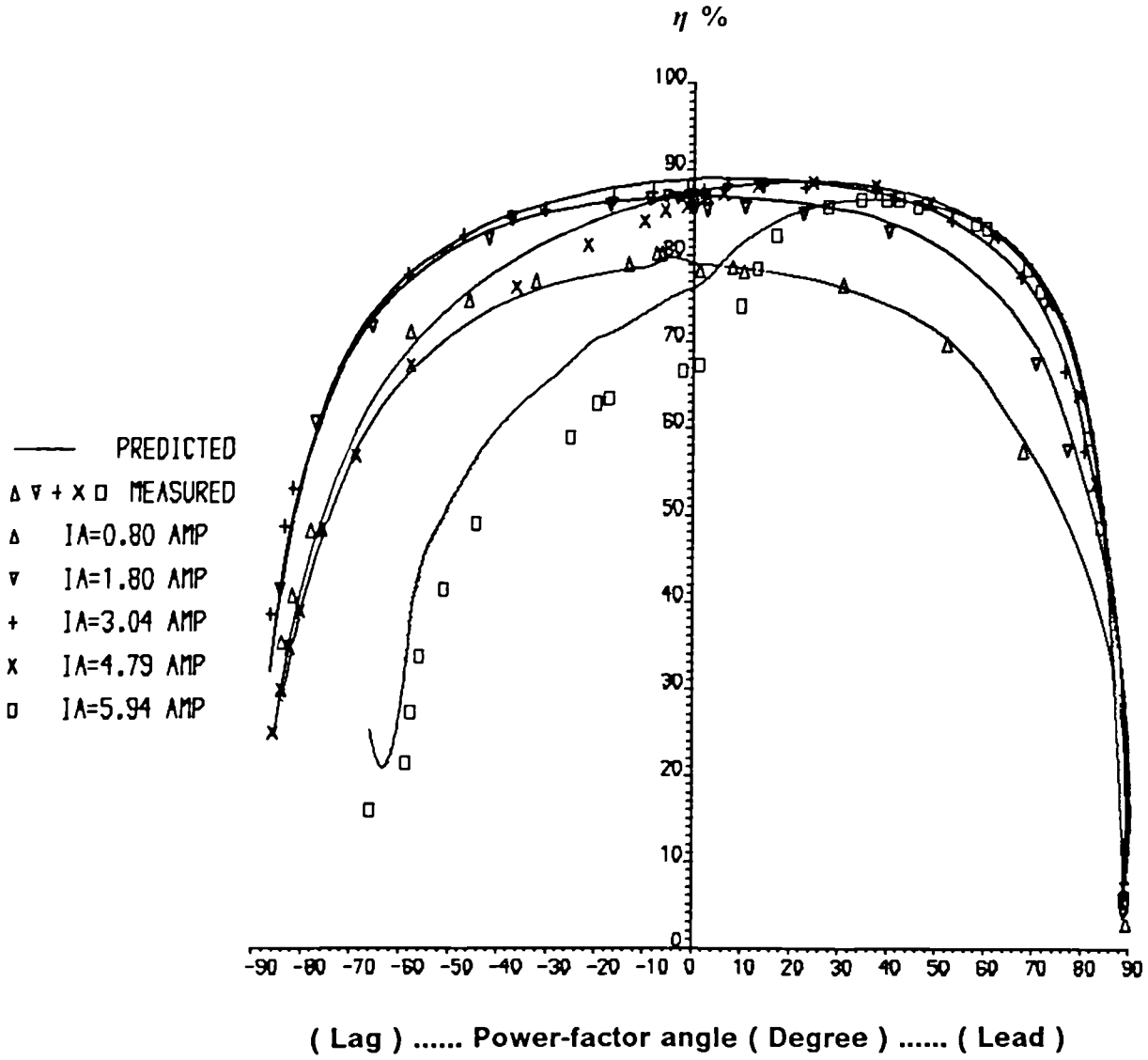


**Fig.(2-25) Generator efficiency versus power-factor angle for variable stator current at 50 Hz.**

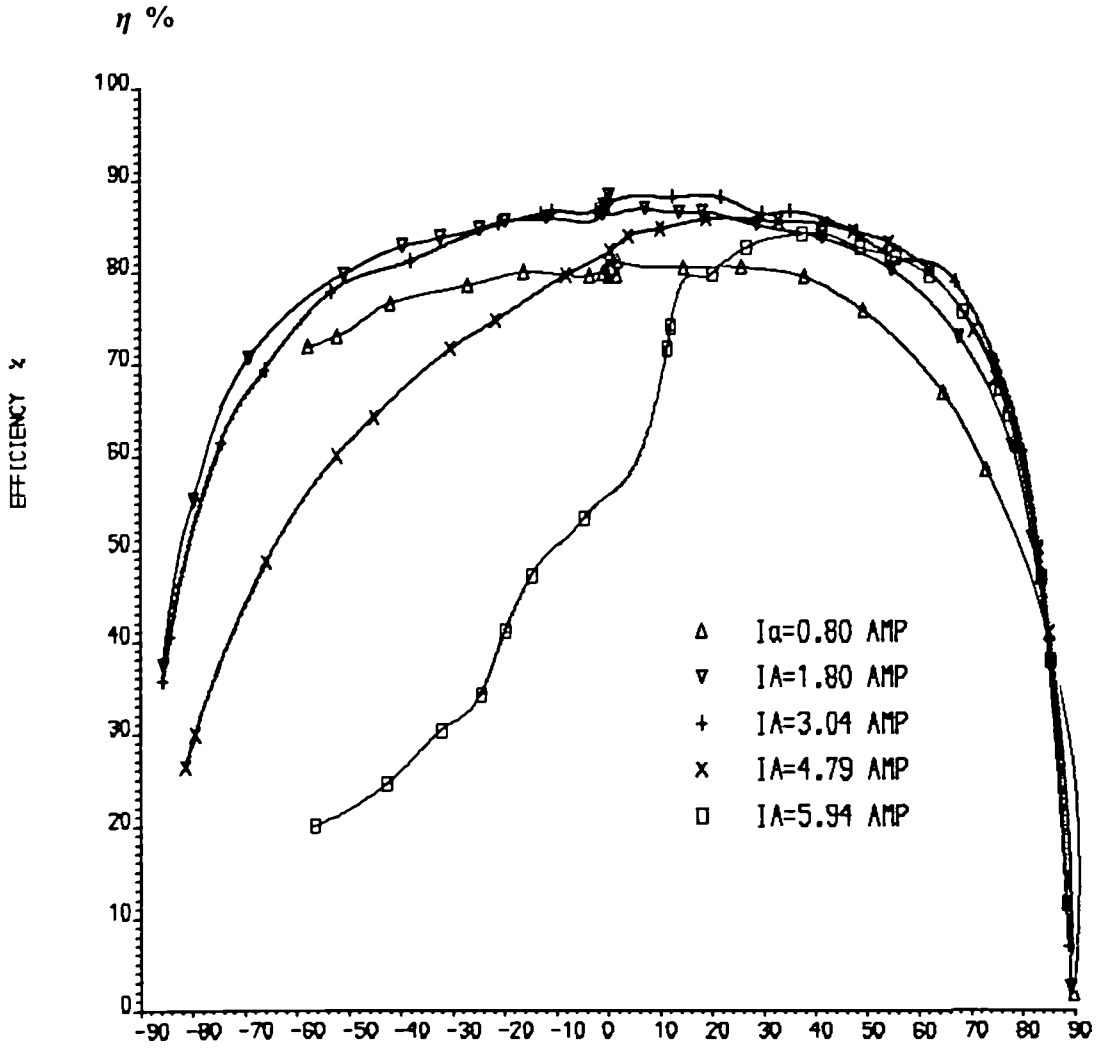


**Fig.(2-26) Generator efficiency versus power-factor angle for variable stator current at 30 Hz.**

*CHAPTER THREE*

# THE PWM, GTO CONVERTER

## 3.1 INTRODUCTION.

The purpose of the converter is to transfer the power from the variable frequency a.c. source of the permanent magnet synchronous machine to a d.c. or a fixed frequency a.c. source. Such sources may include batteries, heaters or the main a.c. utility network. This chapter discusses the design and performance characteristics of a three phase GTO converter which is switched under sine-weighted pulse width modulation (PWM) control.

Two topologies of converter were considered. The first was the three-phase, six GTO bridge shown in fig.(3-1) which can be operated fully over two quadrants to act both as a rectifier and an inverter. The three phase three-switch fully controlled ac dc converter bridge used by Malesani and Tenti [80] was also constructed. This converter has 12-diodes and three GTO thyristors as shown in fig.(3-2). It has the advantages of simplicity and cost effectiveness since it halves the number of GTO thyristors. The disadvantages are that it is limited to single quadrant operation as a rectifier only and the delay angle control is restricted to $\pm 30°$ . Thus, it is possible, to some extent, to use this in conjunction with the PM-generator proposed in this work. However, its performance is the same as for the six GTO converter bridge described here in detail, with the exception of the limitations specified above.

A digital control using a phase locked loop ( PLL ) circuit is implemented which provides PWM signals to control the switches of the GTO converter. The PWM strategy is optimised to minimise the harmonic content of the a.c. line current drawn by the converter. Thus only three small capacitors are needed for filtering at the a.c. input of the power converter.

The digital circuit provides independent control of the modulation depth, hence the amplitude of the current waveform, and the phase, or delay angle, between the input current and voltage.

The method of producing the PWM pattern is by comparing sine-weighted signals stored in the EPROM with a digital triangular waveform from a counter. Each sample of the sine-weighted signal is compared with both edges of the triangular waveform, which produce a uniform sampling PWM signal as shown in fig.(3-3). The methods of uniform sampling techniques, which lead to symmetrical modulation are discussed in [100, 101]. In the present work there are ( 48 ) samples per cycle which is kept constant with frequency, but this is extended, in the current waveform, to (66) samples due to flywheel action of the converter.

### 3.2 OPERATION OF THE SIX SWITCH BRIDGE:

The main circuit of the converter bridge which contains six GTO thyristors to form a three-phase bridge circuit is shown in fig.(3-1). In practice switching aid circuits are connected across each GTO and these are discussed later. Three capacitors are connected in a star configuration on the input and are used to absorb the high frequency components of the current. In addition three small inductors are inserted in series with each phase to filter the a.c. current when the converter is connected to the a.c. network. These coils are not necessary when the converter is connected directly to the PM-synchronous generator, since the synchronous inductance of the machine acts to filter the a.c. current.

The converter operates by switching the GTOs on the positive and the negative halves of the bridge under PWM control. The PWM process is designed to ensure a flywheeling path to the output d.c. current $I_{dc}$ of the converter and at the same time a sinusoidal current at the input of the converter. At any one time at least one switch in each half of the bridge will be conducting to ensure a continuous current path through the bridge. An example of the gate PWM-waveforms that are used to form the sinusoidal input currents of the converter, and to control the output d.c. voltage ($V_{dc}$) of the converter are shown in fig.(3-4) and fig.(3-5). The magnitude of the a.c. current is controlled by providing flywheel periods when both devices in the arm of a converter are conducting and the input current is therefore zero. The width of the flywheeling period will also control the average value of the d.c. voltage ($V_{dc}$). Fig.(3-4) shows examples of the flywheeling action. Referring to the device numbering giving in figure (3-1), if initially GTO1 and GTO6 are switched ON as shown in fig.(3-4a), when GTO6 is switched OFF, to insure a continuous flow of output d.c. current $I_{dc}$ , GTO4 is switched ON over the same interval to form the flywheeling action. Similarly fig.(3-4b) shows the middle pulse (or the narrowest pulse) of the PWM pattern that will occur at the crest of the sine wave. Here the pulse is created by introducing a flywheel period using GTO3 and GTO6. The complete PWM pattern for one cycle of the input current is shown in fig.(3-5). In addition this figure shows all the gate pulses supplied to the GTO thyristors. The effects of the flywheel action described in fig.(3-4a) can be seen to produce a double pulse around the zero crossing of the a.c. current waveform.

Some consideration of the switching behaviour of the GTO thyristors and their operation with this PWM strategy is needed. Fig.(3-6) shows the

typical driving gate signals, and the GTO anode voltage and current of two GTOs in the same half of the bridge. It is clear from this figure that the falling edge of both anode voltage and current of the GTO thyristor is faster than the rising edge. For example as the GTO5 anode current falls to zero, the anode current of say GTO1 still has not been established. To overcome this a delay of 2$\mu$sec is introduced into the Off state of the driving gate signal to form an overlap between the PWM gate signals, which compensates for different "Turn off" delay and "Turn on" delay times of the GTO thyristors. This will ensure a continuous flow of the d.c. current in each half of the bridge.

### 3.3 OPERATION OF A THREE SWITCH BRIDGE:

A 3-phase three-switch GTO converter has been also designed and the main bridge circuit is shown in fig.(3-2). The basic operation of the converter is similar to that of the six-switch GTO converter except that each GTO thyristor carries the current for both the positive and negative half of the cycle. This is achieved by the diodes around the GTOs which direct the current through the one switch in each leg of the converter. The method of operation under PWM control is slightly different to the previous converter in that at any one time two GTOs will be switched according to a sinusoidal PWM pattern, while the third GTO is used for flywheeling the d.c. current at the off periods of the other switches. Apart from this detail, the operation is the same as for a six-switch converter. However, the controllable phase-shift between the input voltage and current is limited to between 30° lagging and 30° leading. This will be explained when the control signals of the bridge are considered.

## 3.4 THE GTO THYRISTOR AND GATE DRIVE:

The GTO thyristor is a bistable semiconductor switch which, like a conventional thyristor, blocks a high-level forward voltage in the off-state, and can pass a peak current far in excess of its rated average current when in the on-state. Unlike an ordinary thyristor, however, it can be turned off by the extraction of reverse current from the gate, essentially a self-commutated semiconductor switch. In this respect it is similar to a high voltage transistor, and combines the most desirable properties of both types of device. Therefore, when applying a GTO to a thyristor converter or any power application, forced commutation components are not needed. Hence, the GTO thyristor offers several advantages over the conventional fast switching thyristors, which may be summarised as:

1- Simplified power circuit configuration, resulting in reduced volume and weight.

2- Less electrical and audible noise, due to the removal of commutation circuits.

3- Fast turn-on and turn-off, permitting the use of higher switching frequencies.

4- Improved power conversion efficiency because of the lower commutation losses.

The major disadvantages of the GTO thyristor are the higher conduction loss and the cost of the sophisticated gate firing circuit to perform the turn-on and more particularly turn-off function. The GTO thyristor has a poor reverse blocking capability, where it behaves like a resistor which is unable to block voltage or conduct significant current. When it is used in a.c. switching, a diode must be connected in series if reverse voltage blocking is required, or

alternatively a diode is connected in anti-parallel with the GTO thyristor, if a reverse current is required to flow.

GTO thyristor gate drive circuits are similar to power transistor base drive circuits with some exceptions which will be discussed below. Two types of gate drive circuits were considered for the GTO thyristor used in this project, the first circuit is designed with a single power supply, and the second is designed with a dual power supply, as shown in fig.(3-7). The first type is only suitable for use up to a 50% duty cycle, and a switching frequency of not less than 45Hz. It is then, a simpler gate drive circuit which has limited applications. On the other hand, the second circuit can be used for full 100% duty cycles at any switching frequency. It is this circuit which has been used for this project.* The type of GTO used is a 10Amp average anode current, 1000Volt device ( BTV58-1000R ), but the gate drive circuit can drive a higher power device to be used in future work with higher rated PM-generators. The gate drive circuits are supplied from an isolated switch mode power supply which is discussed in appendix B. The low power control signal is isolated from the power stage by an optical-isolator, driven from an open collector logic driver gate.

The action of the gate drive circuit of the GTO thyristor occurs in two parts. One section of the circuit acts as a current source which provides the forward current to the gate during turn-on. The second section operates during the turn-off, when the gate drive circuit acts like a negative voltage source of low impedance. The general recommended gating condition of a GTO thyristor is shown in fig.(3-8). The turn-off time is limited by the switching aid circuit components ( $R_s$, $C_s$, $D_s$ ) across the device, while the



*After [ Mullard technical notes ].

turn-on time depends on the ability of the gate drive circuit to supply sufficient forward current. Therefore the switching characteristics of the GTO thyristor are applied with requirement needed in the data sheet (appendix D). The switching characteristics are explained separately at turn-on and turn-off as below:

### 3.4.1 Turn-on:

In the on-state the GTO thyristor has two stable states. At low anode currents, less than the latching current of the device, it behaves like a high power transistor with an associated gate-anode amplification gain of $I_A/I_G$ , which increases with increasing anode current. In this mode of operation, the forward gate current ($I_G$) should be kept continuously flowing to the gate-else the device will fail to conduct. The other mode of operation is similar to a conventional thyristor, and occurs when the anode current exceeds the latching current, when the GTO is triggered and remains in the on-state even when the gate current is removed. However, for safe operation the forward gate current $I_G$ is usually maintained in this mode of operation. In addition the presence of a gate current will tend to reduce the voltage drop across the anode and cathode of the device, [this is explained in the data sheets of the GTO thyristor given in Appendix D].

The experimental gate voltage and current of the power device used ( BTV58-1000R ) are shown in fig.(3-9). At turn-on a sufficient initial value of gate current is needed to ensure fast turn-on of the device. Therefore, an RC circuit is connected in parallel across the collector resistor (22 Ω) of the upper transistor shown in fig.(3-7). This RC circuit gives an initial gate

current of 3 times the continuous forward value $I_G$. Fig.(3-10a) shows the experimental switching characteristics of the anode voltage and current at "Turn on". Here the anode voltage is 220 volts (d.c.) and the average current is up to 10 Amps. The GTO thyristor has also operated successfully at higher voltage of 430 Volt (d.c.) with an average current of up to 8 Amp, and switching frequencies up to 4 kHz.

### 3.4.2 Turn-off:

It has been mentioned earlier that the GTO thyristor has the ability to be switched off from the gate during the conducting period. A negative voltage source (-10 Volt) is needed to switch-off the device. The source is realised experimentally by switching on the lower transistor shown in fig.(3-7) to the negative rail of the d.c. bias source. It is essential that a low stray inductance exists in this path with an expected value of not more than (1.0 $\mu$H), (this value is specified in the data sheets of the GTO thyristor). If the stray inductance is increased above this value the device will be destroyed.

At turn-off, precautions have to be taken to limit the current which is interrupted, and the rate of rise of anode voltage ($dV_D/dt$). The maximum controllable anode current is defined as a function of ($dV_D/dt$) as shown in the data sheets appendix D. The ($dV_D/dt$) is controlled by the switching aid circuit connected across each device in the power bridge discussed below. Fig.(3-10b) shows both anode voltage and current of the GTO thyristor at "Turn off". The gate drive circuits were tested over a range of duty cycles. The GTO thyristor switching waveforms when it is turned-off for about 14%

of the switching cycle as shown in fig.(3-11a), while it is turned-off for 95% of the switching cycle in fig.(3-11b).

### 3.5 SWITCHING AID CIRCUIT:

A polarised ( RCD ) type of switching aid circuit is used to protect the GTO thyristor as shown in fig.(3-12). Assuming initially that the device has been turned-on and the capacitor is fully discharged through the GTO and the snubber resistor $R_s$, when the device is turned-off, the capacitor $C_s$ will be charged through the fast recovery diode $D_s$ . Some tests have been conducted in order to find the minimum on-time ( $t_{on}$ ) of the GTO to give satisfactory results with the aid network. This $t_{on}$ is defined as,

$$t_{on} - 5 \times R_s C_s \qquad (\mu \text{ sec}) \qquad (3.1)$$

where $R_s$ in Ohm, and $C_s$ in $\mu$F.

The minimum $t_{on}$ achieved is (13.35 $\mu$s) for [$C_s$=26.7 nF and $R_s$= 100 $\Omega$]. The snubber circuit will reduce the switching losses in the device, but the losses in the snubber resistor $R_s$ will tend to increase the overall switching loss. The complete physical power circuit board (gate driver circuit, and switching aid circuit) is shown in fig.(3-13).

## 3.6 METHOD OF PROVIDING CONDUCTION OVERLAP FOR THE GTO THYRISTORS:

During the operation of the converter, the current is transferred from one GTO to another GTO in the same half of the converter bridge. At the transition period of the current during which the current is forced to pass through the switching aid circuit of each GTO, a voltage overshoot may occur between the anode and cathode of the devices. To combat this, an overlap of 2 $\mu sec$ has been introduced between the gate PWM switching pulses in the same half of the bridge, as shown in fig.(3-14). Fig.(3-14a) shows the circuit implementation of this which consists of a simple AND gate with an $R_xC_x$ delay at the input. The diode $D_x$ is parallelled with $R_x$ to discharged the capacitor at turn-on, while being reverse-biased at turn-off. By this mechanism the input (x) is switched on until the capacitor is charged to the threshold point and therefore the on time of the pulse is increased. The inverted signal of this phase is passed to another circuit of the same specifications. The resulting overlap of the switching signals is shown in fig.(3-14b). The logic signals required by the converter are complementary.

### 3.7 PWM GENERATOR AND CONTROL CIRCUITS:

The block diagram of the proposed digital sinusoidal pulse width modulation (SPWM) scheme is shown in fig.(3-15). It contains, broadly, a frequency multiplier in a phase locked loop (PLL), a look-up table, an 8-bit 8-bit divider and logic gates used for timing and producing the carrier signal. The last block in the figure is used to combine the PWM pattern with control signals stored in an EPROM to drive the GTO gate circuits in the correct sequence.

The PWM waveforms are generated by comparing a sine-weighted signal stored in a look-up table with a digital triangular waveform. This procedure generates symmetrical uniform pulse width modulated signals. The sine-weighted waveform is stored as a series of positive half cycles, one for each phase, as shown in fig.(3-16b). The address in the look-up table is controlled by the frequency multiplier and by an external digital input which changes the phase of the PWM pattern with respect to a reference obtained from the input voltage to the converter. The look-up table contains three sampled sine-weighted signals with a 120° phase separation between them. The values in the look-up table are scaled by passing them through an eight-bit divider. These signals are then transformed to latch circuits and compared individually with the carrier triangular waveform using an 8-bit magnitude comparator. The pulses produced are then separated and fed to a C-type flip flop to form the PWM signals.

A triangular waveform carrier is used instead of sawtooth to obtain symmetrical pulse width modulated signals, and hence a better current waveform. The amplitude and phase of the PWM waveform is directly

controlled by a programmable digital 8-bit/8-bit divider and a phase shifter respectively. The division process is performed using a sequential logic circuit with the output ranging from (00)Hex to (FF)Hex in steps of one digit. The 8-bit divisor of the divider is used to control the amplitude of the sine-weighted signal, and therefore controls the modulation index (M) of the PWM pattern. The input dividend is set by an A/D converter, or it can be controlled by a microprocessor control unit. This method of sinusoidal pulse width modulation ( SPWM ) is simpler than the strategy of storing many switching angles in a large memory and accessing them at each frequency [101]. The proposed technique saves memory and gives a linear relationship between switching angle and frequency.

The phase-shift circuit is simply consists of an 8-bit full adder. A 6-bit phase shift input is used to give the phase shift desired between the input phase voltage and current. This 6-bit number is added to the 6-bit from the frequency multiplier which gives an offset to the address of the sine-weighted signal stored in the look-up table. At present the phase shifter has a resolution of 7.5°.

### 3.7.1 Phase locked loop:

The phase locked-loop is used to synchronise the digital control circuit to the frequency of the a.c. voltage input to the bridge. A frequency multiplier is used in the feedback loop of the PLL circuit as shown in fig.(3-15). The frequency multiplier is a synchronous counter, which multiplies the input a.c. frequency by (12288), i.e. ($2^{12}x3$). The output of the synchronous counter performs the following functions:

1- To provide an access address to the look-up table which contains the sampled 3-phase sine waves.

2- To provide all the timing clock pulses to the digital circuits.

3- To generate the carrier triangular waveform of the PWM pattern.

The voltage controlled oscillator (VOC) in the PLL circuit is used as the system clock (SYS CLK) for the whole PWM generator. Some logic gates were added in the feedback loop to increase the lock range of the PLL as shown in fig.(3-17)

### 3.7.2 8-bit/8-bit divider:

The sine-weighted signal is stored in the EPROM as a positive half of the signal in order to be compatible with the 8-bit/8-bit divider, which controls its amplitude. The division process is restricted due to the time needed to access the data and a combinational logic circuit was used to give a very fast access time. The circuit developed for 8-bit 8-bit division is simply composed of three EPROMs and two 8-bit full adder circuits as shown in fig.(3-18). This allows the samples of the sine-weighted signal to be divided simultaneously by an 8-bit word which is used as a modulation index (M). A full range of division is obtained (FE to 00)Hex. The time needed is only the access address time of the EPROM, which in this case equal to (250 nsec). A computer program reproduced in appendix A.3 was used to generate the data stored in the EPROM. An alternative approach has been developed to combine the sine-weighted signal and the 8-bit/8-bit divider in a single EPROM and is discussed in appendix (C). This method was developed to reduce the amount of hardware involved, but was not finally incorporated.

### 3.8 CONTROL SIGNALS OF THE CONVERTER BRIDGE:

Control signals are needed to drive the switching PWM pulses in the correct sequence to the desired GTO thyristor. Twelve digital signals are required to control the PWM waveform for switching the six-switch converter as shown in fig.(3-19). These signals together with the PWM pattern are combined to form the logic equation as discussed in the next section. The control logic equations for the 6-switch used for this control strategy are illustrated as shown below,

$$Z_1 \quad W_1.W_2 \tag{3.2}$$

$$Z_3 \quad W_3.W_4 \tag{3.3}$$

$$Z_5 \quad W_5.W_6 \tag{3.4}$$

$$Z_4 = W_4.W_5 \tag{3.5}$$

$$Z_6 - W_1.W_6 \tag{3.6}$$

$$Z_2 = W_2.W_3 \tag{3.7}$$

The control logic signals ( $Z_1$ , $Z_3$ , $Z_5$ ), ( $W_1$, $W_3$ , $W_5$ ) are for the positive half of the bridge, and ( $Z_4$, $Z_6$, $Z_2$ ), ( $W_4$ , $W_6$ , $W_2$ ) are for the negative half of the bridge. The signals $W_1$ with $W_4$ form the R-phase leg, where as $W_3$ with $W_6$ form the Y-phase leg, and $W_5$ with $W_2$ form the B-phase leg. The logic signals ( $W_1$ - $W_6$ ), $Z_2$ and $Z_5$ are stored in an EPROM to make the controller easy to implement. The $W_n$ and $Z_n$ address

is determined by the phase shift signal. However, in the next sections these equations are discussed for each type of control.

### 3.9 SIX-SWITCH CONTROL FOR SPWM CURRENT WAVEFORM:

The pulse width modulated signals obtained from the PWM generator need to be combined with some control signals to drive the GTO thyristors in the correct sequence. For the 6-GTOs converter the switching logic equations for the GTO thyristors are described as below:

The switching equations for the positive half of the bridge are,

$$SW_1 \quad Z_2 Y + W_1 \overline{R} + W_4 + Z_5 B \tag{3.8}$$

$$SW_3 \quad Z_1 R + W_3 Y + W_6 + Z_4 B \tag{3.9}$$

$$SW_5 \quad Z_3 Y + W_5 \overline{B} + W_2 + Z_6 R \tag{3.10}$$

and the switching equations for the negative half of the bridge are:

$$SW_4 - Z_2 B + W_4 \overline{R} + W_1 + Z_5 Y \tag{3.11}$$

$$SW_6 = Z_1 B + W_6 \overline{Y} + W_3 + Z_4 R \tag{3.12}$$

$$SW_2 = Z_6 Y + W_2 \overline{B} + W_5 + Z_3 R \tag{3.13}$$

The above logic equations are represented in the diagram shown in fig.(3-19).

The logic signals ( $Z_1$ - $Z_6$ ) each have duration ($\pi$ / 3) of the sine wave cycle. The logic signals ( $W_1$ - $W_6$ ) have duration ($2\pi$ / 3) of the cycle. These logic signals enable the PWM waveform to switch the GTOs at selected time

periods ($2\frac{\pi}{3}/\omega$) and ($\frac{\pi}{3}/\omega$) as shown in fig.(3-20). The control logic signal $W_1$ has logic "1" for a period $2\pi/3$ of the R-phase current when the R-phase voltage is more positive than the other phases and GTO1 is forward biased. This logic signal $W_1$ controls the positive half switch of the R-phase, i.e. GTO1 in the converter bridge. Similarly the control logic signal $W_4$ has logic "1" for a period of $(2\pi/3)$ of the negative half of the cycle of the R-phase voltage, when the R-phase voltage is less negative than the Y and B-phases, ( i.e. $W_4$ is logic "1" for a period of $(2\pi/3)$ shifted by an angle $\pi$ to the left of $W_1$ ). This logic signal is applied to the negative half of the R-phase, and controls GTO4 in the converter bridge.

The control logic signal $Z_5$ has a logic "1" for a period of $(\pi/3)$. This is to fill the gap between $W_1$ and $W_4$, where a certain PWM waveform is combined with them to form a flywheeling action that makes the current sinusoidal at the start of the cycle. Similarly the other logic signal $Z_2$ is the same as $Z_5$, but shifted by $\pi$ to fill the gap between $W_1$ and $W_4$ at the trailing edge in order to complete the flywheeling action for all the current waveform. The other control logic signals ($Z_1$, $Z_4$) are made up in the same sequence, but they are lagging the 1st group by $(2\pi/3)$ for the Y-phase and for ($Z_3$, $Z_6$)by $(4\pi/3)$ for the B-phase to form the 3-phase control.

### 3.10 CONTROL SIGNALS OF 3-SWITCH CONVERTER:

The controller used for the three-switch converter uses the same circuit as for the 6-switch converter used in this work. The 3-switch converter controller is implemented simply by changing the address of the control signals stored in the EPROM. For three-switch converter 9-control logic

signals are needed as shown in fig.(3-21). The control logic signals with the switching signals are shown in the equations below:

$$SW_{14} = Z_2YB + W_{14}\overline{R} + Z_5BY \tag{3.14}$$

$$SW_{36} = Z_1RB + W_{36}\overline{Y} + Z_4BR \tag{3.15}$$

$$SW_{52} - Z_3YR + W_{52}B + Z_6RY \tag{3.16}$$

The switching signal $W_{14}$ has the same function of the combined switching signals $W_1$ , $W_4$ of the 6-GTO converter. Similarly $W_{36}$ and $W_{52}$ have the same function of the switches placed for the Y-phase and the B-phase respectively. This type of control however is limited to a freedom of + 30 in the phase-shift [80].

## 3.11 ANALYSIS AND HARMONIC REDUCTION OF THE PWM WAVEFORM:

### 3.11.1 Modelling of the sine-weighted signal and the carrier triangle waveform:

Twenty-four 8-bit samples are stored in the EPROM per half cycle of the sine wave for each phase, each representing values of the sine function at 7.5° intervals. Then, the sine-weighted signal is compared with a digital triangular wave created by an 8-bit counter. If the first sample is taken at 7.5° then the last sample of the sine-weighted signal (no. 24) will have an amplitude of zero and the shape of the input phase current to the converter will not symmetrical about the zero crossing points (i.e. each 180°). To overcome this an additional sample is added at the middle of the peak of each of the sine-weighted signals in the EPROM, to give the shape of the input

phase current half wave symmetry. This sample is added at 97.5° of the maximum amplitude, thereafter all the samples are shifted to the left (of the 90° point) to keep the same number of samples (24) per half cycle. The sine-weighted signal is thus derived from the formula,

$$v_s = K_{swo} |255 \sin x| \qquad 90° \leq x \leq 7.5° \tag{3.17}$$

$$v_s \quad K_{swo} |255 \sin(x - 7.5)| \qquad 97.5° \geq x \geq 180°$$

Where $K_w$ is a constant used to introduce a minimum pulse width equal to (0.968) and the angle $x$ is defined in degrees between (0° to 180°). In total two half cycles are stored for each phase, i.e. 48 samples per phase.

The instantaneous value of each sample is approximated to the nearest decimal number and converted to a Hex-decimal number to be stored in the EPROM as shown in table ( 3-1 ). A computer program has been written (appendix A.1) to calculate the data for the 3-phase system, as sine-weighted signals to be stored in the EPROM. The experimentally generated signals are shown in section (3.7) where the PM-generator is explained.

The carrier signal is taken from the counter of the frequency multiplier as a sawtooth waveform. This waveform is converted to a triangle waveform by EXOR gates and compared with each individual phase after the 8-bit 8-bit divider. The carrier signal is represented in fig.( 3-22 ). The positive edge of the triangle is described by the line equation,

$$Y_o = 68x - c \tag{3.18}$$

And, the edges with negative slope are represented by the equation,

$$Y_e = -68x + 510 + c \qquad (3.19)$$

Where c is a constant which changes with the edge number ( m ) of the triangle in the sequence (0, 510, 1020, 1530, ....).

The switching angles are determined by the intersection of the sine-weighted signal and the triangle waveforms. These are then calculated from the above equations after re-arranging as a function of amplitude. Therefore, eqns.(3.18 and 3.19) will be

$$x_o \quad \frac{1}{68} Y + (n \quad 1)7.5 \qquad (n = 1,2,3,.....,24) \qquad (3.20)$$

$$x_e \quad \frac{1}{68} Y + 7.5 + (n \quad 1)7.5 \qquad (n = 1,2,3,.....,24) \qquad (3.21)$$

Where $n$ is the number of the sample of the sine-weighted signal and $Y$ is the sample value expressed as an integer lying between 0 and 255. Table ( 3-2) lists the intersection angles of the two signals of the R-phase stored in the EPROM and the carrier signal for m = 0.95. The other two phases have the same intersection angles, but shifted 120° and 240° from the R-phase respectively.

### 3.11.2 Line current harmonic analysis:

In this section the analysis and the reduction of the harmonic content of the a.c. line current $i_{a2}$ of the proposed PWM, GTO current source converter is discussed, and in particular a method for eliminating the 5th harmonic from the frequency spectrum of the line current is presented. The

harmonic analysis of the line current waveform of a current source converter is useful for many purposes. Firstly, the determination of the harmonic content gives a qualitative estimation of the additional harmonic loss in the generator, and the likely interference caused to the a.c. supply. Secondly, it gives an indication of the size of the filter to be installed on the a.c. side.

The switching devices in any converter operating at high frequencies result in a non-sinusoidal currents being drawn from the a.c. network. Therefore, the load can be a harmonic generator which transmits harmonic power back into the a.c. network. The harmonics of low order, if high enough may cause disturbance in the a.c. network and connection of a converter of such type to the a.c. network is restricted, or may increase losses in the case of connection to a generator. The presence of harmonics can distort the supply waveforms and cause problems such as radio interference where the supply line acts as a high-frequency transmitting aerial, and causes losses in other systems connected to the a.c. network. Some solutions to be taken into consideration are the placing of filters at the input terminals of the converter to bypass the high frequencies, or by using complex circuits to modify the switching of the converters to remove the low order harmonics. The 5th harmonic is the dominant harmonic in the line current frequency spectrum. This can be eliminated by a certain simple technique, that will be discussed in the next section.

The harmonic content in the current waveform $i_{a2}$ of the converter is calculated with reference to fig.(3-23). This waveform is a periodic PWM pattern, and it is represented by a Fourier series [98, 99] in terms of its switching angles as follows:

$$i_{a2}(\omega t) = \frac{1}{2} a_o + \sum_{n=1}^{\infty} a_n \cos \omega t + \sum_{n=1}^{\infty} b_n \sin \omega t \qquad (3.22)$$

where, $(\frac{1}{2} a_o)$ is the average d.c. value for the current waveform and would be expected to be zero.

$$a_n - \frac{1}{\pi} \int_0^{2\pi} i_{a2}(\omega t) \cos n\omega t \, d(\omega t) \qquad (3.23)$$

$$b_n \quad \frac{1}{\pi} \int_0^{2\pi} i_{a2}(\omega t) \sin n\omega t \, d(\omega t) \qquad (3.24)$$

The line current waveform is redrawn in fig.(3-23) to show the switching angles more clearly. This waveform is a periodic function of $i_{a2}(\omega t)$, which has half-wave symmetry since,

$$i_{a2}(\omega t) \quad -f(\omega t + \pi) \qquad (3.25)$$

Therefore, the Fourier series coefficients of the waveform are given as follows:

For n odd:

$$a_n - \frac{2}{\pi} \int_o^{\pi} i_{a2}(\omega t) \cos n\omega t \, d(\omega t) \qquad (3.26)$$

$$b_n = \frac{2}{\pi} \int_o^{\pi} i_{a2}(\omega t) \sin n\omega t \, d(\omega t) \qquad (3.27)$$

For n even:

$$a_n = 0$$

$$b_n - 0$$

Expanding equations (3.26 and 3.27) for all the waveform pulses,

$$a_n \quad \frac{2I_{dc}}{\pi}\left[\int_{x_1}^{x_2} \cos n\omega t\, d\omega t + \int_{x_3}^{x_4} \cos n\omega t\, d\omega t + \ldots\ldots + \int_{x_k}^{x_{(k-1)}} \cos n\omega t\, d\omega t\right]$$

$$b_n \quad \frac{2I_{dc}}{\pi}\left[\int_{x_1}^{x_2} \sin n\omega t\, d\omega t + \int_{x_3}^{x_4} \sin n\omega t\, d\omega t + \ldots\ldots + \int_{x_k}^{x_{(k\ 1)}} \sin n\omega t\, d\omega t\right]$$

Where k is the number of switching points per half cycle of the current waveform and it is equal to (66). This number is increased for the current waveform from 48 points to 66 because of the flywheel periods introduced by the converter operation. Therefore for K = 66 ,

$$a_n \quad \frac{2I_{dc}}{\pi n}\left[\sin nx_2 - \sin nx_1 + \sin nx_4 - \sin nx_3 + \ldots\ldots + \sin nx_k - \sin nx_{(k-1)}\right]$$

$$b_n - \frac{2I_{dc}}{\pi n}\left[\cos nx_1 - \cos nx_2 + \cos nx_3 - \cos nx_4 + \ldots\ldots + \cos nx_{(k-1)} - \cos nx_k\right]$$

Then,

$$a_n = \frac{2I_{dc}}{\pi n}\sum_{i=1}^{66}(-1)^i \sin(nx_i)$$

$$b_n = \frac{2I_{dc}}{\pi n} \sum_{i-1}^{66} (-1)^{(i+1)} \cos(nx_i) \tag{3.28}$$

The $a_n$ coefficient is found equal to zero when both halves of the full cycle are symmetrical about 180°. Therefore, replacing ($b_n$) by $I_{a2}$ , the amplitude of the nth harmonic of the a.c. line current is given by:

$$I_{a2} - \frac{2I_{dc}}{\pi} \sum_{n\ 1}^{\infty} \frac{1}{n} \sum_{i-1}^{66} (-1)^{(i+1)} \cos(nx_i) \tag{3.29}$$

Equation (3.29) represents the amplitude of the nth harmonic of the line current at unity power-factor. The angle (α) is added to the equation to include the phase shift between the line current $i_{a2}$ and the phase voltage of the converter ($V_{ip}$), and includes $a_n$ coefficient, though α has no effect on the harmonic content, so the current equation will be,

$$I_{a2} = \frac{2I_{dc}}{\pi} \sqrt{\left[\sum_{n=1}^{\infty} \frac{1}{n} \sum_{i=1}^{66} (-1)^{(i+1)} \cos(nx_i + \alpha)\right]^2 + \left[\sum_{n=1}^{\infty} \frac{1}{n} \sum_{i=1}^{66} (-1)^{i} \sin(nx_i + \alpha)\right]^2} \tag{3.30}$$

A computer Fortran program has been developed to find the values of the switching angles, and to carry out the harmonic analyses in the input a.c. line current ($i_{a2}$) [appendix A.2]. Table(3-3) shows the theoretical and the experimental results of the harmonic content in $i_{a2}$ . A very small value of

some second-order harmonics are appeared in the experimental results. This is due to the presence of small d.c. component added to the a.c. current measurement by the current transducer used. In the theoretical model the values of the second-order harmonics exist, but in a very small amount which can be neglected. Fig(3-24a) shows the frequency spectrum of ($i_{a2}$). The 3rd harmonic appears to a small degree in the frequency spectrum, this is due to the imbalance of the filter capacitors, resulting from finite capacitor tolerances. The 5th harmonic appears as the only predominant harmonic in the frequency spectrum shown in fig.(3-24a), therefore, the modification has carried out in the stored sine-weighted signal has improved the frequency spectrum to an acceptable level.

**3.11.2a Harmonic minimisation:**

The harmonic content in the a.c. line current of the converter is minimised to an acceptable level as shown in table (3-4). The 5th harmonic has been reduced from -27 dBv to -68.8 dBv, which is a more acceptable level. Fig.(3-24b) shows the frequency spectrum of the reduced line current harmonics. The harmonic minimisation has been achieved by adding the 3rd harmonic in a certain ratio to the sine-weighted signal. The amount of harmonic added to the signal is very small, and will be cancelled by the 3-phase connection. The sine-weighted signal stored in the EPROM after adding the 3rd harmonic is,

$$i_{a2}(\omega t) - 247k_{sw}[\sin \omega t - (0.028)\sin(3\omega t - 60)] \qquad (3.31)$$

Where ( $k_{sw}$ ) is a constant used for pulse limit protection and it is equal to (0.985).

### 3.11.2b Harmonic content with respect to modulation index :

The harmonic content in the a.c. line current $i_{a2}$ remains small, even as the modulation index is reduced. For the present design fig.(3-25) shows all the low order harmonics are reduced with the reduction of the modulation index ( M ) except for the 7th harmonic which is increased, but the increase is very small keeping it within an acceptable level. For example at M = 0.1, the amplitude of the 7th harmonic will be (-45 dBv), which represents (0.56% ) of the fundamental component of the line current $i_{a2}$. Table (3-5) shows the harmonics with respect to (M).

## 3.12 CONVERTER PERFORMANCE AND CHARACTERISTICS:

In conventional 6-pulse converters, the output d.c. voltage of the converter can be controlled only by varying its delay angle. But in the present work the output d.c. voltage ($V_{dc}$) of the converter can be regulated by changing the delay angle ($\alpha$) or by reducing the modulation index ( M )of the PWM signal. The output d.c. voltage is decreased, when the delay angle ($\alpha$) is changed from 0° to 90° leading or 90 ° lagging as shown in fig.(3-26). This figure shows the experimental results of the output d.c. voltage ($V_{dc}$) versus the delay angle for different values of the modulation index. Here it can be seen that even at low modulation index the output voltage has a cosine function with respect to the delay angle ( $\alpha$ ). Consequently the output d.c. voltage can be represented approximately in terms of ( $\alpha$ ) and ( M ) by the mathematical expression;

$$V_{dc} = \frac{3\sqrt{2}}{\pi} M V_{tcl} \cos \alpha \qquad (3.32)$$

Where $V_{tcl}$ is the line to line terminal voltage.

For a constant delay angle and variable modulation index, ($V_{dc}$) is plotted as shown in fig.(3-27). The relationship between the output d.c. voltage and the modulation index is linear. Fig.(3-27a) shows ($V_{dc}$) versus ( M ) for lagging delay angle, While in fig.(3-27b) is plotted for leading delay angle.

The experimental waveforms of the output voltage and the input line current are shown in fig.(3-28). Fig.(3-28a) shows 30° lagging phase-shift between the phase voltage and phase current, and fig.(3-28b) shows a phase-shift of 30 leading. In addition figs.(3-29 and 3-30) show the PWM pulses experimentally with both input and output voltage, and current. Fig.(3-29) shows the experimental waveforms of the output d.c. voltage, and the PWM gate signals. Finally fig.(3-30) shows the experimental waveforms of the gate pulses and the input a.c. line current and voltage. The a.c. current has an (rms) value of 4.0 Amp.

The fundamental component of the converter input current $i_{a2f}$ is derived from the phasor diagram shown in fig.(3-31b). Therefore, it may be calculated from the formula

$$i_{a2f} = \sqrt{{i_{a1f}}^2 - 2 i_{a1f} i_{cf} \sin \phi + {i_{cf}}^2} \qquad (3.33)$$

where $i_{a1f}$ is the fundamental component of the line current before the filter , $i_{cf}$ is the fundamental component of the capacitor current, and $\phi$ is the power-factor angle. The fundamental component of the input a.c. current

$i_{a2f}$ versus output d.c. current is plotted as shown in fig.(3-32). The results plotted in this figure are obtained by connecting the converter to the main a.c. network, and shows both the measured input a.c. currents before and after the capacitor filter as a function of the output d.c. current. The linear relationship between them and the output d.c. current indicates the linearity of the system.

### 3.13 OUTPUT POWER AND EFFICIENCY:

High efficiency was achieved from the 1.6 kWatt prototype PWM GTO converter as shown in fig.(3-33). The peak efficiency of the converter is 94.4%, and high efficiency is obtained even at low output power. The efficiency of larger power converters of similar design would be expected to be even higher. In addition the efficiency of the converter has been measured for a constant output d.c. current ($I_{d.c.} = 1 Amp$) for different delay angles ranging from -90 lagging to 90 leading and different modulation index, as shown in fig.(3-34). These characteristics demonstrate that high efficiency is obtained even at a low modulation index and large delay angle. The output power increases linearly with the output d.c. current for constant input frequency as shown in fig.(3-33).

| Data X (Hex.) | Data Y (Hex.) | Data Z (Hex.) |
|---|---|---|
| BC | ED | 42 |
| A7 | F6 | 5D |
| 90 | F7 | 78 |
| 78 | F7 | 90 |
| 5D | F6 | A7 |
| 42 | ED | BC |
| 25 | DF | CF |
| 25 | CF | DF |
| 42 | BC | EF |
| 5D | A7 | F6 |
| 78 | 90 | F7 |
| 90 | 78 | F7 |
| A7 | 5D | F6 |
| BC | 42 | ED |
| CF | 25 | DF |
| DF | 25 | CF |

**Table (3-1)**
**The sine weighted data stored in the EPROM.**

| Pulse no. | Pulse margin | Intersection angle | | Pulse width |
|---|---|---|---|---|
| (m) | (degree) | Order no. | Degree | (degree) |
| 1 | 0.0°-7.5° | 1 | 0.47° | 6.559° |
| | | 2 | 7.029° | |
| 2 | 7.5°-15° | 3 | 8.455° | 5.589° |
| | | 4 | 14.044° | |
| 3 | 15°-22.5° | 5 | 16.426° | 4.647° |
| | | 6 | 21.073° | |
| 4 | 22.5°-30° | 7 | 24.367° | 3.765° |
| | | 8 | 28.132° | |
| 5 | 30 -37.7° | 9 | 32.264° | 2.971° |
| | | 10 | 35.235° | |
| 6 | 37.5 -45 | 11 | 40.132° | 2.235° |
| | | 12 | 42.367° | |
| 7 | 45 -52.5 | 13 | 47.955° | 1.589° |
| | | 14 | 49.544° | |
| 8 | 52.5 -60 | 15 | 55.735° | 1.029° |
| | | 16 | 56.764° | |
| 9 | 60 -67.5 | 17 | 63.455° | 0.589° |
| | | 18 | 64.044° | |
| 10 | 67.5 -75 | 19 | 71.102° | 0.295° |
| | | 20 | 71.397° | |
| 11 | 75 -82.5 | 21 | 78.617 | 0.265° |
| | | 22 | 78.882 | |
| 12 | 82.5 -90 | 23 | 86.117° | 0.265° |
| | | 24 | 86.382° | |
| 13 | 90 -97.5 | 25 | 93.617° | 0.265° |
| | | 26 | 93.882° | |
| 14 | 97.5 -105 | 27 | 101.117° | 0.265° |
| | | 28 | 101.382° | |
| 15 | 105 -112.5 | 29 | 108.602° | 0.295° |
| | | 30 | 108.897° | |
| 16 | 112.5 -120 | 31 | 115.955° | 0.589° |
| | | 32 | 116.544° | |
| 17 | 120 -127.5 | 33 | 123.235° | 1.029° |
| | | 34 | 124.264° | |
| 18 | 127.5 -135 | 35 | 130.455 | 1.589° |
| | | 36 | 132.044° | |
| 19 | 135 -142.5 | 37 | 137.632° | 2.235° |
| | | 38 | 139.867° | |
| 20 | 142.5 -150 | 39 | 144.764 | 2.971° |
| | | 40 | 147.735° | |
| 21 | 150 -157.5 | 41 | 151.867° | 3.765° |
| | | 42 | 155.632° | |
| 22 | 157.5 -165 | 43 | 158.926° | 4.647° |
| | | 44 | 163.573° | |
| 23 | 165 -172.5° | 45 | 165.955° | 5.589° |
| | | 46 | 171.544° | |
| 24 | 172.5 -180° | 47 | 172.970° | 6.559° |
| | | 48 | 179.529° | |

**Table (3-2)**
**The intersection angles of the sine-weighted signal with the carrier signal.**
**[ modulation depth M = 0.95 ]**

| Harmonic order no. (n) | f (Hz) | Experimental Amplitude (dBv) | Theoretical Amplitude (dBv) |
|---|---|---|---|
| 1 | 50 | 0.0 | 0.0 |
| 2 | 100 | -59.2 | -122.1 |
| 3 | 150 | -43.5 | -109.3 |
| 4 | 200 | -60.3 | -108.4 |
| 5 | 250 | -27.0 | -27.69 |
| 7 | 350 | -43.2 | -43.10 |
| 9 | 450 | -51.1 | -135.7 |
| 11 | 550 | -37.4 | -37.83 |
| 13 | 650 | -46.0 | -44.96 |
| 17 | 850 | -47.2 | -52.64 |
| 19 | 950 | -47.1 | -51.31 |
| 21 | 1.05k | -52.9 | -149.7 |
| 22 | 1.10k | -59.4 | -118.3 |
| 23 | 1.15k | -37.6 | -39.30 |
| 24 | 1.20k | -56.1 | -101.4 |
| 25 | 1.25k | -38.5 | -37.18 |
| 26 | 1.30k | -60.2 | -111.2 |
| 27 | 1.35k | -45.5 | -130.8 |
| 28 | 1.40k | -53.4 | -129.3 |
| 29 | 1.45k | -33.4 | -34.69 |
| 30 | 1.50k | -50.6 | -121.8 |
| 31 | 1.55k | -34.3 | -31.92 |
| 32 | 1.60k | -53.6 | -119.3 |
| 33 | 1.65k | -39.2 | -115.5 |
| 34 | 1.70k | -47.0 | -125.4 |
| 35 | 1.75k | -28.5 | -28.74 |
| 36 | 1.80k | -44.7 | -103.6 |
| 37 | 1.85k | -31.0 | -27.20 |
| 38 | 1.90k | -45.1 | -111.3 |
| 39 | 1.95k | -29.9 | -115.3 |
| 40 | 2.00k | -38.3 | -121.9 |
| 41 | 2.05k | -20.5 | -19.67 |
| 42 | 2.10k | -37.0 | -109.8 |
| 43 | 2.15k | -21.7 | -17.50 |
| 44 | 2.20k | -49.0 | -104.7 |
| 45 | 2.25k | -28.5 | -110.1 |
| 46 | 2.30k | -46.9 | -104.5 |
| 47 | 2.35k | -30.0 | -23.37 |
| 48 | 2.40k | -41.0 | -120.7 |
| 49 | 2.45k | -19.5 | -18.94 |

**Table (3-3)**
**Frequency spectra of the a.c. line current $i_{a2}$ without harmonic minimisation. [ modulation depth M = 0.95 ]**

| Harmonic order no. (n) | f (Hz) | Experimental Amplitude (dBv) | Theoretical Amplitude (dBv) |
|---|---|---|---|
| 1 | 50 | 0.0 | 0.0 |
| 2 | 100 | -63.9 | ------ |
| 3 | 150 | -44.0 | ------ |
| 4 | 200 | -65.4 | ------ |
| 5 | 250 | -68.8 | -71.43 |
| 7 | 350 | -53.5 | -53.24 |
| 9 | 450 | -64.3 | ------ |
| 11 | 550 | -50.1 | -50.68 |
| 13 | 650 | -53.5 | -49.55 |
| 15 | 750 | -50.5 | ------ |
| 17 | 850 | -39.6 | -42.00 |
| 19 | 950 | -40.7 | -39.74 |
| 21 | 1.05k | -43.9 | -36.70 |
| 22 | 1.10k | ----- | ------ |
| 23 | 1.15k | -34.3 | -36.70 |
| 24 | 1.20k | -69.0 | ------ |
| 25 | 1.25k | -38.1 | -35.13 |
| 26 | 1.30k | ----- | ------ |
| 27 | 1.35k | -37.5 | ------ |
| 28 | 1.40k | -66.3 | ------ |
| 29 | 1.45k | -30.0 | -31.92 |
| 30 | 1.50k | -65.0 | ------ |
| 31 | 1.55k | -36.0 | -30.47 |
| 32 | 1.60k | -69.7 | ------ |
| 33 | 1.65k | -31.6 | ------ |
| 34 | 1.70k | -59.2 | ------ |
| 35 | 1.75k | -25.3 | -27.25 |
| 36 | 1.80k | -59.1 | ------ |
| 37 | 1.85k | -32.3 | -25.03 |
| 38 | 1.90k | -57.3 | ------ |
| 39 | 1.95k | -23.0 | ------ |
| 40 | 2.00k | -49.2 | ------ |
| 41 | 2.05k | -16.8 | -19.83 |
| 42 | 2.10k | -48.3 | ------ |
| 43 | 2.15k | -21.5 | -15.47 |
| 44 | 2.20k | -64.5 | ------ |
| 45 | 2.25k | -21.2 | ------ |
| 46 | 2.30k | -61.8 | ------ |
| 47 | 2.35k | -47.5 | -19.33 |
| 48 | 2.40k | -52.5 | ------ |
| 49 | 2.45k | -18.6 | -16.21 |

**Table (3-4)**

**Frequency spectra of the a.c. line current $i_{a2}$ after adding the 3rd harmonic to the signal.**

| Modulation index M | 5th Har. (dBv) | 7th Har. (dBv) | 11th Har. (dBv) | 13th Har. (dBv) | 17th Har. (dBv) |
|---|---|---|---|---|---|
| 0.95 | -71.43 | -53.24 | -50.68 | -49.55 | -42.00 |
| 0.90 | -70.24 | -53.17 | -50.82 | -49.68 | -42.13 |
| 0.80 | -82.23 | -52.04 | -57.86 | -49.73 | -42.54 |
| 0.70 | -79.19 | -52.00 | -52.56 | -51.40 | -43.15 |
| 0.60 | -79.06 | -51.09 | -54.45 | -53.22 | -44.16 |
| 0.50 | -67.63 | -50.00 | -57.69 | -56.34 | -45.59 |
| 0.40 | -61.93 | -48.77 | -64.24 | -62.88 | -47.70 |
| 0.30 | -57.87 | -47.56 | -72.80 | -73.64 | -51.11 |
| 0.20 | -54.79 | -46.36 | -58.54 | -57.92 | -57.35 |
| 0.10 | -52.01 | -45.26 | -52.82 | -52.07 | ------ |

Table (3-5)

**The low order harmonics in the a.c. line current $i_{a2}$ with respect to modulation index.**

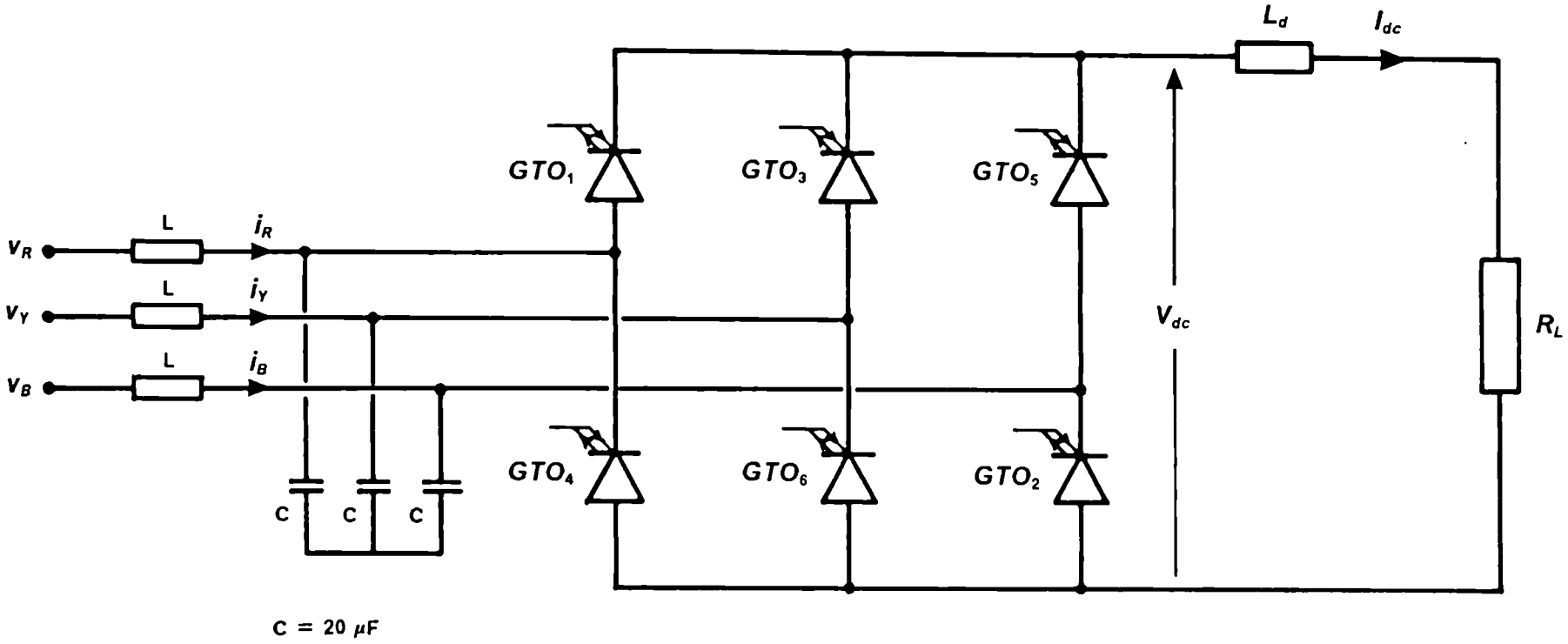


Fig.(3-1) GTO converter bridge circuit.

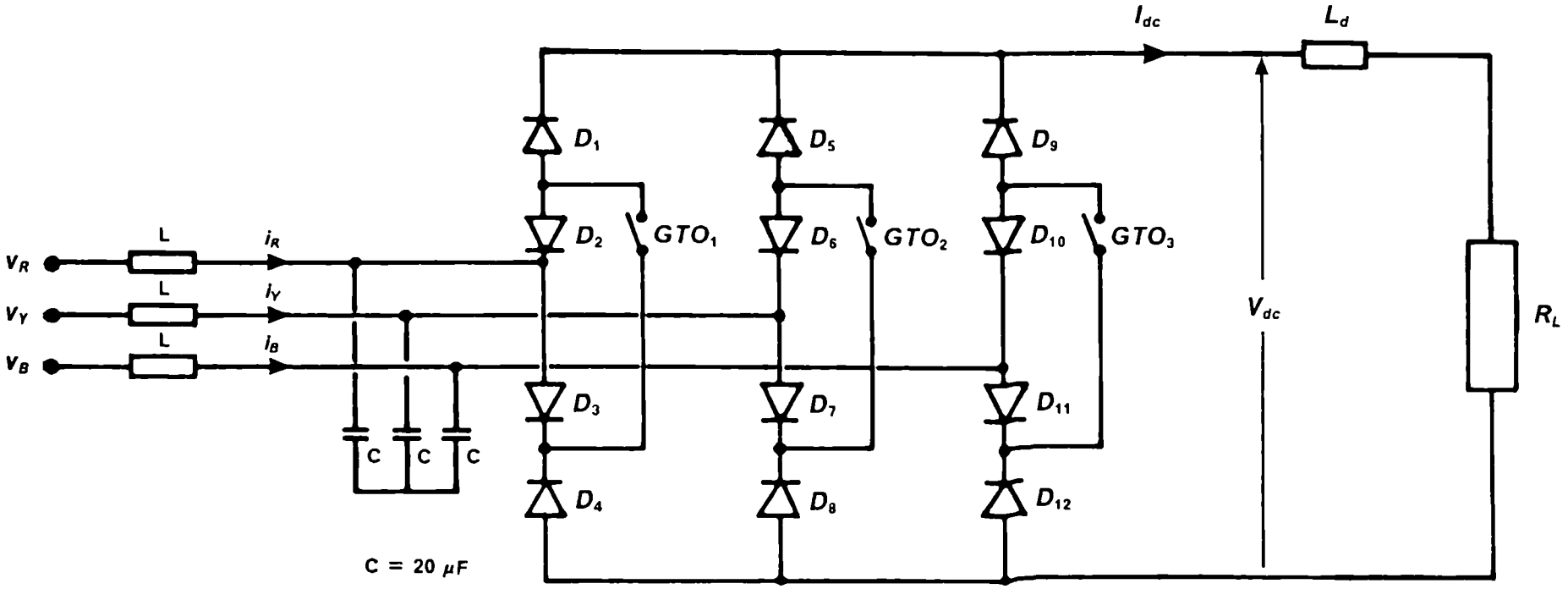


Fig.(3-2) Three-switch fully controlled a.c./d.c. rectifier.

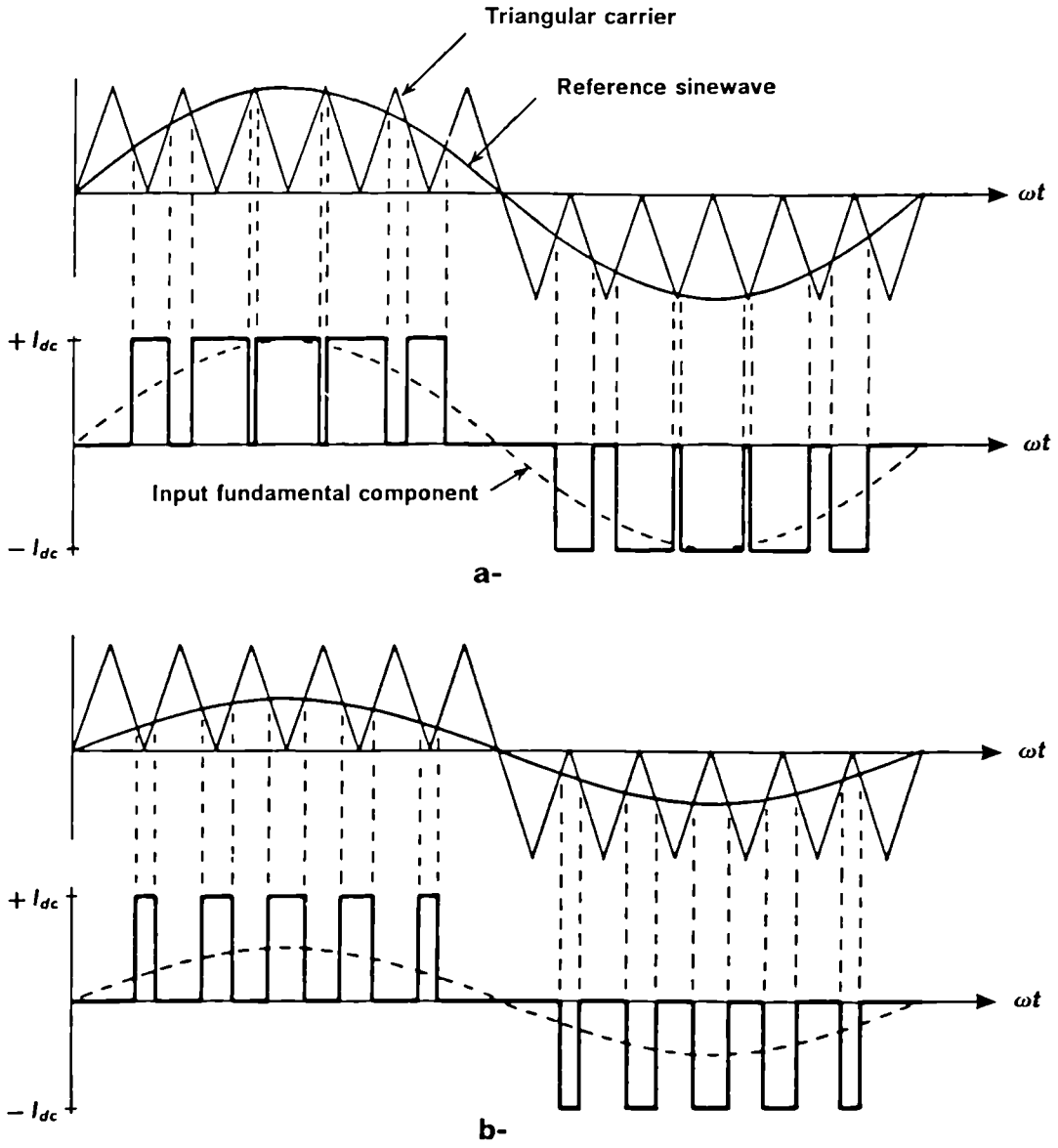


Fig.(3-3) Uniform sampling pulse width modulation.

a- At maximum modulation index.
b- At half modulation index.

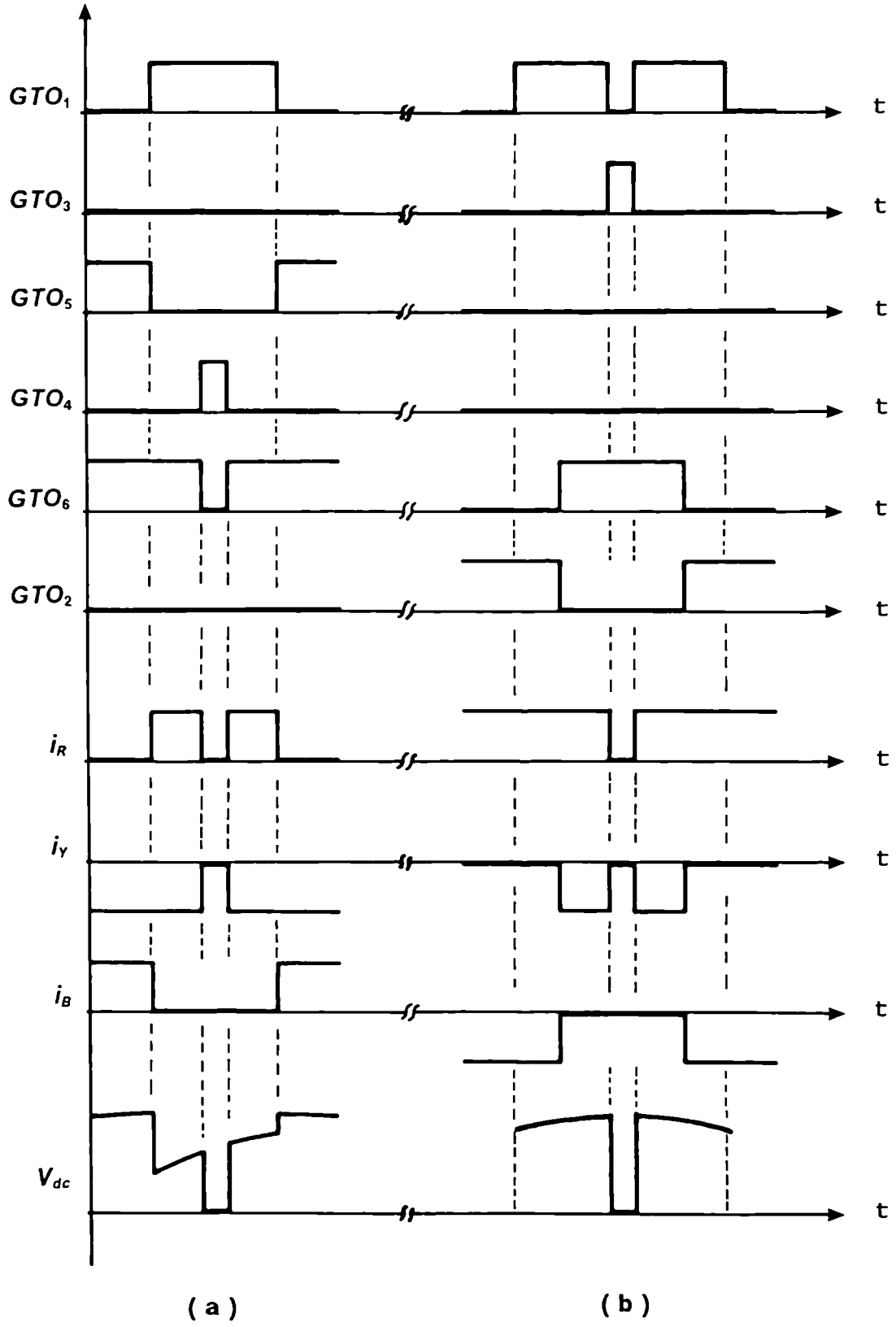


Fig.(3-4) GTO gate Signals and output d.c. voltage.
a- First Sample of each gate from the pulse pattern.
b- Middle sample of each gate from the pulse pattern.

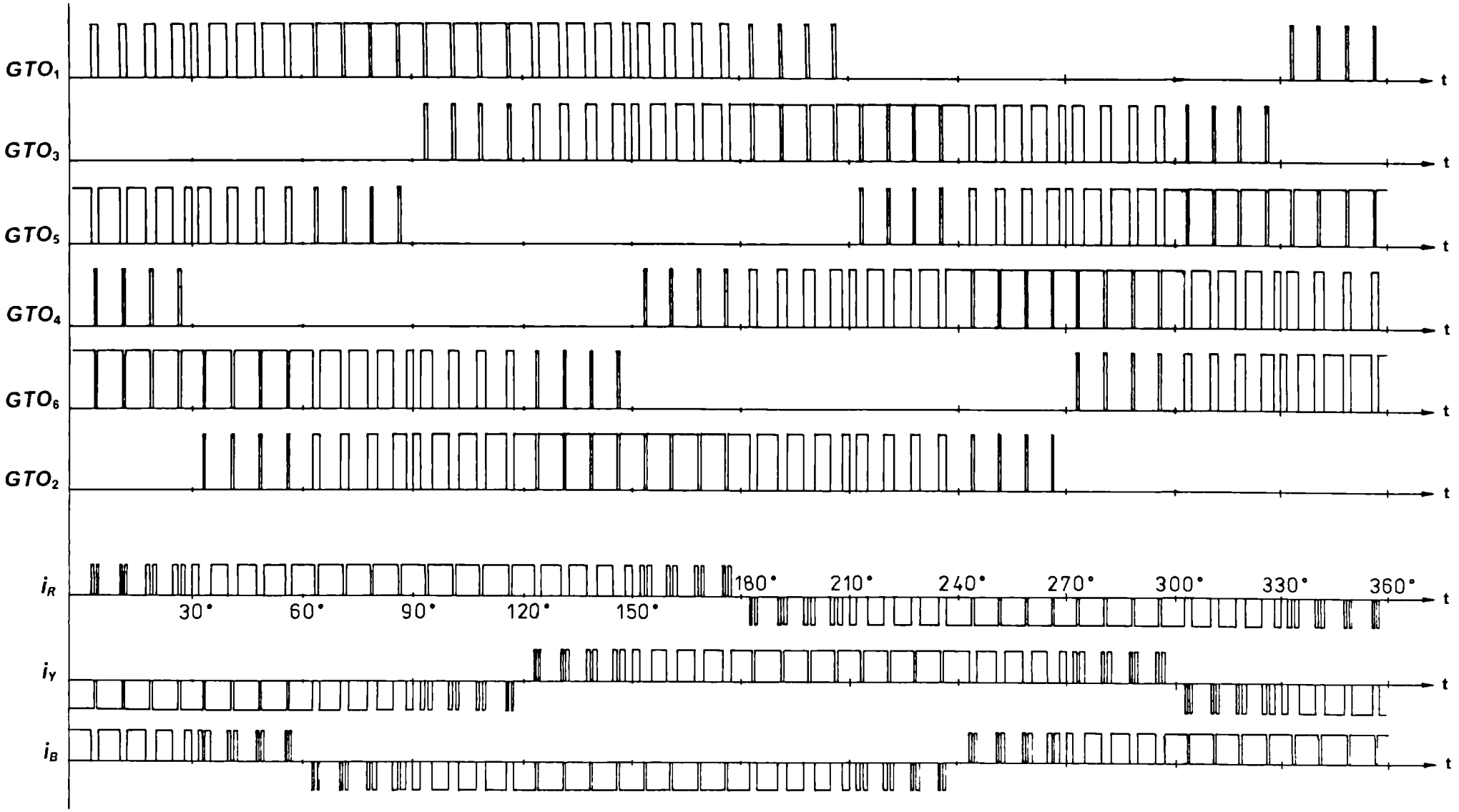


**Fig.(3-5) PWM gate pulses and the 3-phase current waveforms.**

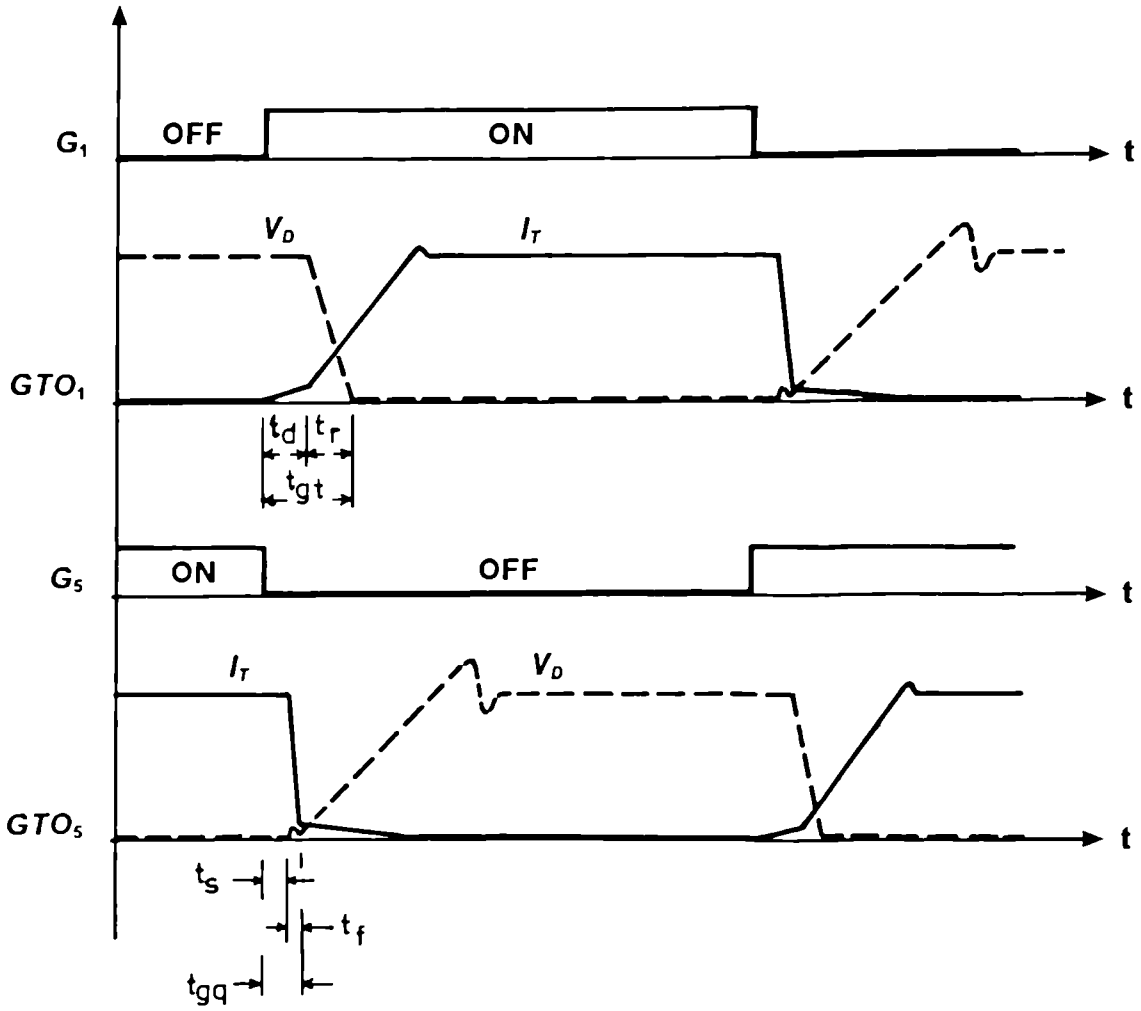


$t_d = 0.25\mu sec$ $t_s = 0.5\mu sec$

$t_r = 1.0\mu sec$ $t_f = 0.25\mu sec$

$t_{gt} = 1.25\mu sec$ $t_{gq} = 0.75\mu sec$

**Fig.(3-6) Switching characteristics of two GTOs at the same half of the bridge.**

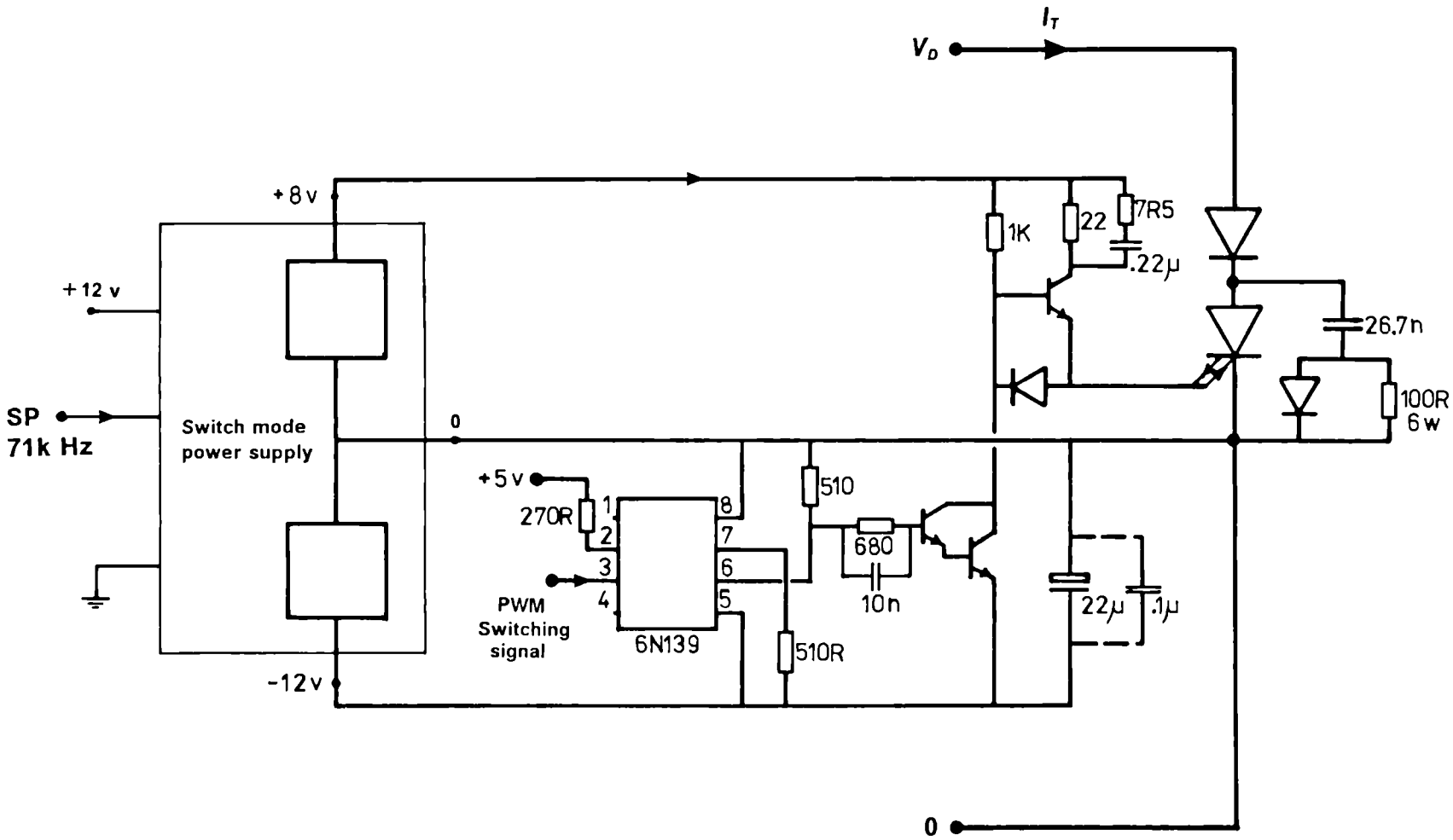


**Fig.(3-7) GTO gate drive circuit.**

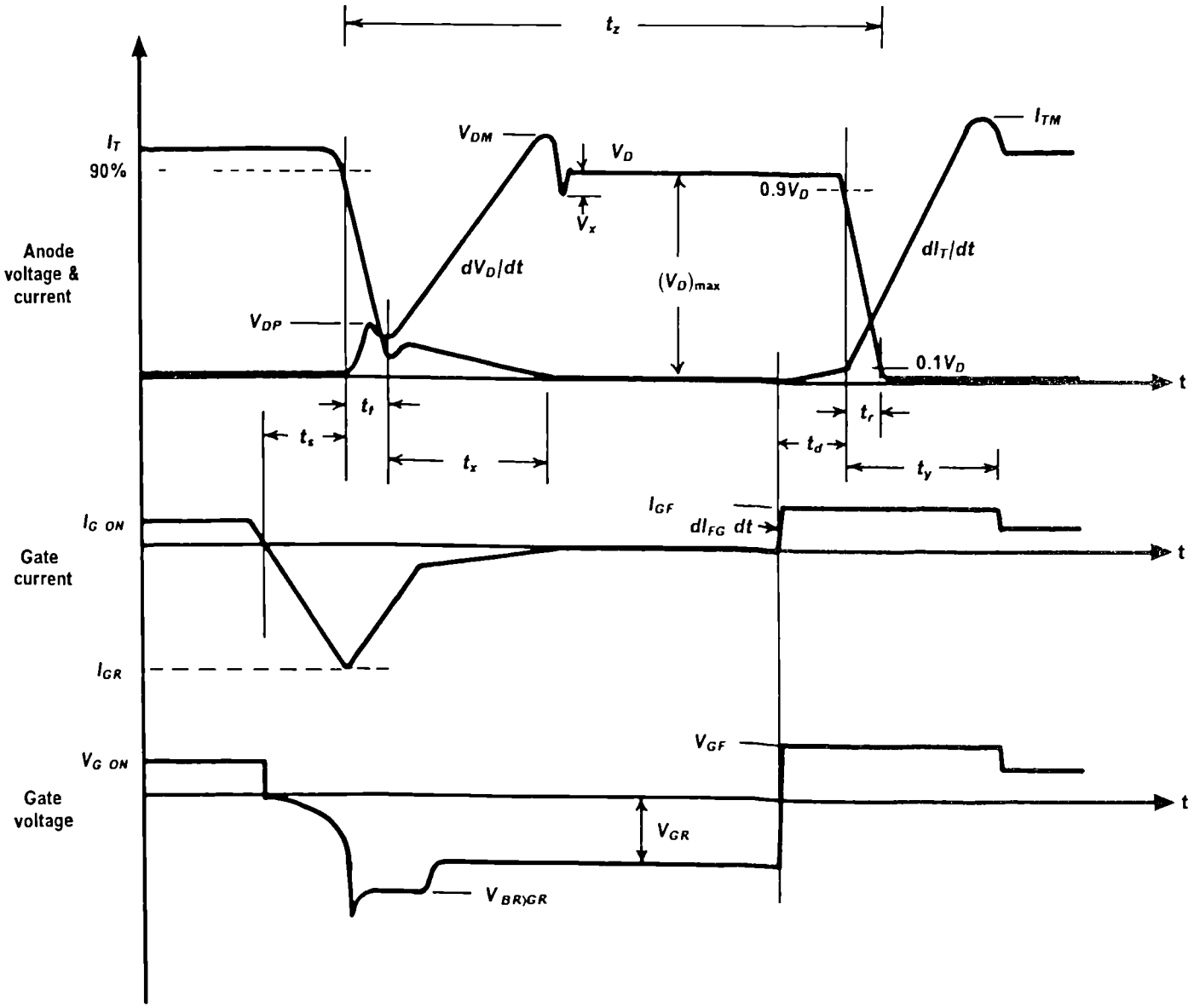


Fig.(3-8) Recommended gating conditions of the GTO thyristor.

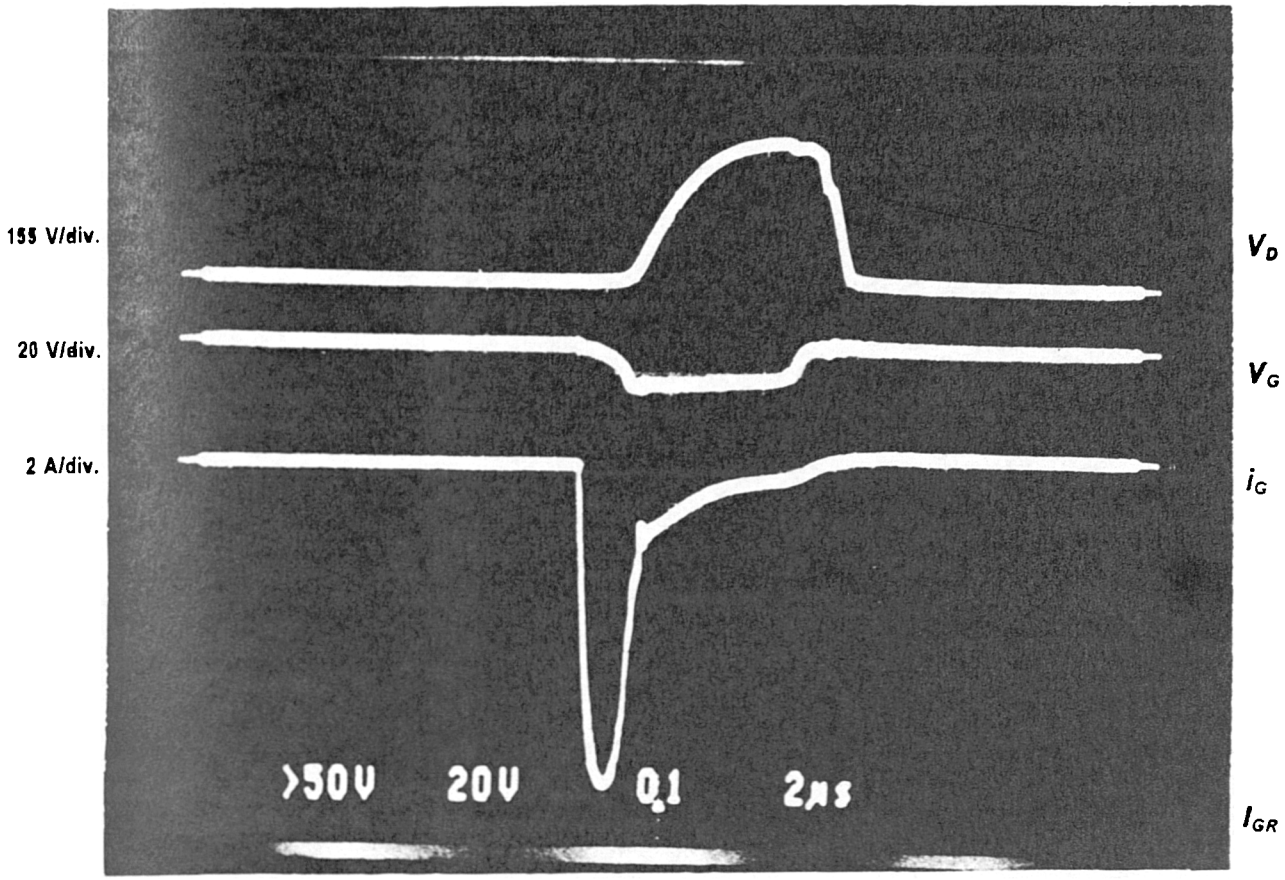


Fig.(3-9) Gate drive voltage and current of the GTO thyristor at [ $V_D = 230$ *Volt*, $I_T = 10$ *Amp* ]

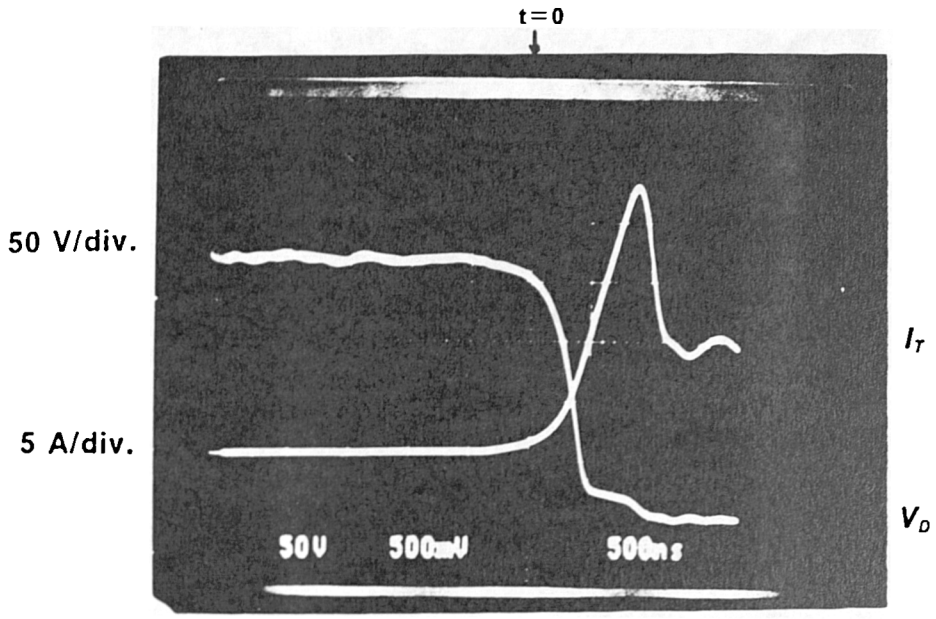


a- Turn on [ $t_d = 0.25\mu s$, $t_r = 0.7\mu s$ ].

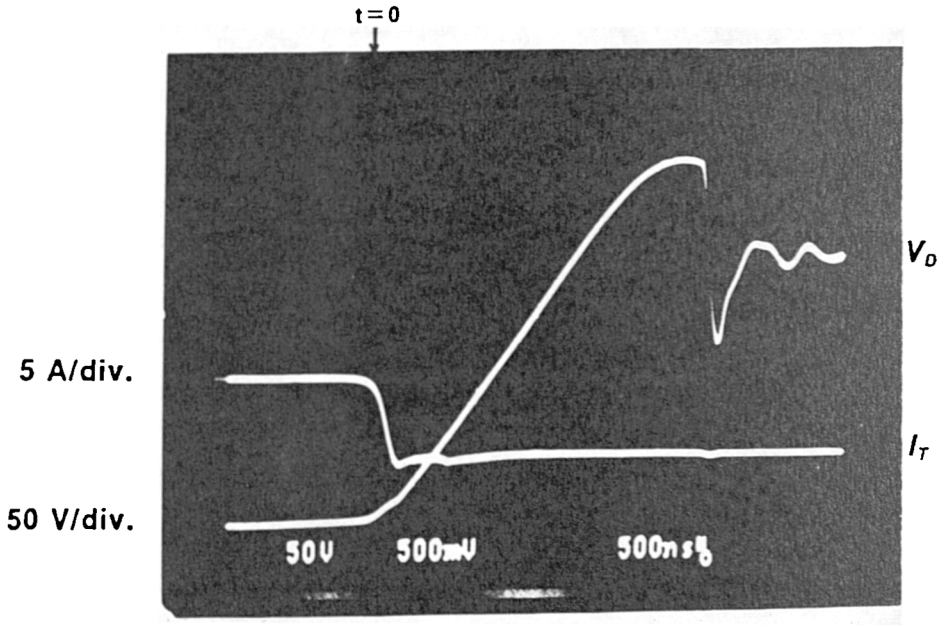


b- Turn off [ $t_f = 0.25\mu s$, $t_s = 1.0\mu s$ ].

**Fig.(3-10) Anode voltage and current of the GTO thyristor at f= 7.8 kHz, $V_D$ = 220 volt, and $I_{T(av.)}$ = 10 amp.**

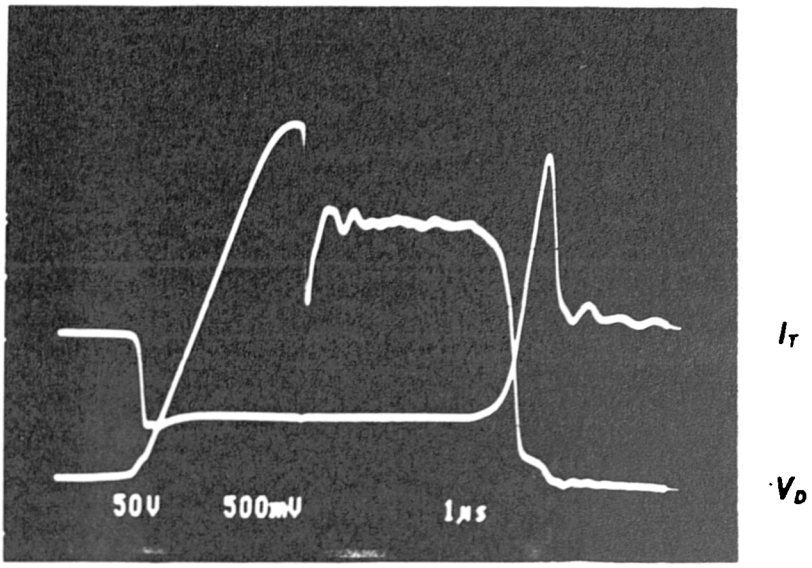


a- Anode voltage and current for 95% of the switching cycle.

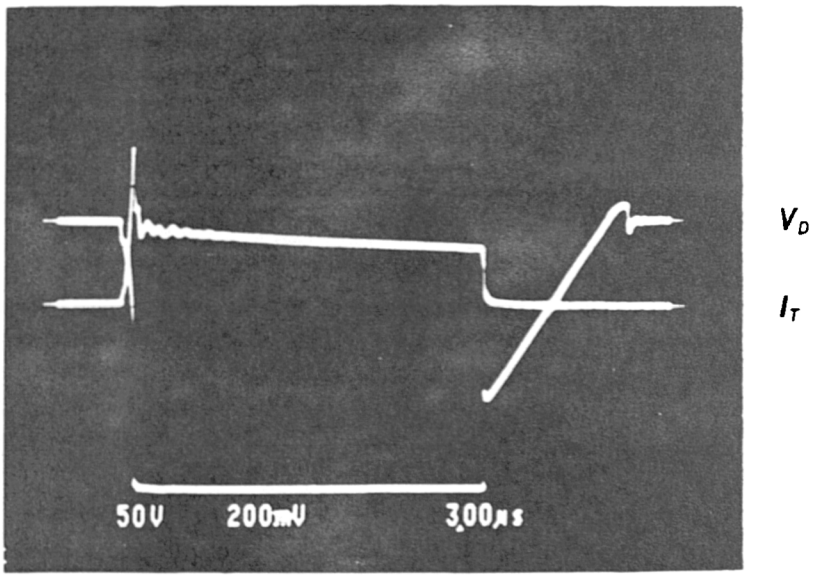


b- Anode voltage and current for 14% of the switching cycle.

Fig.(3-11) Switching characteristics of the GTO thyristor.

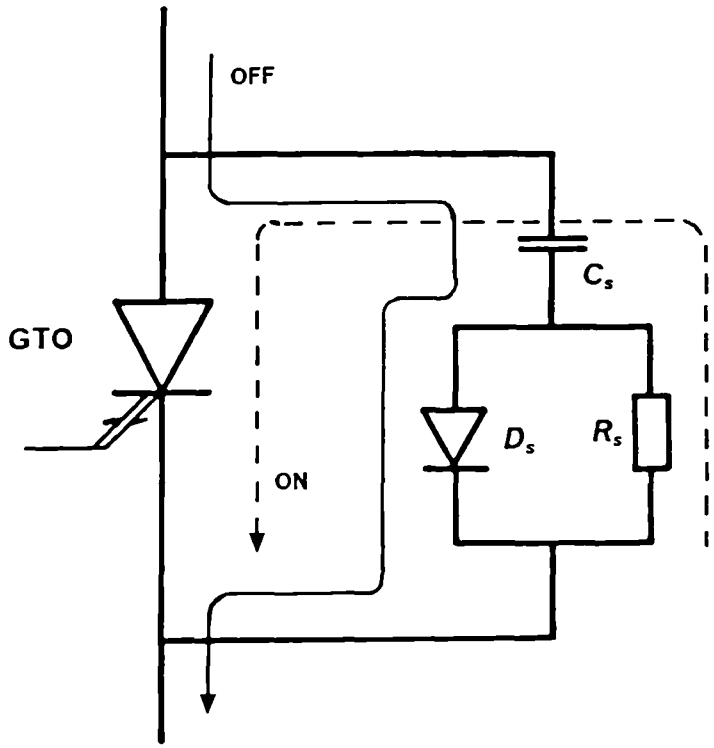


Fig.(3-12) RCD switching aid circuit.

Fig.(3-13) Experimental layout of the GTO board module.

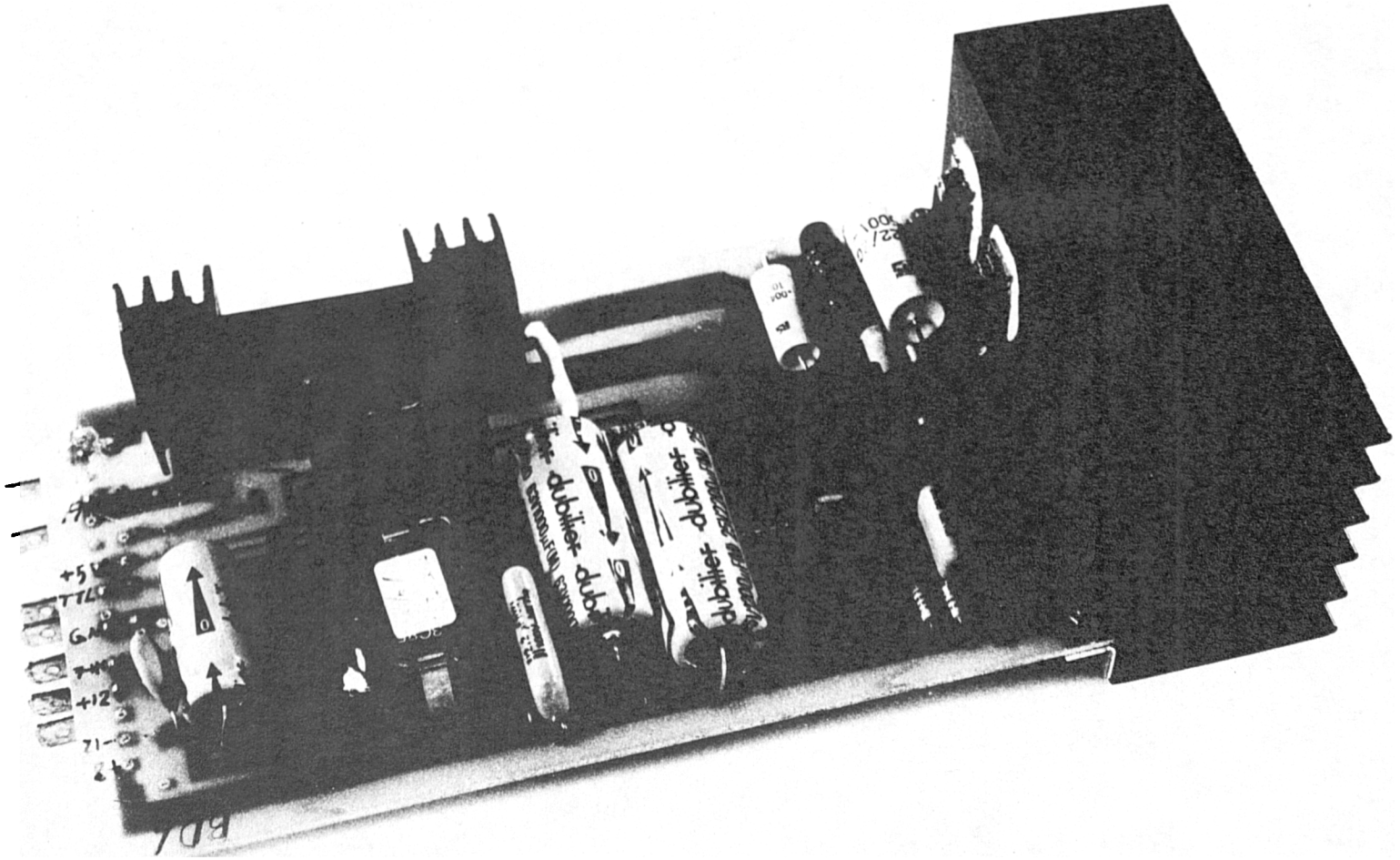

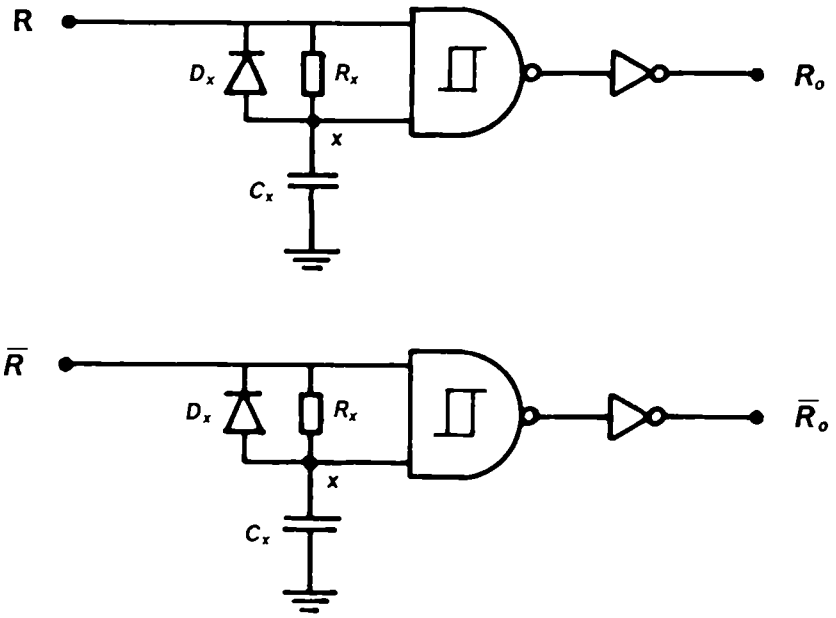


$R_x$ = 1 k Ω, $C_x$= 1 nF.

a- Circuit diagram.

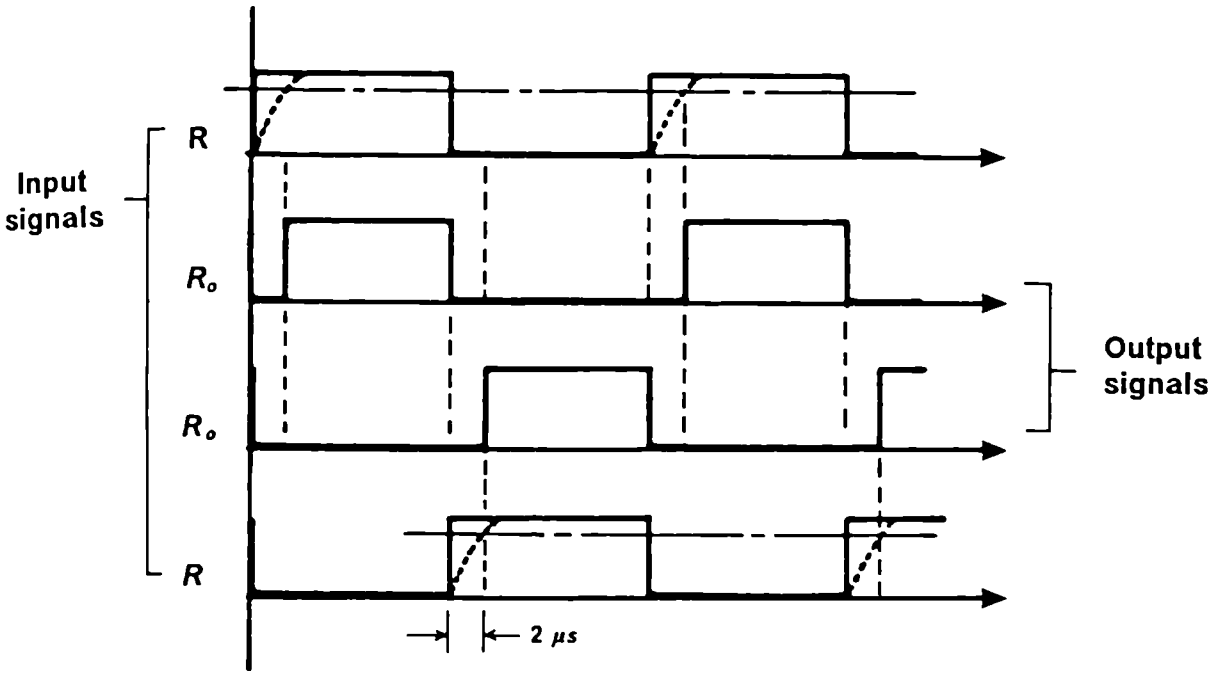


b- Timing waveforms.

Fig.(3-14) Overlap circuits for the switching signals.

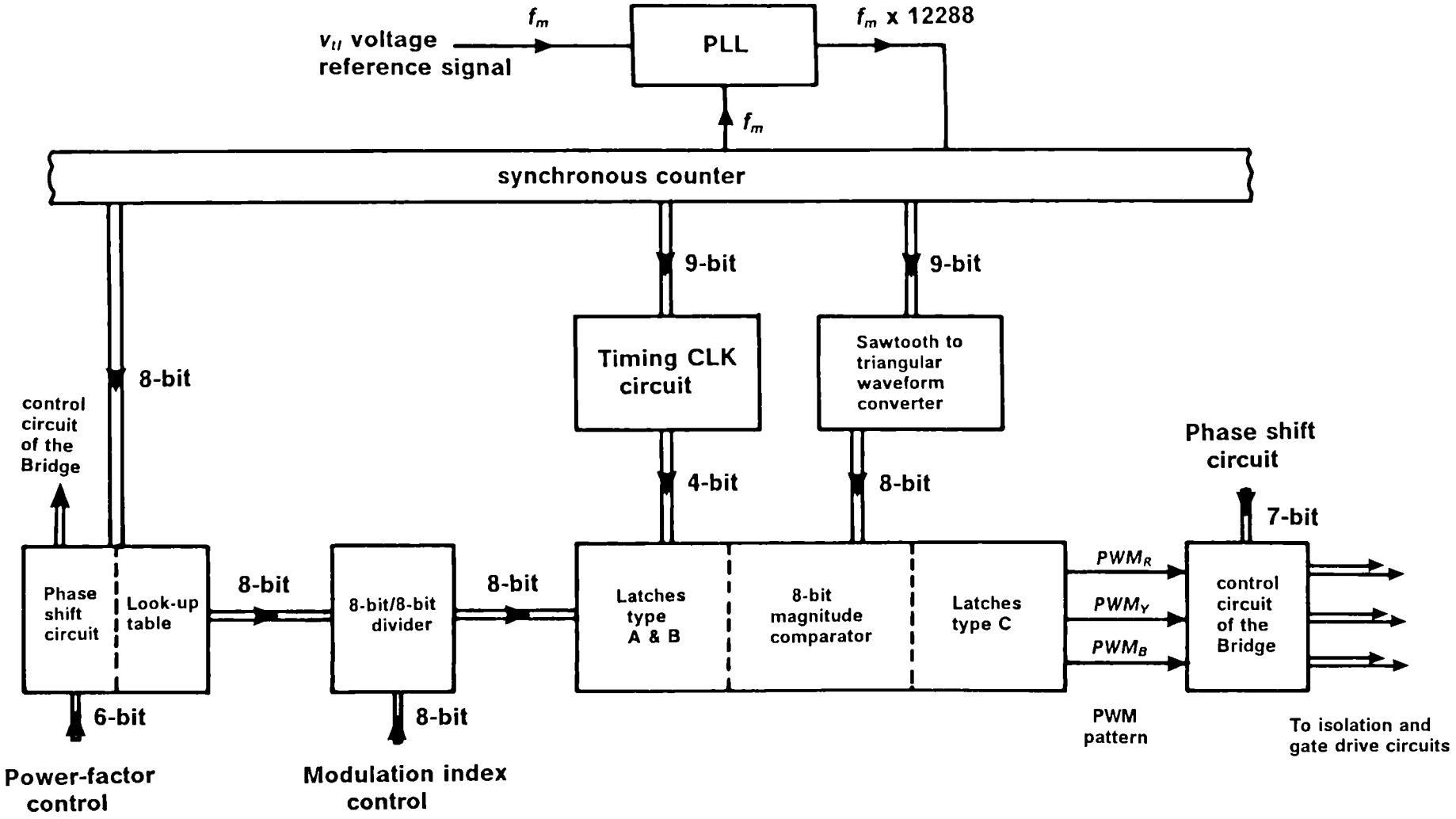


Fig.(3-15) Schematic diagram of the PWM generator.

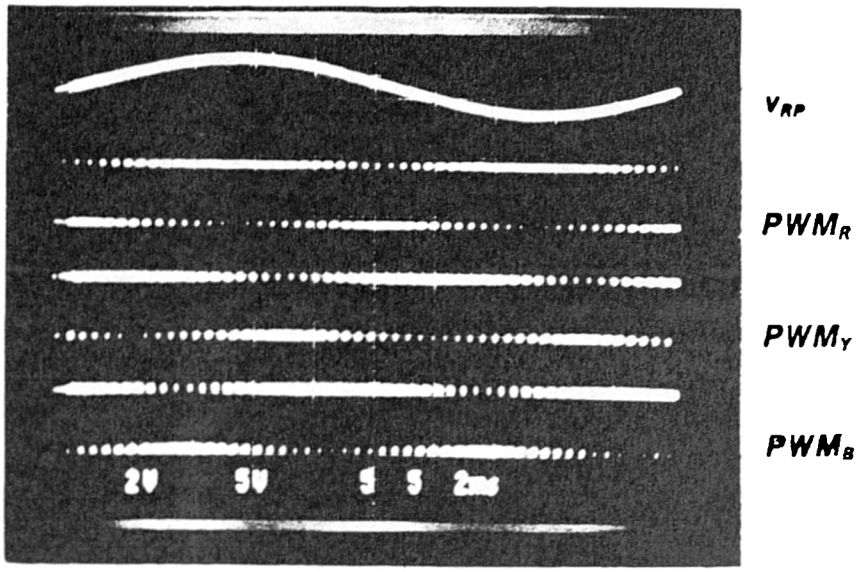


a- After latches type (c).

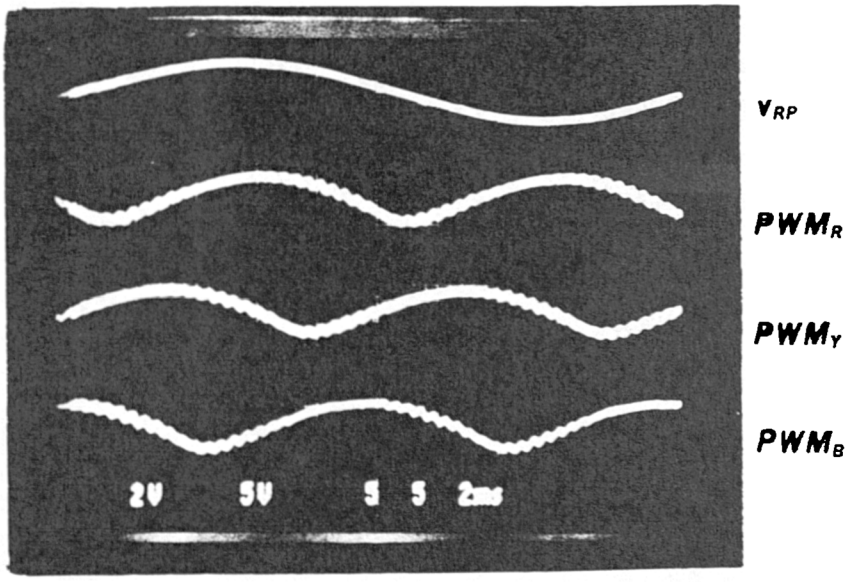


b- After an RC filter.

Fig.(3-16) Sine-weighted signals stored in the look-up table.

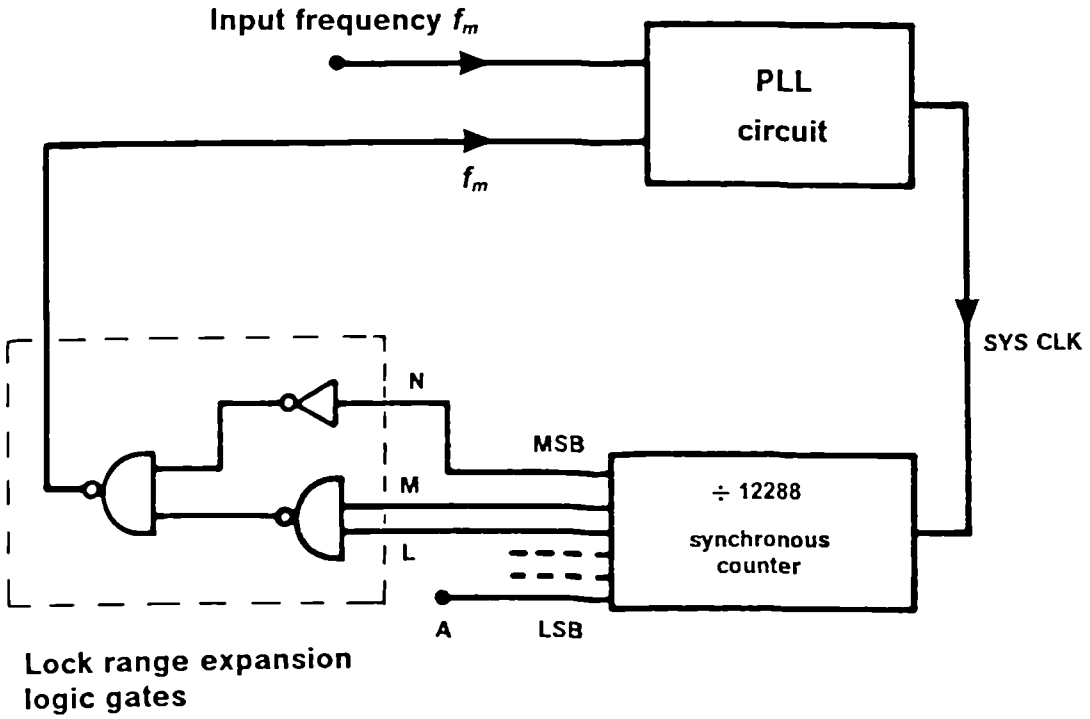


Fig.(3-17) Expansion of the lock range of the PLL circuit.

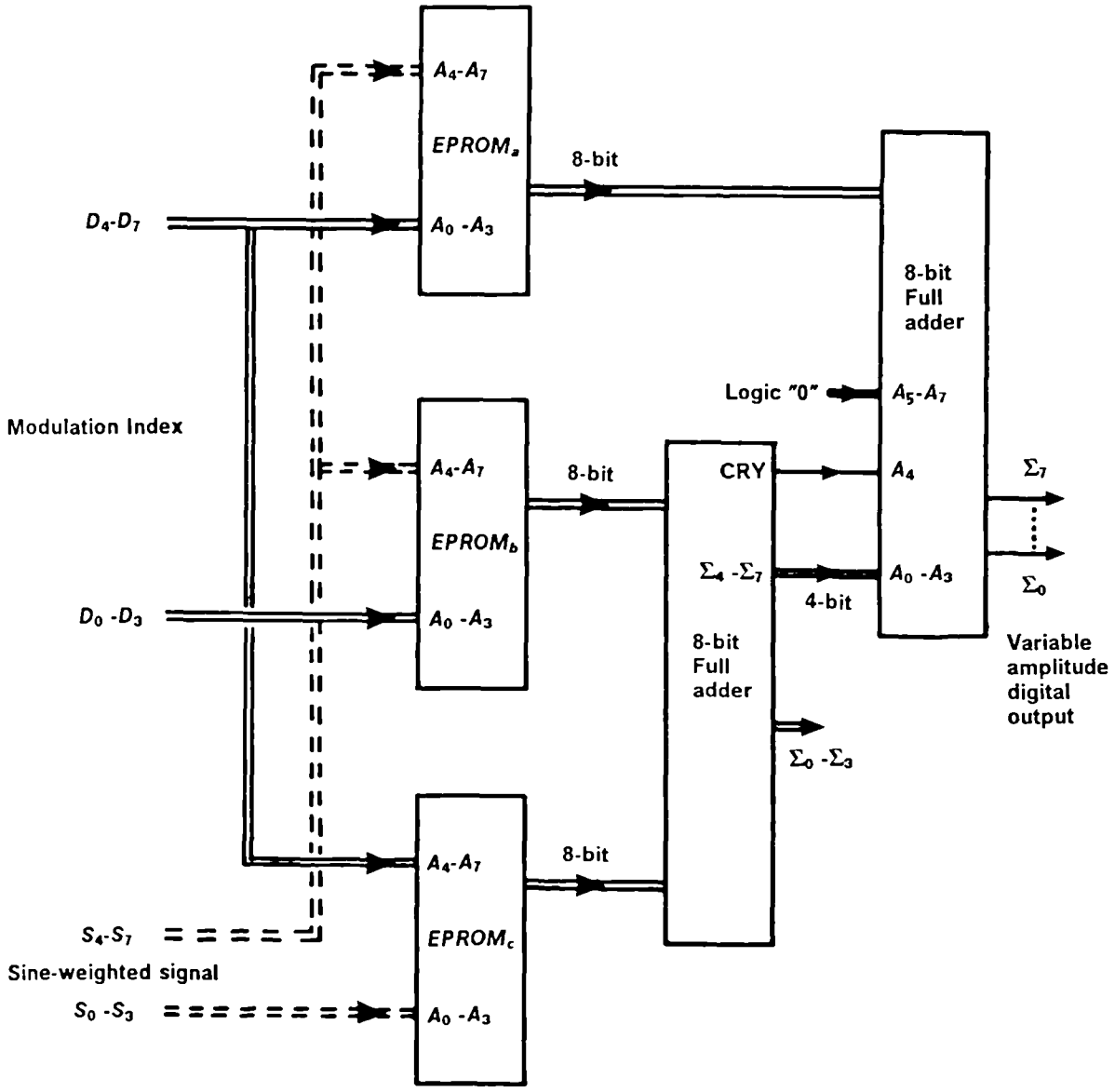


Fig.(3-18) Schematic diagram of the 8-bit/8-bit divider.

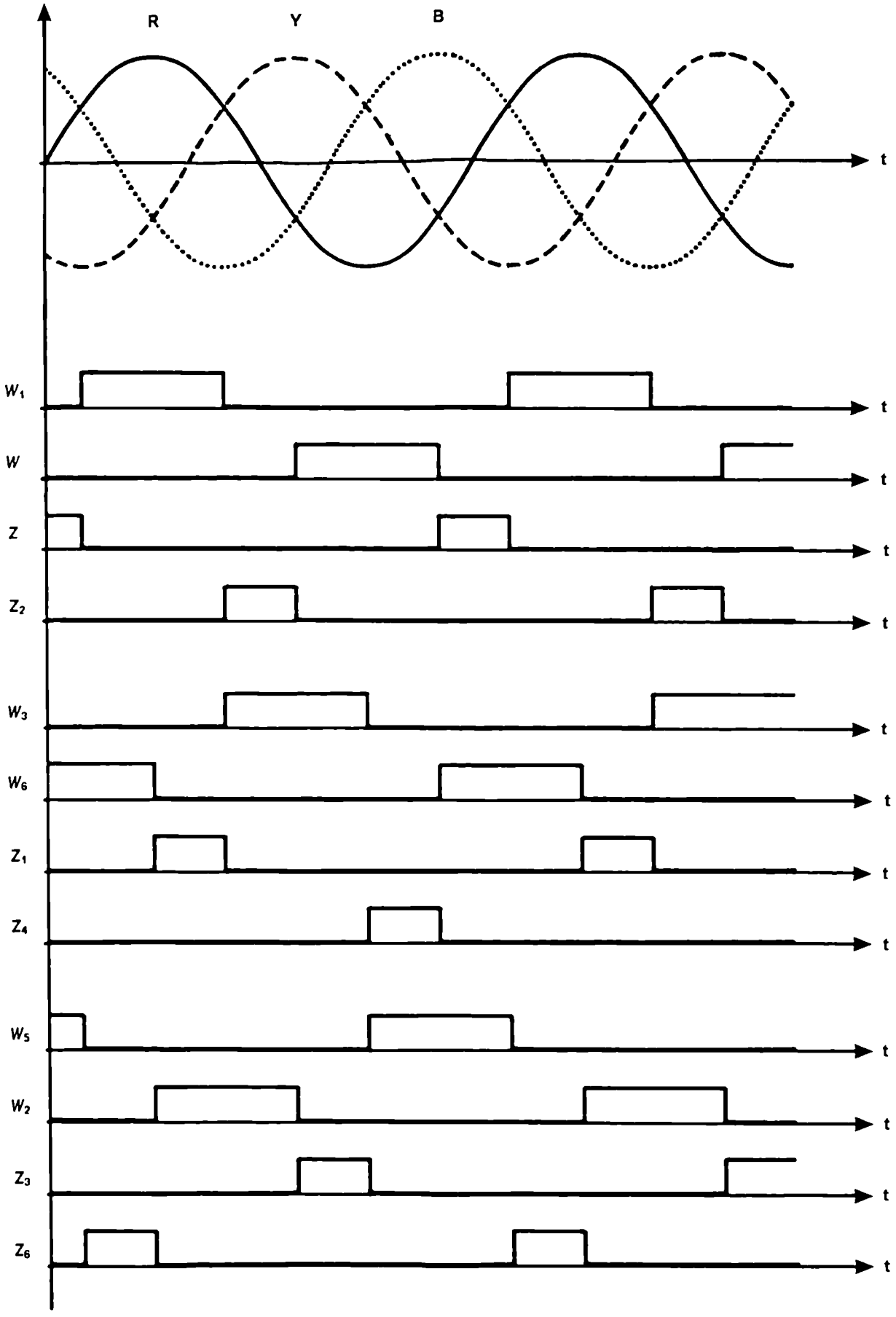


Fig.(3-19) Control signals of the current source converter.

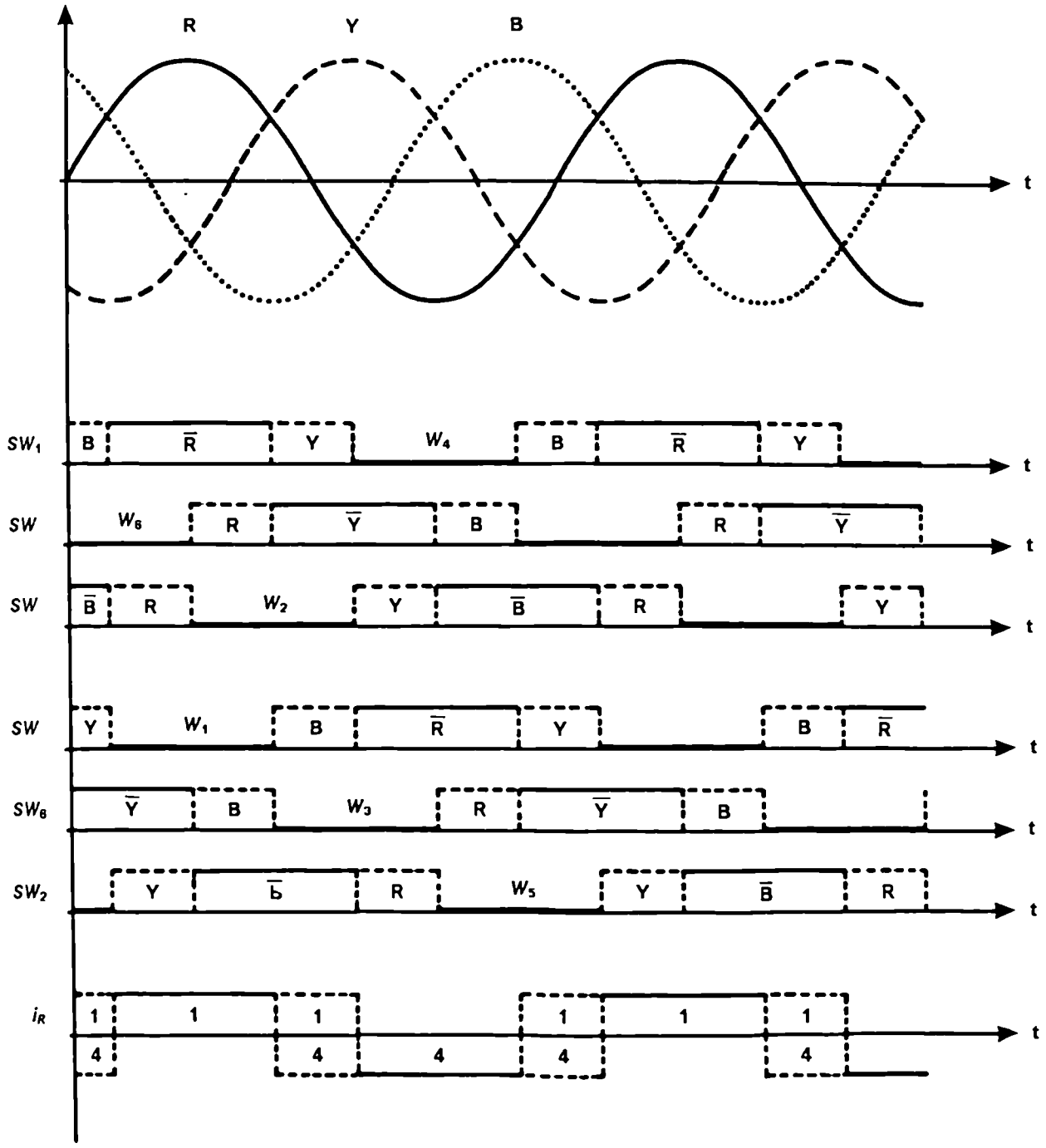


Fig.(3-20) Switching signals of the PWM, GTO converter.

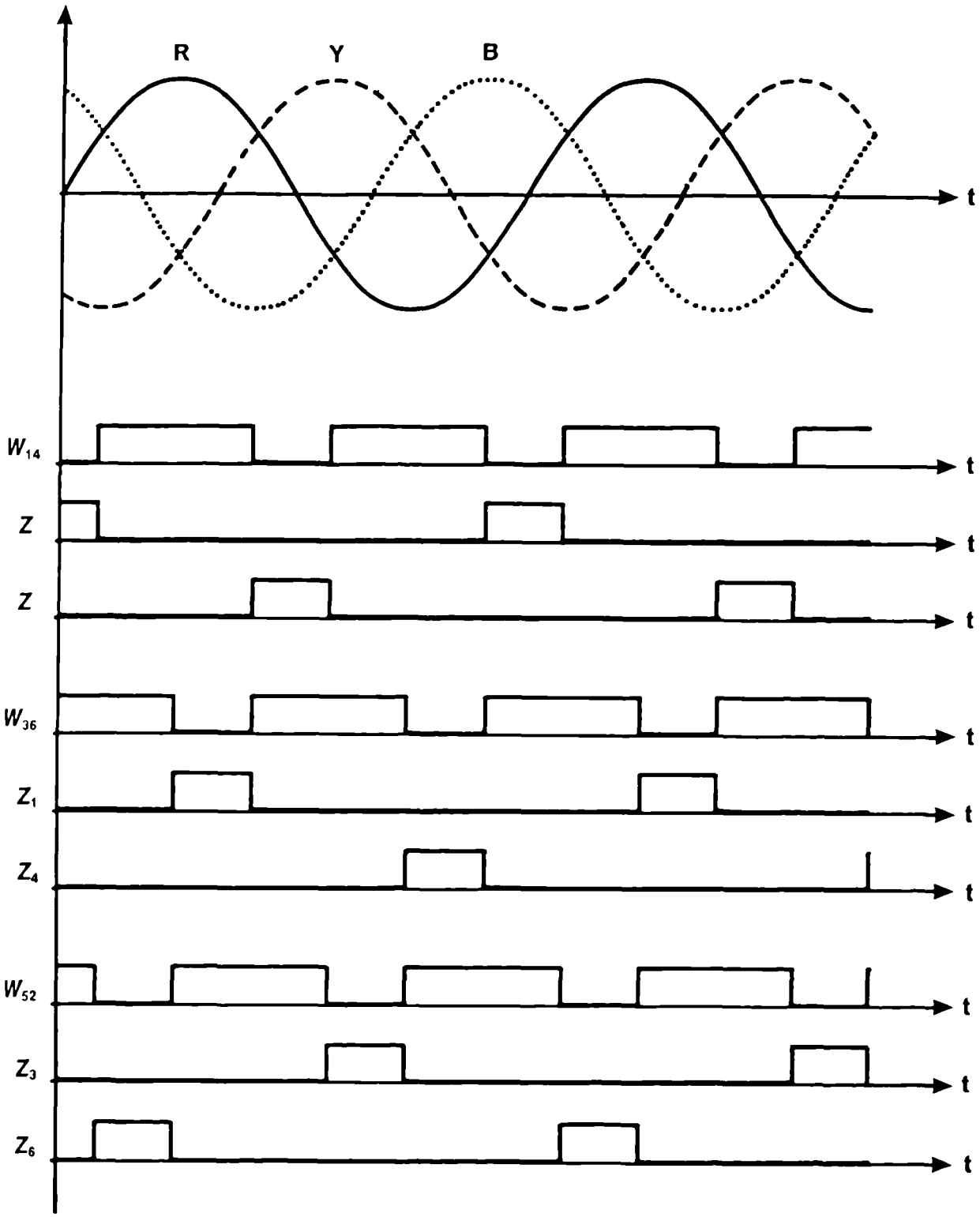


Fig.(3-21) Control signals of 3-switch converter.

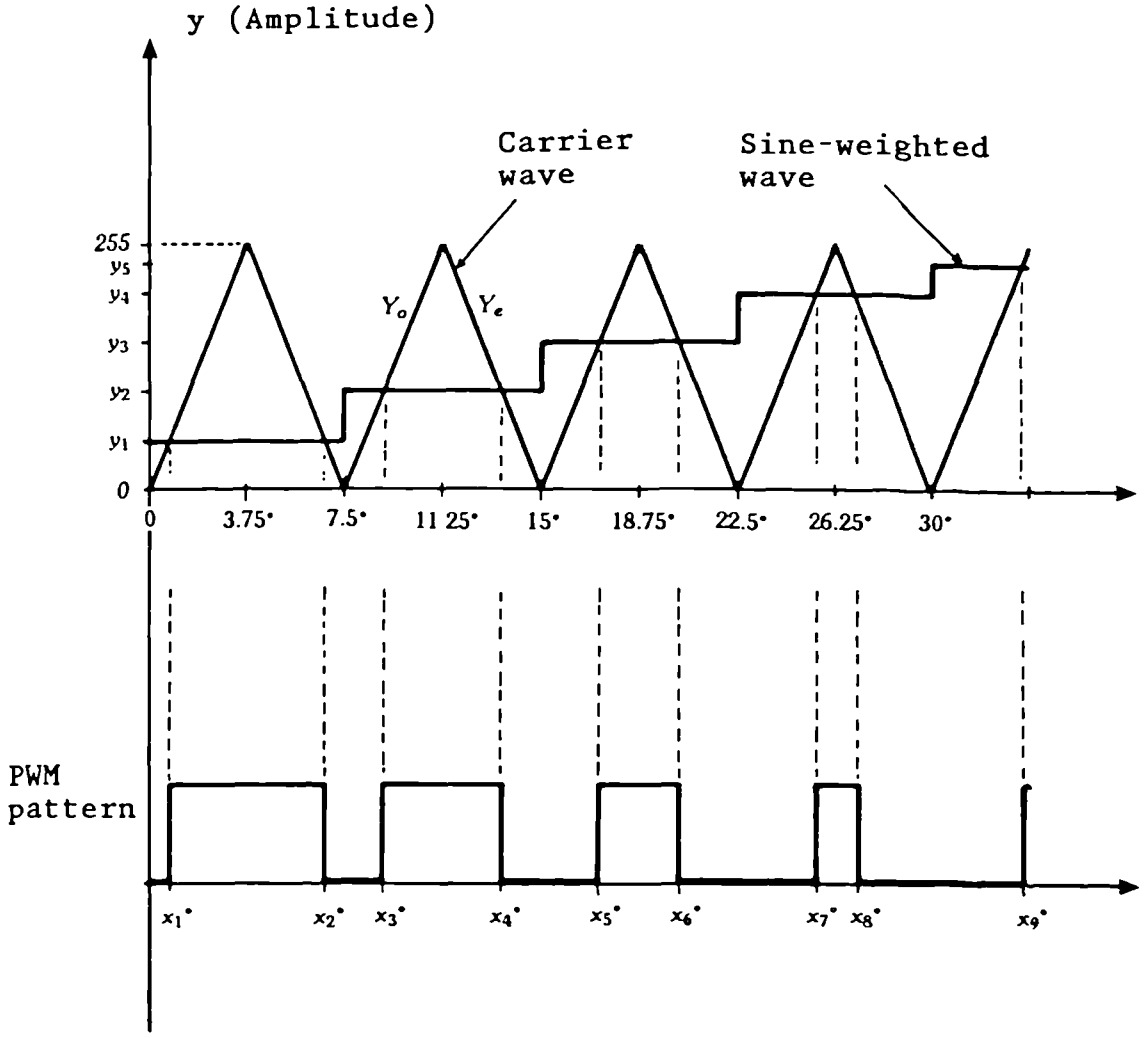


**Fig.(3-22) PWM pattern generation.**

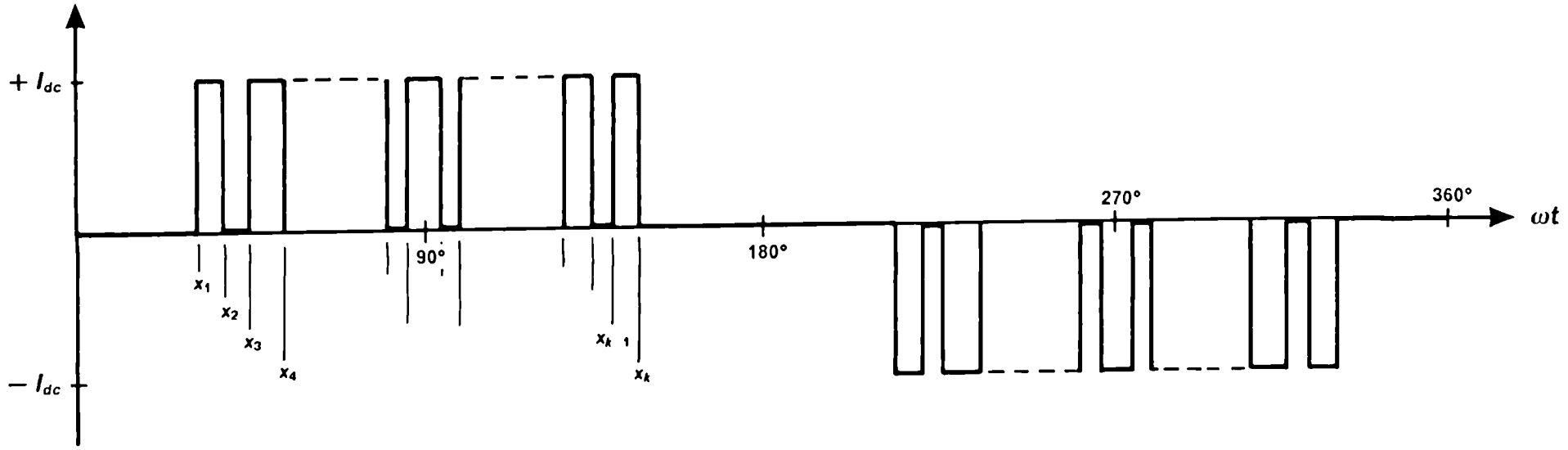


**Fig.(3-23) PWM pattern switching angles of the input line current [ $i_{a2}(\omega t)$ ]**

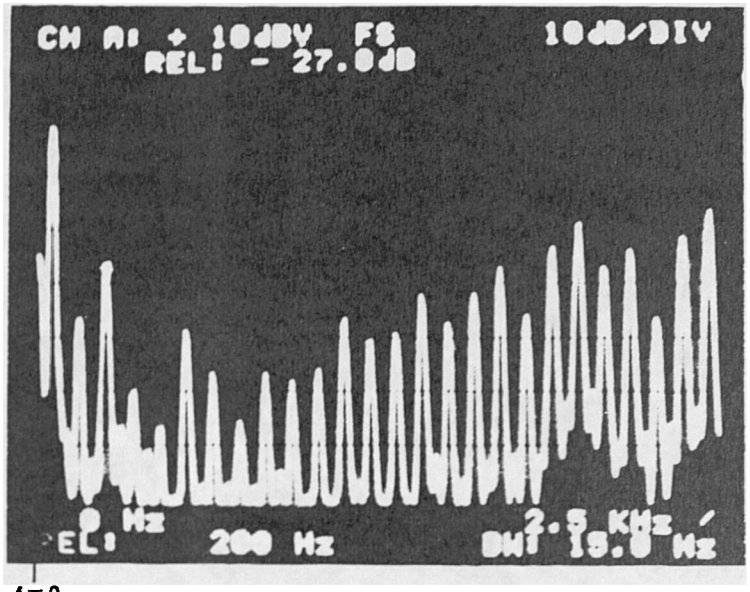


a- Without harmonic minimisation.

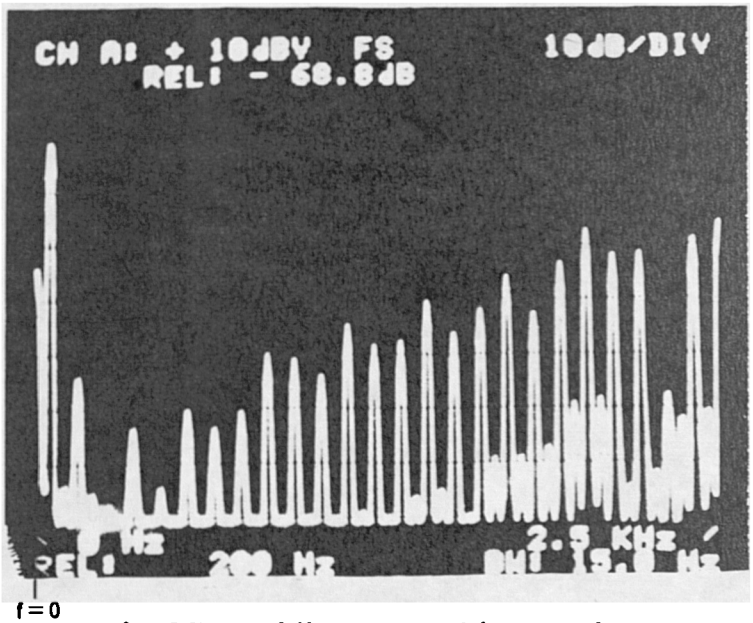


b- After adding the 3rd harmonic.

Fig.(3-24) Frequency spectrum of the input a.c. line current [$i_{a2}(\omega t)$] of the converter before and after adding the 3rd harmonic to the sine-weighted signal.
[ $i_{a2}$ = 3.24 Amp(rms), $I_{dc}$ = 4.045 Amp ]

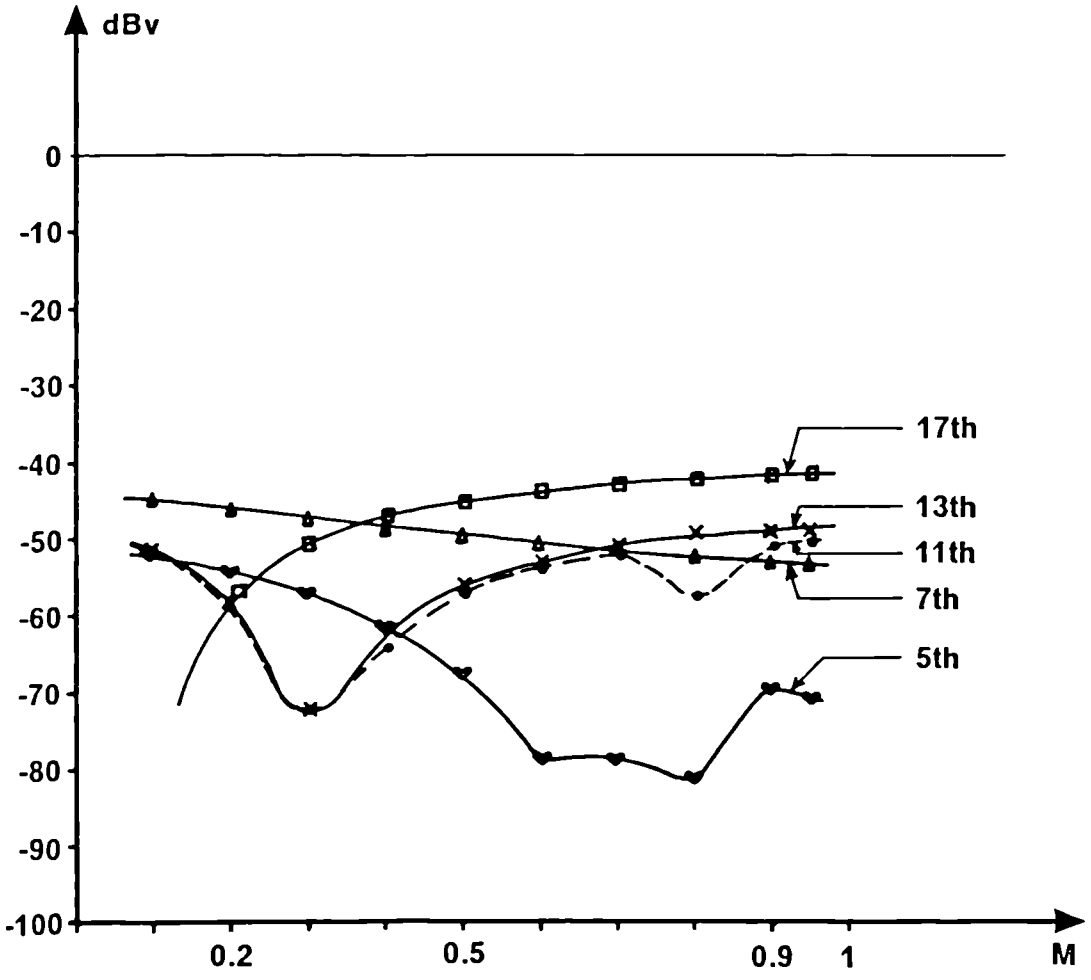


Fig.(3-25) Harmonic content versus Modulation index of the input line current $i_{a2}$

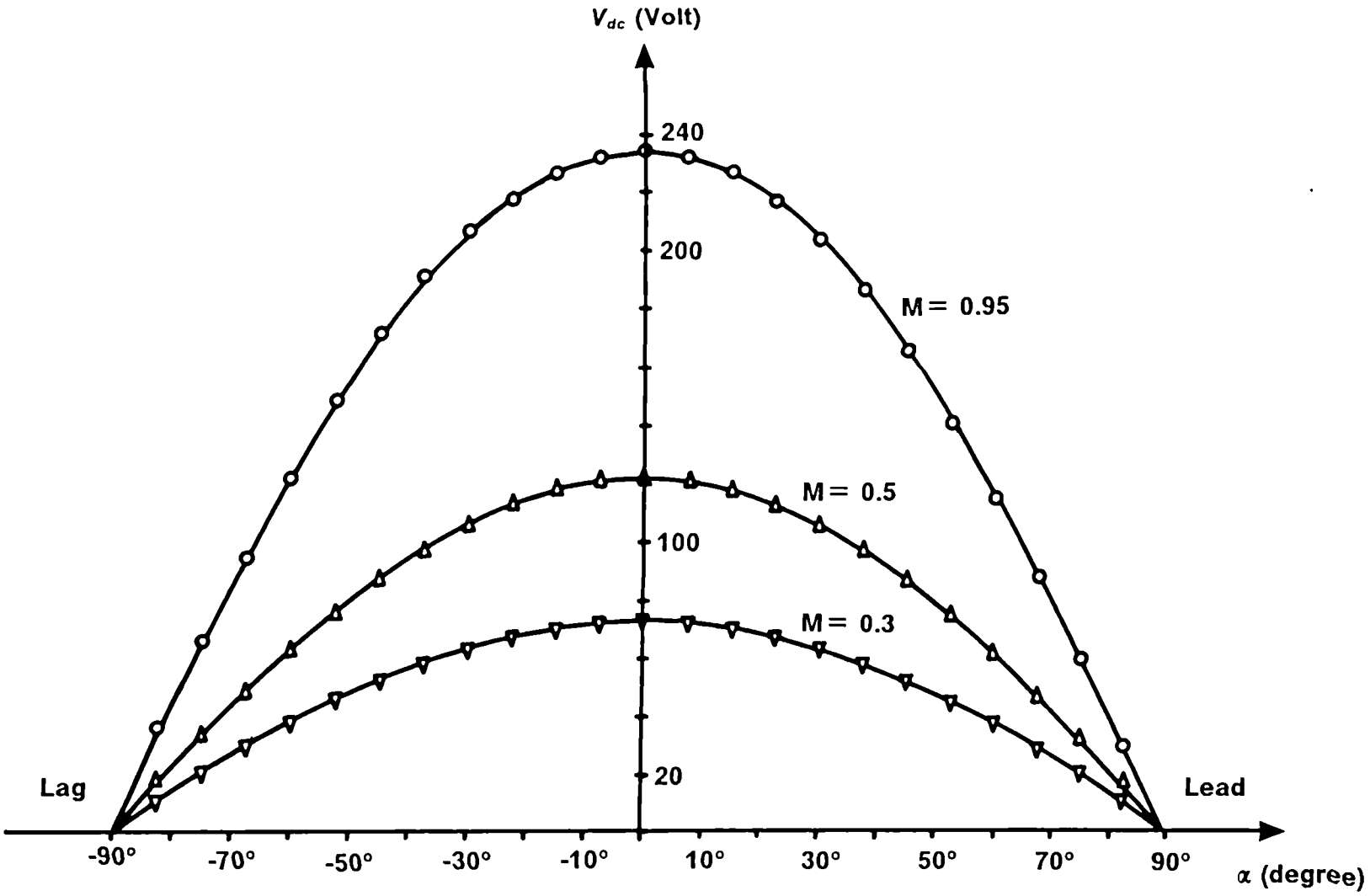


Fig.(3-26) Output d.c. voltage versus the delay angle of the converter.[ $V_{tl} = 200volt$ and $I_{dc} = 1.0Amp$]

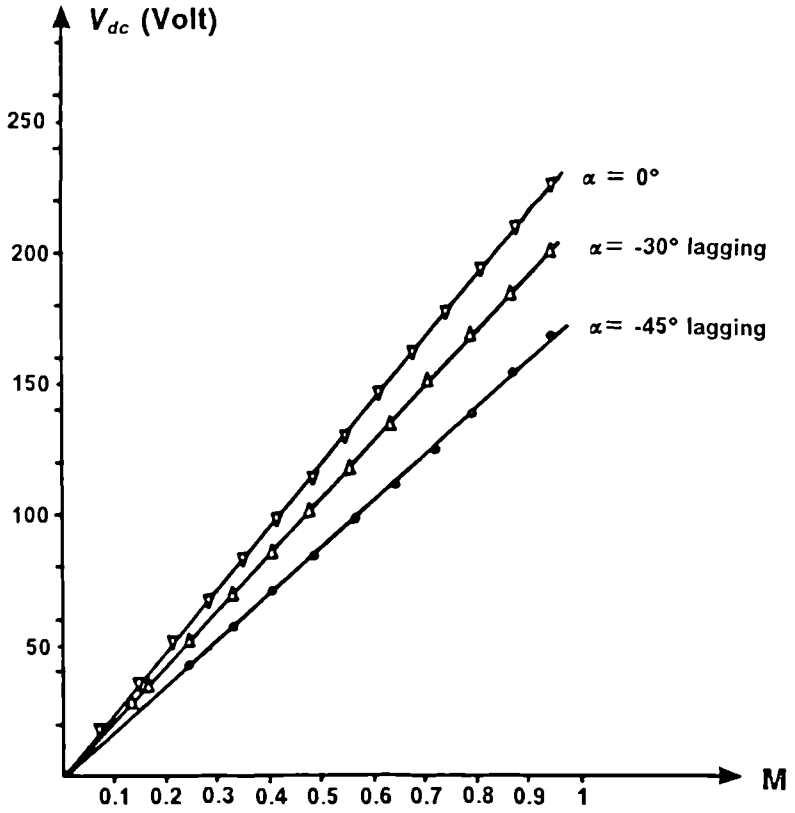


a- At lagging power-factor.

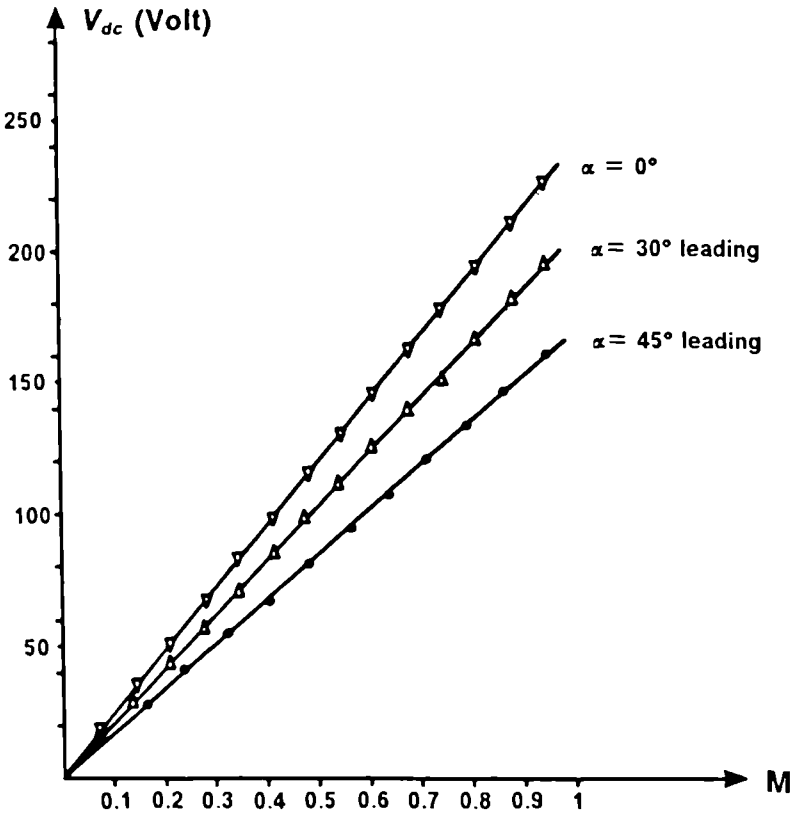


b- At leading power-factor.

Fig.(3-27) Converter output d.c. voltage versus modulation index.
[ $V_{tl} = 200\ volt$, $I_{dc} = 6\ Amp$ ]

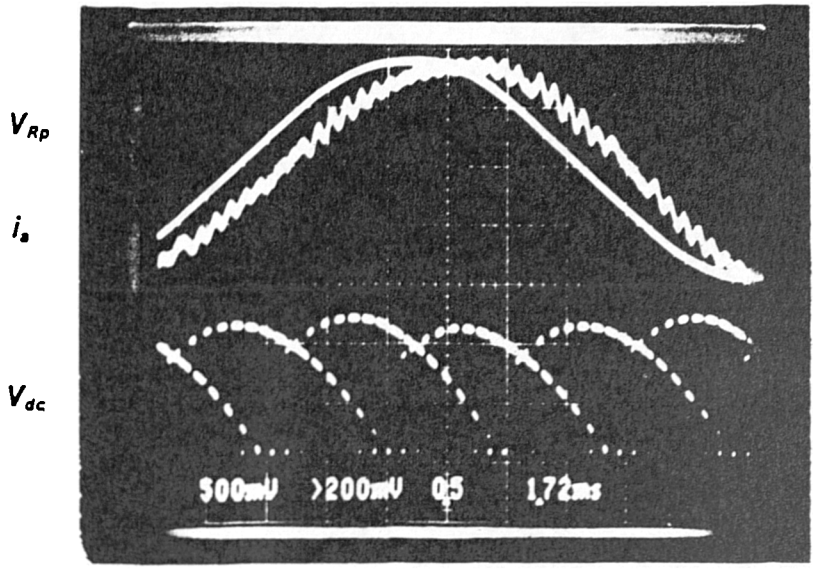


a- At lagging power-factor.

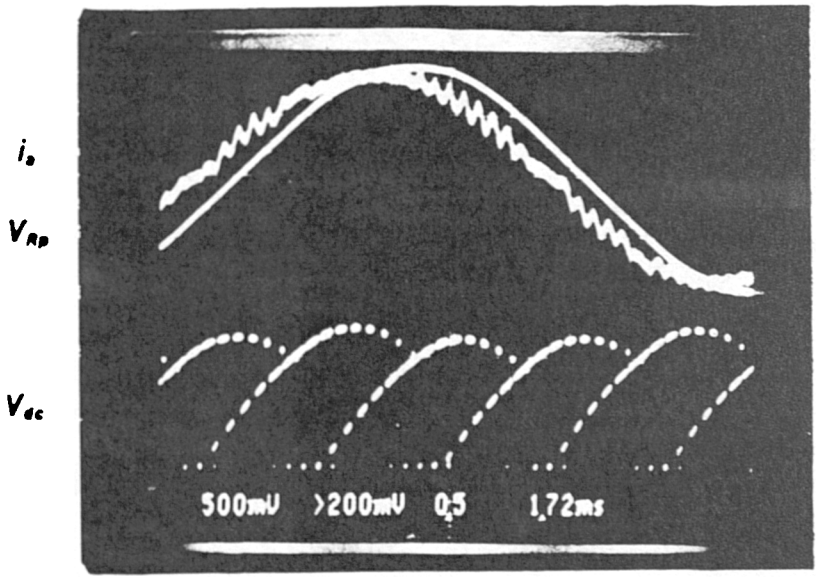


b- At leading power-factor.

Fig.(3-28) Converter voltage and current.

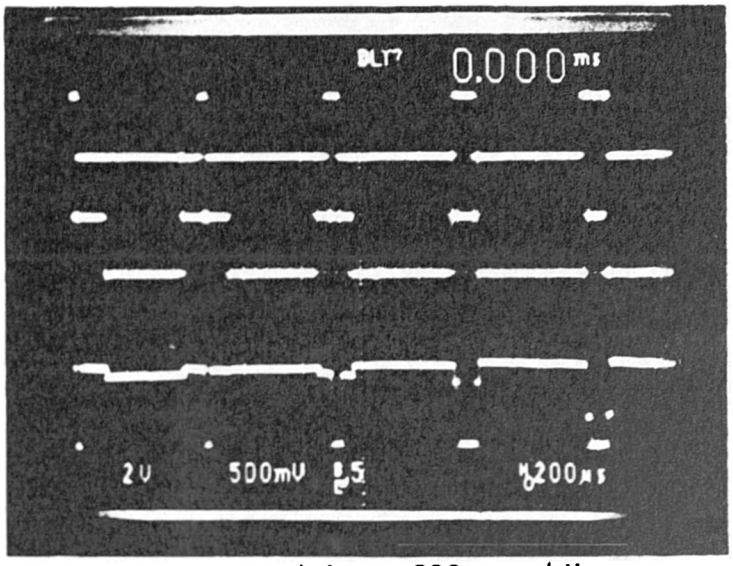


a- *T/div.* = **200 µsec/div.**

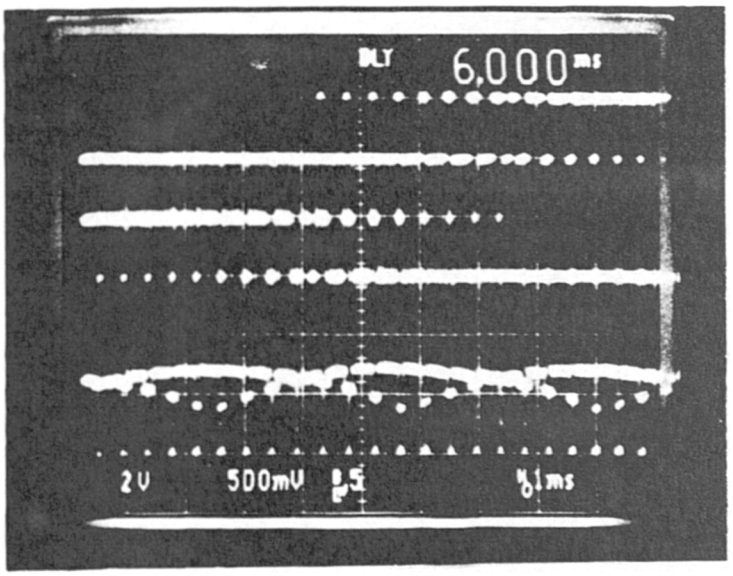


b- *T/div.* = **1 msec/div.**

**Fig.(3-29) PWM gate signals and output d.c. voltage ($V_{dc}$ = 230 volt)**

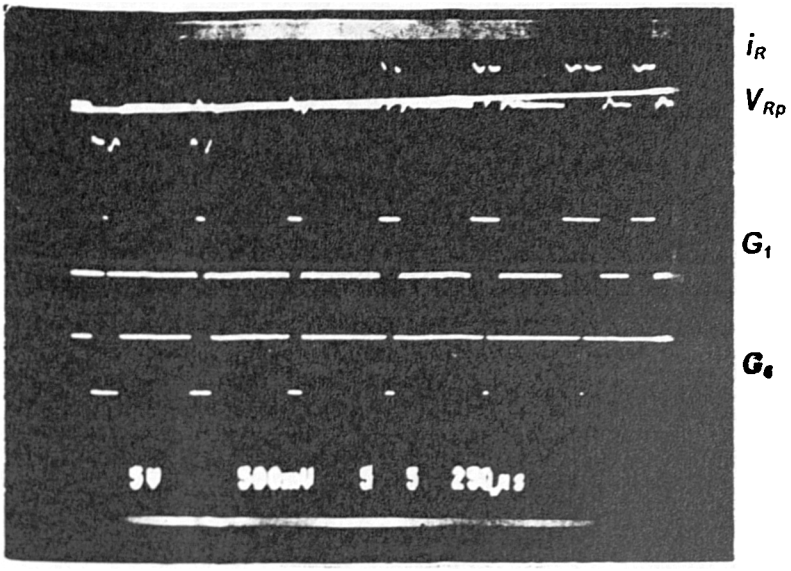


a- *T/div.* = 250 *μsec/div.*

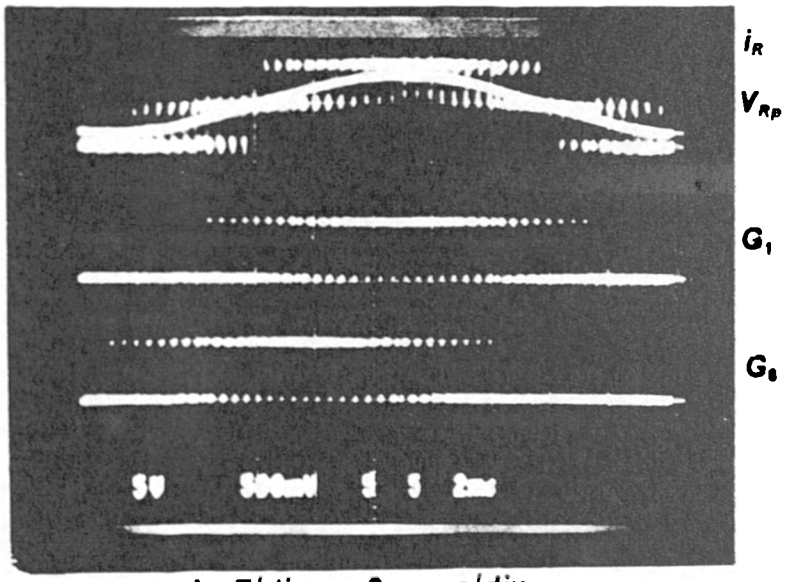


b- *T/div.* = 2 *msec/div.*

Fig.(3-30) PWM gate pulses of the Red-phase current and phase voltage.

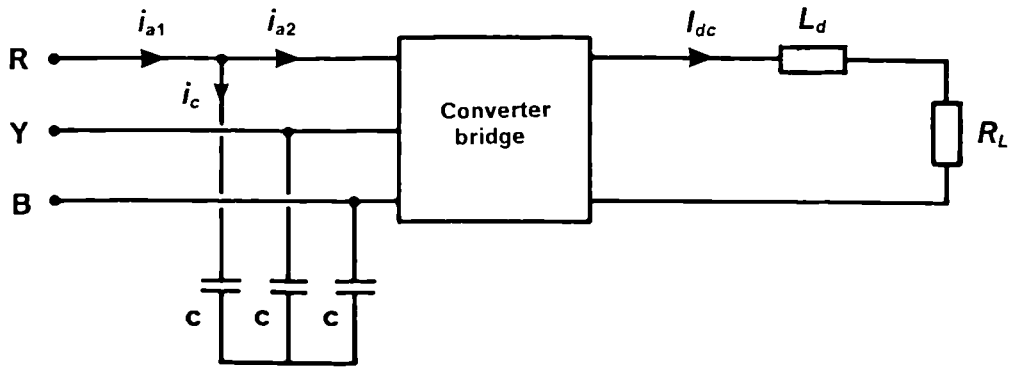


a- Converter block diagram.

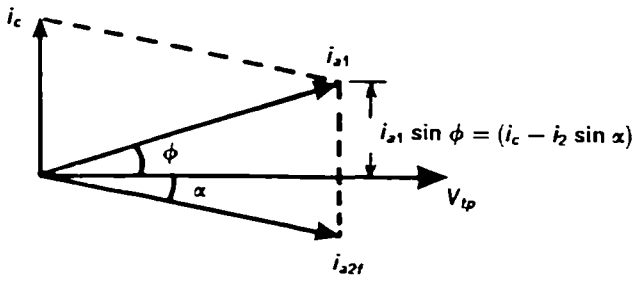


b- Phasor diagram.

Fig.(3-31) Calculation of fundamental component of the input current ($i_{a2}$).

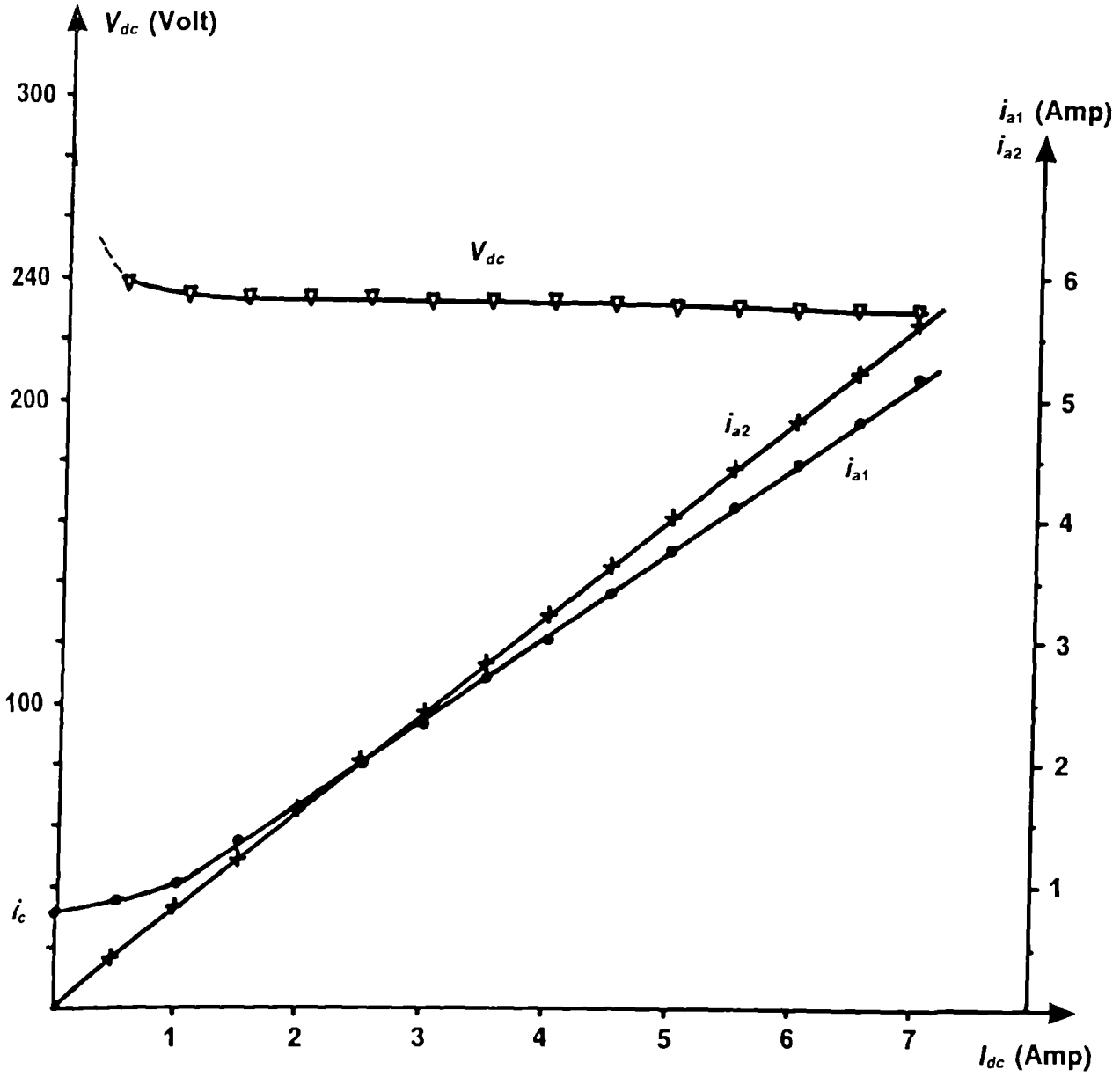


Fig.(3-32) Output d.c. voltage and input line currents versus d.c. current.

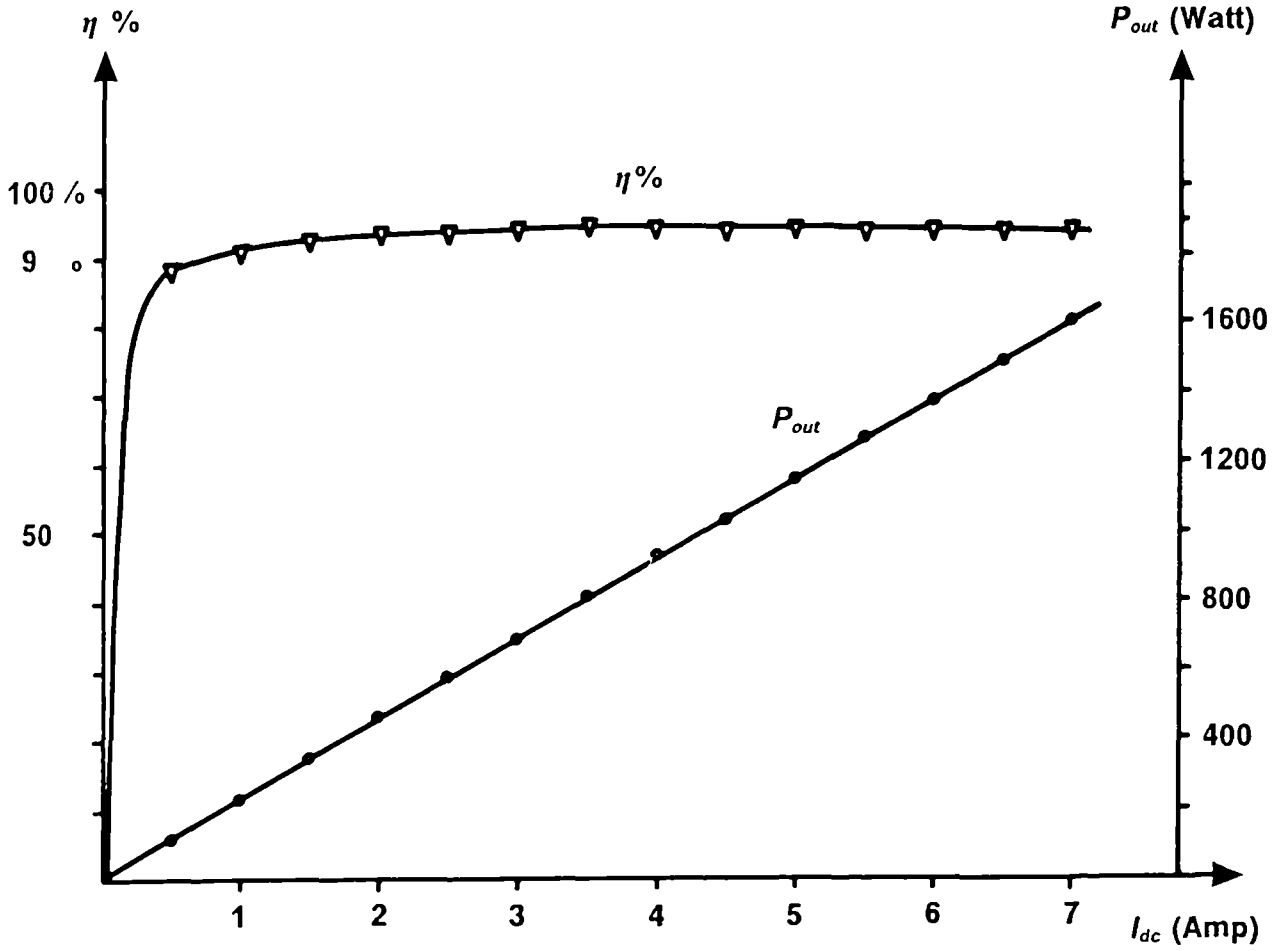


Fig.(3-33) Output power and efficiency versus d.c. current.

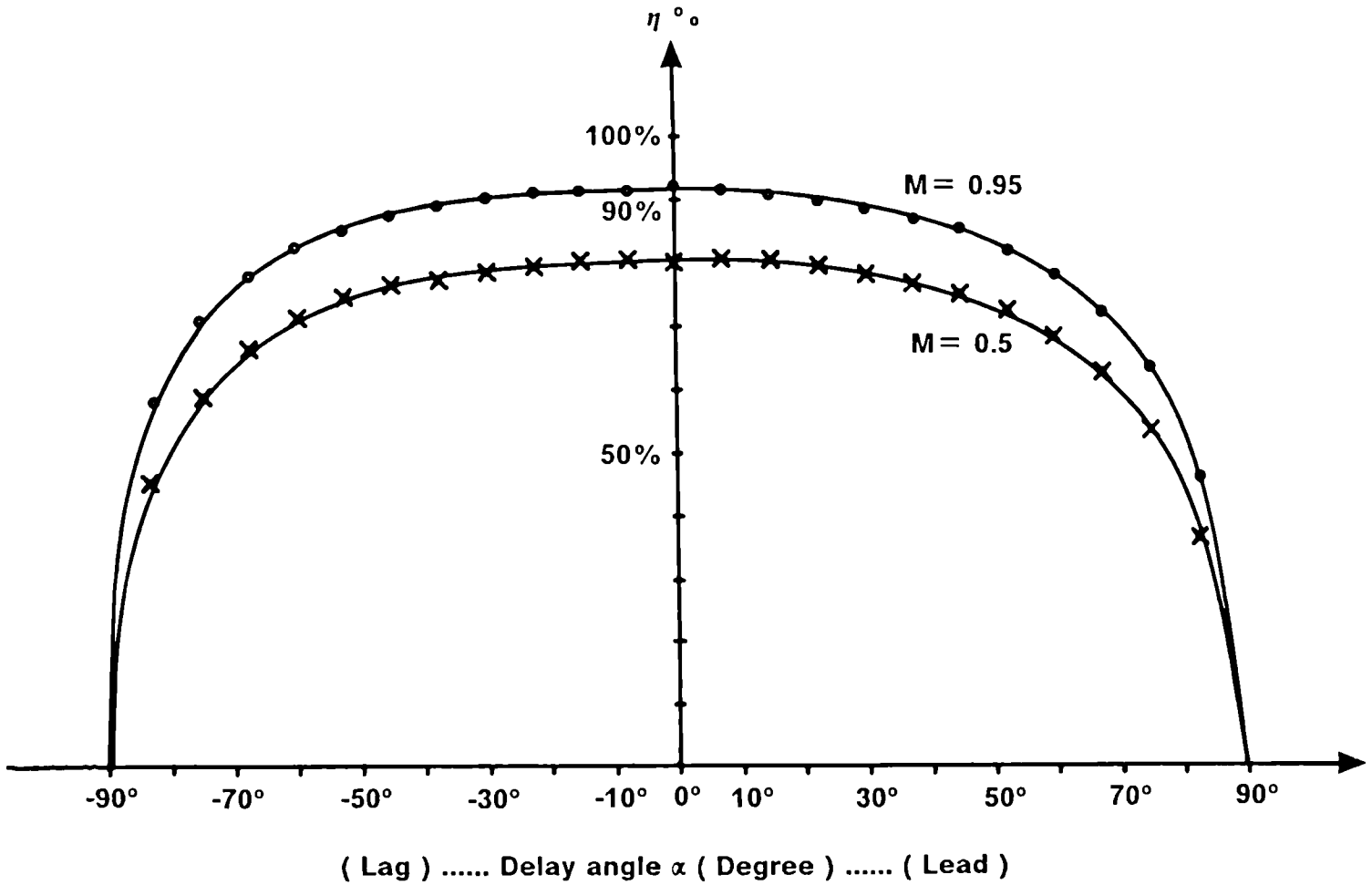


**Fig.(3-34) Efficiency of the converter at constant d.c. current versus the delay angle. [ $V_{tl} = 200volt$, $I_{dc} = 1\ Amp$ ]**

*CHAPTER FOUR*

# COMBINED PERMANENT MAGNET GENERATOR AND CONVERTER PERFORMANCE CHARACTERISTICS

4.1 Introduction.
4.2 System operation and control.
4.3 System operation in the inversion mode.
4.4 Output power and d.c. voltage characteristics.
4.5 System efficiency.
Figures 4.1 to 4.13

## 4.1 INTRODUCTION:

The results of testing the PM-synchronous machine as a generator using a passive load at different speeds has already been discussed and was seen to exhibit a very good performance even though inexpensive magnets were used in the rotor. In this chapter the machine will be used as a generator connected to the PWM, GTO converter and tested as a complete system with open loop control. The implication of testing the PM-synchronous generator with the converter is to form a power source which could be used with wind or tidal turbines as an alternative source of energy.

The main system comprises of the GTO converter which converts power at both variable frequency and voltage from the 8-pole PM-synchronous generator to d.c. power as shown in fig.(4-1). This power can be used for different applications, which will be discussed in the next chapter. A d.c. motor was used as the prime mover for test purposes. Some additional circuits are used to complete the system, for instance a coil placed in the d.c. link, and a 3-phase capacitor filter in the a.c. side.

The PM-synchronous machine can operate either as a generator or as a motor, thus four quadrant operation is possible and are described in most electrical machine books. In the proposed work the machine can be used with the converter to work in two quadrant operation, i.e. as a generator or as a motor. However the machine works mainly as a generator. But it may be used in a back to back converting scheme, for example may be used as a motor for pump storage. The proposed six-GTO thyristor PWM converter can transfer the power in both directions, and is classified as a two quadrant operation converter. Therefore, the six-switch PWM, GTO converter was

tested in the inversion mode to be used as a converter of variable d.c. input power connected to the main a.c. network in a back to back system ( or so called d.c. transmission). The 3-switch converter discussed earlier is similar to a diode bridge rectifier in that it can convert the power from a.c. to d.c. only and therefore it is classified as a one quadrant operation converter.

Multi-function controller has been designed to control all possible parameters that make the combination of the PM-generator and the converter working at maximum power transfer and high efficiency. The controller maximises the generator power for a wide range of frequency throughout the phase locked loop (PLL). However a disadvantage arises from the PLL circuit because of the instability when the synchronous reactance of the PM-generator is increased by more than 49 mH, when the power-factor angle vary towards lagging and the generator supplies high current to the load. This is investigated by placing three inductors in series with each phase of the machine.

## 4.2 SYSTEM OPERATION AND CONTROL:

The work has concentrated on the six-switch GTO thyristor converter, due to its capability of full two quadrant operation, with the delay angle $\alpha$ variable in the range $\pm$ 180° . The detailed schematic diagram of the whole system controller is shown in fig.(4-2). Here the controller is discussed as an open circuit control to illustrate the principal operation of the system. Essentially the input voltage of the converter is controlled by the delay angle $\alpha$ of the converter, by varying the power-factor at which the generator is operated at. Similarly the output voltage is controlled independently by the

modulation index of the PWM pattern as well as to the delay angle control. The closed loop control operation of the system, to control the power-factor and output power, is discussed in Chapter 6. Fig.(4-2) shows the full control block diagram of the conversion system.

As the frequency of the PM-generator changes with any speed variation, the PLL circuit will automatically synchronise the generator with the electronic circuits of the converter. But there is a problem arising with this synchronism due to the presence of the PLL filter. The system being discussed here is an open loop circuit, therefore the change in the desired power-factor angle caused by the speed variation is corrected by changing the set value to the A D converter (2) as shown in fig.(4-2), i.e. the setup value for the delay angle ( $\alpha$ ) is altered. Fig.(4-3) shows the open loop characteristics of the delay angle versus speed. The angle has been setup for a constant value and the plotted results were recorded. Therefore, such a controller require the power-factor angle to be fixed at the precise value, this will be discussed letter. As can be seen from fig.(4-1) the current $i_{a1}$ is the stator current of the generator, while $i_{a2}$ is the line current of the converter. However, the stator current of the generator has a power-factor angle of 90° leading when the converter has no-load. Therefore, this angle starts to decrease towards 0 as the converter is loaded towards full load as shown in fig.(4-4). Hence the power-factor angle is a function of two parameters, firstly the delay angle $\alpha$ which implicitly depends on the speed (n), secondly the output d.c. current which is also depend on the input a.c. current. These parameters have been controlled by the controller through a phase control function as shown in fig.(4-2). The control function is a look-up table that has the angles that makes the system work linearly with respect to speed and

to the input a.c. current. The output power of the system is controlled by another controller which controls the output characteristics. Here the A/D converter (1) controls the output d.c. current by controlling the width of the PWM pulses. The full circuit operation of this controller is discussed in section (6.6).

### 4.3 SYSTEM OPERATION IN THE INVERSION MODE:

It has been mentioned earlier that the six-switch PWM, GTO converter can work in the inversion-mode as well as the rectifier-mode. This is controlled by the same controller shown in fig.(4-2), except that the setup value of the A D converter (2) is changed to shift the delay angle $\alpha$ by 180°. As before the synchronism between the machine and the electronic circuits of the converter is achieved by using the induced line voltage in the stator as a reference for the control system. Therefore, it will act in the feedback loop of the PLL circuit to keep the switching frequency in synchronism with the machine frequency.

Furthermore, the PM-synchronous machine has been tested as a motor after placing a d.c. power source on the d.c. side of the converter to supply the PM-machine. In this case the PWM, GTO converter works in the inversion mode, while the d.c. current flows in the same direction, since the GTO thyristors conduct in only one direction (as in the rectifier mode of operation). Then power can be reversed when the output d.c. voltage $V_{dc}$ of the converter is reversed in polarity. This is achieved by changing the delay angle ( $\alpha$ ) of the converter from 0° to 180°. However, the system has been tested for different speeds. Then, the voltage $V_{dd}$ of the d.c. power supply is

fixed at any suitable value, and the converter voltage $V_{dc}$ allow to vary. This can be achieved in two ways, either by controlling the delay angle of the converter or by varying the modulation index M of the PWM pattern. Thus, to let the power flow to the PM-synchronous machine, $V_{dc}$ must be slightly smaller than $V_{dd}$ to provide a current flow through the circuit. Therefore, the d.c. current is defined as

$$I_{dc} - \frac{V_{dd} \quad V_{dc}}{R_d} \tag{4.1}$$

Where $R_d$ is the effective resistance of the d.c. link.

Therefore, it is possible to control the speed with the above factors. The machine was operated as a motor on load. An example of the converter waveform are shown in fig.(4-5). In this particular case the d.c. voltage was -214 Volt, the d.c. current (1.2 Amp) and the motor speed was 720 rpm. Fig.(4-5a) shows that the converter d.c. voltage has a negative average value, while the d.c. current has a positive magnitude as shown in fig.(4-5b). The experimental waveforms of the input line voltage and phase current of the PM-synchronous machine as a motor are shown in fig.(4-6). Due to the PWM techniques used for this converter, even for the converter working in the inversion mode, the voltage and current waveforms keeping their shape as a sinusoidal waveform.

## 4.4 OUTPUT POWER AND D.C. VOLTAGE CHARACTERISTICS :

In the normal operation of a line commutated converter the input phase current will lag the phase voltage. However using the GTO converter the

delay angle can be advanced to make the phase of the current lead the voltage. This kind of operation is required for the PM-synchronous generator to optimise its power as shown in fig.(4-7). This figure shows that the maximum output power of the generator occurs at leading power-factor angle for different frequencies. The generator is therefore tested for constant leading power-factor angle for a variable speed from 375 rpm up to 900 rpm as shown in fig.(4-8). A constant resistive load was applied on the d.c. side at a constant modulation index M. This power can be changed by varying the input power factor angle of the generator. The effect of this procedure is to increase the terminal voltage of the generator, and thus supply more power to the load. Fig.(4-8) illustrates the system output power for the speed range specified above at two different power-factor angles. It may be seen that the generator gives twice the power at 37.5° leading power-factor angle than for 0 power-factor angle, while the output current is kept constant.

The power-factor angle $\phi$ is dependent on the delay angle $\alpha$ of the converter. Therefore, the system output power is controlled entirely by the delay angle, which is termed the advance angle when the phase current leads the phase voltage. In this respect some factors have been changed with the PM-generator speed. These factors are plotted in fig.(4-9), with the optimum value of the power-factor angle. It is clear that these factors are linear with speed, and thus easy to control.

Fig.(2-23) is repeated and redrawn in fig.(4-10), where the experimental results of the power factor-angle using the PWM, GTO converter are plotted on it. In the first case, the load was a capacitive and resistive one connected to the PM-synchronous generator. It can be seen that the experimental points

are close to the theoretical line. In the second case, the load was the PWM, GTO converter with variable delay angle ( $\alpha$ ). These experimental points are also near the theoretical line. This is so because of the accuracy ($\pm$ 7.5°) of the power-factor angle controller.

The combination of the GTO converter and the PM-synchronous generator has the potential of giving a high output even at low speed, when the machine is run at leading power-factor angle $\phi$ as shown in fig.(4-11). The figure shows the characteristics of the PM-generator running at constant speed, while the power-factor angle is kept constant at 30° leading. It may be noted that the maximum rated output power given by this generator at frequency of 25 Hz is approximately equal to the same output power when the generator runs at unity power-factor angle at a frequency of 50 Hz and the same value of the input current ($I_{a1}$). The PM-generator output at 50 Hz is boosted in the same way by advancing the power-factor angle to leading as shown in fig.(4-11).

The current waveform of the PM-synchronous generator has very low harmonic content when connected to the GTO converter. The harmonic content was discussed earlier in Chapter 3. However, fig.(4-12) shows examples of the input current and output voltage waveforms of the generator when connected to a full-wave rectifier bridge, and the PWM, GTO converter. It is clear from the current waveform of the PWM converter shown in this figure, that it is more easily filtered than the rectangular waveform of the rectifier bridge.

## 4.5 EFFICIENCY :

The system efficiency can be divided into two parts, the machine efficiency $\eta_m$ % and the converter efficiency $\eta_c$ % . The total system efficiency $\eta_s$ % is equal to the product of these two quantities. The efficiency of the PM-generator alone was discussed in chapter two and is equal to 90 % at full load current and 50 Hz. Under the same conditions the efficiency of the converter is 94.5 %, therefore the total system efficiency will be 84.6 % as shown in fig.(4-13a). Fig.(4-13b) shows the system efficiency at 25 Hz. At low frequency the system efficiency reduced as more current was drawn by the load, because of the higher proportion of copper ( $I^2R$ ) loss at low output power.

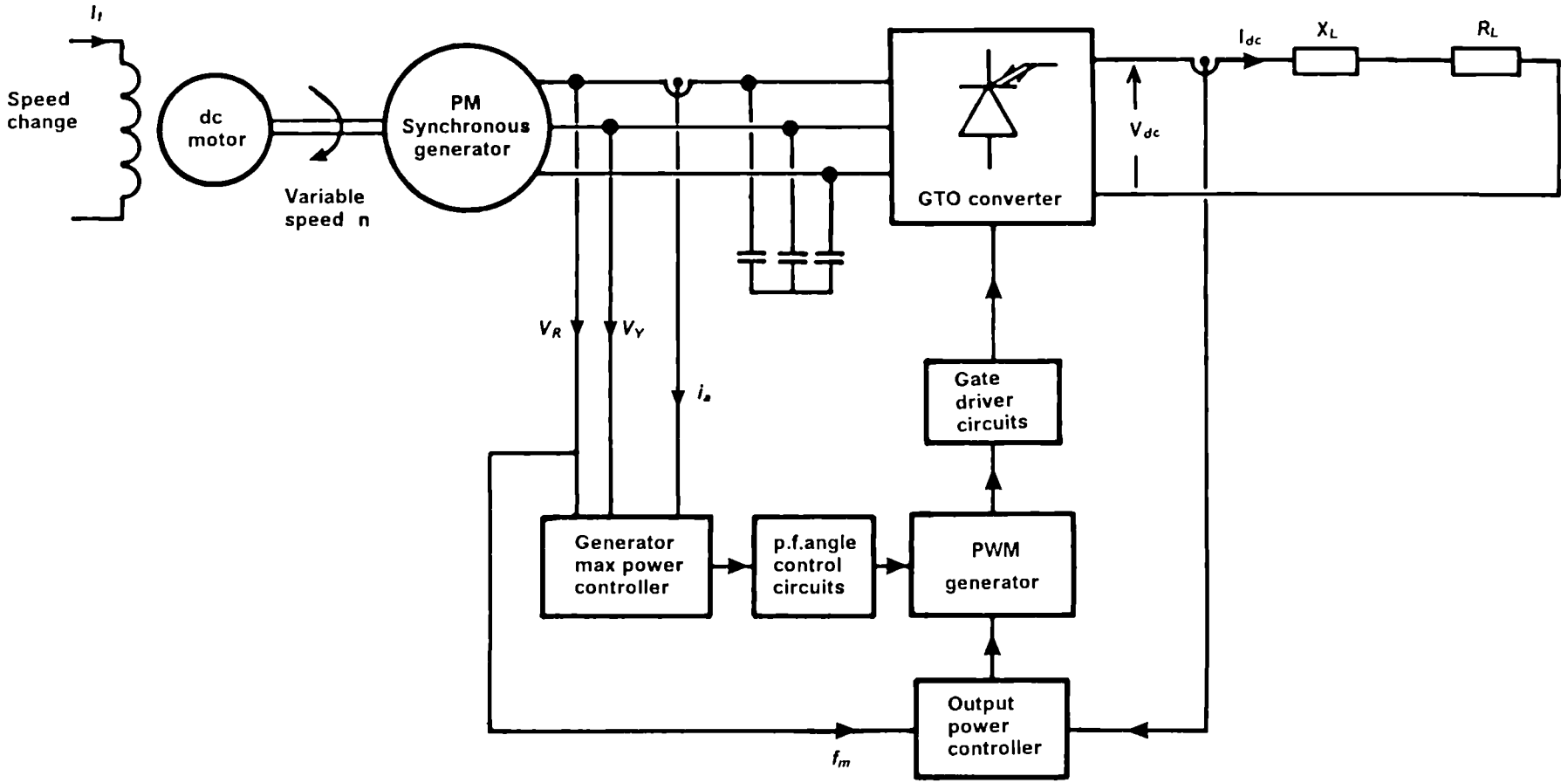


**Fig.(4-1) Schematic d'agram of the energy conversion system.**

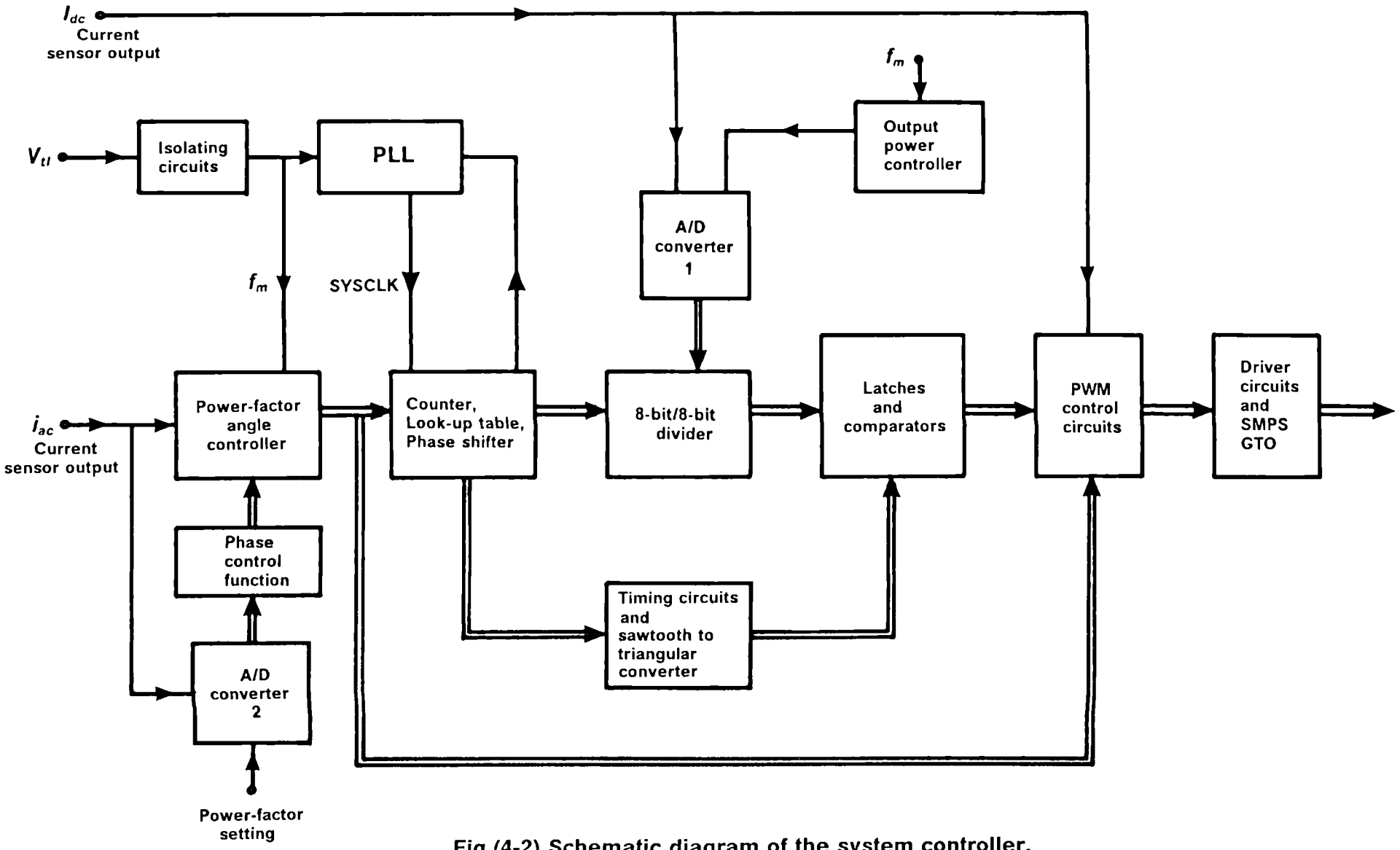


Fig (4-2) Schematic diagram of the system controller.

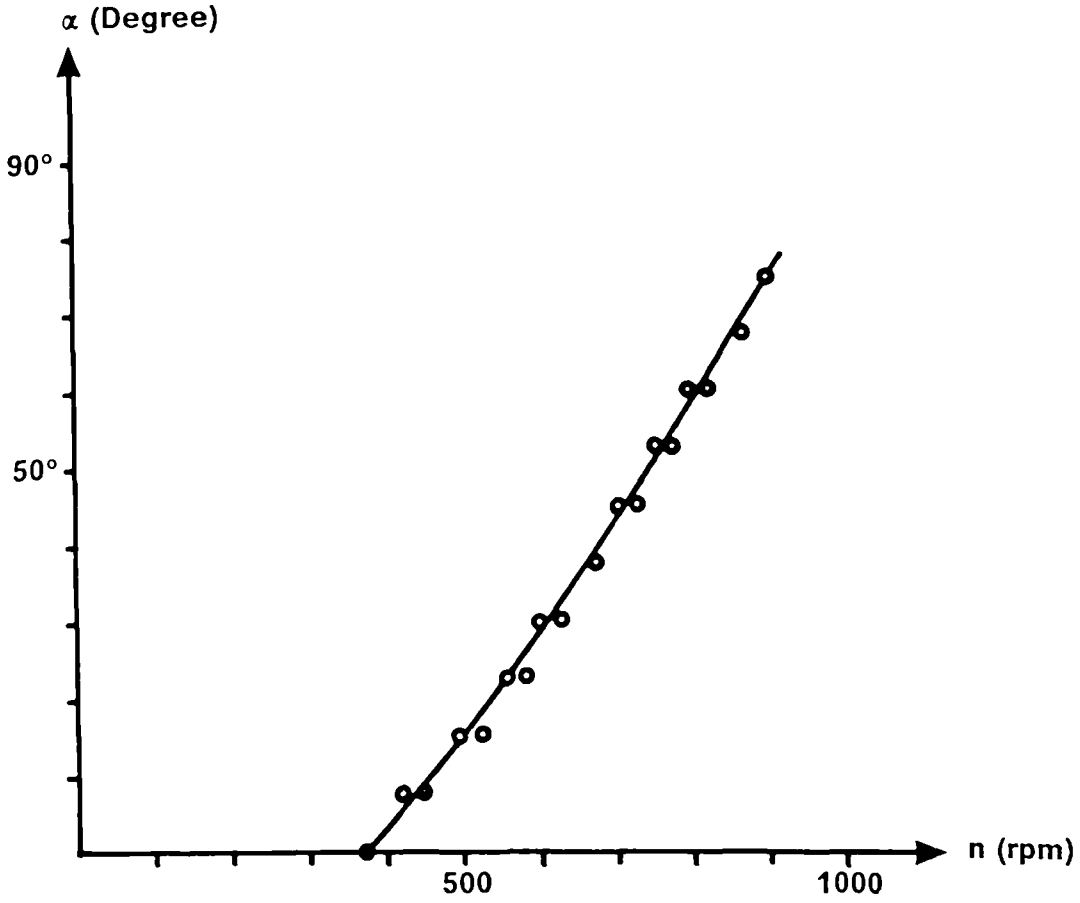


Fig.(4-3) Converter delay angle versus machine speed without power-factor angle controller.

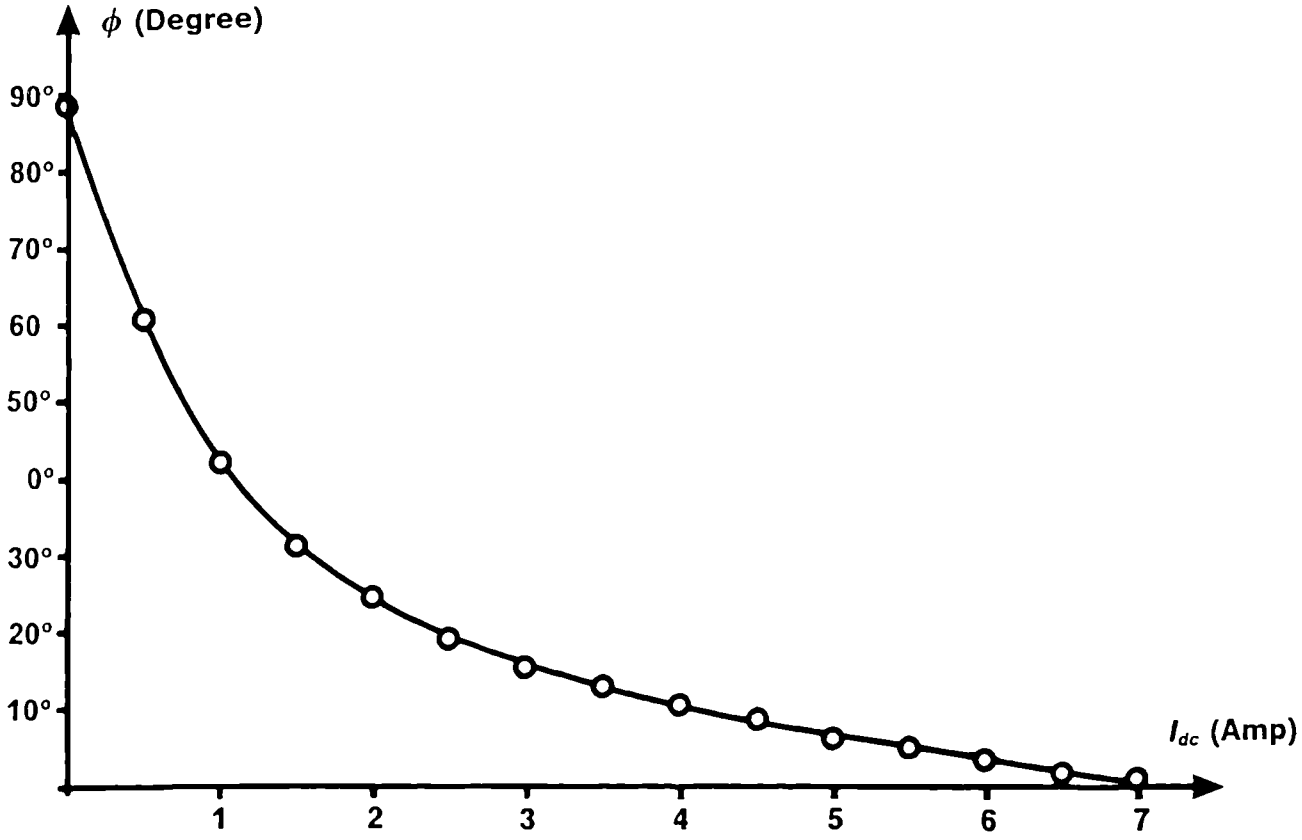


**Fig.(4-4) Input power-factor angle of the converter versus output d.c. current without its controller.**

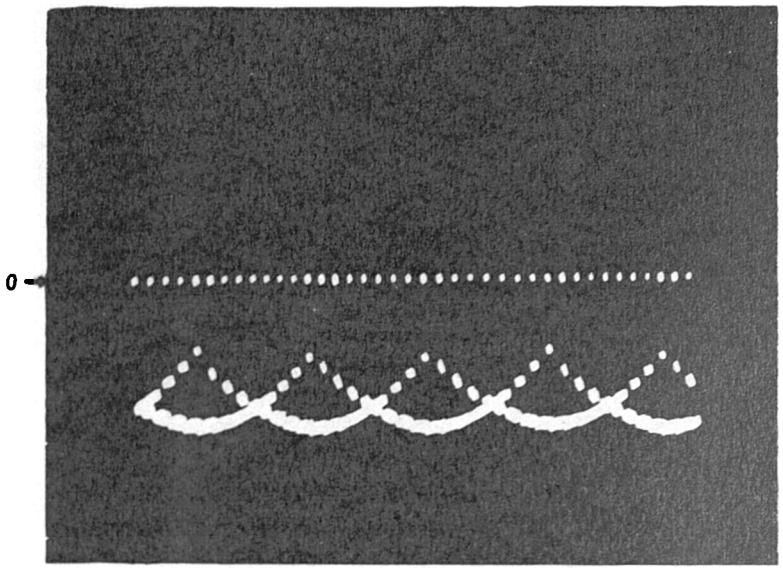


a- Converter d.c. voltage.

T/div.= 2 ms/cm, V/div.= 100 v/cm
$V_{dd}$ = 300 Volt , $V_{dc}$ = -214 Volt

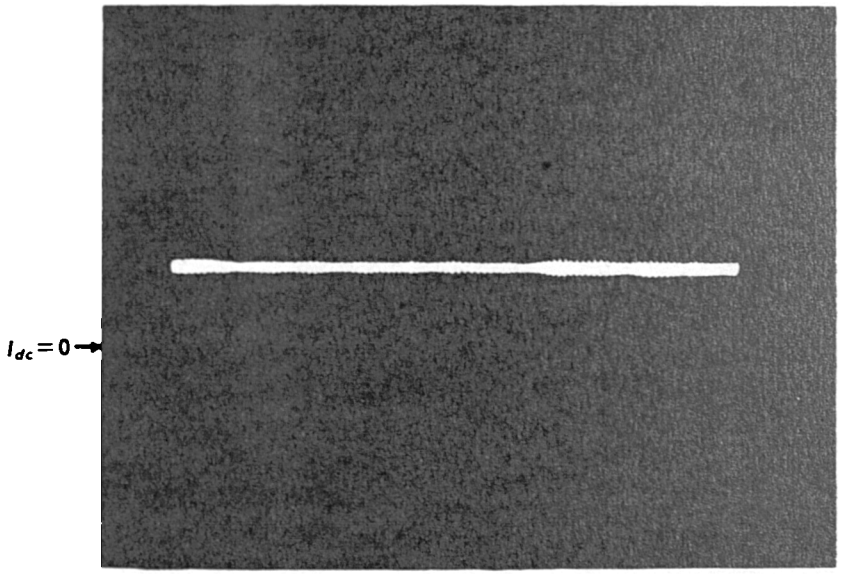


b- Converter d.c. current.

T/div.= 2 ms/cm, I/div.= 1.25 A/cm
$I_{dc}$ = 1.2 Amp

Fig.(4-5) Converter waveforms in the inversion mode.

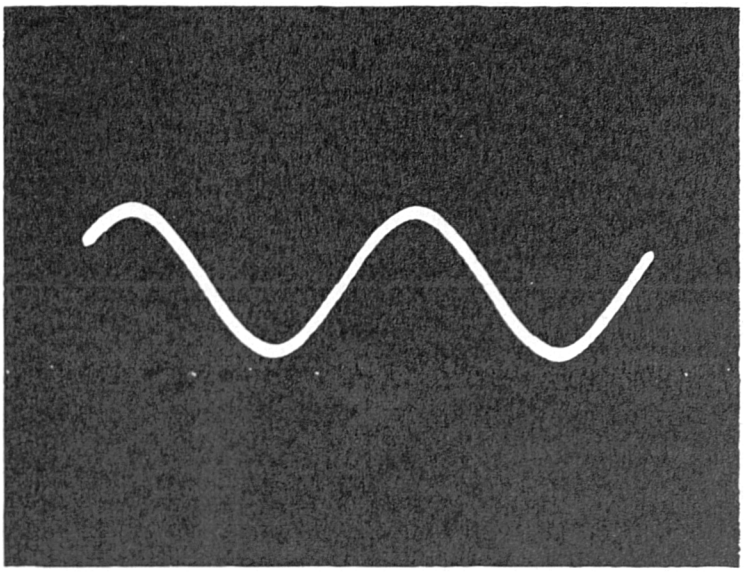

a- Line voltage $V_{ll}$ [200 v/cm].

$V_{ll}$ = 175.5 volt

T/div.= 2 ms/cm

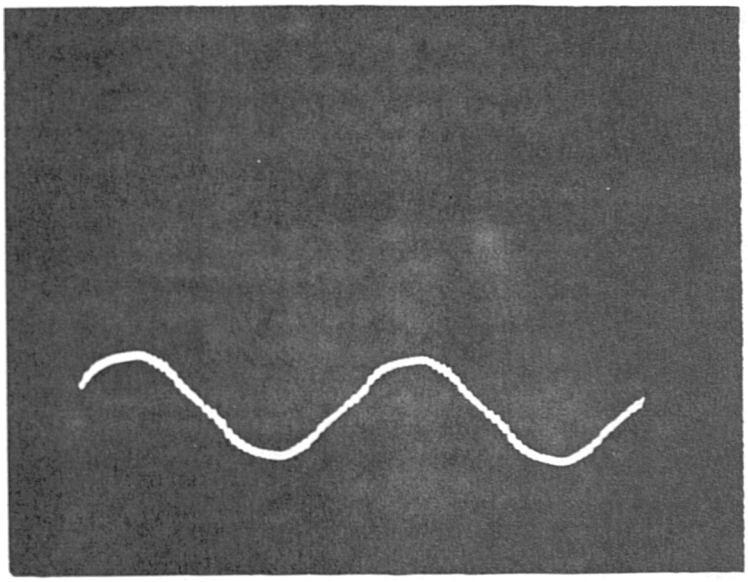

b- Phase current $I_{a1}$ [5 A/cm].

$i_{a1}$ = 2.1 Amp

Fig.(4-6) Input voltage and current of the PM-synchronous machine as a motor fed from the PWM, GTO converter.

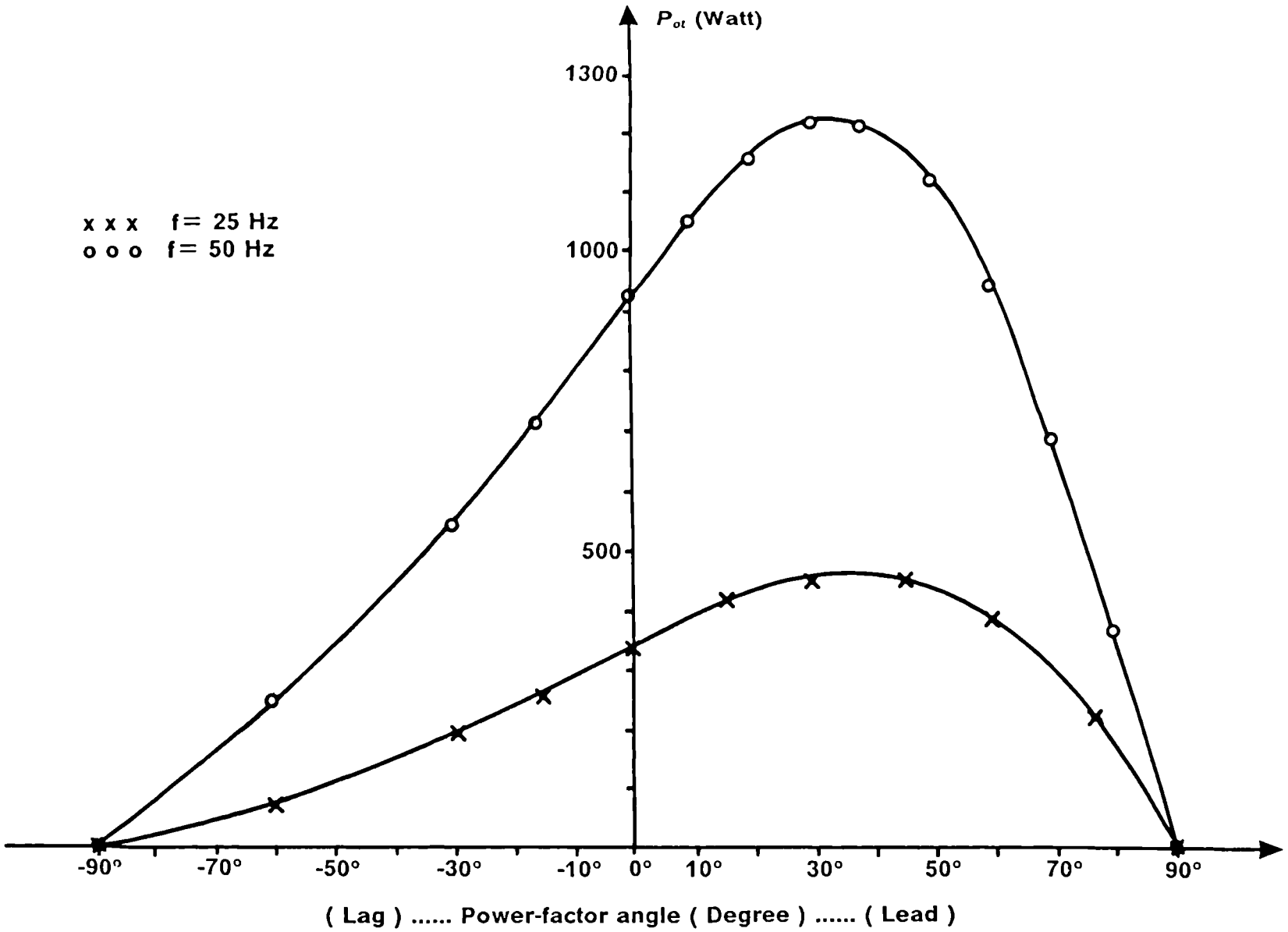


Fig.(4-7) Output power of the generator at constant stator current.
[ $i_a$ = 4.3 Amp]

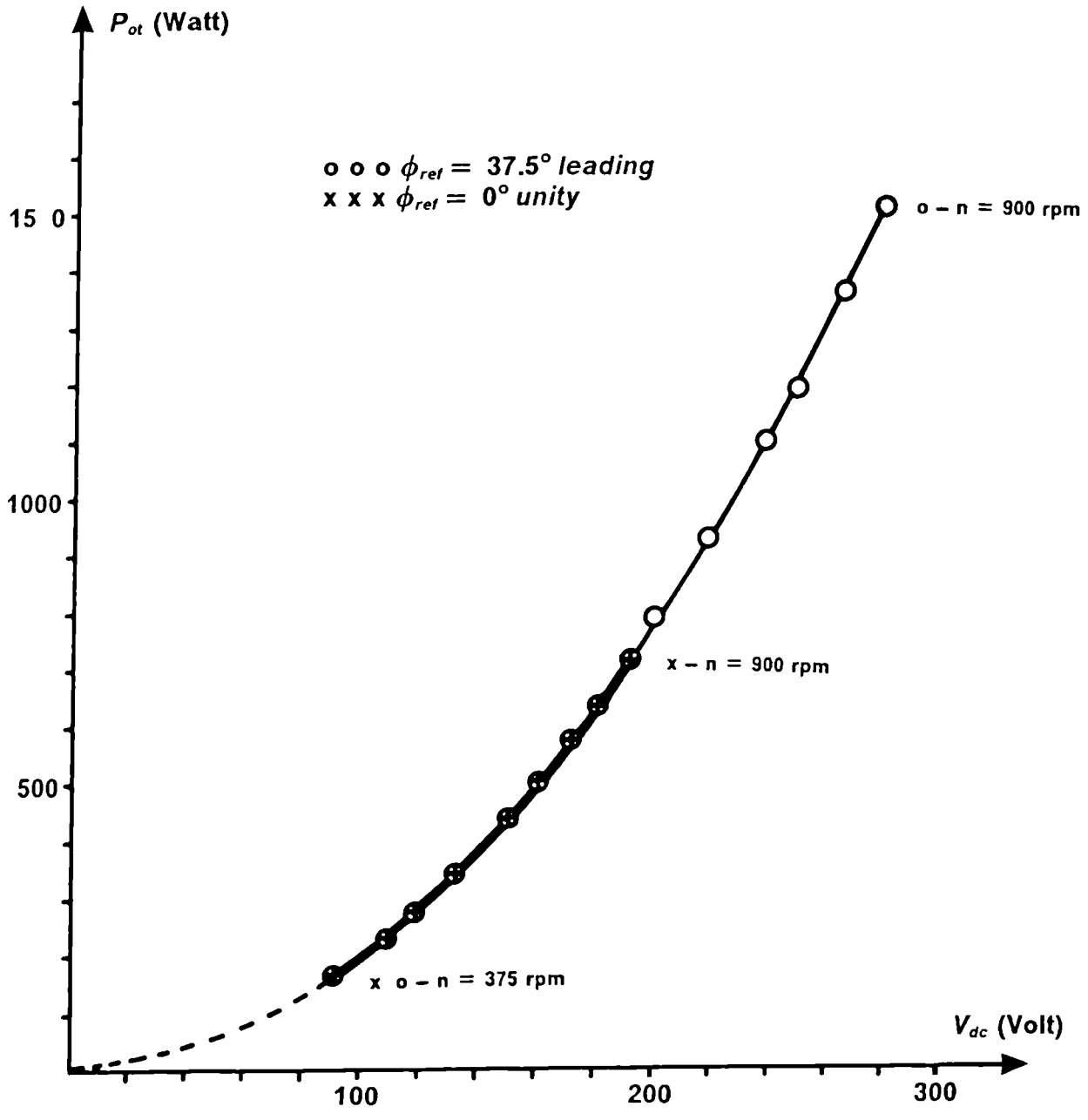


Fig.(4-8) Output power of the converter versus d.c. voltage controlled by the power-factor controller. [n = 375 – 900 rpm]

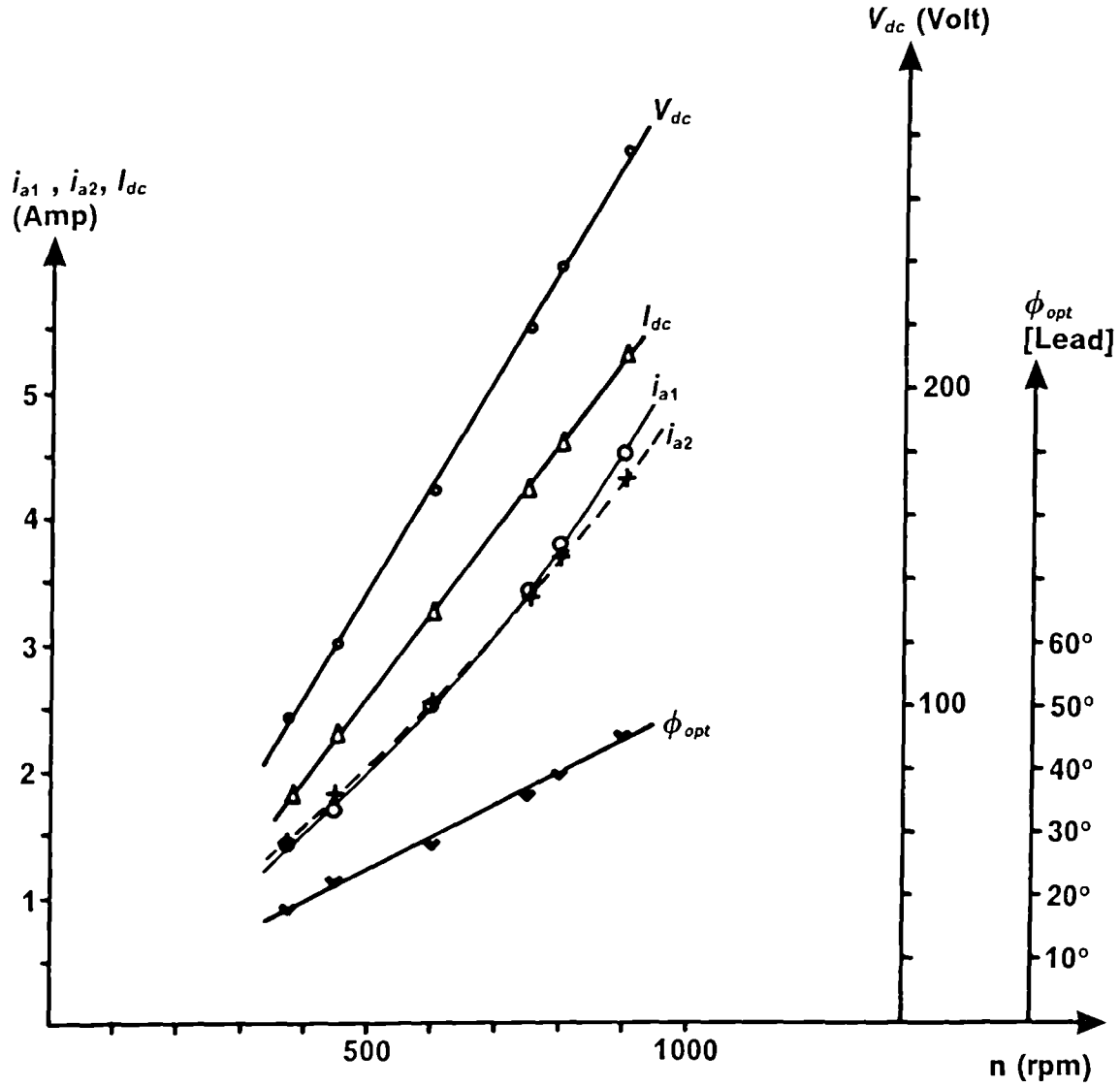


Fig.(4-9) Converter characteristics at maximum power transfer.

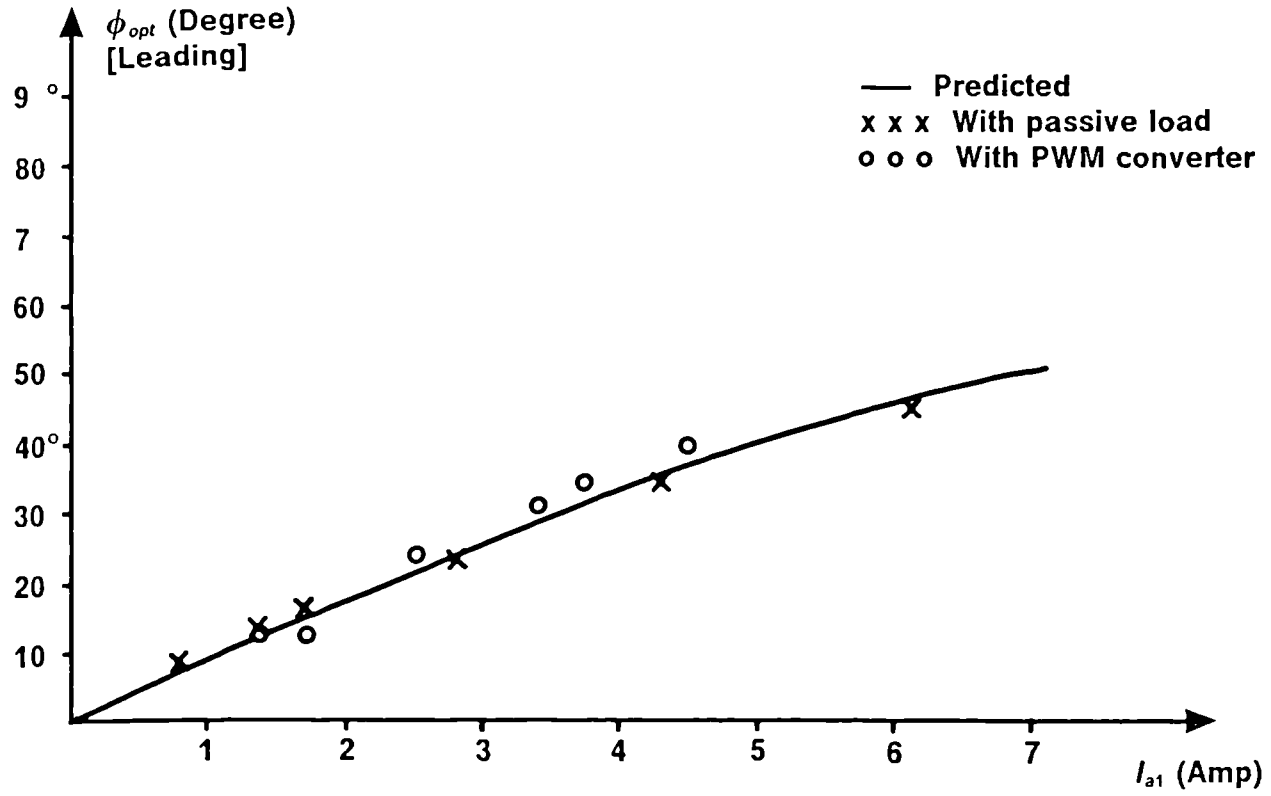


Fig.(4-10) Optimal power-factor angle versus stator current at maximum power transfer.

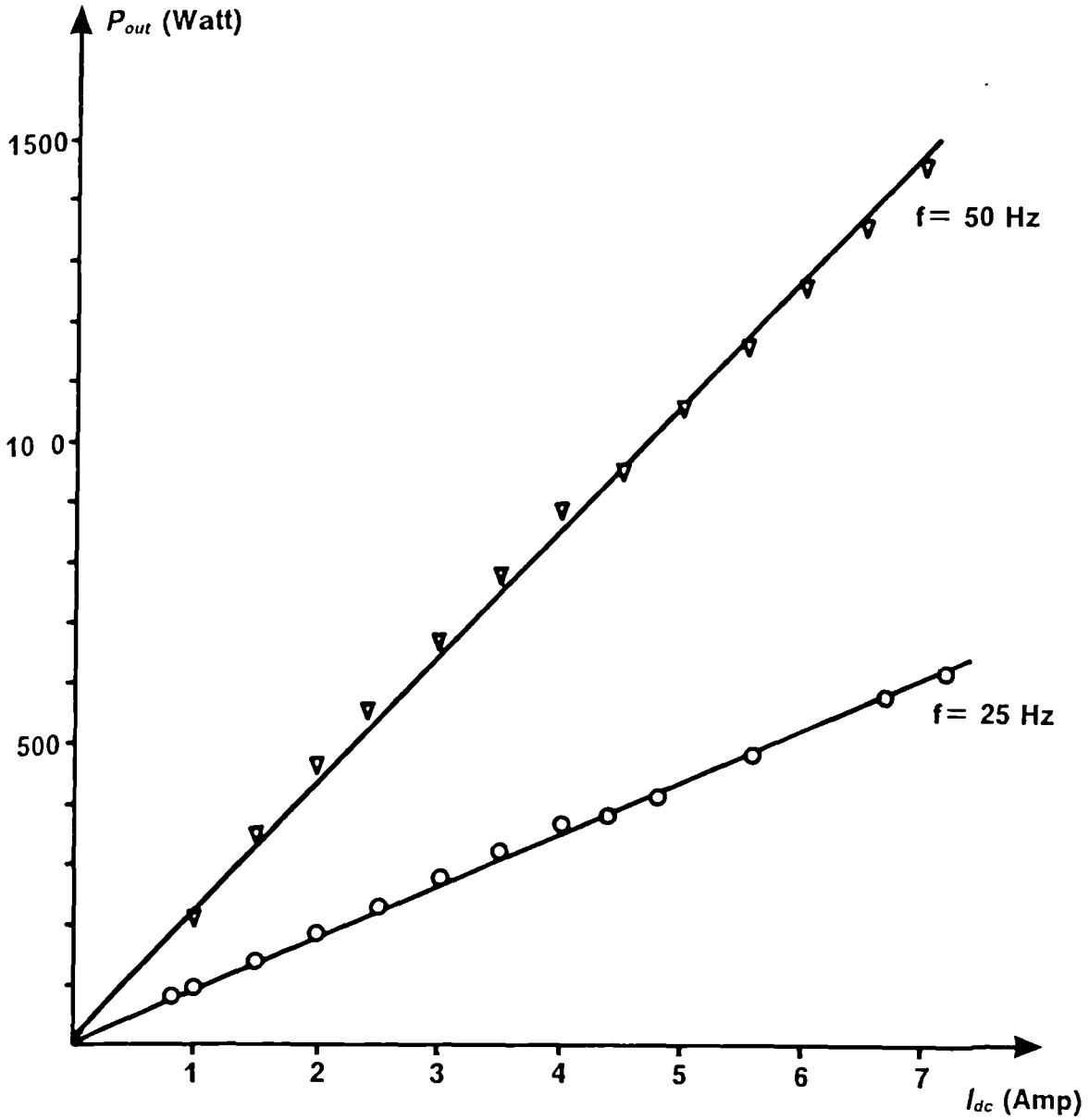


Fig.(4-11) System output power at $\phi = 30°$ *Leading* .

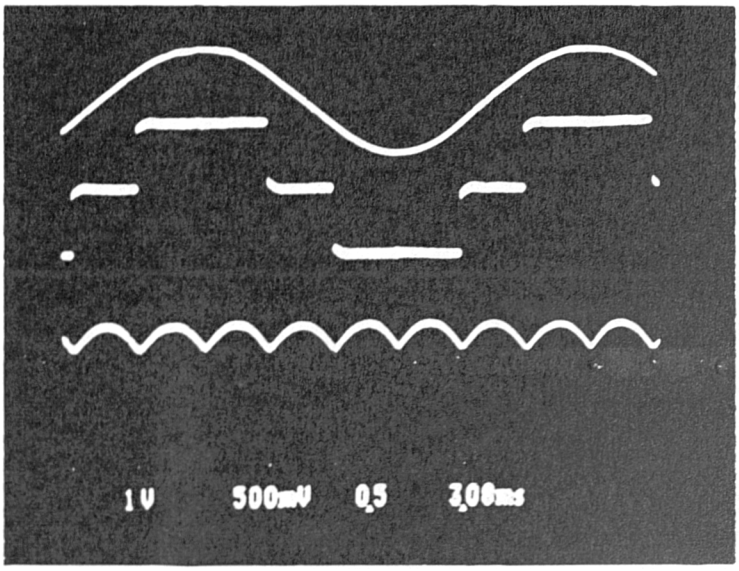


a- Rectifier bridge waveforms.

T/div.= 3.08 ms/cm

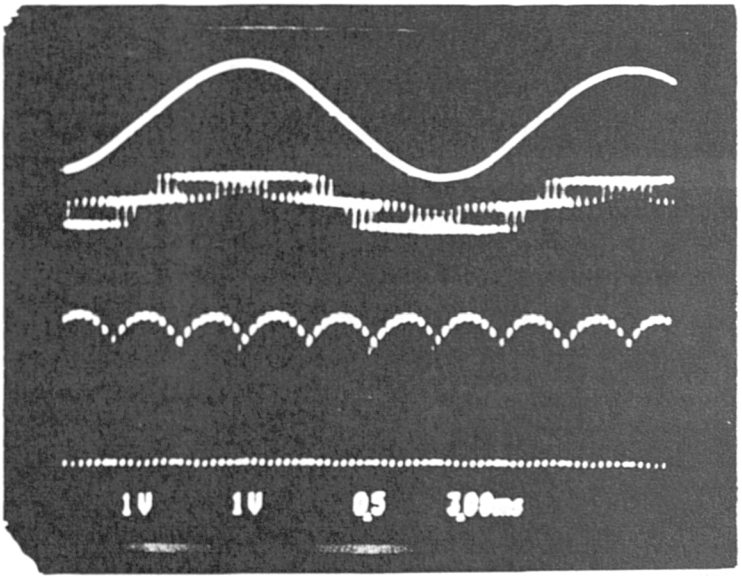


b- PWM, GTO converter waveforms.

Fig.(4-12) Waveforms of two types of the three-phase fully controlled rectifier.

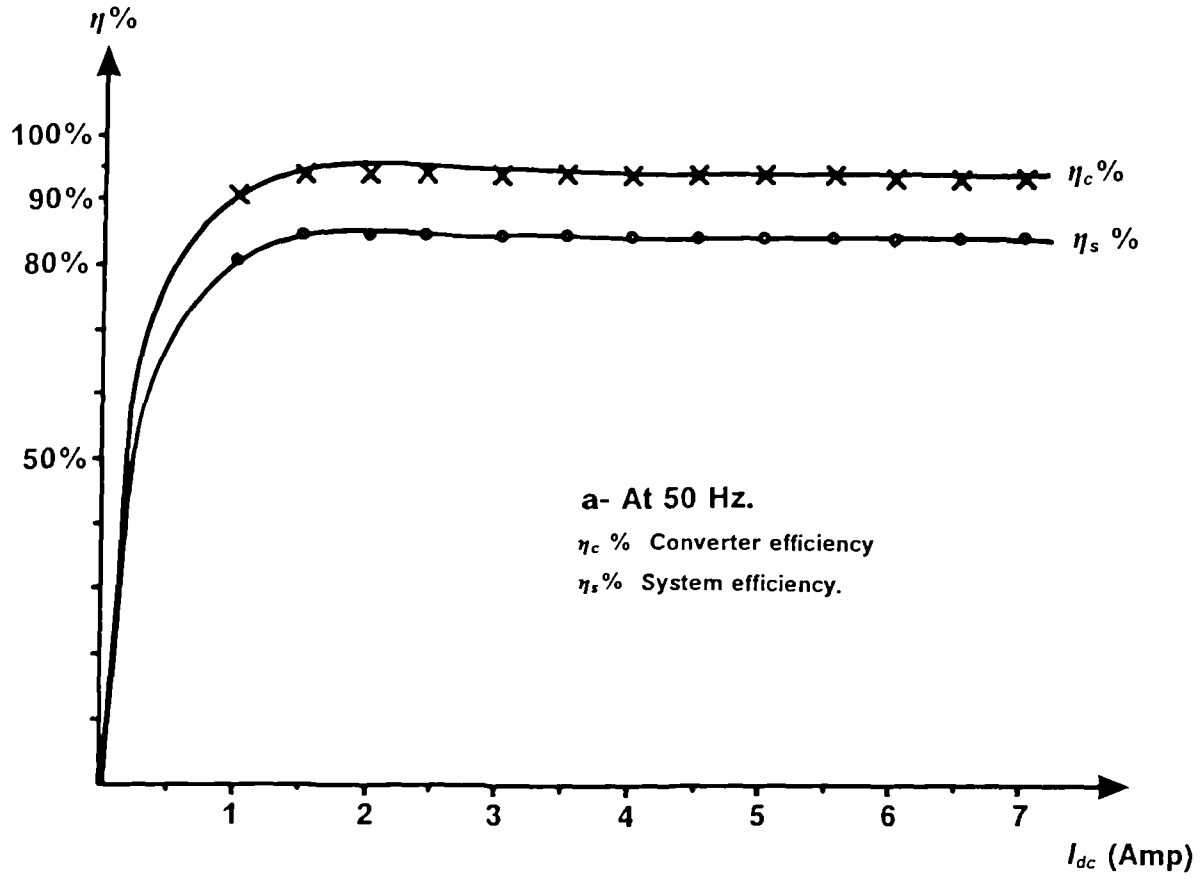


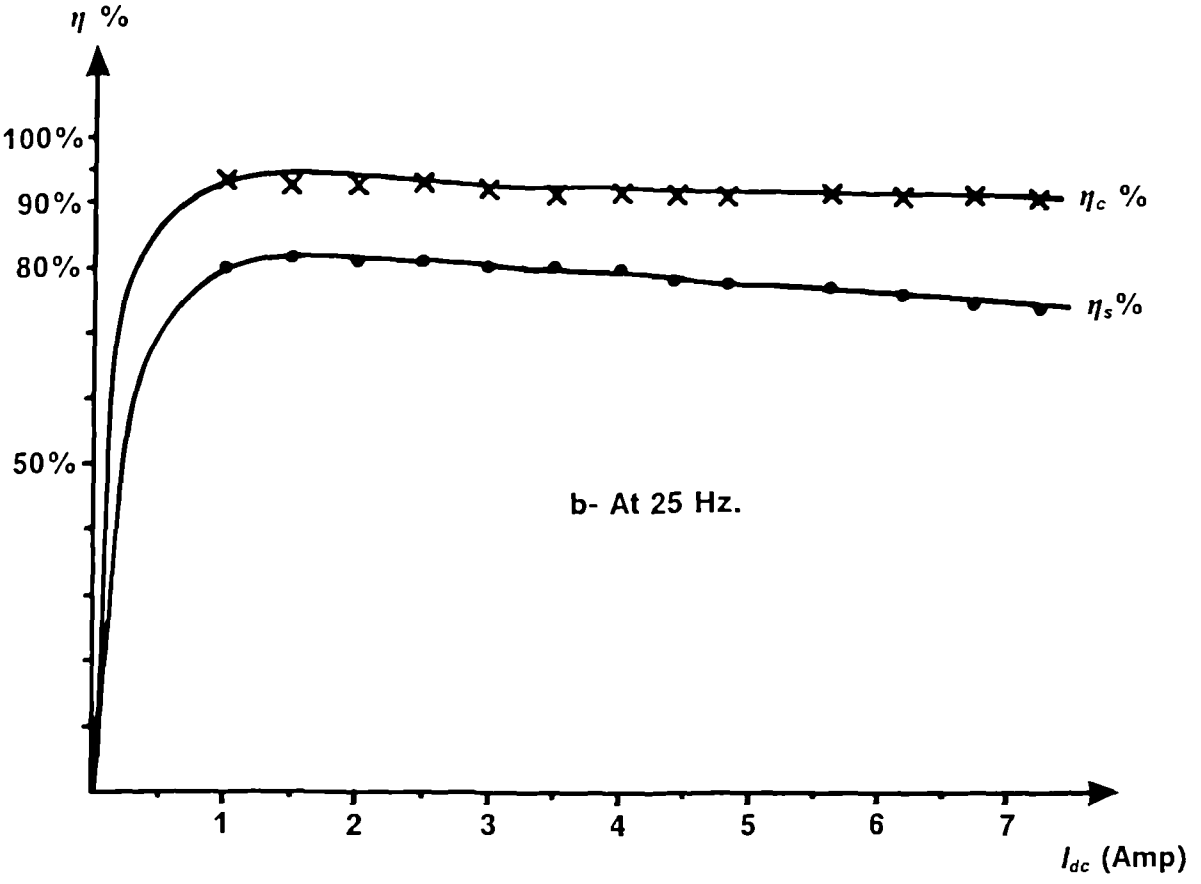


Fig.(4-13) Efficiency of the PWM, GTO converter and the complete system at two different frequencies.

*CHAPTER FIVE*

# CHARACTERISTICS AND APPLICATIONS OF WIND ENERGY CONVERSION SYSTEMS

## 5.1 INTRODUCTION

Human beings have always wished to convert wind power to mechanical and latter to electrical power. Wind, more than any other renewable energy source, has intrigued serious and amateur inventors over the ages. It is said that more patents for wind systems have been applied for than almost any other device to date. The earliest reference to windmills appeared in Arab writings from the ninth century A.D. that described mills that operated on the borders of Persia and Afghanistan some two centuries earlier [1]. The first recorded Northern European mills were built in France in 1180, and in England in 1190 [2]. P.La Cour of Denmark built the first windmill to drive an electric generator, late in the nineteenth century.

Wind-turbines can be classified into many categories because of the great variety in their design. In designing a wind system it is therefore essential to gain some insight into the mechanical properties of wind turbines and their performance. However, they are mainly classified into two categories, based on the orientation of the blade axis. These are horizontal axis machines (like propeller-type blades) or vertical axis machines such as the (Darrieus type turbine) as shown in fig.(5-1). In general, the propeller-type blades are the most common for use in electric power generation. Each turbine has an optimum rotational speed with respect to the wind speed. This is defined by a factor called the tip speed ratio, and is equal to the ratio of the blade tip speed to the speed of the wind perpendicular to the turbine. This ratio is a non dimensional factor used to evaluate the performance of the turbine. Fig.(5-2) shows typical wind turbine characteristics where it can be seen that the propeller-type blade turbine is the most efficient. In any case the detailed mechanical discussion can be

found in many books and papers [1-2, 19-21, 23-25], and is beyond the scope of this work. The size of the turbine used also has great bearing on the type of application. Small wind turbines are usually used locally for generating power in a particular location (stand alone systems) [24, 31]. Large turbines are used to generate power for the utility network. The latter can be synchronous or asynchronous power systems connected to the utility network.

## 5.2 CHARACTERISTICS OF A TYPICAL WIND-TURBINE:

The power harnessed from the wind is created by a volumetric mass of air moving at variable speed in some particular direction. This power is captured by a wind turbine placed in the path of the wind, where in practice only a fraction of this power can be extracted as mechanical power, because of the mechanism of the aerodynamic system.

A wind-turbine generator produces variable amounts of power and usually generates for less than 50% of the time [24]. There are other forms of power generation (e.g. hydro, standby diesel, battery), that can be combined to form a reliable total system. As the output of the wind turbine changes, the load should immediately be changed so as to maintain a match between the wind power and the demand.

The total power available in a wind stream ( $P_{wd}$ ) is equal to the rate of the incoming kinetic energy of that stream and is proportional to the cube of the wind speed ( $v$ ). (i.e. the total power of a wind stream is directly proportional to its density, area, and the cube of its velocity). It is defined by [23-26],

$$P_{wd} - \frac{1}{2}\rho A v^3 \tag{5.1}$$

Where ( $\rho$ ) is the air density (Kg/$m^3$), ( $A$ ) is the cross-sectional area of the wind stream intercepted by the blade ( $m^2$ ), and ( $v$ ) is the wind speed before interception (m s).

The efficiency of the wind turbine is represented by the power coefficient ( $C_p$ ), or Betz coefficient [23-26]. It has been found theoretically that $C_p$ can have a maximum value equal to 0.593. $C_p$ is defined as the ratio of the power available in the wind-stream $P_{wd}$ to the mechanical power $P_m$ available on the shaft of the rotor of the wind turbine, therefore,

$$C_p \quad \frac{P_m}{P_{wd}} \tag{5.2}$$

So, the mechanical power delivered by the turbine rotor shaft is defined as

$$P_m \quad C_p \frac{\rho}{2} A v^3 \tag{5.3}$$

In practice $C_p$ can vary between 0.45 to 0.15 depending on the design of the wind turbine. This arises from a compromise between cost effectiveness and efficiency. Many types of wind energy conversion systems have been discussed in the literature [1-26].

The power extracted from the wind stream is dependent on blade tip to wind speed ratio ( $\lambda$ ). The non dimensional factor, tip speed ratio $\lambda$, represents an important factor, which relates the wind-turbine rotor's radius of rotation ( $R$ ), angular speed of rotation ( $\omega$ ) and wind speed ( $v$ ), (or in

other words it is the ratio of the tangential blade speed to wind speed), therefore

$$\lambda = \frac{\omega R}{v} \tag{5.4}$$

Fig.(5-3) shows $C_p$ versus $\lambda$ characteristic for a typical fixed-pitch horizontal axis wind turbine, thus $\lambda$ represents all possible speed variations [25, 30]. From the graph shown in fig.(5-3), the power coefficient $C_{p(max)}$ is achieved at only one tip speed ratio ( $\lambda_m$ ) for any particular design. So to operate the wind rotor at maximum power coefficient $C_{p(max)}$ at $\lambda_m$ irrespective of variations in $v$, the dotted curve $P_m$ in fig.(5-5) should be followed. It is clearly seen that a constant tip speed ratio operation is desirable for maximum energy extraction from a wind energy system.

The torque developed by a horizontal axis rotor blade of fixed pitch angle varies with both the shaft speed and the wind velocity. If the rotational speed is too slow in a wind stream of a given velocity, the blade will stall, and the output torque of the wind machine will decrease as shown in fig.(5-4). Therefore, to develop maximum output power from a wind stream shown in fig.(5-5), as the speed of the wind-stream varies, either the pitch-angle of the blade or the rotational speed of the blade must be varied. Most of the modern wind machines are designed with variable-pitch blades. A control mechanism is provided that will adjust the pitch of the blades to maintain a constant rotational speed, irrespective of wind speed changes or output load variations [23].

From wind turbine theory [25], the wind turbine torque and power characteristics are plotted against the shaft speed ( n ) as shown in figs.(5-4 and 5-5). From the graphs it is obvious that the maximum power delivered by the turbine occurs at high rotational speed rather than at maximum torque. So the maximum power line is represented by

$$P_m - k_1 n^3 \qquad (Watt) \tag{5.5}$$

and the torque corresponds to that power line is defined as

$$T_{tm} \quad k_2 n^2 \qquad (N.m) \tag{5.6}$$

Where $k$ and $k_2$ are constants [25].

The torque developed on the shaft is defined as

$$T_s \quad \frac{P_m}{\omega} \tag{5.7}$$

Substituting eqns. 5.3 and 5.4 into eqn. 5.7 results in

$$T_s \quad \frac{C_p \frac{\rho}{2} A v^2 R}{\lambda} \tag{5.8}$$

Therefore,

$$\frac{C_p}{\lambda} \quad \frac{T_s}{\frac{\rho}{2} A v^2 R} = C_T \tag{5.9}$$

Where $C_T$ is called the torque coefficient of the wind turbine, and this is used to evaluate the solidity of the aerodynamic turbines.

## 5.3 APPLICATIONS OF ENERGY CONVERSION SYSTEMS TO WIND TURBINES:

As we discussed earlier, wind energy can be used for a number of different applications. The implication of these to the control of a wind system, which uses the permanent magnet machine and the GTO converter as the means of energy conversion, is discussed in Chapter 6. The experimental results are discussed below:

### 5.3.1 Resistive load:

The mechanical power delivered to the PM-generator is converted to a d.c. power. A resistive load is used as a heater on the d.c. side. The heat could be used for many purposes. Such as in boilers to be used for factories, or for heating houses. A heater of 2 kWatt was used with the proposed system. The control unit and its function is very simple. As the wind speed is increased more load is inserted into the system to absorb that power. Fig.(5-6) shows the output power versus d.c. voltage characteristic for a speed range of 250-900 rpm. The system is tested for two loads, however, as the load is increased the extracted output power is increasing also. The output power from the PM-generator is increased at high speeds by increasing the power-factor angle towards leading as shown in fig.(5-7). The load must capable of handling this increased power.

### 5.3.2 Battery charging:

One of the useful applications of wind energy is its use in battery charging. The turbines used for that purpose are classified as small scale wind turbines. Use is generally in remote places, such as in communication

repeater-stations or used for changing batteries in camps and remote villages. The PM-synchronous generator was tested for this purpose to give both constant output voltage $V_{dc}$ and current $I_{dc}$ at any speed. $V_{dc}$ and $I_{dc}$ are kept constant by adjusting the modulation index of the PWM pattern. Fig.(5-8) shows the output d.c. voltage versus the generator speed n . The percentage of error in the output d.c. voltage is within $\pm$ 0.9%, therefore, good accuracy is achieved. The PM-generator presented in this work can be replaced with an induction generator [5] or by a conventional synchronous generator used by Bolton and Nicodemou [30], but both of them are considered to have disadvantages as discussed in chapter one, such as reactive power demand for the former and the maintenance for the latter, as well as the harmonic content.

### 5.3.3 Back to back converting scheme:

The variable wind energy can be supplied to the main a.c. network, but of course, the main a.c. network has a constant terminal voltage and constant frequency, which is vital to be connected to a wind or tidal power system directly. However, in order to implement the connection of variable sources of energy to the main a.c. network, some consideration has to be given to the characteristics of the generator and the a.c. network. Many different systems have been employed to date. In principle they are similar, but each has been designed for a different requirement. It has been mentioned in Chapter 1 that some systems use induction generators directly connected to the a.c. network, but that they have the disadvantage of frequency limitation. Some systems, on the other hand, use pole changing of the generator adding complexity to the system, and increasing its cost effectiveness.

In a sense d.c. transmission offers such important advantages to make it more attractive at present to a.c. transmission. Some of them are discussed below:

1- D.c. power can carry higher power than for a.c. power transmission, because of the effect of capacitance in a.c. transmission. Therefore, d.c. cables are more likely to be used for longer distances than those for a.c. cables.

2- D.c. power can be transmitted between two different stations in spite of the frequency difference between them. However, for a.c. transmission there is need to match the frequency as well as the effect of reactance and phase difference at the connection ends.

However d.c. transmission is not in common use because high voltage power electronic converters are a recent development involving complexity and cost. Furthermore the d.c. transmission can be used only between two points due to the difficulty of tapping the d.c. power along the line. However in the work presented here we have only two converters adjacent to each other to form a conversion scheme.

The present work is focused on new power electronic devices called GTO thyristors. A current source converter of six-GTO thyristors has been implemented in this study and is used as a controllable voltage and power-factor rectifier. Another converter of the same specification, but simpler in its control circuitry has been constructed, for connection to the a.c. network to reconvert the wind energy to a form suitable for connection to the

a.c. network. Thus, the GTO converter is used in the inversion mode. Such a system is called a (back to back) converting scheme, or a d.c. transmission system as shown in fig.(5-9). The advantages of this system, can be exploited extracting the power from the wind or the tide in spite of the power fluctuations. In a wind-energy conversion system, as discussed earlier, the power is inevitably variable in terms of voltage and frequency. This variation can be very large and a controller has been designed to adapt all these variations within its limits. The case of a tidal-energy conversion system is less complex, since there is smaller range of voltage and frequency of the generator. Therefore the controller is simpler in its function. However, the present work has the capability for controlling either of the two systems.

Fig.(5-9) shows the schematic diagram of the whole transmission power system. This system transfers the power into two directions from the PM-synchronous generator to the a.c. network, or from the a.c. network to the PM-machine (working as a motor). The rotor of the PM-generator is coupled to a prime mover turbine and electrically connected to a 6-switch GTO converter (converter-1), working as a rectifier. The output of this converter is connected through a d.c. link to another 6-switch GTO converter (converter-2), working as an inverter. The a.c. side of converter-2 is connected to the main a.c. network of constant frequency and voltage. d.c. reactors were placed between the two converters to separate the output d.c. voltages of both converters, and to smooth the d.c. current. The principle of operation is divided into two modes:

1- The power transmitted from the generator to the a.c. network.

2- The power transmitted from the a.c. network to the PM-machine.

In the first case when the PM-generator supplies the power to the a.c. network. Converter-1 works as a fully controlled rectifier with a delay angle $\alpha_1 = 0°$. The converter d.c. voltage $V_{d1}$ may be varied by adjusting the modulation index $M_1$ of the PWM pattern. The second converter (which is identical to the first one) operates as an inverter receiving the power through the d.c. link, and transferring it to the main a.c. network. The delay angle of converter-2 will be $\alpha_2 - 180°$, and its d.c. voltage $V_{d2}$ may be similarly varied by adjusting the modulation index $M_2$ of the PWM pattern. However, the delay angle $\alpha_2$ can be expressed as an advanced angle defined by [ $\beta$ 180 $\alpha_2$]. Therefore for simplicity $\alpha_1$ and $\beta$ can be adjusted from 0° (Which gives maximum output d.c. voltage of both converters) to 90° (which gives zero volts of the output d.c. voltage). It is obvious that the resistance in the d.c. link unless very small will cause a high voltage drop causing large system losses. Therefore any small variation in the d.c. link voltages $V_{d1}$ and $V_{d2}$ will cause large amount of d.c. current. According to this the d.c. current is defined as

$$I_{dc} \quad \frac{V_{d1} \quad V_{d2}}{R_d} \tag{5.10}$$

Hence, in practice certain precautions should be taken to limit the high current fluctuation. Thus for this type of power transmission, the output d.c. voltage should be controlled in such a way to overcome the above problem.

For d.c. power transmission the output d.c. voltage $V_{d1}$ and current $I_{dc}$ characteristics should have the function shown in fig.(5-10) [8]. The characteristics of either of these converters has been explained in this figure. The output d.c. voltage $V_{d1}$ is kept constant for the d.c. current which can

vary from zero up to a reference level called $I_{d1}$ as shown in fig.(5-10a). Then, when $I_{dc}$ reaches this value, $V_{d1}$ is reduced sharply to zero, (the reduction is done by adjusting $M_1$ ). Converter-2 d.c. voltage $V_{d2}$ has the same shape, but in reverse order, i.e. $V_{d2}$ is kept zero until the d.c. current reaches a reference value of the d.c. current $I_{d2}$ setup by converter-2 as shown in fig.(5-10b). Fig.(5-10c) shows the two curves superposed to show the operating point of the d.c. link (which is the intersection point of the two curves). It is clearly seen that $V_{d2}$ is made slightly smaller than $V_{d1}$. It is the same as in the converter when working in the inversion mode and connected to a d.c. source (discussed in chapter Four). $I_{d2}$ also is made smaller than $I_{d1}$ to produce a working margin stated in some books to be as 10% of the rated load current. From the shape of the curves good protection is obtained against a fault condition in the d.c. link. The voltage will reduce quickly to zero when a fault occurs.

For the second mode of operation of this conversion system the power is transferred back from the a.c. network to the PM-machine; hence a regeneration process. In order to do this the delay angles $\alpha_1$ and $\beta$ of both converters need only to be changed. Taking into account the voltage and current characteristics need to be reversed. $\alpha_1$ now operates in inversion mode and $\beta$ in rectification mode. Adjustment of machine speed is made by changing the modulation index $M_1$.

In the present work the controller can be programmed to any desired function. Therefore each converter has its controller working separately with programmed values which have been setup for any working condition as shown in fig.(5-9). Each controller can work individually with mutual effect

on the other. Then, if the set values need to be changed, these will be adjusted for both converters at the same time. The controller will be discussed in chapter Six, but it is worth to mention that the functions of the output d.c. voltage and current characteristics shown in fig.(5-10) can be stored in an EPROM.

## a- Horizontal axis types.

U.S.Farm windmill

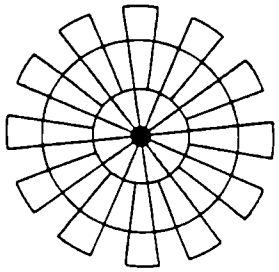

Dutch windmill

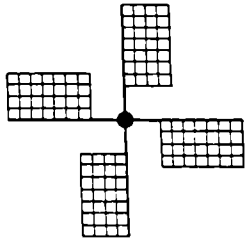

2, and 3-blade Propellers

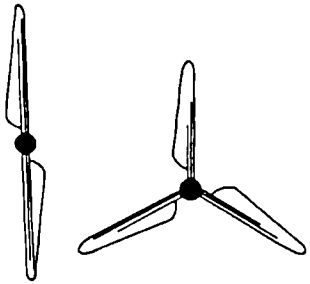

Cross-wind paddles

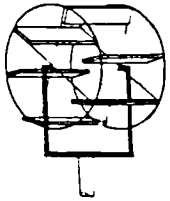

## b- Vertical axis types.

$\phi$ -Darrieus

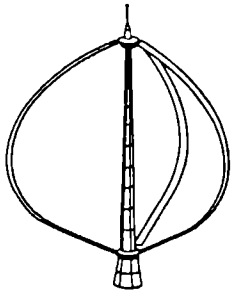

$\Lambda$-Darrieus

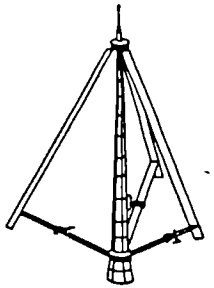

Giromill

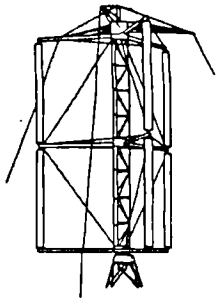

Savonius

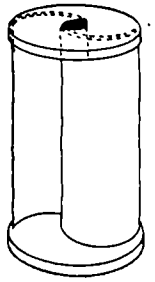

**Fig.(5-1) Types of windmill blades in use.**

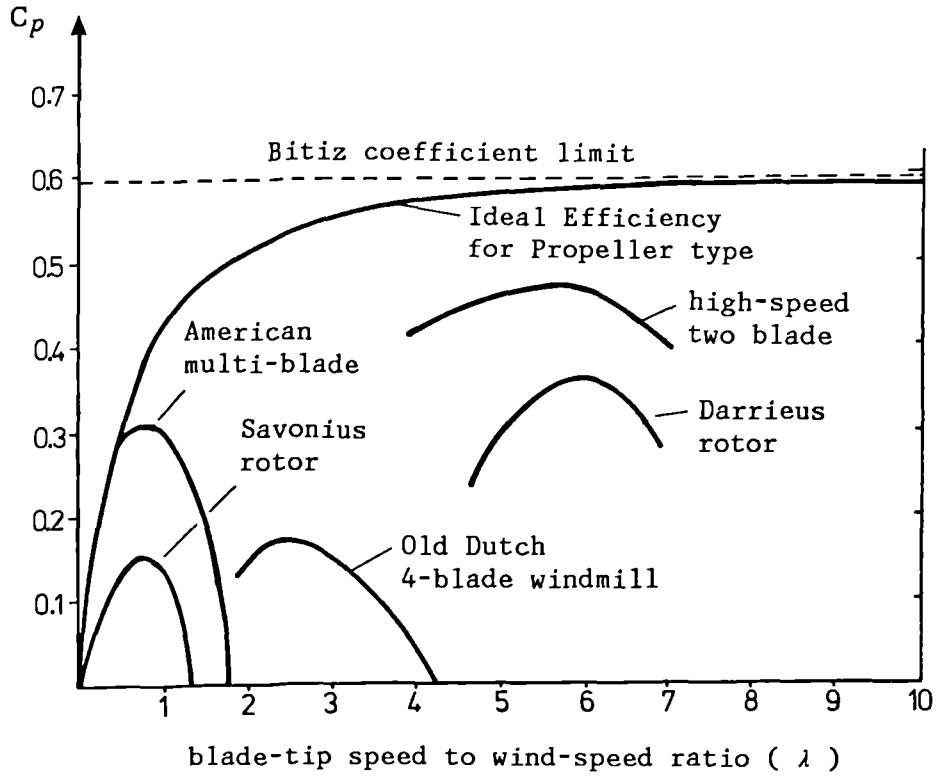


**Fig.(5-2) Typical performances of wind turbines.**

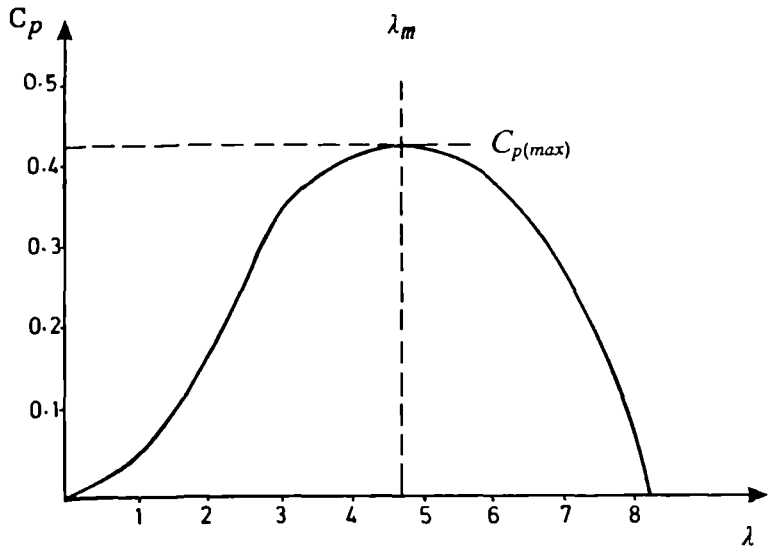


**Fig.(5-3) Typical Power Coefficient versus tip speed ratio characteristics.**

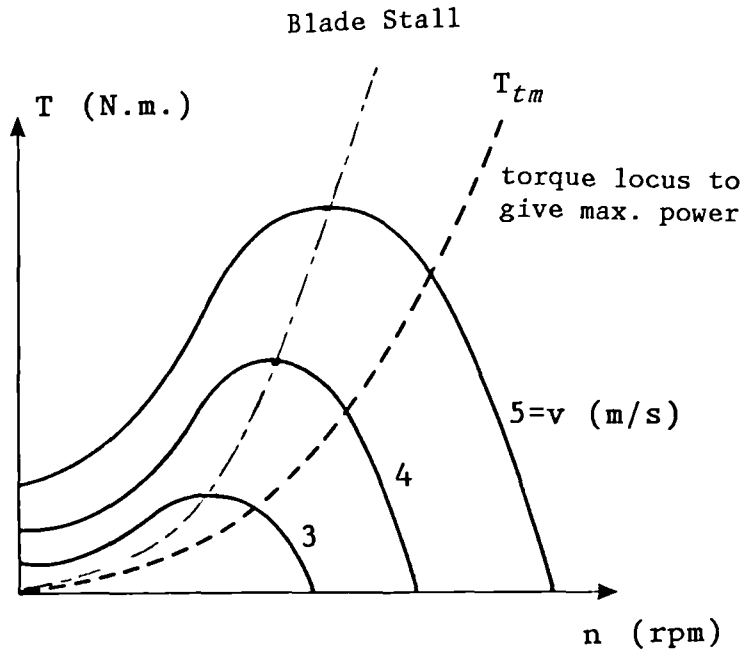


**Fig.(5-4) Characteristics of wind-rotor torque versus its shaft speed for different wind velocity.**

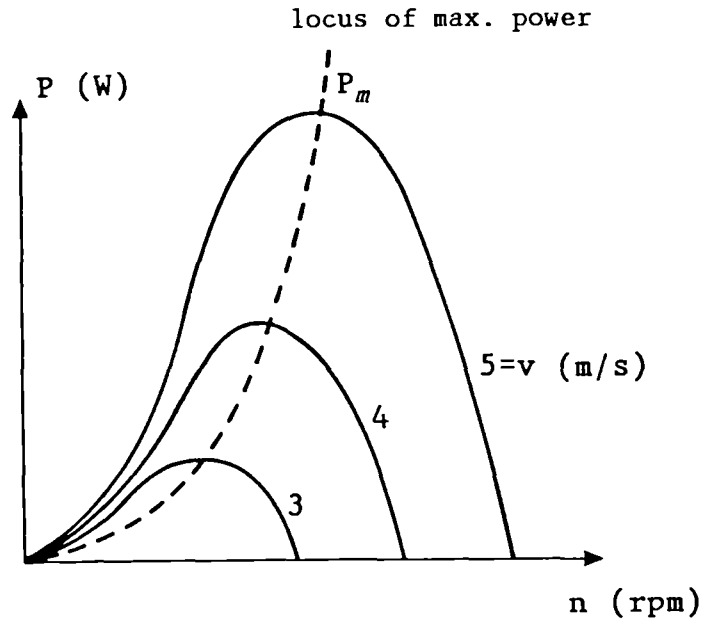


**Fig.(5-5) Characteristics of wind-rotor power versus its shaft speed for different wind velocity.**

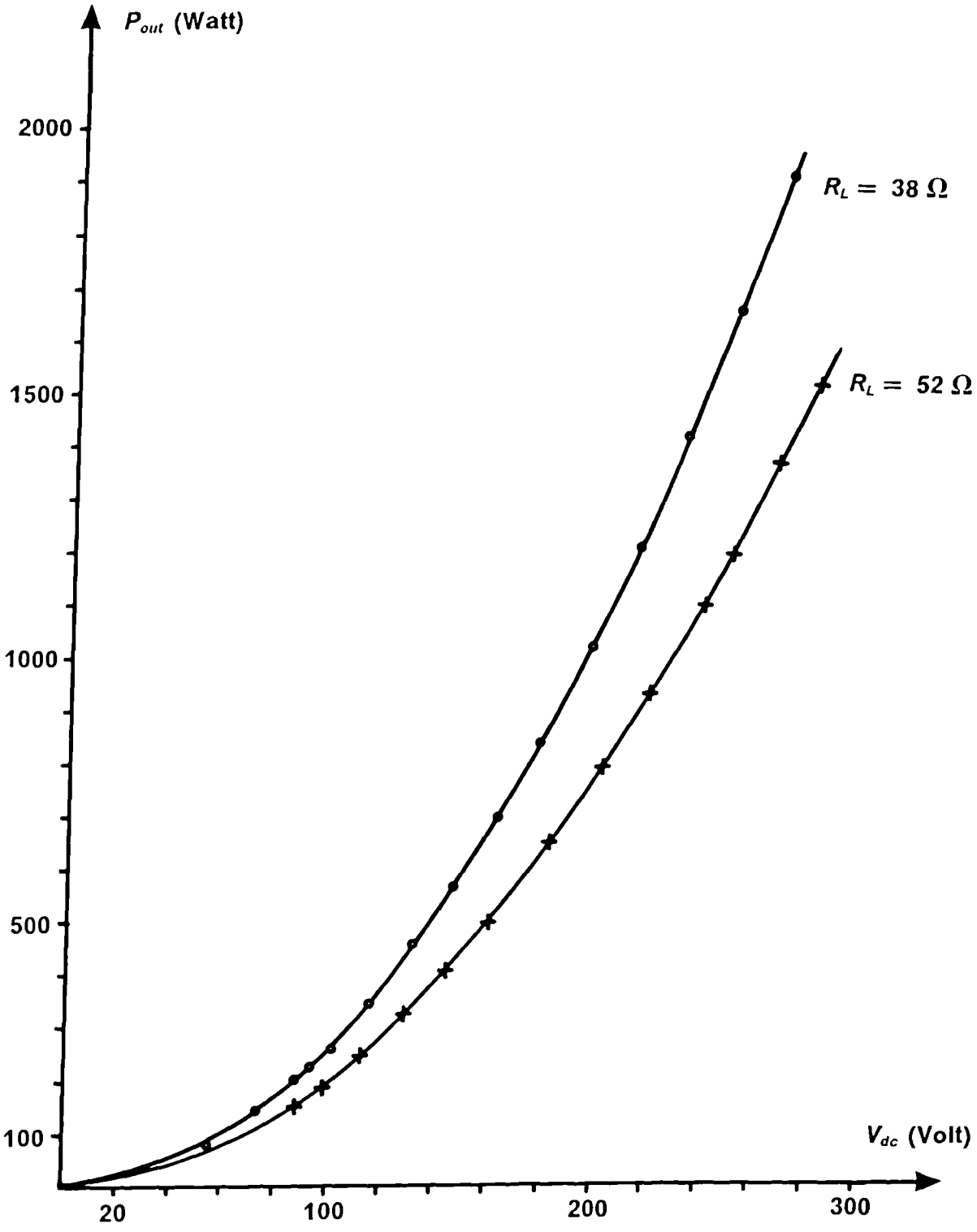


Fig.(5-6) Output power of the System at different load for speed [n = 250 -- 900 rpm, $\phi_{ref} = 37.5°$ ].

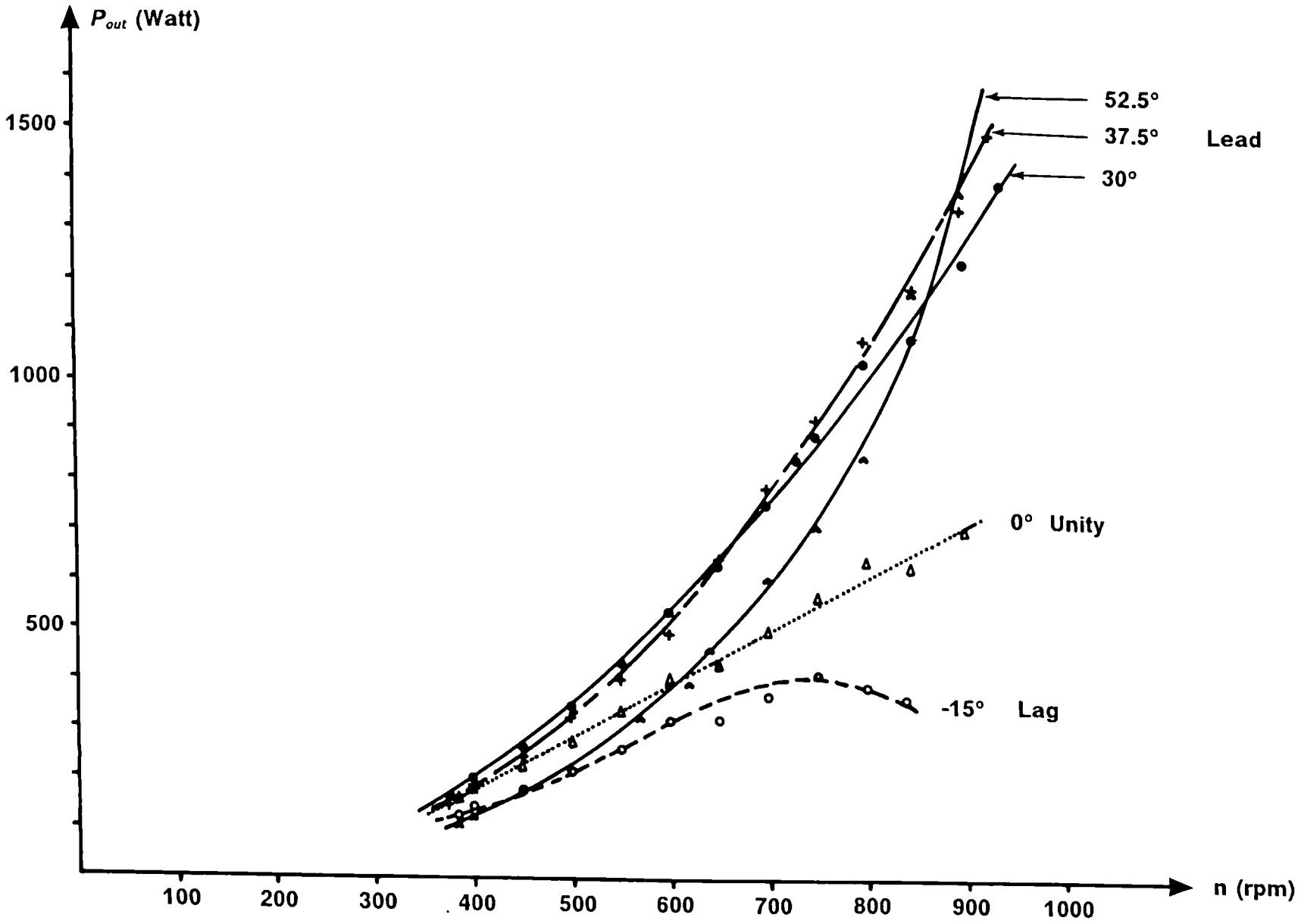


Fig.(5-7) System output power at constant load impedance.

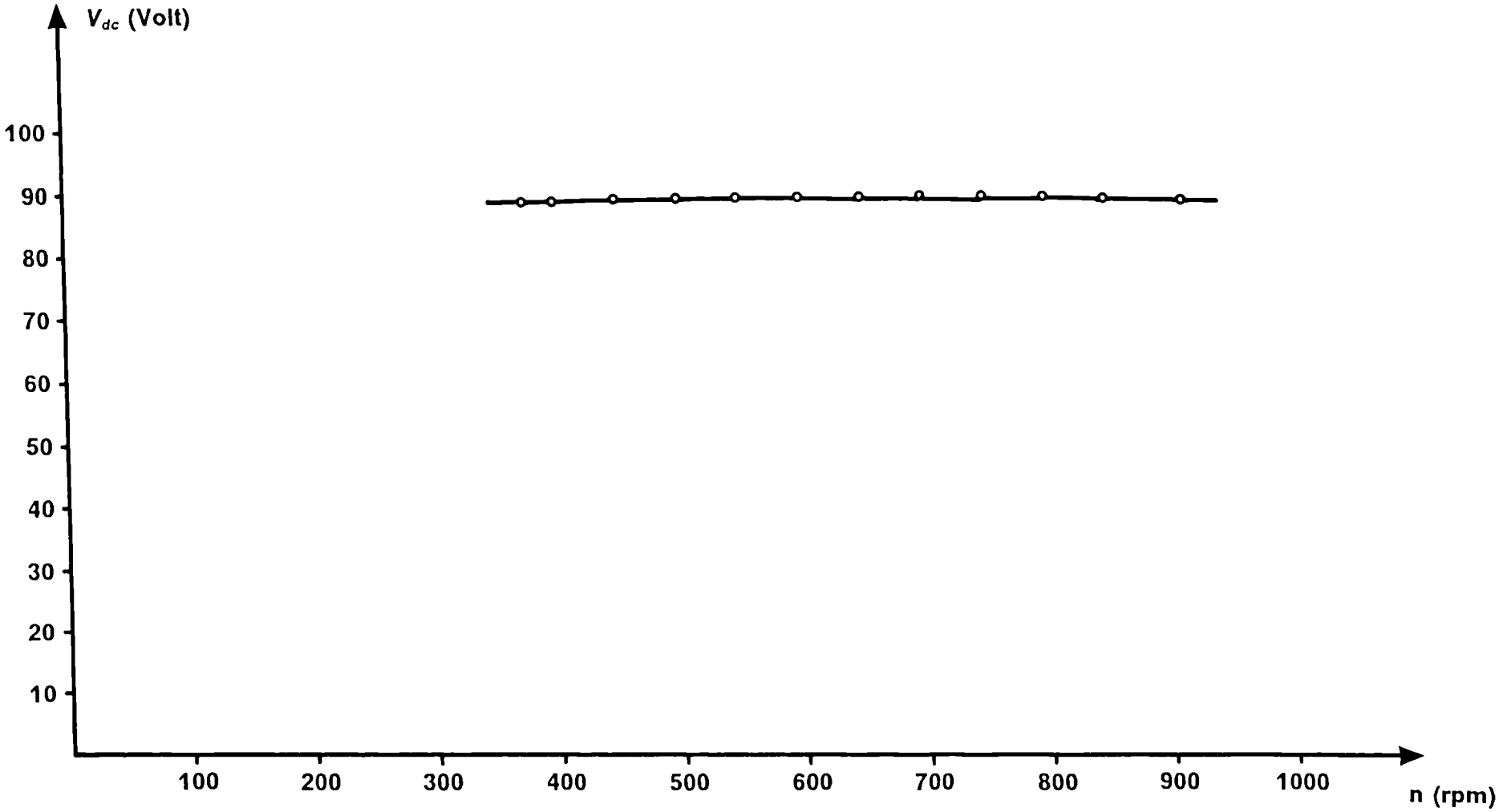


Fig.(5-8) Converter output characteristics when used for battery charging.

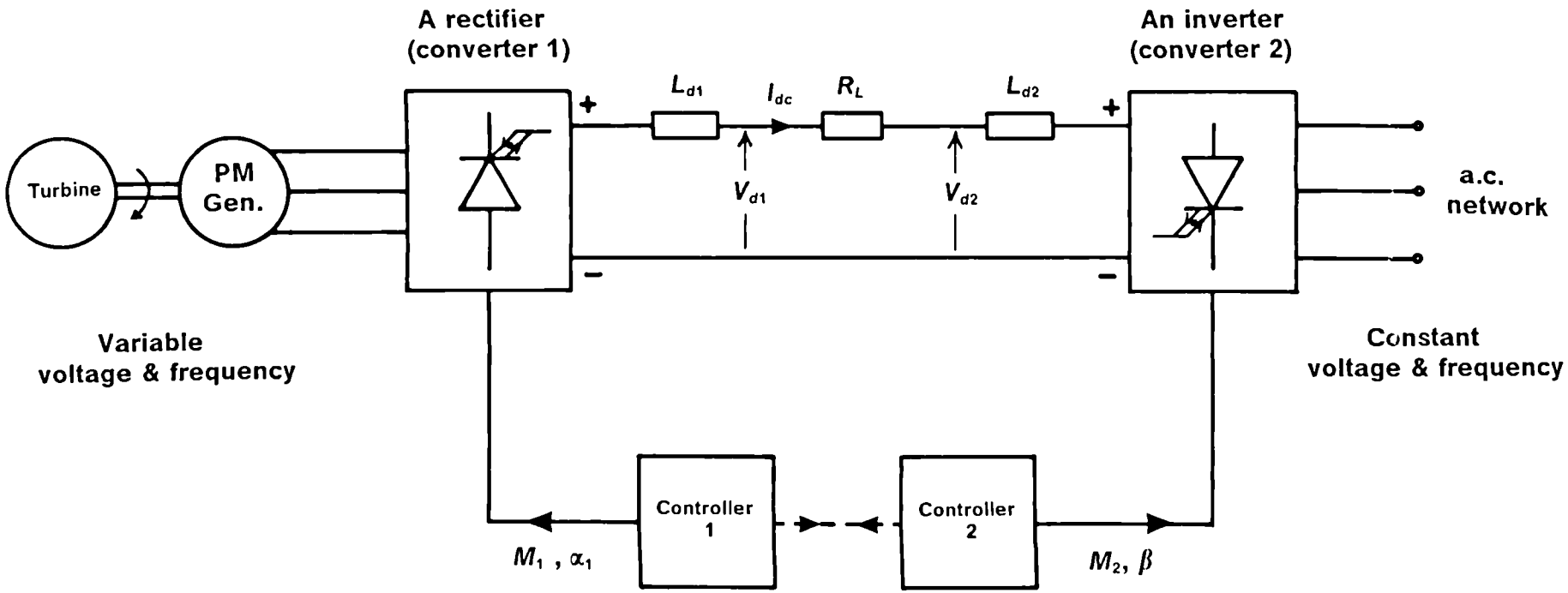


**Fig.(5-9) Power transmission system using PWM, GTO converters in a back to back converting scheme.**

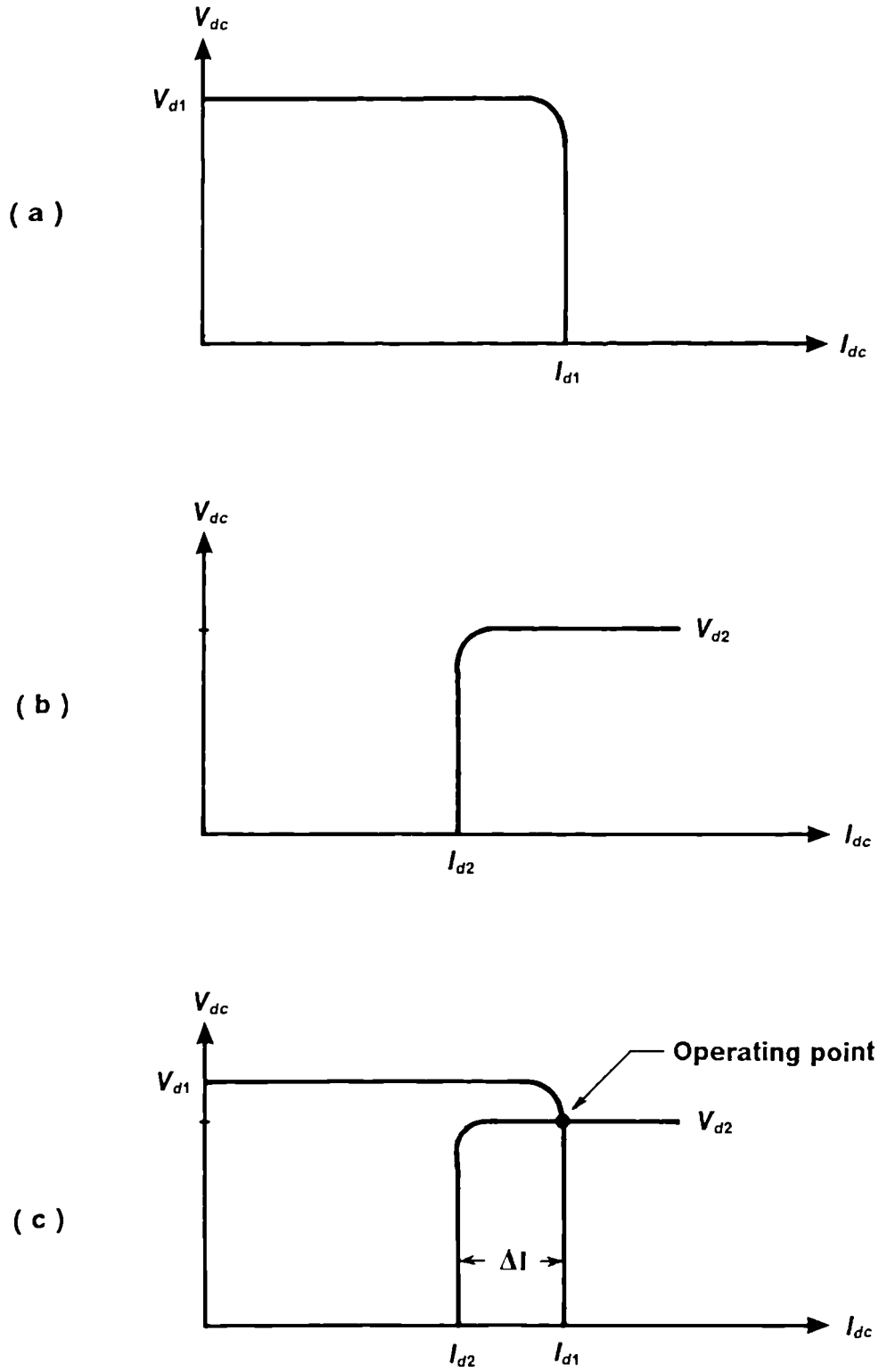


Fig.(5-10) Output d.c. voltage and current characteristics of the back to back converting scheme.

a- Converter-1 as a rectifier. b- Converter-2 as an inverter.

c- Voltage operating point for both converters.

*CHAPTER SIX*

# POWER-FACTOR AND OUTPUT POWER CONTROLLER FOR A WIND ENERGY SYSTEM

## 6.1 INTRODUCTION.

The combined PM-generator and PWM, GTO converter system may be controlled to be used in variable energy sources at its maximum power and efficiency. The controller is used to optimise the generator performance and to match the implemented converting scheme. In this chapter the system controller will be discussed and applied to the examples used in Chapter 5. The system controller is divided into two controllers which are used to control three parameters as shown below,

1- The first controller controls the power-factor angle $\phi$ as a function of both frequency and output d.c. current. The power-factor is controlled for its optimal value by a reference function stored in an EPROM { $\phi_{opt} \propto f(I_{dc}, f)$ }. As mentioned earlier in wind energy schemes the speed of the turbine is changing with wind speed, therefore the frequency of the electric generator will be changed, as will as the power-factor angle. Then to optimise the output power and the efficiency of the generator the power-factor angle will be controlled as a function of the d.c. current of the converter.

2- The modulation index control is used as a second controller to control the output power of the power-conditioner (converter) by changing the amplitude of the average d.c. current, to match the wind-turbine power, i.e. the modulation index controller is used to match the converter performance to the application needed. Furthermore it is used to protect the converter from high voltage and high current that could occur.

## 6.2 POWER FACTOR ANGLE CONTROLLER OPERATION:

In this section the circuit operation of the phase controller shown in fig.(6-1) is discussed. Two reference signals were used for the phase control operation, the first signal is from the line voltage $V_{tcl}$ , and the second signal is from the stator phase current $i_{a1}$, which is used as a reference for power-factor angle $\phi$ measurement. The controller is very simple and active, and utilises the delay angle ( $\alpha$ ) of the converter to correct any changes in the power-factor angle $\phi$. The delay angle $\alpha$ of the converter is the angle between the terminal phase voltage $V_{tp}$ and the input line current ( $i_{a2}$ ) to the converter, and can be varied from -180 to 180°.

The difference in the phase angle between the terminal voltage $V_{tl}$ and the line current $i_{a1}$ is measured and added to an offset value for calibration reasons, it is then compared with the phase reference command $\phi_{ref}$ to the setup value required. The output from the 6-bit comparator is the error signal which sets the second up down counter to change the delay angle $\alpha$ to correct the phase angle $\phi$ between $V_{tp}$ and $i_{a1}$. Then, the changes will continue until the error signal becomes zero. However the power-factor angle controller makes the angle $\phi$ independent of both system frequency ( f ) and the output d.c. current from the converter. These characteristics will be discussed in the next sections.

The signal ( v ) shown in the waveform diagram in fig.(6-2) represents the voltage reference signal ($V_{tcl}$). This signal is taken from the first input to the PLL phase-comparator, while the other reference is from the stator line current $i_{a1}$ through a current transducer. Then, the current signal ( $i_Q$ ) shown in fig.(6-2) is generated by the positive going edge of $i_{a1}$ and the negative going

edge of ( v ). The current signal $i_Q$ is fed with the voltage signal ( v ) to an EXOR gate to give the phase difference between the converter input voltage and the stator line current $i_{a1}$. This phase difference ($\phi_{in}$) is measured by the first 8-bit up/down counter shown in fig.(6-1). Then an offset value is added to the counter reading by loading the counter at each measurement cycle as shown in fig.(6-2). This phase ( $\phi_{in}$ ) represented by the 8-bit output of the counter, and is fed to a latch circuit to prevent the changes of the phase shift, when the counter to be loaded at the next measurement cycle until the right phase to be latched. A D-type flip flop (not shown in the figure) was used to set the first counter for lead or lag operation, which gives the input line current $i_{a1}$ a range of leading and lagging phase shift referred to input phase voltage.

The phase reference $\phi_{ref}$ command represents the phase required after the correction in phase between the phase voltage $V_{tp}$, and the stator line current $i_{a1}$ . The error signal ( $\phi_E$ ) of the phase difference from the output of the comparator is defined as,

$$\phi_E = \phi_{in} - \phi_{ref} \tag{6.1}$$

This error is zero for a steady state condition. However, if a change will be in $\phi_{ref}$ side or $\phi_{in}$ side there will be an error signal $\phi_E$ which is used to correct the power-factor angle $\phi$ using the second up/down counter as shown in fig.(6-1). Here again the second 8-bit up down counter is used for lead and lag changes . The lead and lag in phase demand is calculated by the same 8-bit comparator. Six-bits from this up/down counter were used to correct the power-factor angle by adjusting the value of the delay angle $\alpha$.

The speed of changing the power-factor angle $\phi$ is dependent on the clock (CLK3) of the second up/down counter. This clock CLK3 is taken from the terminal voltage frequency ( f ) through a 4-bit binary counter. Then, the terminal voltage frequency ( f ) is divided by (16) to produce (CLK3) Hz, therefore, the gain ( K ) in this case of the closed loop counter is equal to (1 16). The gain is chosen at this value, since the mechanical response of the system is slow compared with the power-factor angle $\phi$ changes .

### 6.2.1 POWER FACTOR CONTROL WITH OUTPUT D.C. CURRENT CHANGES:

The stator current $i_{a1}$ has been taken as a reference for power-factor angle control. The phase $\phi$ will be changed with the magnitude of the converter input current $i_{a2}$ from ($\phi = 90°$ leading at $i_{a2} = 0$ Amp up to $\phi = \alpha°$ for $i_{a2} = \infty$), this happens due to the presence of the capacitive filter at the input of the converter. Fig.(6-3) shows the fundamental components of the stator current $i_{a1}$ and the input converter current $i_{a2}$ . The capacitor filter current $i_c$ always leads the terminal voltage $V_{tp}$ by 90°. The converter input current $i_{a2}$ is dependent on the output d.c. current $I_{dc}$ of the converter. Given that $V_{tp}$ used as a reference then if $i_{a2}$ is changed in its magnitude, $i_{a1}$ will vary in both magnitude and phase angle, while $i_c$ is kept constant. Because this mechanism occurs at any variation of $i_{a2}$ , therefore such a control is needed to make the phase $\phi$ independent of the magnitude of $i_{a2}$. For example in fig.(6-3) if $i_{a2}$ is reduced, the new value of the stator current will be $i'_{a1}$ at a

phase angle of $\phi'$. However, the power-factor controller is designed to correct any changes in the angle $\phi$. The control strategy is then applied, for example, when the angle $\phi$ decreases, then the delay angle $\alpha$ will decrease instead to compensate the changes in $\phi$. So the current vector of $i_{a2}$ moves towards $V_{tcp}$ automatically to keep $\phi$ at the same value. This process will be reversed if the angle $\phi$ is increased.

As mentioned earlier the speed of changing $\alpha$ is dependent on the clock to the second up down counter. A 4-bit synchronous counter is used at the input clock of the second up/down counter to set the gain of (1/16).

Fig.(6-4) shows some examples of the experimental results which have been plotted for power-factor angle $\phi$ and the delay angle $\alpha$ with respect to the output d.c. current, at a constant frequency. It can be seen that from the graph, to keep $\phi$ constant, then the delay angle $\alpha$ should be reduced. This is done automatically by the power-factor controller.

### 6.2.2 POWER FACTOR CONTROL WITH INPUT FREQUENCY CHANGES:

The phase locked loop (PLL) circuit used in this system has a versatile synchronisation with a wide speed ( n ) range of about 250 - 900 rpm. Therefore, it has excellent control at this range of speed, but there is a disadvantage of using the PLL circuit, since the phase is varied with the input frequency between the two comparator inputs of the PLL circuit. Then, due to the phase change of the two comparator inputs, the delay angle $\alpha$ of the converter changes with frequency, and therefore the angle $\phi$ will change. This process means that at any speed there is a certain power-factor angle $\phi$ at

that speed. This has been discussed in Chapter 4, where an example form the experimental results was given, and have been plotted in fig.(4-3), which shows the change in the delay angle $\alpha$ of the converter without the power-factor controller, at a wide speed range of 375 - 900 rpm.

After introducing the power-factor angle controller in the circuit, all the problems of the phase changes are solved. The clock to the first up/down counter shown in fig.(6-1) is taken from the frequency multiplier of the PLL circuit. The timing waveforms are shown in fig.(6-2). This clock has the same carrier frequency as the PWM signal, and is proportional to all the frequencies of the frequency multiplier. Therefore, at any time the accuracy of the controller is ( 48 ) steps per cycle, i.e. 7.5° per one step in the phase shifter. Therefore the degree of sensitivity is $\pm$ 7.5° , which sets the dead zone of the angle control. The degree of sensitivity of the power-factor controller can be increased by increasing the number of samples per cycle of the sine-weighted signal, which is, in this work fixed for any frequency. Many experimental tests have been carried out for different power-factor angles $\phi$, for speed from 375 - 900 rpm, an example is shown in fig.(6-5).

### 6.3 MODULATION INDEX CONTROLLER:

The modulation index control is simpler than the phase shift control because of altering only the pulse width of the PWM pattern. The process is carried out through the first 8-bit A/D converter shown in the complete system block diagram of fig.(4-2). The modulation index ( M ) will change the average amplitude of the sine-weighted signal through the 8-bit/8-bit divider. Because the current is strongly affected by the PWM pulses, therefore the

output d.c. current is a function of the modulation index. Therefore this controller is used to match the output power for the combined system of the PM-generator and the PWM, GTO converter to the output power generated from a variable energy turbines. The system is discussed in the next section.

## 6.4 SYSTEM CONTROLLER USED IN WIND-POWER SYSTEM:

### 6.4.1 Output power control using power-factor controller:

As mentioned earlier the power extracted from a wind turbine is strongly dependent on the turbine wheel area and the wind speed, i.e. in other words the output power from a wind turbine is proportional to the square of its diameter, and to the cube of the wind speed ( $v^3$ ) [1]. Therefore, the power produced by windmill turbines is affected inherently by the wind speed, (i.e., any small reduction in the wind speed, results in a large change of the output power).

Generally the output power from electric generators used in windmill applications varies with the square of the speed of rotation ( $n^2$ ). For for a wound rotor synchronous generator the excitation field of the rotor can be adjusted to increase or decrease its output voltage. But the permanent-magnet generators may benefit from capacitances which could be switched into the system to match its output power [13]. The work proposed has the advantage of flexible converter operation, where the delay angle can be varied for leading or lagging power factor. Therefore, an inductive load, through the converter operation, can appear as a capacitive load.

It is found experimentally and supported by the theoretical model, that, the maximum output power $(P_{out})_{max}$ from the 8-pole PM-synchronous generator used, occurs at leading power-factor angle $\phi$. Then, the generator can give maximum power at any value of stator current $i_{a1}$ when the power-factor angle $\phi$ is adjusted from ($\phi = 0°$) at $i_{a1} = 0$ Amp to ($\phi = \phi_{opt}°$) at the rated value of the stator current of the PM-synchronous generator. Therefore, at any instant of maximum power transfer and when the stator current $i_{a1}$ is increased, then $\phi$ should be increased towards leading power-factor angle. The relation between $i_{a1}$ and $\phi$ is found to be linear experimentally, which is supported by theoretical analyses as shown in the past sections. Thus, the controller maximises the generator power for any value of any stator current.

### 6.4.2 Output power control using modulation index controller [steady state]:

It is obvious that the output power from a windmill is proportional to the cube of the shaft speed, and the output power from the electrical generator is proportional to the square of the shaft speed. Thus, the output power from the generator is controlled to match the wind-turbine power. Assuming a resistive load to be connected at the output of the GTO converter, which involves most types of loads. Therefore, the output d.c. current of the converter connected to the PM-synchronous generator is controlled to give the matching condition. Assuming that the power from the windmill is defined by,

$$P_{ow} \propto n^3 \qquad (6.2)$$

Then, the output power of the converter ( $P_{oc}$ ) should be the same as ( $P_{ow}$ ), assuming converter efficiency is (100%), therefore,

$$P_{oc} \propto n^3 \tag{6.3}$$

where the converter power is defined by

$$P_{oc} \quad I_{dc}^2 R \tag{6.4}$$

and the shaft speed ( n ) for this 8-pole PM-generator is illustrated as,

$$n \quad 15f \tag{6.5}$$

Substituting eqns.(6.5) and (6.4) into eqn.(6.3), gives,

$$I_{dc}^2 R \propto (15f)^3 \tag{6.6}$$

Therefore, the output d.c. current is defined as

$$I_{dc} \propto f^{1.5} \tag{6.7}$$

Eqn.(6.7) indicates that, the output d.c. current of the converter is proportional to the generator frequency to the power ( 1.5 ) making its output power match the wind-turbine output power. This equation is represented as a function stored in an EPROM placed in the control circuit of the modulation index controller. The address to this EPROM is proportional to the generator frequency. Certain limits have been added for the working frequency range from (25 - 60 Hz), therefore after 60 Hz, the d.c. current is to be reduced, since high voltage is developed on the a.c. side of the

converter. The decrease of the current is to reduce the stresses on the GTO devices of the converter.

Fig.(6-6) shows the controller of the output power to match the wind turbine power. The input control signal to this controller is from the R-phase of the PM-synchronous generator, and its output is fed to the d.c reference of the output d.c. current of the converter. The controller operation is by measuring the duration of the input frequency of the PM-synchronous machine ($f_m$), using a a constant frequency ($f_g$) oscillator. The resultant frequency is fed through an AND gate to an 8-bit counter, then to a latch circuit. The clock (L CLK) to the latch circuit is derived from the delayed frequency ($f_{md}$) from the machine as shown in fig.(6-7a). The output from this counter will be the address of the control function that will be fed to an 8-bit D A converter. Therefore the output from this circuit is compared with the sensed d.c. current in the circuit, then it is adjusted to be proportional to the same value of the stored function in the EPROM. The adjustment is carried out by changing the modulation index of the PWM waveform. The EPROM shown in fig.(6-6) contains the function of ( $I_{dc} \propto f^{1.5}$ ) as shown in fig.(6-7b). The working range is between (25 - 166 Hz). Fig.(6-8) shows two different functions, so either can be used. The difference occurs only after 60 Hz. Fig.(6-8a) shows the current should be reduced linearly after reaching its maximum limit specified by the maximum frequency range. Fig.(6-8b) shows that the current is kept constant after reaching its maximum limit. Thus, any function can be chosen to suit the electrical generator and the converter. The function shown in fig.(6-8) is the output of the power controller which is the d.c. reference of the output d.c. current. These functions are stored in the reverse way to reduce the hardware of the electronic circuits.

For battery charging the output d.c. voltage should be constant for any change in the input a.c. voltage. The output d.c. voltage is defined by equation (3.32). The modulation index should be altered as a function of the input a.c. voltage. Therefore equation (3.32) is redefined in terms of the modulation index (M) as,

$$M \propto \frac{1}{V_{tcl}} \tag{6.8}$$

The modulation index is inversely proportional with the input a.c. voltage. The experimental results are shown in section (5.3.2).

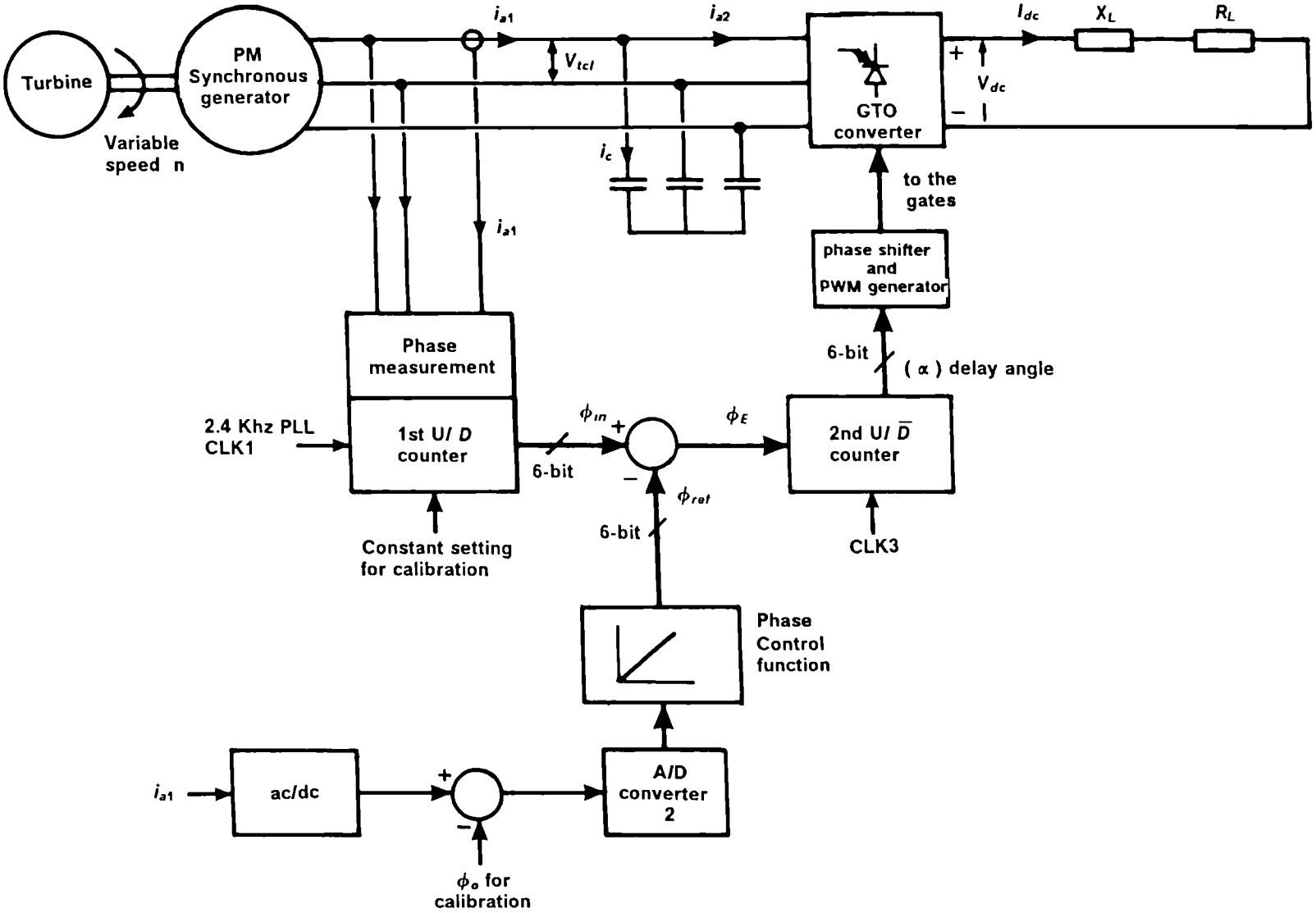


**Fig.(6-1) Power-factor angle controller block diagram.**

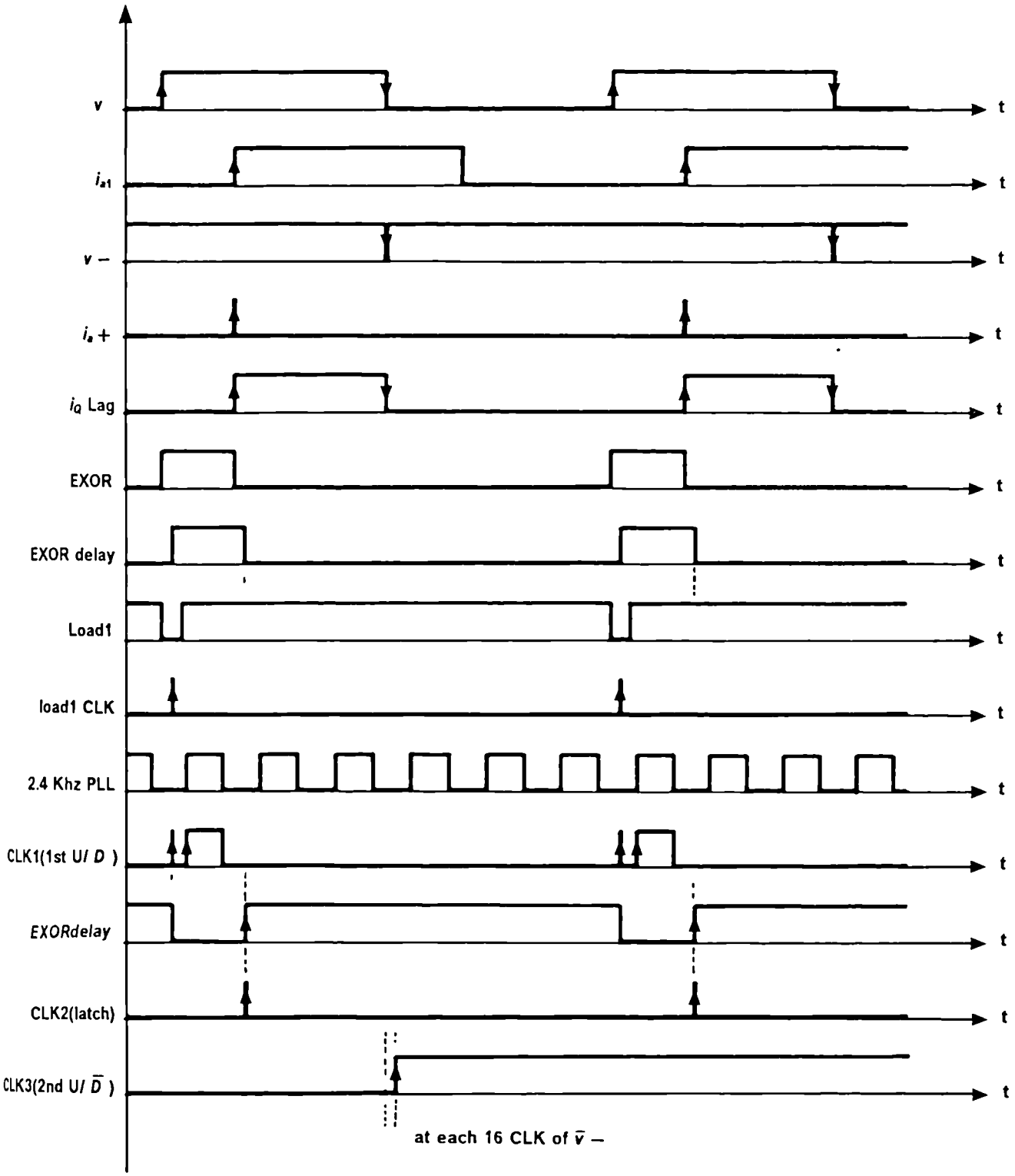


Fig.(6-2) Timing waveforms for the power-factor angle controller.

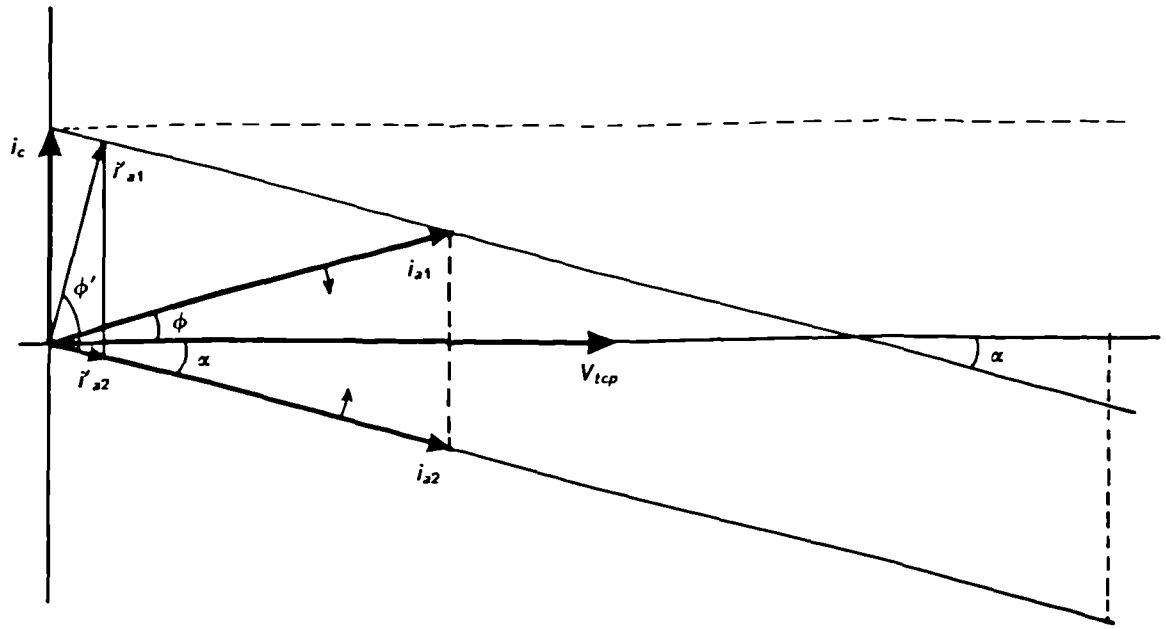


**Fig.(6-3) Power-factor angle locus diagram with converter current $i_{a2}$**

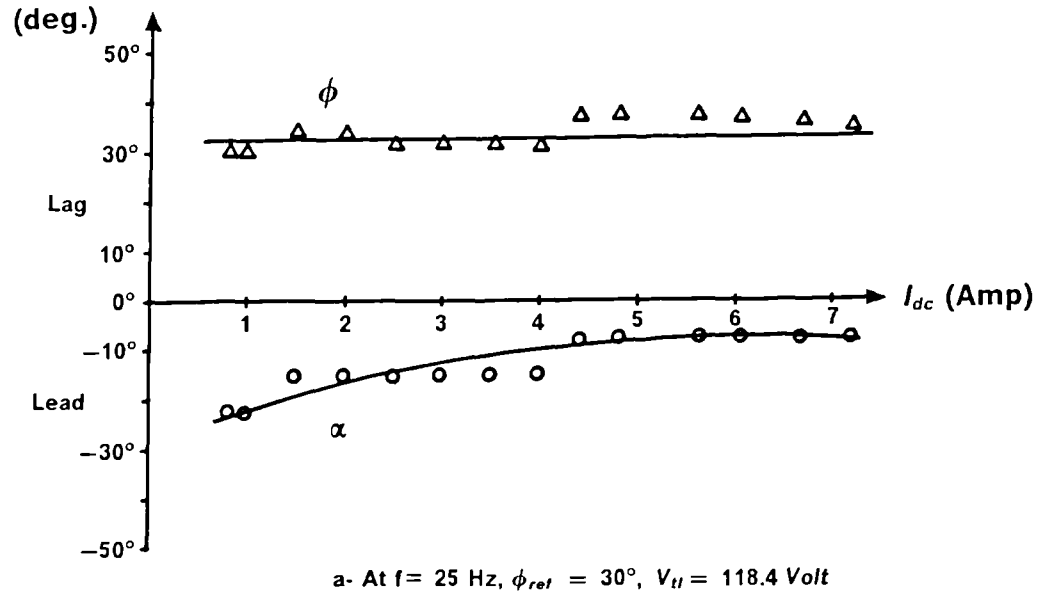


a- At f= 25 Hz, $\phi_{ref}$ = 30°, $V_{tl}$ = 118.4 *Volt*

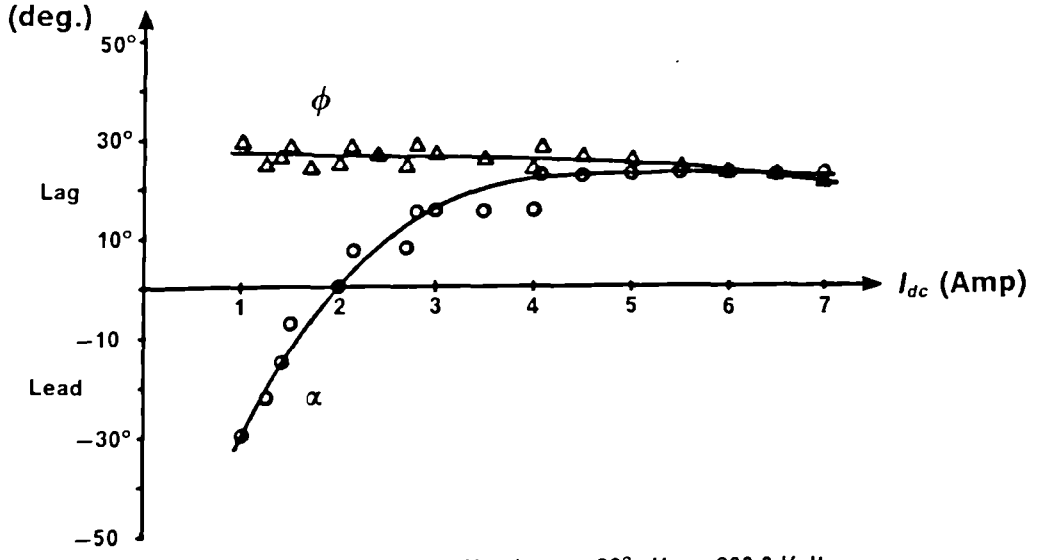


b- At f= 50 Hz, $\phi_{ref}$ = 30°, $V_{tl}$ = 200.0 *Volt*

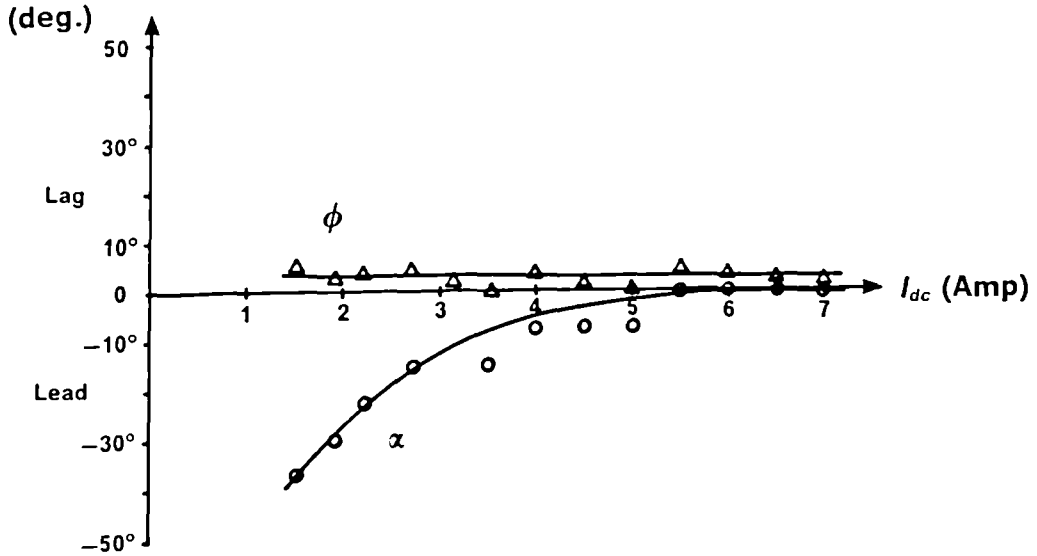


c- At f= 50 Hz, $\phi_{ref}$ = 0°, $V_{tl}$ = 200.0 *Volt*

**Fig.(6-4) Power-factor angle $\phi$ and delay angle $\alpha$ versus output d.c. current.**

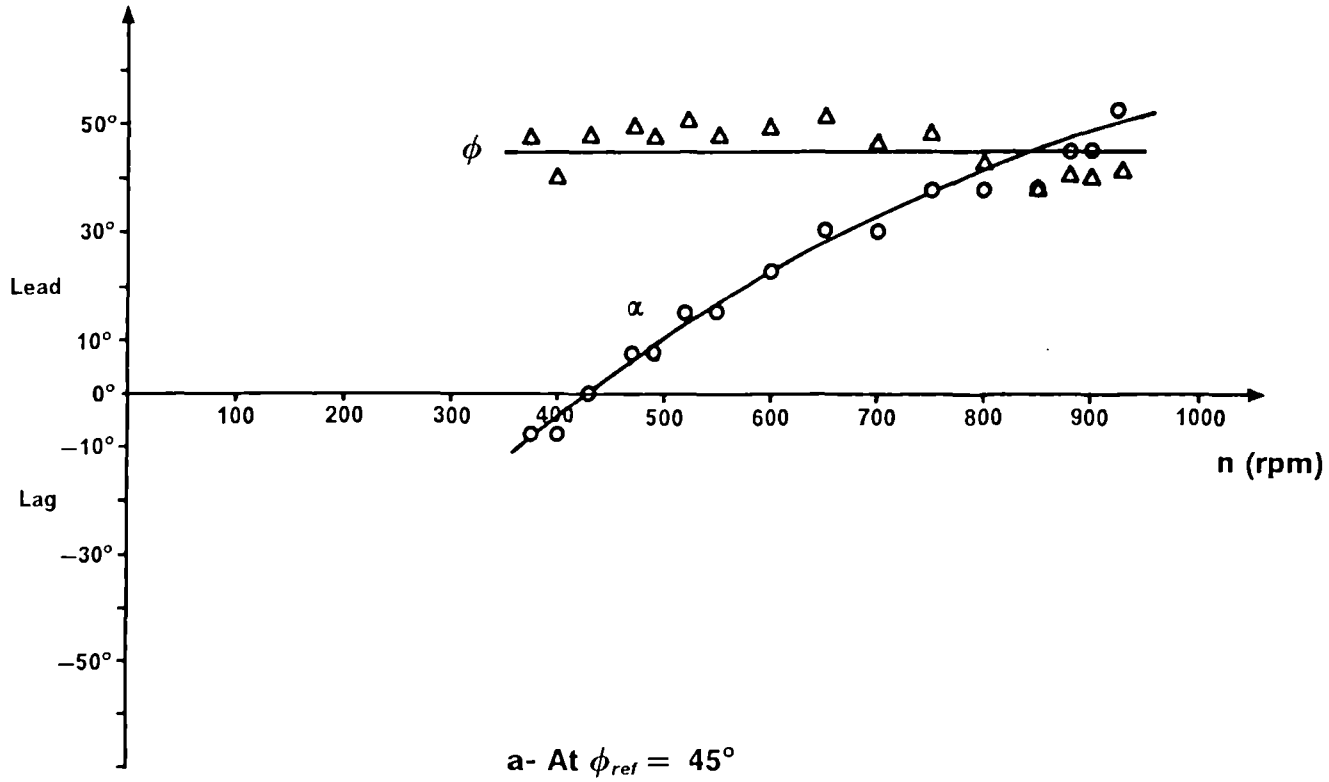


a- At $\phi_{ref} = 45°$

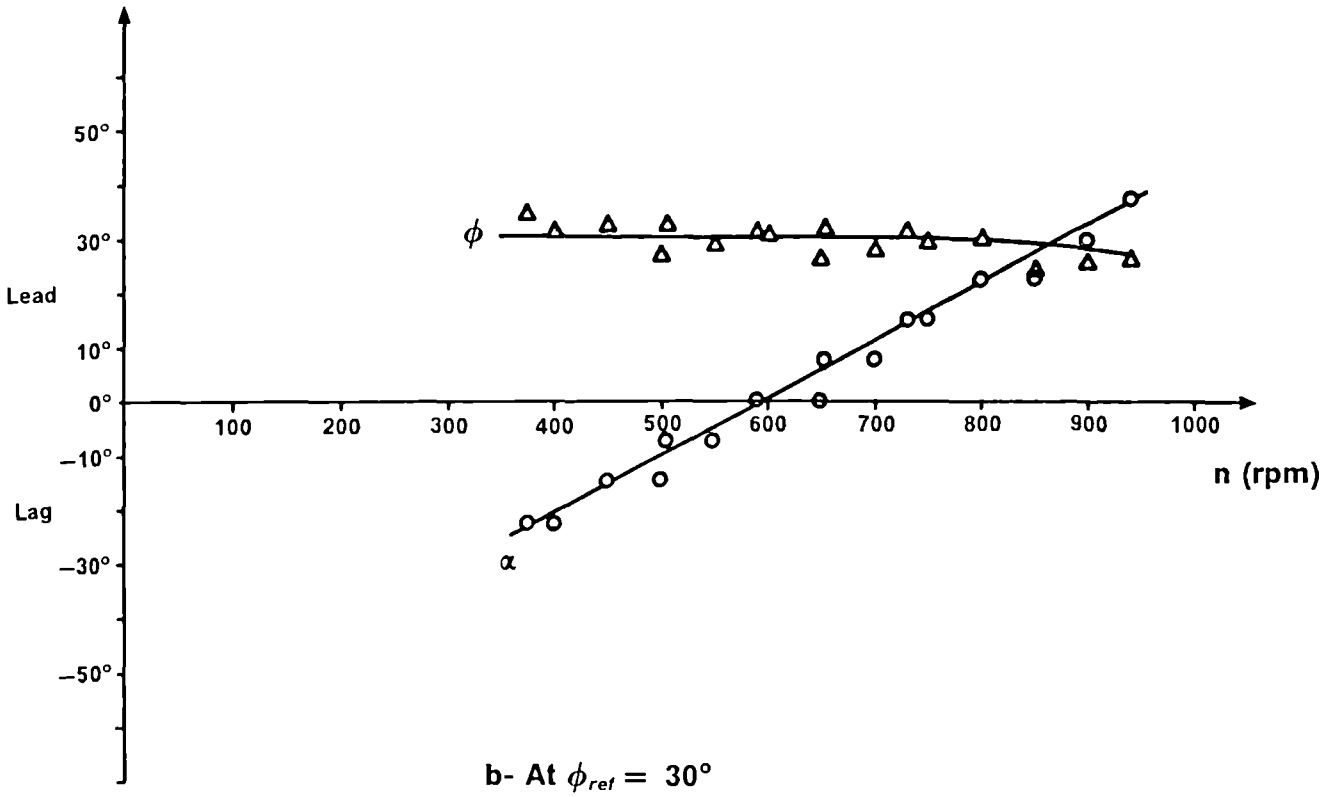


b- At $\phi_{ref} = 30°$

Fig.(6-5) Power-factor angle $\phi$ and delay angle $\alpha$ versus synchronous speed of the generator.

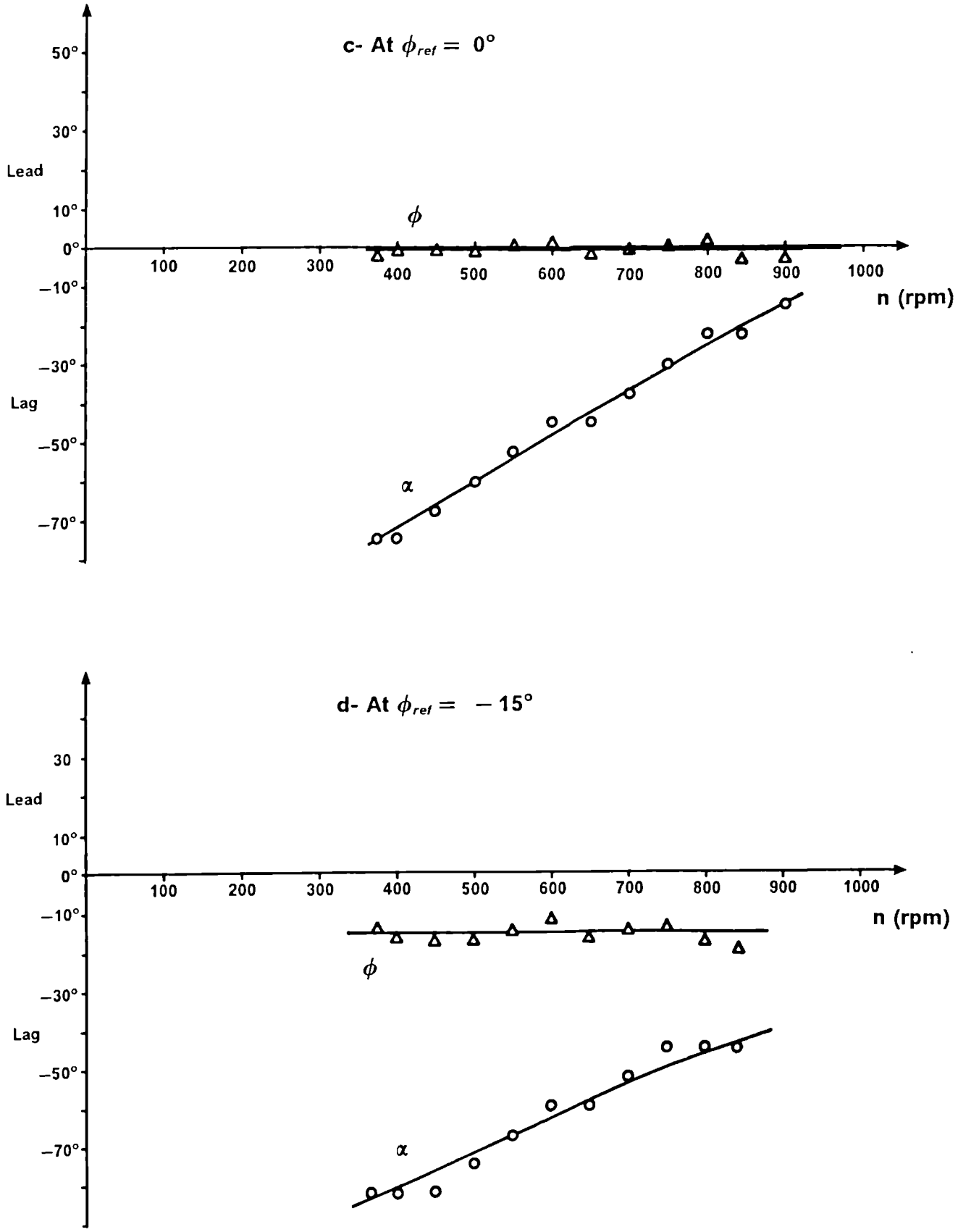


**Fig.(6-5) Power-factor angle $\phi$ and delay angle $\alpha$ versus synchronous speed of the generator.**

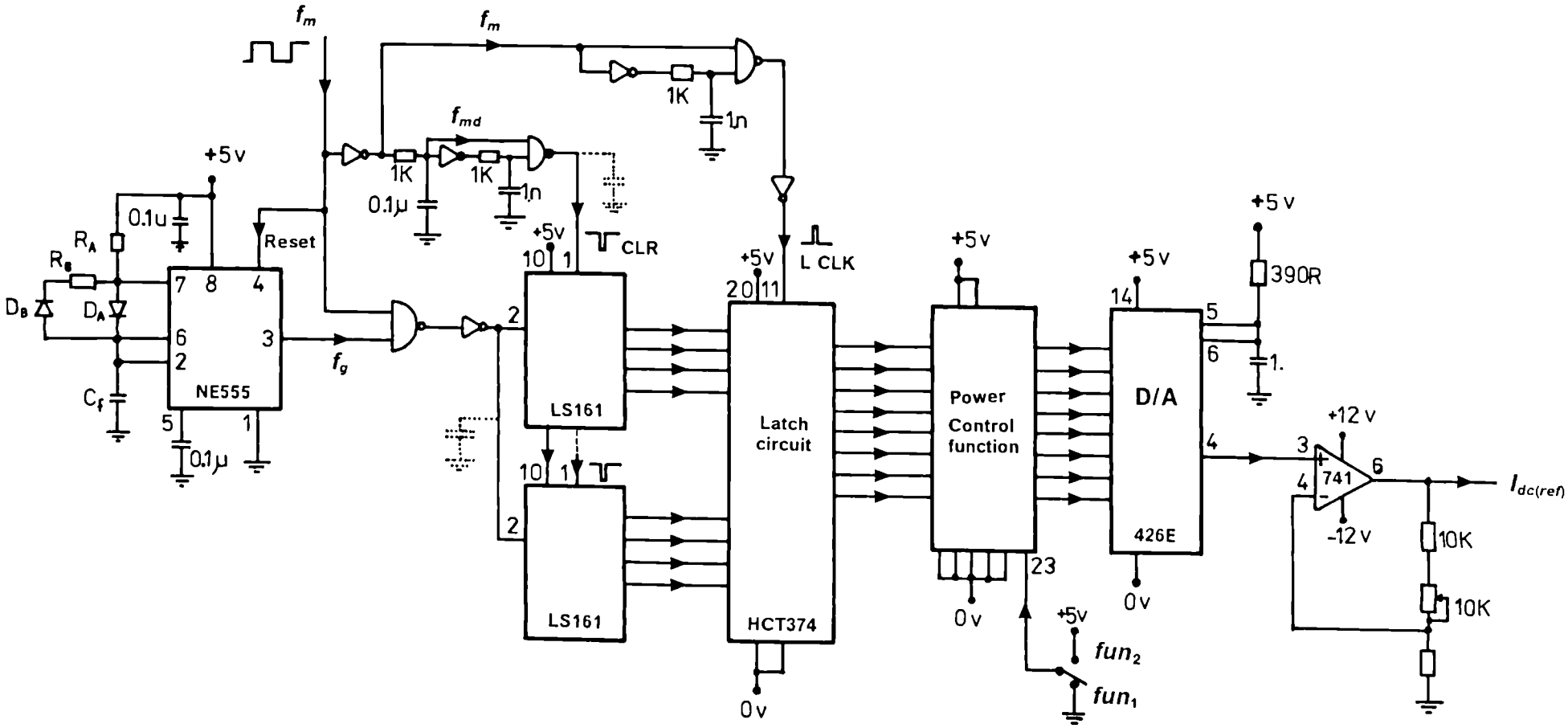


**Fig.(6-6) Output power controller.**

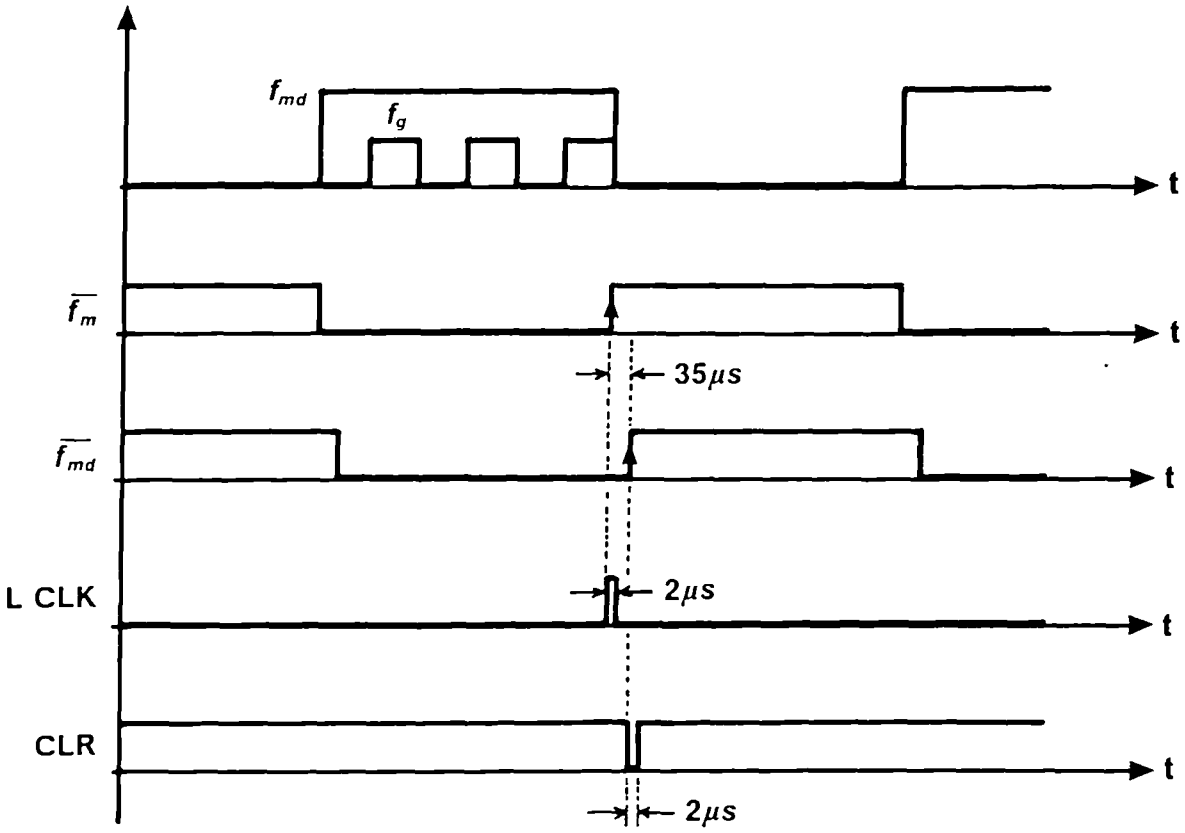


a- Timing waveform diagram.

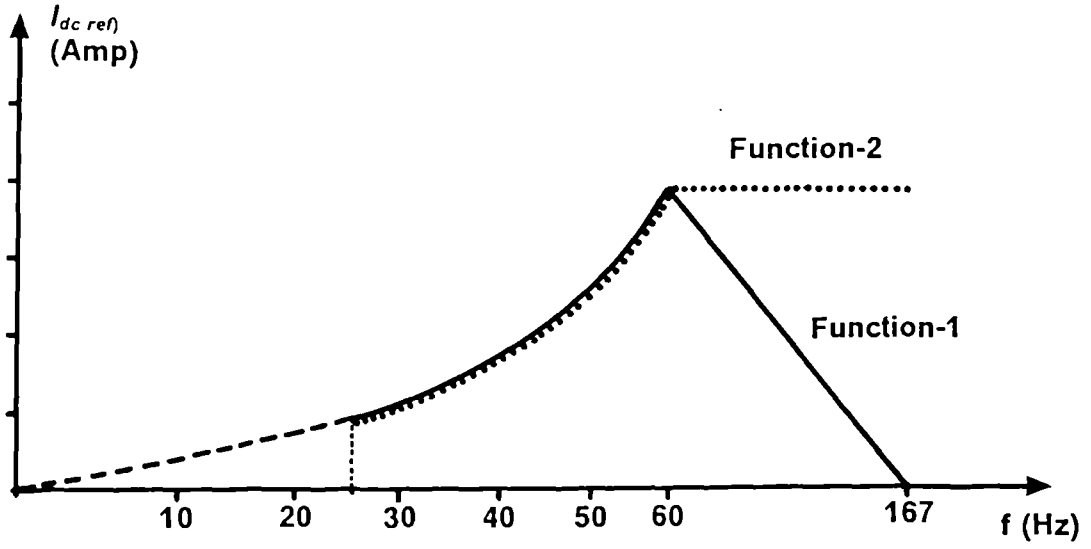


b- Power control functions.

Fig.(6-7) Timing signals and output power function of the controller.

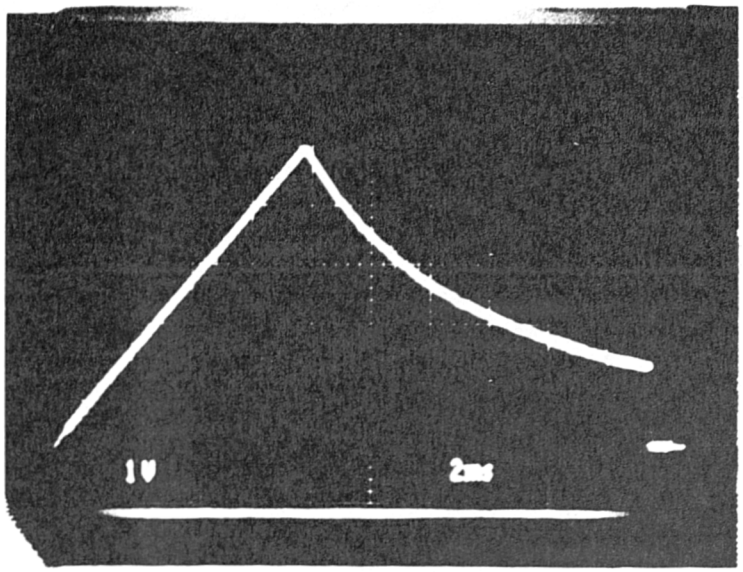


a- Function-1

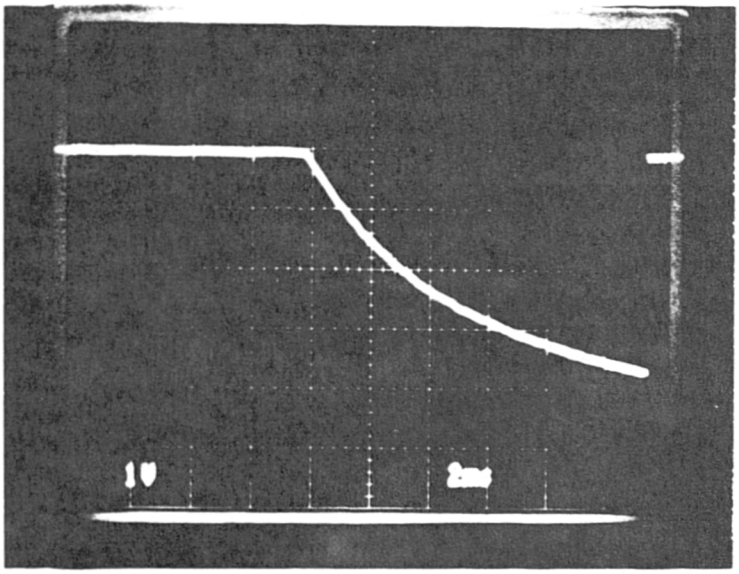


b- Function-2

Fig.(6-8) The control functions used to match the wind-turbine characteristics.

*CHAPTER SEVEN*

# CONCLUSIONS AND FUTURE WORK

7.1 Conclusions.
7.2 Suggestions for future work.

## 7.1 CONCLUSIONS:

This work demonstrates the development of an economical power conversion scheme. This is achieved by the design of a new pulse width modulated static power converter using GTO thyristors and the incorporation of a permanent magnet synchronous generator. The generator has an 8-pole multistacked imbricated rotor of Ceramic-8 Ferrite material, and has a conventional type of 3-phase induction machine. The system designed has high efficiency and a high power capability especially when run at a certain leading power factor, and may operate over a wide machine speed range. The GTO converter can accomplish this and also give a sinusoidal machine current. The GTO converter has two controllers, the delay angle and the modulation index, hence it can match both the optimum machine characteristics and the load characteristics. The complete system is ideally suitable for use with alternative sources of energy. An application was chosen, as an example, which involves an effective and efficient wind energy conversion scheme.

The characteristics of the PM-synchronous generator and its equivalent circuit have been examined with a view to providing a static model of the machine. The parameters of the 8-pole PM-synchronous generator are determined experimentally and verified with the theoretical equivalent circuit model presented. The PM-synchronous machine has permanent magnet excitation, rather than wound rotor. Therefore its leakage reactance is calculated by a method derived from the phasor diagram of the equivalent circuit for the machine. A computer program was used to find the best value of the reactance which is suitable for this machine. The core loss is determined experimentally and is represented theoretically by a shunt resistor

across the air gap induced voltage in the equivalent circuit model. The generator has large values of direct and quadrature synchronous reactance, which were found to be approximately equal. Therefore, the permanent magnet generator modelled as if it had a rotor of a cylindrical shape rather than a salient pole. This cylindrical model was verified by running experimental tests on the machine's characteristics. Good agreement was found between the two. Both the machine model and the experimental characteristics showed, that the generator has maximum power at a leading power factor for particular speed.

The performance characteristics of the 8-pole PM-synchronous generator were good, though for thoroughness another two types of high field permanent magnet synchronous machine were tested. The first one was a 12-pole generator with NdFeB type magnets. In fact this generator was designed to run at high speeds and because of the very low output voltage, could not be used with the converter proposed. However it was tested to demonstrate its operation with the converter. The other permanent magnet generator tested was a 4-pole type using $SmCo_5$ magnets. The generator was physically smaller in size than the original 8-pole type tested and gave a high output power. However for wind power purposes the 8-pole type was chosen as a compromise between the 12-pole low output power type and the 4-pole high output power type.

Two A.C. D.C. converters have been designed and tested using GTO thyristor devices for high power rating at a reasonable high carrier frequency. The advantage of using the GTO thyristor is that it has both characteristics of the transistor to be switched on and off from the gate, and has the

capability of high currents like normal thyristors. But the disadvantage is the cost, and the complex gate drive circuits. The first type of converter, the three-GTO bridge operated in one-quadrant due to its limited delay angle restriction to $\pm 30°$ . The second type tested was that of a six-GTO bridge in which full control of delay angle produced two-quadrant operation, with total control over reactive output power. Thus this type was most favourable for the proposed scheme.

For PWM operation a new design of sinusoidal pulse width modulation technique has been introduced. The sinusoidal pulse width modulation of uniform sampling was used because of low harmonics in the current waveform. The carrier used is a triangular waveform to give a uniform sampling. With the techniques used for this PWM a low harmonic content is achieved. All the low order harmonics are absent from the frequency spectrum. The analysis of the harmonic content in the line current of the converter is presented. The coincidence between the experimental results and the theoretical model gives high confidence in the accuracy results obtained. The reduction of the 5th harmonic in the frequency means that, a reduction in the generator loss is achieved. The reduction in the low order harmonics of the line current and voltage gives the system an excellent performance. In the controller a phase locked-loop was used to offer the advantages of synchronism to the digital signals for a wide frequency range of operation.

The system is supplied by an automatic controller which allows a wide speed range capability of (250 - 940 rpm). The controller allows power-factor angle adjustment to give an optimum value of power-factor angle $\phi_{opt}$ control. This in turn optimises the maximum output power $(P_{out})_{max}$ at any speed or

load, and hence maximum efficiency achieved. The degree of sensitivity of the controller is $\pm 7.5^{o}$ and can be increased by increasing the number of samples per cycle to give more precise values of the optimum power-factor angle $\phi$ control.

The system because of its wide speed range and high power capability, is very attractive and adaptable to wind or tidal power systems. The present prototype of the 8-pole generator and the GTO converter, has an overall efficiency of 84.6 %. The compact size, free maintenance, and high efficiency give the attraction to permanent magnet generators to be used in alternative sources of energy, in spite of the disadvantages of high expenses of the new magnet materials and the demagnetisation of these materials. In fact the generator working at leading power-factor to maximise its output power, gives the advantage of reducing the demagnetisation effect.

An insight into the many different types of design of wind turbine and their mechanical operation has been given. Characteristics of general wind turbine have been derived mathematically demonstrating the dependence of efficiency with turbine design. In fact for a particular design there is an optimal tip speed ratio for which maximum power output is obtained. It is shown that the propeller blade turbine has the best overall efficiency and hence would be ideal for integration into the present proposed system.

A variety of applications of wind turbine systems have been discussed, the most simple being resistive loading such as that found in heaters. The principle of operation is a simple one altering load power-factor angle and modulation index M as the wind speed varies in order to control the load

power. The second application discussed was that of d.c. battery charging requiring a simple controller in order to maintain constant $V_{dc}$ and $I_{dc}$. The third and final application discussed was that of the back to back conversion scheme. This scheme is used to connect two systems of different frequencies, and convert and generate power from one to another. Thus this scheme is particularly advantageous in connection to the main utility network. Control of the system has been briefly discussed, and may be implemented with the system described in this thesis.

A novel controller for a wind energy conversion scheme has been implemented. It is a digital programmable controller used to control the generator terminal voltage and power-factor angle. These factors are a function of the machine frequency and stator current, and are controlled easily using the proposed techniques and the use of the phase locked loop for wind speed range. For application to wind energy system, low power prototypes of three example load have been discussed, that is a resistive load, battery charging and back to back energy conversion system. These models were successfully investigated with high efficiency achieved. High power generation would improve overall efficiency since the ratio of output power to losses would be increased. The system model proposed in this work has an output power of ( 2kWatt ). For extended higher power models, the control would be the same, but only the design of the converter power stage would need to be altered for a greater VA rating.

## 7.2 SUGGESTIONS FOR FUTURE WORK:

The work presented in this thesis can be extended to higher powers, and some suggestions are but as follows:

1- Output power:-

The possibility of increasing the converter ratings is realisable. For medium power, high volt-ampere power devices can be used, but for high power systems, each GTO thyristor within one converter can be composed of many thyristors connected in series parallel to form one higher rating GTO thyristor. Then all these thyristors should be triggered simultaneously. Another way to increase the power of the converter is by connecting two converters of the same type in series to increase the voltage rating of the total system.

2- Applications:-

High field PM-generators can be used with this type of converter to form a powerful compact system of small size suppling high output power. In addition to the use of this converter in alternative source of energy, it can be used for another applications such as in pumped storage systems to be used as a motor.

3- System controller:-

The controller of both PWM generator and the converter can be dedicated in integral form since most of the control signals are stored in EPROMs. Then it can be used in commercial use. The sensitivity of the power-factor controller can be increased from $\pm 7.5°$ to $\pm 1.87°$, by increasing the number of samples stored in the EPROM. An analogue PLL circuit is used in the present work. This PLL circuit can be replaced with a

digital PLL circuit to be used in conjunction with a microprocessor control technique, since some authors are interested in using a microprocessor control. The difference between the two PLL circuits is that the digital PLL circuit has a digital comparator instead of analogue one. The advantage of a digital PLL circuit is that it is easily controlled by a microprocessor, and the controller is integrated in a modular form so as to give a universal operation to the system in terms of reliability and system speed. The stability analysis of the system would also be well worth investigating.

# REFERENCES


1. EL-WAKIL M.M., "Powerplant Technology", Mcgraw-Hill book company, 1988.

2. GERALD FOLY, "The Energy Question", Apelican book currents events, 1987.

3. HIRSCHFELD, F. , "Wind power-pipe dream or reality ?", Mech. Eng., Vol. 99, no.9, pp. 20-28, September 1977.

4. JAYADEV T. S., "Windmills stage of comeback", IEEE Spectrum Vol. 13, Nov. 1976, pp. 45-49.

5. ARRILLAGA J. ,WATSON D. B. , "Static power conversion from self-excited induction generators", Proc. IEE, Vol. 125, No. 8, August 1978.

6. OGUCHI K., OUCHIN N., "Characteristics of experimental self-cascaded induction motors", Faculty of Eng. Ibaraki Univ. Hitachi Japan No. 27, 1979, pp. 67-74.

7. SCHWEICKARDT H. and SUCHANEK V., "Converter-Fed synchronous generator systems for wind power plants", Brown Boveri Rev. (Switzerland), Vol. 69, No. 3, March 1982, pp. 57-64.

8. NORIAKI S., HIDETOSHI U., YOICHI H., "Induction generator connected to a utility network through a static frequency changer", IEEE-IAS Conference 1983.

9. JEFFERSON J. M., LARSEN N., "The application of flywheels in short-term energy storage", Proceedings of the Conf. (97-104), 10-12 Sept. 1984, Coventry England.

10. BRUNETTI V., CRESCIMBINI F., SANGIOVANNI G., "A newly conceived AC/DC static converter for wind power plants", Power Electronics & Applications Proceedings 1985 Brussels Belgium, Part 2, Vol. 1, 1985, pp. 271-6.

11. STEINBUCH M., BELGIUM J.A., "Dynamic modelling and analysis of a wind turbine with variable speed", Dept. of Mech. Eng. Univ. of Technol Netherlands, Journal A, Vol. 27, No. 1, 1986.

12. KOCZARA W., MICHALSKI W., "Reactive power in variable-speed converter-fed drives connected to the three-phase supply Network", 17th Annual IEEE Power Electronics Specialists Conference 1986.

13. BINNS K.J., LOW T.S., "Performance and application of multistacked imbricated permanent magnet generators", IEE Proceedings, Vol. 130, Pt. B, No. 6, Nov. 1983.

14. BINNS K.J., CHAABAN F. B., "The relative merits of Rare Earth permanent magnet Materials for use in the Excitation of permanent magnet machines", Inter. conf. on Electrical Machines, Pisa, Sept. 1988.

15. BINNS K. J., KURDALI A., "Permanent-magnet a.c. generators", Proc. IEE, Vol. 126, No. 7, July 1979, pp. 690-696.

16. BINNS K. J., "The use of permanent magnetic machines for low speed generation", 1st Symposium on wave energy utilisation, Proce. of Gothenburg 30Oct.-1Nov. 1979.

17. TECK-SENG LOW, WAI-HOONG LEE, "Characteristics and performance analysis of a permanent-magnet motor with a multistacked imbricated rotor", IEEE Transactions on Energy conversion, Vol. EC-2,No. 3, September 1987, pp. 450-457.

18. OFFRINGA L. J. J., DE ZEEUW W. J., "A twelve pulse current source inverter as a static VAR compensator in the link between a local power plant and a weak power Grid", Power Electronics and applications Proceeding, Vol. 1, Part 2, 1985, pp. 17-121.

19. Colston Papers No. 30, "Tidal Power and Estuary Management, Symposium of the Colston Research Society, held in Univ. of Bristol, 1987.

20. FRANK M. WHITE, "Fluid Mechanics", 1986, 2nd Ed.

21. TOWNE R. A., "Trends in hydro generator design and application to pumped storage", an Engineering Foundation conference of American Society of Civil Engineers, Frankling Pierce College Ringe, N.H., August 18-23, 1974.

22. LOW T. S., "The optimal configuration of a multi-stacked permanent magnet generator", Ph.D. thesis presented at Univ. of Southampton, March 1982.

23. ELDRIDGE, FRANK R., "Wind machines", 1980, 2nd Ed.

24. JOHN TWIDELL, "A guide to small wind energy conversion systems", Cambridge University Press 1987.

25. British Wind Energy Association, "Wind Energy for the Eighties", 1982.

26. GOLDING E. W., "The generation of electricity by wind power", 1976.

27. HAWLEY R., "Power generation in the future", Proc. IEE, Vol. 125, No. 10, Oct. 1978.

28. RAJAGOPALAN V., VEILLLETTE D., "Contribution to the development of wind energy systems using static power electronic converters", IEEE Power Electronics Specialists Conf. 1978, pp. 69-75.

29. KLOSS A., "Interaction between variable-speed converter-fed drives and the supply network", BBC Brown, Boveri & CO., IPEC-Tokyo 1983.

30. BOLTON H.R., NICODEMOU V.C., "Operation of self-excited generators for windmill application", Proc. IEE, Vol. 126, No. 9, Sept. 1979.

31. SUZUKI T., OKITSU H., KAWAHITO, "Characteristics of a small wind-power system with D.C. generator", IEE Proc., Vol. 129, Pt. B, No. 4, July 1982.

32. OOI B.T., DAVID R.A., "Induction generator/Synchronous-condenser system for wind-turbine power", Proc.IEE, Vol.126, No.1, Jan. 1979.

33. HOLMES P.G., ELSONBATY N.A., PHIL M., "Cycloconverter-excited divided-winding doubly-fed machine as a wind-power convertor", IEE Proc., Vol. 131, Pt. B, No. 2, March 1984.

34. KANT M., BERNA M., VIDONI E., "Wind energy conversion system with electromagnetic stabiliser", Proc. IEE, Vol. 126, No. 11, Nov. 1979.

35. WATSON D.B., ARRILLAGA J., DENSEM T., "Controllable d.c. power supply from wind-driven self-excited induction machines", Proc. IEE, Vol. 126, No. 12, December 1979.

36. MILLER T.J.E., "Method of testing permanent magnet polyphase AC motors", IEEE proc. of IAS-1981, pp.494-499.

37. SLEMON G.R., STRAUGHEN A., "Electric Machines", Addison-Wesley Publ. Comp., 1982.

38. WOOD W.S., "Theory of electric machines", London Butterworths scientific Publ., 1958.

39. NASAR S., "Handbook of electrical machines", McGraw-Hill, 1987.

40. LINDASAY J.F. and RASHID M.H., "Electromechanics and Electrical machinery", Printice-Hall, Englewood Cliffs (N.J.), 1986.

41. HONSINGER V.B., "Performance of polyphase permanent magnet machines", IEEE Trans. on Power Apparatus and Systems, Vol. PAS-99, No.4, July/Aug. 1980.

42. JONES C.V., "The Unified theory of electrical machines", London Butterworths, 1967.

43. Leland A.Schlapch, "Conduction Limits Of A 3-Phase Controlled Converter In Inversion", IEEE Trans. Ind. Appl., pp. 298,MARCH/APRIL 1986.

44. V.R. Stefanovic, "Power Factor Improvement With A Modified Phase- Control led Converter", IEEE Trans. Ind. Appl., Vol. IA-15,No. 2, MARCH/APRIL 1979.

45. S.B. Dewan & W.G. Dunford, "Improved Power Factor Operation Of a Three Phase Rectifier Bridge Through Modified Gating", IEEE IAS.Conf. 1980.

46. J.Rosa & P.T. Finlayson, "Power Factor Correction Of Thyristor Dual Converter Via Circulating Current Control", IEEE IAS. Annual Meeting, 1978.

47. H.Huisman & S.W.H. De Haan, "A DC To 3-Phase Series-Resonant Converter With Low Harmonic Distortion", IEEE Trans. on Industrial Electronics Vol. 32, No. 2, MAY 1985.

48. S.K. Tso & F.W. Pu, "Software Realisation Of Synchronisation and Firing Control Of Thyristor Converters", IEE Proceedings, Vol. 131, Pt. B,No. 4, JULY 1984.

49. P. Marino, C. Picardi & A. Russo, "AC Characteristics In AC/DC/DC Conversion", IEE Proc., Vol. 130, Pt. B, No. 3, MAY 1983.

50. N.G. Hingorani & J.K. Hall, "Use Of Capacitors For Reduction Of Commutation Angle In Static High-Pwer Converters", IEE Proc., Vol. 112,No. 12, DEC. 1965.

51. D.T. Slattery & J.D. Watson,"Extension Of Regenerative Control Range In Phase-Controlled 3-Phase,6-Pulse Thyristor Converters", Second International Conference On Power Electronics & Variable Speed Drives, 24th-26th, NOV. 1986.

52. K. Taniguchi,& H. Mori, "Applications Of A Power Chopper TO The Thyristor Scherbius", IEE Proc., Vol. 133, Pt. B, No. 4, JULY 1986.

53. Ali Mirbod & Ahmed El-Amawy, "Performance Analysis Of A Novel Microprocessor Based Controller For A phase-Controlled Rectifier Connected To A Weak AC System", IEEE Trans. On Ind. Appl., Vol. IA-23, No. 1, JAN./FEB. 1987.

54. Sjoerd W.H. De Haan, "Analysis Of The Effect Of Source Voltage Fluctuations On The Power Factor In 3-Phase Controlled Rectifiers ", IEEE Trans. Ind. Appl., Vol. IA-22,No. 2, MARCH/APRIL 1986.

55. J. Rosa, "Utilisation and Rating Of Machine Commutated Inverter-Synchronous Motor Drives", IAS 1978 :15A.

56. Hirofumi Akagi, Yoshihira Kamazawa & Akira Nabae, "Instantaneous Reactive Power Compensators Comprising Switching Devices Without Energy Storage Components", IEEE-IAS Conf. 1983.

57. F. Fallside & R.D. Jackson, "Direct Digital Control Of Thyristor Amplifiers", IEE Proc., Vol. 116, No. 5, MAY 1969.

58. J. Arrillaga & D.G. Baldwin, "Direct Digital Closed-Loop Control Of h.v.d.c. Converters", IEE Proc., Vol. 121, No. 12, Dece 1974.

59. W. Drury, W. Farrer & B.L. Jones, "Performance Of Thyristor Bridge converters Implying Flywheeling", IEE Proc., Vol. 127, Pt. B, No. 4, JULY 1980.

60. Z. Zabar & G. Bronner, "Bypass Operation By Cyclic Firing Of The Bridge Thyrister", IEE Proc., Vol. 126, No. 9, SEPT. 1979.

61. A.M. Ali, "Fast Changing Four Quadrant Converter", IEE Proc., Vol. 124, No. 10, OCT. 1977.

62. A. Skjellnes & T. Arnulf, "Phase-Locked Loop Control Of Thyristor Converters", IEE Proc., Vol. 123,No. 10,OCT. 1976.

63. L. Malesani, L. Rossetto & P. Tenti, "Active Filter For Reactive Power And Harmonics Compensation", IEEE 1986.

64. Khai D.T. Ngo, "A New Flyback AC/AC Converter", IEEE 1986.

65. Deepakraj M. Divan & Thomas H. Barton, "Harmonic Reduction In Synchronous Chopper-Converter Combinations", IEEE 1985.

66. Noriaki Sato, Hidetoshi Umida & Yoichi Hayashi, "Induction Generator Connected To A Utility Network Through A Static Frequency Changer", IEEE-IAS Conf., 1983.

67. D.M. Divan & T.H. Barton, "Consideration On The Application Of Improved Power Factor Converter Structures", IEEE-IAS 1983.

68. C.P. Henze & N. Mohan, "A Digitally Controlled AC to DC Power Conditioner That Draws Sinusoidal Input Current", 17th Annual IEEE Power Electronics Specialists Conf. 1986.

69. Kwang-Hwa Liu & Fred C. Lee, "Zero-Voltage Switching Technique In DC/DC Converters", 17th Annual IEEE Power Electronics Specialists Conf. 1986.

70. W. Koczara & W. Michalski, "Reactive Power In Variable-Speed Converter Fed Drives Connected To The 3-Phase Supply Network", 17th Annual IEEE Power Elect., Spct. Conf. 1986.

71. Teruo Kataoka, Kazuhiro Mizumachi & Shota Miyairi, "A Pulswidth Control led AC-to-DC Converter To Improve Power Factor and Waveform Of AC Line Current", IEEE Trans. Ind. Appl., Vol. IA-15, No. 6, NOV./DEC. 1979.

72. Nvpr Durga Prasad, Sr Doradla & Yvvs Murthy, "Versatile Digital Firing Schemes For Pulse-Width Modulated AC-DC Converters", IEEE Power Elect. Spct. Conf. 1984.

73. S.P. Yeotikar, S.R. Doradla & Sachidanand, "Digital Simulation Of 3-Phase AC/DC PWM Converter Motor System Using A New State Space Converter Model", IEEE Power Elect. Spct. Conf. 1986.

74. S.K. Riswas & B.S.R. Iyengar, "Simple New PWM Patterns for Thyristor 3-Phase AC/DC Converters", IEE Proc., Vol. 133, Pt. B, No. 6, NOV. 1986.

75. Boon Teck Ooi, John C. Salmon, Juan W. Dixon & Ashok B. Kulkarni, "A 3-Phase Controlled-Current PWM Converter With Leading Power Factor", IEEE Trans. Ind. Appl., Vol. IA-23,No. 1, JAN./FEB. 1987.

76. Eduardo P. Weichmann, Phoivos D. Ziogas & Victor R. Stefanovic, "Generalised Functional Model For 3-Phase PWM Inverter/Rectifier Converters", IEEE Trans. Ind. Appl., Vol. IA-23, No. 2, MARCH/APRIL 1987.

77. P.D. Ziogas, Young, Gookang & V.R. Stefanvioc, "Optimum System Design Of A 3-Phase PWM Rectifier-Inverter Type Frequency Changer", IEEE Power Elect. Spect. Conf. 1984.

78. P.D. Ziogas, Yong-Gookang & V.R. Stefanovic, "PWM Control Techniques For Rectifier Filter Minimisation", IEEE Power Elect. Spect. Conf. 1984.

79. Paolo Tenti, "Feed-Forward Control of Multilevel PWM Converters", IEEE power Electronics Specialists Conference, 1984.

80. Luigi Malesani & Paolo Tanti, "Three Phase AC/DC PWM Converter With Sinusoidal AC Current and Minimum Filter Requirement", IEEE Trans. Ind. Appl., Vol. IA-23, No. 1, JAN./FEB. 1987.

81. S. Nonaka & K. Shinohara, "GTO Current Source Inverter", IEEE Power Elect. Spect. Conf. 1984.

82. J.D. Edwards, "Three-Phase Digital PWM Inverter", IEE Proc., Vol. 122, No. 3, MARCH 1975.

83. Mitsuyuki hombu, Shigeta veda, Akiteru Veda and Yasuo Matsuda, "A New Current Source GTO Inverter with Sinusoidal Output Voltage and Current", IEEE Trans.Ind.Appl., Vol.IA-21, No.5., SEPT./OCT. 1985.

84. Sakutaro Nonaka & Yasuhiko Neba, "Analysis Of PWM GTO Current Source Inverter-Fed Induction Motor Drive System", IEEE Trans. Ind. Appl., Vol. IA-23,No. 2, MARCH/APRIL 1987.

85. Makoto Hashii, Kenji Kousaka & Masahiro Kaimoto, "New Approach To A High Power GTO PWM Inverter For AC Motor Drives", IEEE Trans. Ind. Appl., Vol. IA-23, No. 2, MARCH/APRIL 1987.

86. Mitsuyuki Hombu, Shigeta Veda & Akiteru Veda, "A Current Source GTO Inverter With Sinusoidal Inputs & Outputs", IEEE Trans. Ind. Appl., Vol. IA-23, No. 2, MARCH/APRIL 1987.

87. H. Inaba, S. Shima, A. Veda., T. Ando, T. Kurosawa & Y. Saki, "A New Speed Control System for DC Motors Using GTO Converter and Its Application to Elevators", IEEE Trans. Ind. Appl., Vol. IA-21, MARCH/APRIL 1985.

88. F.L. Luo, R.D. Jackson & R.J. Hill, "Digital Controller for Thyristor Current Source", IEE Proc., Vol. 132, Pt. B, No. 1, JAN. 1985.

89. A.R. Daniels & R.T. Lipczynski, "Digital Firing-Angle Circuit For Thyristor Motor Controllers", IEE Proc., Vol. 125, No. 3, MARCH 1978.

90. S.K. Tso & P.T. Ho, "Dedicated-Microprocessor Scheme for Thyristor Phase Control Multiphase Converters", IEE Proc., Vol. 128, Pt. B.No. 2, MARCH 1981.

91. D.J. Miller, "Power-Station Construction in UK Which Way for The
Future ?", IEE Proc., Vol. 125, No. 1, JAN. 1978.

92. J.D. Van Wyk, H.-Ch. Skudelny & A. Muler-Hellmann, "Power Electronics, Control of The Electromechanical Energy Conversion & Some Applications", IEE Proc., Vol. 133, Pt. B, No. 6, NOV. 1986.

93. J. Arrillaga & D.B. Watson,"Static Power Conversion From Self-excited Induction Generators", IEE Proc., Vol. 125, No. 8, AUG. 1978.

94. Bowes S.R. & Mount M.J., "Microprocessor Control of PWM Inverters", IEE Proc., Vol. 128, Pt. B, No. 6, NOV. 1981.

95. S.R. Bowes & T. Davies, "Microprocessor-Based Development System for PWM Variable-Speed Drives", IEE Proc., Vol. 132, Pt.B, No.1, JAN.1985.

96. T.L. Grant & T.H. Barton, "A Highly Flexible Controller for A Pulse Width Modulation Inverter", Annual Meeting, IAS 1978:15 E, pp. 486-492.

97. A. Abbondanti, "A Digital Modulator Circuit for PWM Inverters", Annual Meeting, IAS 1978:15 F, pp. 493-501.

98. KORNER T.W., "Fourier Analysis", 1989, Trinity Hall, Cambridge.

99. DODES I.A., "Numerical Analysis for Computer Science", 1978, Elsevier North-Holland, Inc.

100. BOWES S.R., "New sinusoidal pulse width-modulated inverter", Proc. IEE, 1975, 122(11), pp.1279-1285.

101. HUANG I.B. and LIN W.S., "Harmonic reduction in inverters by use of sinusoidal pulse width modulation", IEEE Trans., 1980, IECI-27(3),pp.201-207.

102. KIM MOH LIM, "A Microprocessor-controlled 3-phase PWM inverter for Variable-speed induction motor

Drives", Ph.D. thesis Submitted to the Univ. of Wales, 1983.

103. Chaaban Farid B., "Computer Aided Analysis, Modelling and Experimental Assessment of Permanent Magnet Synchronous Machines with Rare Earth Magnets", Ph.D. thesis submitted to the University of Liverpool, Tune 1989.

104. Langsdorf A.S., "Theory of Alternating-current machinery", McGraw-Hill, 1937.

105. Woodworth A. and Burgum F., "Simple rules for GTO circuit design", Mullard Technical Publication, M88-0137.

106. McMurray W., "Efficient Snubbers for voltage source GTO inverters", IEEE Transac. on Power Elect., Vol. PE-2, No.3, July 1987, pp. 264-272.

# *APPENDICES*

## *Appendix A*

### *PWM software*

The Fortran-77 programming language is used to write all the programs in this project. An IBM 8081 mainframe computer has been used in this University to run these programs.

### A.1 SINE-WEIGHTED SIGNAL GENERATION

This program has been written to generate the sine weighted signal, and then stored in the EPROM. The output data from this program will be used for the analysis of the current waveforms.

```
C SINE WEIGHTED GENERATION PROGRAM
C   ------------------------------------------------------------
C     CHARACTER DIGITS(0:15),HEX(2)
C     DATA DIGITS/'0','1','2','3','4','5','6','7','8','9','A','B','C',
C    1'D','E','F'/
C   ------------------------------------------------------------
      DIMENSION NI(48)
      CHARACTER DIGITS(0:1),BIN(8)
      DATA DIGITS/'0','1'/
C- READING THE AMPLITUDE(AMP) AND PHASE SHIFT (PHA) OF THE 3RD HARMONIC
**      READ(*,*)AMP,PHA
           READ(*,*)DELTA
CC      DO 500 II -5,80,5
        PHA=60.
        AMP=0.028
CC      AMP=II/1000.
**
**    WRITE(2,90)
**    WRITE(2,95)
90    FORMAT(8X,'X',9X,'I',10X,'AM',10X,' NI',11X,'HEX',6X,'BINARY')
95    FORMAT(5X,'********',3X,'******',4X,'**********',5X,'**********',5X,
     1 '********',2X,'**********')
C-       [48] IS THE NUMBER OF SAMPLES PER CYCLE
      DO 200 I=1,48
      IF(I.GT.24) GOTO 105
C-       AX IS THE SWITCHING ANGLE IN RADIAN.
C-       AX = [7.5*(PY/180)]*I
C-       THE SWITCHING ANGLE FOR +VE HALF.
      AX=(0.130899693)*I
      GOTO 107
```

```
C-       THE SWITCHING ANGLE FOR -VE HALF.
105    AX=(0.130899693)*(I-24)
C-       X IS THE SWITCHING ANGLE IN DEGREE.
107    X=180/3.141592654*AX
         PYT=3.141592654/180.
C_____________________________________________________________________
C-       [-1] IN THE BELOW EQUATIONS IS USED FOR FOURIER ANALYSES
C-       ONLY TO MATCH THE O/P OF THE 8-BIT/8-BIT DIVIDER.
*110        AM=255.0*SIN(AX)+0.0001-1.
110    AM=(247.0/259.)*255.*(SIN(AX)-AMP*SIN(3.*(AX+
     1 DELTA*PYT)-PHA*PYT))+0.0001-1.
C_____________________________________________________________________
C-         CALCULATION OF THE  HALF SINEWAVE
C-         CONVERSION TO THE NEAREST INTEGER.
C-         CONVERTING THE AMPLITUDE TO BINARY AND HEX DECIMAL NUMBER.
130    NI(I)=NINT(AM)
C  ------------------------------------------------------------
       N=NI(I)
C      DO 30 K =2,1,-1
       DO 30 K =8,1,-1
C      M=N/16
       M=N/2
C      IREM=N-M*16
       IREM=N-M*2
C      HEX(K)=DIGITS(IREM)
       BIN(K)=DIGITS(IREM)
       N=M
30     CONTINUE
C-         WRITING ALL THE DATA IN A TABLE.
C      WRITE(2,100)X,I,AM,NI,HEX
C100   FORMAT(5X,F7.1,5X,I2,7X,F7.2,7X,I5,10X,A,A)
C  ------------------------------------------------------------
******
**     WRITE(2,100)X,I,AM,NI(I),NI(I),BIN
100    FORMAT(5X,F7.1,5X,I2,7X,F7.2,7X,I5,10X,Z2,6X,4(A),2X,4(A))
200    CONTINUE
C------------------------
C-     WRITING THE SAMPLED DATA TO BE STORED IN THE EPROM FOR ALL THE
C-     3-PHASE SYSTEM.
**     WRITE(2,290)
**     WRITE(2,300)(NI(I),NI(I+16),NI(I+32),I=1,16)
**     WRITE(2,295)
**     WRITE(2,300)(NI(I),NI(I+16),NI(I+32-48),I=17,32)
**     WRITE(2,295)
**     WRITE(2,300)(NI(I),NI(I+16-48),NI(I+32-48),I=33,48)
**     WRITE(2,295)
**     WRITE(2,300)(NI(I),NI(I+16),NI(I+32),I=1,16)
C------------------------
C-         WRITING THE SAMPLED AMPLITUDE OF THE SINE WAVE TO BE USED FOR
C-       FOURIER ANALYSES IN PROGRAM [SWITCH FORTRAN].
300    FORMAT(5X,Z2,5X,Z2,5X,Z2)
290    FORMAT(4X,'SIN 1  SIN 2  SIN 3')
295    FORMAT(1X,'--------------------------------')
       WRITE(2,330)(NI(I),I=1,12)
       WRITE(2,330)(NI(I),I=12,1,-1)
CCCCC                                        500      CONTINUE
330    FORMAT(5X,I5)
       STOP
       END
```

## A.2 CURRENT WAVEFORM GENERATION AND HARMONIC MINIMISATION

This program used the data of the sine-weighted signal generated in the last appendix. A PWM pattern is produce to form the current waveform of the input current. In this program the harmonic content is calculated.

```
C THE PROGRAM IS TO CALCULAT THE CURRENT WAVEFORMS OF THE SPWM CONVERTER
C Y(I) IS THE SWITCHING LEVEL OF 48 SAMPLES AT PERIOD OF 180 DEGREE.
C IPHS IS THE PHASE SHIFT BETWEEN THE INPUT PHASE VOLTAGE & LINE CURRENT
C DCI IS THE OUTPUT D.C. CURRENT OF THE CONVERTER.
C M IS THE MODULATION INDEX
C
      REAL IR(400),IY(400),IB(400),M(255),N(246),XR(400),XY(400),XB(400)
     1,Y(50),XR1(200),XR2(200),BN(150),BN1(150),BN2(150),XRR(400),
     1BN3(150),BBN(150),CN(150),CCN(150),CN3(150),AN(150),AAN(150),
     1AN3(150),AAN3(150),AN1(150),AN2(150),IRMS(150),CN4(150),IPHS,
     1ANB(150),BNB(150),BN1B(150),AN1B(150)
*     PRINT*,'(INTER PHASE SHIFT IP*7.5=IPHS.AS 0 1,2,3...,IP'
        READ(*,*)IP
      READ(2,*)(Y(I),I=1,24)
*     IP=01
5     DCI=4.00
C START CALCULATION OF SWITCHING ANGLES.
      N(1)=000.0
      M(1)=(246.-N(1))/255.
 10   DO 20 I=1,24
      Y(I)=Y(I)-N(1)
      XR2(I)=(-1./68.)*Y(I)+(I)*7.5
      XR1(I)=(1./68.)*Y(I)+(I-1)*7.5
 20   CONTINUE
*     WRITE(3,30)(XR1(I),XR2(I),I=1,24)
*30   FORMAT(1X,F7.3,1X,F7.3)
      J=1
      K=2
      DO 40 I=1,24
      XR(J)=XR1(I)
      XR(K)=XR2(I)
      J=J+2
      K=K+2
 40   CONTINUE
C  END CALCULATION OF SWITCHING ANGLES.
C
C WRITE THE SAMPLED DATA OF HALF SINE WAVE (48)SAMPLES.
*     WRITE(3,50)(I,XR(I),I=1,48)
*50   FORMAT(1X,I5,1X,F7.3)
C FORMING THE RED PHASE LINE CURRENT IR(I) BY ARRANGING THE SWITCHING
C POINTS OF THE SINE-WEIGHTED SIGNAL MANTIOND ABOVE.
C  THIS LOOP TO MAKE 3-PERIOD OF THE SINEWEIGHTED WAVEFORM OF THE R-PASE
```

```
      K=1
      DO 1000 J =1,8
      DO 900 I =1,48
      XRR(K)=XR(I)+((J-1)*180.)
      K=K+1
 900  CONTINUE
1000  CONTINUE
C  THIS LOOP TO MAKE 3-PERIOD OF THE SINEWEIGHTED WAVEFORM OF THE Y-PASE
      DO 2000 I =1,(384-16)
      XY(I)=XRR(I+16)-60.
2000  CONTINUE
C  THIS LOOP TO MAKE 3-PERIOD OF THE SINEWEIGHTED WAVEFORM OF THE B-PASE
      DO 3000 I =1,(384-32)
      XB(I)=XRR(I+32)-120.
3000  CONTINUE
*     WRITE(3,55)(I,XRR(I),XY(I),XB(I),I=1,384)
 55   FORMAT(1X,I5,1X,F8.3,1X,F8.3,1X,F8.3)
*      DO 555 IIP =1,10
*       IP=IIP-1
      IPHS=IP*7.5
C  GROUP 1
C----------
*       J=1
*       K=2
*     DO 4000 I=(1+IP),(8+IP)
*     IR(J)=XB(I)
*     IR(K)=XY(I)
*       J=J+2
*       K=K+2
*4000  CONTINUE
         I=1+IP
       J=1
4000   IF(XB(I).LT.XY(I)) THEN
      IF(I.LT.(8+IP)) THEN
        IR(J)=XB(I)
        IR(J+1)=XY(I)
        IR(J+2)=XY(I+1)
        IR(J+3)=XB(I+1)
       J=J+4
       I=I+2
      GO TO 4000
       ENDIF
      ELSEIF(XB(I).GT.XY(I)) THEN
C - - - - - - - - - - - - - -
4400  IF(I.LT.(8+IP)) THEN
        IR(J)=XY(I)
        IR(J+1)=XB(I)
        IR(J+2)=XB(I+1)
        IR(J+3)=XY(I+1)
       J=J+4
       I=I+2
      GO TO 4000
       ENDIF
      ENDIF
C  GROUP 2
C----------
        J=18
      IR(17)=30.+IP*7.5/2.
      DO 4001 I=(9+IP),(40+IP)
      IR(J)=XRR(I)
```

```
        J=J+1
4001  CONTINUE
C  GROUP 3
C----------
       IR(50)=150.+IP*7.5/2.
*        J=51
*        K=52
*       DO 4002 I=(41+IP),(48+IP)
*       IR(J)=XY(I)+180.
*       IR(K)=XB(I)+180.
*        J=J+2
*        K=K+2
*4002  CONTINUE
         I=41+IP
       J=51
4002   IF(XB(I).LT.XY(I)) THEN
      IF(I.LT.(48+IP)) THEN
        IR(J)=XB(I)
        IR(J+1)=XY(I)
        IR(J+2)=XY(I+1)
        IR(J+3)=XB(I+1)
       J=J+4
       I=I+2
      GO TO 4002
       ENDIF
      ELSEIF(XB(I).GT.XY(I)) THEN
C - - - - - - - - - - - - - -
4402  IF(I.LT.(48+IP)) THEN
        IR(J)=XY(I)
        IR(J+1)=XB(I)
        IR(J+2)=XB(I+1)
        IR(J+3)=XY(I+1)
       J=J+4
       I=I+2
      GO TO 4002
       ENDIF
      ENDIF
C  GROUP 4
C----------
*       J=67
*       K=68
*      DO 4003 I=(49+IP),(56+IP)
*      IR(J)=XB(I)+180.
*      IR(K)=XY(I)+180.
*       J=J+2
*       K=K+2
*4003  CONTINUE
         I=49+IP
       J=67
4003   IF(XB(I).LT.XY(I)) THEN
      IF(I.LT.(56+IP)) THEN
        IR(J)=XB(I)
        IR(J+1)=XY(I)
        IR(J+2)=XY(I+1)
        IR(J+3)=XB(I+1)
       J=J+4
       I=I+2
      GO TO 4003
       ENDIF
      ELSEIF(XB(I).GT.XY(I)) THEN
```

```
C - - - - - - - - - - - - - -
4403  IF(I.LT.(56+IP)) THEN
        IR(J)=XY(I)
        IR(J+1)=XB(I)
        IR(J+2)=XB(I+1)
        IR(J+3)=XY(I+1)
       J=J+4
       I=I+2
      GO TO 4003
       ENDIF
      ENDIF
C  GROUP 5
C----------
      IR(83)=210.+IP*7.5/2.
        J=84
      DO 4004 I=(57+IP),(88+IP)
      IR(J)=XRR(I)
        J=J+1
4004  CONTINUE
C  GROUP 6
C----------
      IR(116)=330.+IP*7.5/2.
*        J=117
*        K=118
*       DO 4005 I=(89+IP),(96+IP)
*       IR(J)=XB(I)+180.+180.
*       IR(K)=XY(I)+180.+180.
*         J=J+2
*         K=K+2
*4005  CONTINUE
          I=89+IP
        J=117
4005    IF(XB(I).LT.XY(I)) THEN
      IF(I.LT.(96+IP)) THEN
         IR(J)=XB(I)
         IR(J+1)=XY(I)
         IR(J+2)=XY(I+1)
         IR(J+3)=XB(I+1)
        J=J+4
        I=I+2
      GO TO 4005
       ENDIF
      ELSEIF(XB(I).GT.XY(I)) THEN
C - - - - - - - - - - - - - -
4405  IF(I.LT.(96+IP)) THEN
        IR(J)=XY(I)
        IR(J+1)=XB(I)
        IR(J+2)=XB(I+1)
        IR(J+3)=XY(I+1)
       J=J+4
       I=I+2
      GO TO 4005
       ENDIF
      ENDIF
C---------------------------------
      WRITE(3,59)M(1),IPHS
 59   FORMAT(1X,'MODULATION INDEX M = ',F7.4,1X,'PHASE SHIFT=',F8.2)
      WRITE(3,60)(IR(I),I=1,132)
 60   FORMAT(1X,1X,F9.3)
```

```
C++++++++++++++++++++++++++++++++++++++
C FURIER SERIES ANALYSIS
C++++++++++++++++++++++++++++++++++++++
      KK=50
      DO 99 NN=1,KK
C 1ST HALF OF THE SIGNAL.
      BN1(NN)=0.0
      AN1(NN)=0.0
      DO 100 I=1,(66-2*IP)
      PY=3.141592654
      BN(I)=(DCI/(PY*NN))*((-1)**(I+1)*COS(NN*IR(I)*PY/180.))
           AN(I)=(DCI/(PY*NN))*((-1)**(I)*SIN(NN*IR(I)*PY/180.))
      BN1(NN)=BN(I)+BN1(NN)
           AN1(NN)=AN(I)+AN1(NN)
      CN(NN)=BN1(NN)
 100  CONTINUE
C------------------
C 2ND HALF OF THE SIGNAL.
      BN2(NN)=0.0
           AN2(NN)=0.0
      DO 101 I=(67-2*IP),(132-2*IP)
      BBN(I)=(DCI/(PY*NN))*((-1.)**(I)*COS(NN*IR(I)*PY/180.))
           AAN(I)=(DCI/(PY*NN))*((-1.)**(I+1)*SIN(NN*IR(I)*PY/180.))
      BN2(NN)=BBN(I)+BN2(NN)
           AN2(NN)=AAN(I)+AN2(NN)
      CCN(NN)=BN2(NN)
 101  CONTINUE
C------------------
C 3RD HALF OF THE SIGNAL.
      BN1B(NN)=0.0
      AN1B(NN)=0.0
      IF(IP.NE.0) THEN
      DO 111 I=(132-2*IP),132
      PY=3.141592654
      BNB(I)=(DCI/(PY*NN))*((-1)**(I-1)*COS(NN*IR(I)*PY/180.))
           ANB(I)=(DCI/(PY*NN))*((-1)**(I)*SIN(NN*IR(I)*PY/180.))
      BN1B(NN)=BNB(I)+BN1B(NN)
           AN1B(NN)=ANB(I)+AN1B(NN)
C     CN(NN)=BN1(NN)
 111  CONTINUE
      END IF
C------------------
 99   CONTINUE
        DO 102 NN=1,KK
          AN3(NN)=AN1(NN)+AN2(NN)+AN1B(NN)
 102    BN3(NN)=CN(NN)+CCN(NN)+BN1B(NN)
          DO 104 NN=1,KK
          AAN3(NN)=20*ALOG10(ABS(AN3(NN)/AN3(1)))
 104    CN3(NN)=20*ALOG10(ABS(BN3(NN)/BN3(1)))
      WRITE(3,219)
 219  FORMAT(6X,' N',2X,'1ST HALF',4X,'2ND HALF',5X,'HAR',5X,'HB(DB)',
     15X,'HA(DB)',5X,'HC(DB)')
       DO 666 I =1,KK
       IF(ABS(BN3(I)).LT.(0.0001)) GO TO 660
      WRITE(3,220)I,CN(I),CCN(I),BN3(I),CN3(I)
 660    IF(ABS(AN3(I)).LT.(0.0001)) GO TO 666
      WRITE(3,230)I,AN1(I),AN2(I),AN3(I),AAN3(I)
 220    FORMAT(1X,I6,2X,F9.5,2X,F9.5,2X,F9.5,1X,F8.3)
 230    FORMAT(1X,I6,2X,F9.5,2X,F9.5,2X,F9.5,13X,F8.3)
```

```
     CN4(I)=20*ALOG10(SQRT(BN3(I)**2+AN3(I)**2)/SQRT(BN3(1)**2+AN3(1)
    1**2))
     WRITE(3,240)CN4(I)
240    FORMAT(63X,F8.3)
666   CONTINUE
     SUM=0.0
     DO 103 NN=1,KK
     IF(ABS(BN3(NN)).LT.(0.0001)) GO TO 103
     SUM=SUM+(BN3(NN))**2/2.
     IRMS(NN)=SQRT(SUM)
     RMS=IRMS(NN)
     NNN=NN
103  CONTINUE
     WRITE(3,218)NNN,SUM,RMS
     WRITE(3,*)
     WRITE(3,*)
555  CONTINUE
218  FORMAT(5X,'N=',I6,2X,'SUM=',F10.3,2X,'IRMS(NN)=',F10.3)
     STOP
     END
```

## A.3 8-BIT/8-BIT DIVIDER DATA GENERATION

This a simple program used to generate the data for the divider, which can be stored in the EPROMs used for this purpose.

```
*                          APPENDIX  A.3
*                         ------------
*          8-BIT / 8-BIT DIVIDER  DATA GENERATION PROGRAM
*         ---------------------------------------------
*   EPROM DATA CRIATION
      DO 20 I =1,16
      DO 10 J =1,16
      IB2=(I-1)
      JA1=(J-1)
      IPR2=IB2*JA1
      WRITE(2,100)IB2,JA1,IPR2,IPR2
100   FORMAT(5X,I5,10X,I5,10X,I5,5X,Z4)
10    CONTINUE
20    CONTINUE
      STOP
      END
```

## A.4 DATA EXCHANGE TO INTEL FORMAT PROGRAM.

This program is used to convert the decimal data generated in the programmes to hexadecimal and into Intel format in order that it can be transformed STRATOS EPROM programmer.

```
************************************************************
*     SUBROUTINE TO OUTPUT INTEGERS (RANGE 0 - 255) IN     *
*     INTEL HEX FORMAT. OUTPUT IS TO CHANNEL 7.            *
*                                                          *
*     CALL HEXOUT(III)  TO OUTPUT A INTEGER VALUE          *
*     CALL HEXEND TO TERMINATE OUTPUT AND FLUSH BUFFER     *
*                                                          *
************************************************************
      SUBROUTINE HEXOUT(INFO)
      INTEGER INFO
      INTEGER ADDR,ADDR2,ADDR3,CKSUM,COUNT,POINT,TEMP
      INTEGER*2 HI,LO
      LOGICAL DONE
      CHARACTER*68 RECORD
      CHARACTER*11 EOF
      CHARACTER*1 DECODE(16)
      EQUIVALENCE (CKSUM,HI)
*
*     ROM START ADDRESS IS 0
*
      DATA ADDR /0/
      DATA COUNT /0/
      DATA DECODE /'0','1','2','3','4','5','6','7',
     *             '8','9','A','B','C','D','E','F'/
      DATA EOF/':00000001FF'/
*
*      IF NEW RECORD THEN PUT OUT PREAMBLE AND INIT COUNTERS
*
      IF (COUNT .EQ. 0) THEN
         RECORD(1:1) = ':'
         CKSUM = 0
         POINT = 10
      ENDIF
*
*      GET NEXT DATA BYTE, STORE IN RECORD AND UPDATE CHECKSUM
*
      TEMP = INFO - (INFO/256)*256
      CKSUM = CKSUM + TEMP
      RECORD(POINT:POINT) = DECODE((TEMP/16)+1)
      RECORD(POINT+1:POINT+1) = DECODE(TEMP+1 - (TEMP/16)*16)
      POINT = POINT + 2
      COUNT = COUNT + 1
*
*      IF RECORD NOT YET COMPLETE JUST RETURN
*
```

```
      IF (COUNT .LT. 28) RETURN
      DONE = .FALSE.
      GOTO 1000
*
*      ELSE FINISH OFF AND OUTPUT
*
      ENTRY HEXEND
*
*     CHECK IF COUNT IS ZERO, IF SO THERE IS NO DATA
*     WAITING IN THE BUFFER SO WE JUST PUT A END MARKER
*
      DONE = .TRUE.
      IF (COUNT .EQ. 0) GOTO 2000
1000  RECORD(2:2) = DECODE((COUNT/16)+1)
      RECORD(3:3) = DECODE(COUNT+1 - (COUNT/16)*16)
      ADDR = ADDR - (ADDR/(256*256))*256*256
      ADDR2 = ADDR/256
      ADDR3 = ADDR - (ADDR/256)*256
      RECORD(4:4) = DECODE((ADDR2/16) +1)
      RECORD(5:5) = DECODE(ADDR2+1 - (ADDR2/16)*16)
      RECORD(6:6) = DECODE((ADDR3/16) +1)
      RECORD(7:7) = DECODE(ADDR3+1 - (ADDR3/16)*16)
      RECORD(8:8) = '0'
      RECORD(9:9) = '0'
*
*     COMPUTE CHECKSUM
*
      CKSUM  = -(CKSUM + COUNT + ADDR2 + ADDR3)
*
*     FIDDLE ABOUT TO COPE WITH NEGATIVE VALUE
*
      HI = 0
      CKSUM = CKSUM - (CKSUM/256)*256
      RECORD(POINT:POINT) = DECODE((CKSUM/16)+1)
      RECORD(POINT+1:POINT+1) = DECODE(CKSUM+1 - (CKSUM/16)*16)
      WRITE(7,700) RECORD(1:POINT+1)
700   FORMAT(A)
      ADDR = ADDR + COUNT
      COUNT = 0
2000  IF (DONE) WRITE(7,700) EOF
      RETURN
      END
```

## *Appendix B*

### *Switch mode power supply design for the GTO thyristor*

Switch mode power supplies (SMPS) are particularly advantageous in the field of power electronics. Their compactness and relatively high output power make them particularly attractive for use in GTO thyristor gate drive supplies. The particular type used here is the flyback isolated d.c./d.c. converter configuration as shown in fig.( B ). The design procedure may be found in the literature for example [1]. The circuit used supplies the gate drive circuit of the GTO with both a positive 8 volts supply for turn on, and a negative 12 volts supply for turn off. The main switching device employed is an IRF510 MOSFET which is switched at 71 kHz from a square wave oscillator (SP). Electrical isolation is provided by a high frequency RM10 transformer wound with four coils. Two secondary coils $F_2$, and $F_3$ are used to provide the positive 8 volts, negative 12 volts supplies, and a tertiary winding $F_4$ is used to prevent saturation in the transformer core.

Reference:

[1] Chryssis G., "High frequency switching power supplies: Theory and design", McGraw-Hill, 1984.

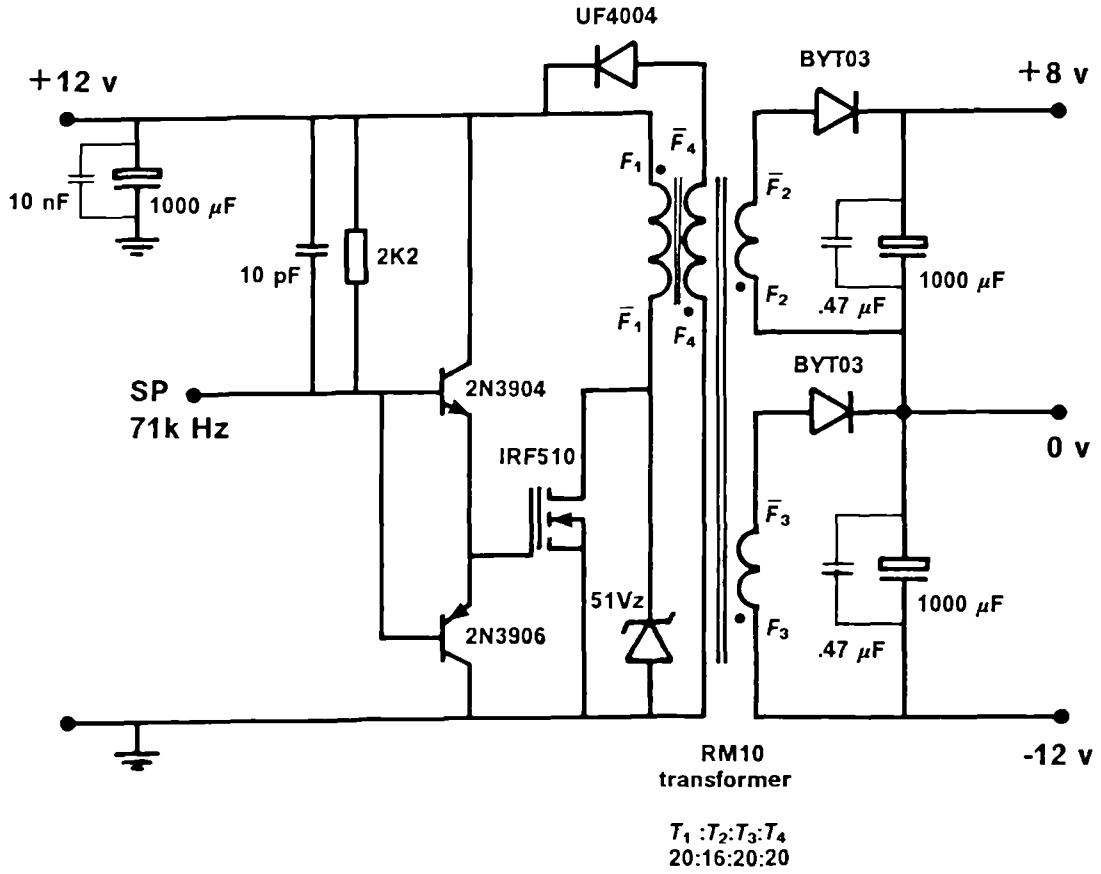


**Fig.( B ) Switch mode power supply circuit diagram.**

## *Appendix C*

### *Modified design of the sine-weighted signal and 8-bit/8-bit divider*

In the original design of the PWM generator a sine-weighted signal is stored as a single look-up table, and then fed to the 8-bit/8-bit divider to control the amplitude. However a more compact digital controller, can be achieved by storing the sine-weighted signal as pages of different amplitudes as shown in table ( C ), hence the digital divider is not needed. Therefore a single EPROM of 16-bit address can be used as both look-up table divider as shown in fig.(C). This EPROM will replace the two blocks representing the look-up table and the 8-bit 8-bit divider shown in fig.(3-15). The first most significant 7-bits are used to address the modulation index, while the other 9-bits are used to address the sine-weighted signal. Therefore, there are 128 pages, each page has a certain level of the sine-weighted signal, which varies from modulation index M = $(00)_{Hex}$ up to M = $(FE)_{Hex}$.

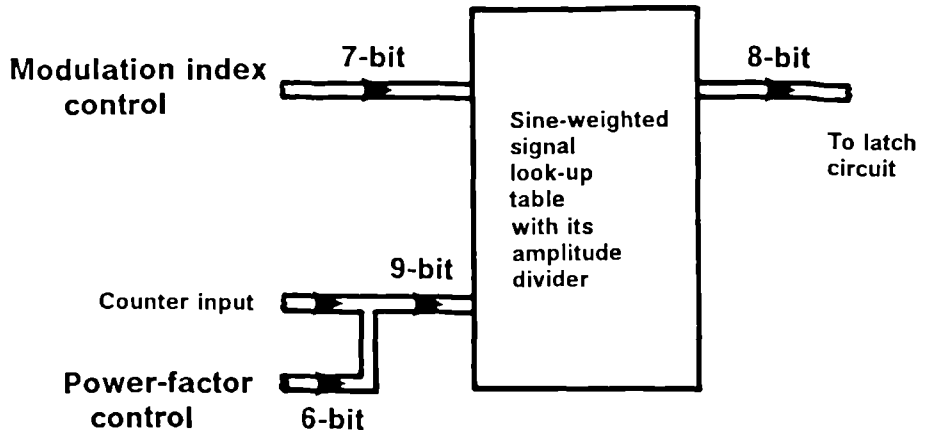


**Fig.( C ) Modified block diagram of the look-up table.**

| Sine Page no. | Modulation index address $A_{15}A_{14}A_{13}$ $A_{12}A_{11}A_{10}A_9$ | Sine-weighted signal address $A_8A_7$ $A_6A_5A_4$ $A_3A_2A_1A_0$ | Phase | No. of states |
|---|---|---|---|---|
| page-1 | 0 0 0 0 0 0 0 0 | 0 0 0 0 0 0 0 0 | B | 128 |
| | 0 0 0 0 0 0 0 0 | 0 1 * * * * * * * | Y | 128 |
| | 0 0 0 0 0 0 0 0 | 1 0 * * * * * * * | R | 128 |
| | 0 0 0 0 0 0 0 0 | 1 1 1 1 1 1 1 1 | - | 128 |
| page-2 | 0 0 0 0 0 0 0 1 | 0 0 0 0 0 0 0 0 | B | 128 |
| | 0 0 0 0 0 0 0 1 | 0 1 * * * * * * * | Y | 128 |
| | 0 0 0 0 0 0 0 1 | 1 0 * * * * * * * | R | 128 |
| | 0 0 0 0 0 0 0 1 | 1 1 1 1 1 1 1 1 | - | 128 |
| page-3 | 0 0 0 0 0 0 1 0 | 0 0 0 0 0 0 0 0 | B | 128 |
| | 0 0 0 0 0 0 1 0 | 0 1 * * * * * * * | Y | 128 |
| ⋮ | 0 0 0 0 0 0 1 0 | 1 0 * * * * * * * | R | 128 |
| | 0 0 0 0 0 0 1 0 | 1 1 1 1 1 1 1 1 | - | 128 |
| page-128 | 1 1 1 1 1 1 1 1 | 0 0 0 0 0 0 0 0 | B | 128 |
| | 1 1 1 1 1 1 1 1 | 0 1 * * * * * * * | Y | 128 |
| | 1 1 1 1 1 1 1 1 | 1 0 * * * * * * * | R | 128 |
| | 1 1 1 1 1 1 1 1 | 1 1 1 1 1 1 1 1 | - | 128 |

**Table ( C )**
**Modified data stored in the EPROM.**

# *Appendix D*

# *Data sheets of the GTO thyristor BTV58-1000R*

## FAST GATE TURN-OFF THYRISTORS

Thyristors in TO 220AB envelopes capable of being turned both on and off via the gate. They are suitable for use in high frequency inverters, power supplies, motor control etc. The devices have no reverse blocking capability. For reverse blocking operation use with a series diode, for reverse conducting operation use with an anti parallel diode.

### QUICK REFERENCE DATA

| | | | BTV58 600R | 850R | 1000R | |
|---|---|---|---|---|---|---|
| Repetitive peak off state voltage | $V_{DRM}$ | max. | 600 | 850 | 1000 | V |
| Non repetitive peak on state current | $I_{TSM}$ | max. | | 75 | | A |
| Controllable anode current | $I_{TCRM}$ | max. | | 25 | | A |
| Average on state current | $I_{T(AV)}$ | max | | 10 | | A |
| Fall time | $t_f$ | max | | 250 | | ns |

### MECHANICAL DATA

Dimensions in mm

Fig 1 TO 220AB

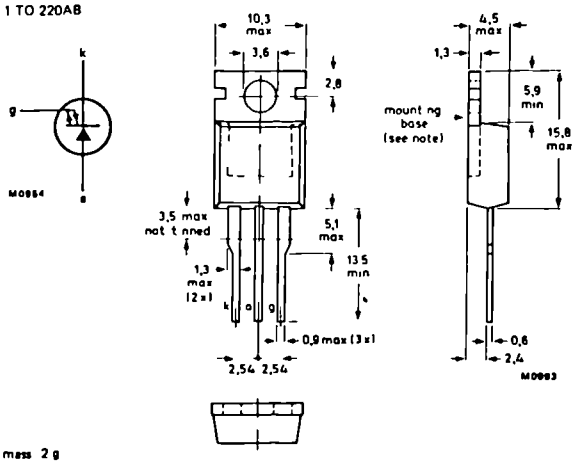


Net mass 2 g

Note The exposed metal mounting base is directly connected to the anode

Accessories supplied on request: see data sheets Mounting instructions and accessories for TO 220 envelopes

### RATINGS

Limiting values in accordance with the Absolute Maximum System (IEC 134)

| | | | BTV58 600R | 850R | 1000R | |
|---|---|---|---|---|---|---|
| **Anode to cathode** | | | | | | |
| Transient off state voltage* | $V_{DSM}$ | max. | 750 | 1000 | 1100 | V |
| Repetitive peak off state voltage* | $V_{DRM}$ | max | 600 | 850 | 1000 | V |
| Working off state voltage* | $V_{DW}$ | max | 400 | 600 | 800 | V |
| Continuous off state voltage* | $V_D$ | max | 400 | 500 | 650 | V |
| Average on state current (averaged over any 20 ms period) up to $T_{mb}$ = 80 °C | $I_{T(AV)}$ | max | | 10 | | A |
| Controllable anode current | $I_{TCRM}$ | max | | 25 | | A |
| Non repetitive peak on state current t = 10 ms half sinewave $T_j$ = 120 °C prior to surge | $I_{TSM}$ | max | | 75 | | A |
| $I^2t$ for fusing t = 10 ms | $I^2t$ | max | | 28 | | $A^2s$ |
| Total power dissipation up to $T_{mb}$ = 25 °C | $P_{tot}$ | max | | 65 | | W |
| **Gate to cathode** | | | | | | |
| Repetitive peak on state current $T_j$ = 120 °C prior to surge gate cathode forward t = 10 ms, half sinewave | $I_{GFM}$ | max | | 25 | | A |
| gate cathode reverse t = 20 µs | $I_{GRM}$ | max | | 25 | | A |
| Average power dissipation (averaged over any 20 ms period) | $P_{G(AV)}$ | max | | 2,5 | | W |
| **Temperatures** | | | | | | |
| Storage temperature | $T_{stg}$ | | | −40 to + 150 | | °C |
| Operating junction temperature | $T_j$ | max | | 120 | | °C |
| **THERMAL RESISTANCE** | | | | | | |
| From junction to mounting base | $R_{th\,j\text{-}mb}$ | = | | 1,5 | | K/W |
| From mounting base to heatsink with heatsink compound | $R_{th\,mb\text{-}h}$ | = | | 0,3 | | K/W |
| with 56367 alumina insulator and heatsink compound (clip mounted) | $R_{th\,mb\text{-}h}$ | = | | 0,8 | | K/W |

* Measured with gate connected to cathode

### CHARACTERISTICS

**Anode to cathode**

| | | | | |
|---|---|---|---|---|
| On state voltage $I_T$ = 5 A; $I_G$ = 0,2 A; $T_j$ = 120 °C | $V_T$ | < | 1.8 | V* |
| Rate of rise of off state voltage that will not trigger any off-state device; exponential method $V_D$ = 2/3 $V_{Dmax}$; $V_{GR}$ = 5 V; $T_j$ = 120 °C | $dV_D/dt$ | < | 10 | kV/µs |
| Rate of rise of off state voltage that will not trigger any device following conduction, linear method $I_T$ = 5 A; $V_D$ = $V_{DRMmax}$; $V_{GR}$ = 10 V; $T_j$ = 120 °C | $dV_D/dt$ | < | 1.5 | kV/µs |
| Off state current $V_D$ = $V_{Dmax}$; $T_j$ = 120 °C | $I_D$ | < | 3 0 | mA |
| Latching current; $T_j$ = 25 °C | $I_L$ | typ. | 1.0 | A** |
| **Gate to cathode** | | | | |
| Voltage that will trigger all devices $V_D$ 12 V; $T_j$ = 25 °C | $V_{GT}$ | > | 1.5 | V |
| Current that will trigger all devices $V_D$ = 12 V; $T_j$ = 25 °C | $I_{GT}$ | > | 200 | mA |
| Minimum reverse breakdown voltage $I_{GR}$ = 1 0 mA | $V_{(BR)GR}$ | > | 10 | V |
| **Switching characteristics (resistive load)** | | | | |
| Turn on when switched to $I_T$ = 5 A from $V_D$ = 250 V with $I_{GF}$ 0 5 A; $T_j$ = 25 °C | | | | |
| delay time | $t_d$ | < | 0 25 | µs |
| rise time | $t_r$ | < | 1.0 | µs |

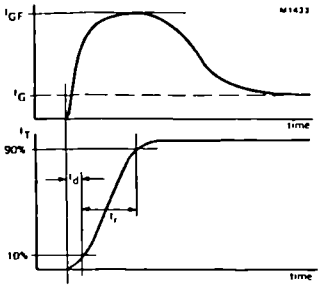


Fig 2 Waveforms

* Measured under pulse conditions to avoid excessive dissipation.

** Below latching level the device behaves like a transistor with a gain dependent on current

**Switching characteristics (inductive load)**

Turn off when switched from $I_T$ = 5 A to $V_D$ = $V_{Dmax}$, $V_{GR}$ 10 V; $L_G$ ≤1 0 µH; $L_S$ ≤0 25 µH; $T_j$ = 25 °C

| | | | | |
|---|---|---|---|---|
| storage time | $t_s$ | < | 0 5 | µs |
| fall time | $t_f$ | < | 0 25 | µs |
| peak reverse gate current | $I_{GR}$ | < | 6 | A |

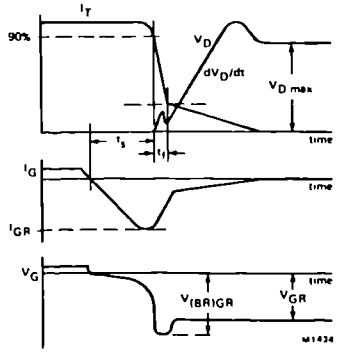


Fig.3 Waveforms.

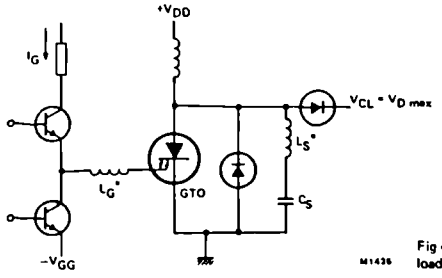


Fig 4 Inductive load test circuit.

*Indicates stray series inductance only.